U.PORTO

FEUP FACULDADE DE ENGENHARIA
UNIVERSIDADE DO PORTO

WEARABLE SENSORS SYSTEMS FOR HUMAN MOTION ANALYSIS

SPORTS AND REHABILITATION

ANA SOFIA MATOS SILVA

THESIS SUBMITTED IN FULFILLMENT OF THE REQUIREMENTS FOR THE DEGREE OF DOCTOR OF PHILOSOPHY IN BIOMEDICAL ENGINEERING BY THE FACULTY OF ENGINEERING OF THE UNIVERSITY OF PORTO, PORTUGAL.

SUPERVISOR: MIGUEL FERNANDO PAIVA VELHOTE CORREIA

CO-SUPERVISOR: ORLANDO JOSÉ DOS REIS FRAZÃO

FEBRUARY, 2014

ABSTRACT

Wearable technologies introduced a refinement to personal signal capturing by permitting a long-term on-person approach. The need for precise training regimes, continuous monitoring and quantitative analysis of movement has taken the athletes and patients out of the laboratory to their "natural environments", in order to improve their performance, monitor their evolution, mitigate the risks of injuries and preventing the adoption of improper strategies.

The system described hereby will provide a functional instrumented wearable device that has the potential to be used in different applications, from sports to rehabilitation, allowing the collection of data capable of quantitatively describe performance and movements. To do so, the system was based on a modular approach, where several sensor modules could be assembled and used together to extract meaningful information. In parallel, a proof-of-concept intensity-modulated fiber optic sensor was designed and characterized with the purpose to measure human joint angles and that could ultimately be integrated in the wearable system.

The experiences developed in swimming have demonstrated that inertial sensors can provide meaningful information about swimmers' performance through the extraction of angular displacements and temporal parameters. Moreover, different swimming styles can be differentiated by analyzing acceleration profiles. In the field of rehabilitation, the system was used in post-stroke subjects in order to establish methods to analyze upper-limb performance during the reaching task, provide quantifiers to characterize the movement and better understand specific motor mechanisms underlined the task, such as the postural control.

Keywords: Inertial sensors, fiber optic sensors, swimming performance analysis, stroke rehabilitation.

RESUMO

As tecnologias denominadas *wearable* (vestíveis) introduziram um refinamento na monitorização pessoal, ao permitir a aquisição centrada no indivíduo e por longos períodos de tempo. A necessidade de obter regimes de treino precisos, de monitorizar de forma contínua e de obter uma análise quantitativa do movimento, conduziu ao afastamento dos atletas e pacientes de laboratórios para o seu "meio natural", de forma a melhorar o seu desempenho, acompanhar a sua evolução, mitigar o risco de lesões e prevenir a adoção de estratégias de movimento desadequadas.

O sistema apresentado nesta tese é um instrumento funcional *wearable* que pode ser utilizado em diversas aplicações, desde o desporto à reabilitação, e que permite a aquisição de dados quantitativos capazes de descrever movimentos. Para isso, foi utilizado um conceito modular que permite a integração e combinação de diversos módulos de sensores de forma a extrair informação relevante. Em paralelo, foi criado e construído um sensor em fibra ótica baseado no efeito de atenuação, com o objetivo de medir ângulos corporais e ser integrado no sistema desenvolvido.

Os resultados da utilização do sistema na natação demonstraram que os sensores inerciais têm potencial para analisar o desempenho do nadador, através de parâmetros cinemáticos. Para além disso, permitem distinguir entre diferentes técnicas de nado. Em reabilitação, o sistema foi utilizado em indivíduos que sofreram um acidente vascular encefálico de forma a estabelecer protocolos de aquisição do movimento do membro superior durante a tarefa de alcance, fornecer quantificadores que caracterizam o movimento e compreender melhor os mecanismos motores específicos da tarefa, tal como o controlo postural.

Palavras-chave: Sensores inerciais, sensores em fibra ótica, análise do desempenho na natação, reabilitação, acidente vascular encefálico.

ACKNOWLEDGMENTS

The number of people directly and indirectly involved in this investigation was very wide. Therefore, to all who had contributed with technical and scientific knowledge and have collaborated in some way for my personal growth, I would like to give you my gratitude.

I would like to thank the *Fundação para a Ciência e Tecnologia de Portugal* for the financial support through a PhD grant (SFRH/BD/60929/2009). In addition, I would like to thank INESC Porto (*Instituto de Engenharia de Sistemas e Computadores do Porto*) and my unit UOSE (*Unidade de Optoelectrónica e Sistemas Electrónicos*) not only for the administrative support as my host institution but also for presenting me with the spirit of union, friendship and cooperation.

A special thank to my supervisor, Prof. Miguel, and co-supervisor, Prof. Orlando, for the guidance during the investigation. I would also like to thank Prof. João Paulo Vilas-Boas for being always available to share his knowledge and advices.

I must thank to all my colleagues and friends at Lab I301 who shared my achievements and anxieties and helped me when everything seemed "stuck".

Last, but definitely not the least, I would like to thank Hugo. Thank you for being my best friend, for the patience to deal with my frustrations, for making me smile and most of all for your love.

To Hugo

There are no mistakes. The events we bring upon ourselves, no matter how unpleasant, are necessary in order to learn what we need to learn; whatever steps we take, they're necessary to reach the places we've chosen to go.

Richard Bach

"The Bridge Across Forever: A True Love Story"

CONTENTS

LIST OF FIGURES

LIST OF TABLES

LIST OF ABBREVIATIONS

AMA	American Medical Association
AP	Application Point
ADC	Analog-to-Digital Converter
BMI	Body Mass Index
BSN	Body Sensor Network
CNS	Central Nervous System
DCM	Direction Cosine Matrix
DNA	Deoxyribo-Nucleic Acid
ECG	Electrocardiography
ED	End Device
EMG	Electromyography
FAB	Functional Assessment of Biomechanics
FBG	Fiber Bragg Grating
FMA	Fugl-Meyer Motor Assessment
FOS	Fiber Optic Sensors
GUI	General User Interface
IDE	Integrated Development Environment

INS	Inertial Navigation System
I2C	Inter-Integrated Circuit
LED	Light-Emitting Diode
LMCA	Left Medial Cerebral Artery
LPG	Long-Period Gratings
MCA	Medial Cerebral Artery
MEMS	Micro-Electro-Mechanical Systems
MMSE	Mini-Mental State Examination
MRI	Magnetic Resonance Imaging
OLE	Optical Linear Encoder
OTDR	Optical Time Domain Reflectometer
PASS	Postural Assessment Scale for Stroke patient
PCB	Printed Circuit Board
PCF	Photonic Chrystal Fiber
POF	Polymer Optical Fiber
PWM	Pulse-Width Modulation
RF	Radio-Frequency
RMA	Rivermead Motor Assessment
RMCA	Right Medial Cerebral Artery
RPS	Reach Performance Scale
RSSI	Received Signal Strength Indicator
sEMG	Surface Electromyography
SMF	Single-Mode Fiber
SPI	Serial Peripheral Interface

TIA	Transient Ischemic Attack
UART	Universal Asynchronous Receiver Transmitter
USB	Universal Serial Bus
WIMU	Wearable Inertial Measurement Unit
WSN	Wireless Sensor Networks
WPAN	Wearable Personal Area Network
W2M2	Wireless Wearable Modular Monitor

CHAPTER 1

INTRODUCTION

1.1. Motivation

In the wide field of human motion analysis, several different areas share technological devices and methods. In the realm of clinical analysis, professionals apply their knowledge for diagnosis and planning of treatments protocols (orthotic or prosthetic prescription, surgical intervention or medication). In rehabilitation, therapists must address the individual's impairment and challenge the motor system by integrating motion analysis strategies to develop new methods to improve rehabilitation processes. With respect to sports, coaches and athletes use motion analysis techniques to access biomechanical data in order to improve athletes' performance while avoiding injuries.

In sports, namely in swimming, numerous devices and setups have been implemented in order to assist on performance analysis. Many of these devices and setups are based on video capturing and analysis (Thompson, MacLaren, Lees, & Atkinson, 2004), while others make direct measurement and signal capturing through awkward setups and apparatus (Pendergast, Termin, & Zaharkin, 1999), generally uncomfortable for the athletes and thus affecting their performance. Although this scenario is very frequent for the majority of sports, there is a relatively reduced number of signal monitoring systems being used for swimming performance analysis today (particularly when compared to the number of wearable monitoring devices for healthcare or even for land based sports), a shift on the approaches for swimming analysis is being noted. Different strategies have been applied by the mentioned systems, however a common element seem to be their dependence on inertial sensors, such as accelerometers and gyroscopes.

At present, in the field of human motor rehabilitation, patient movement analysis is primarily carried out in one of two methods: in a motion laboratory, with full analysis of the motion of body segments using optical tracking sensors, or in a clinical appointment with the physician or physiotherapist making visual observations. The first method is expensive, requires highly qualified technical

skills and expertise, involves the maintenance of a dedicated motion laboratory, and uses cumbersome equipment attached to the patient; but it produces well-quantified and accurate results. The second method is less expensive and does not require special equipment, but the results are qualitative, unreliable, and difficult to compare across multiple appointments (Dobkin, 2004; Knorr et al., 2005).

There is a need for an alternative analysis method that is capable of providing quantitative and repeatable results over extended time periods.

Wearable monitoring systems represent a group of technologies that have changed the way biomechanical and physiological data are acquired, allowing long-term on-site monitoring that do not necessarily occur within controlled environments.

Advances in sensors, namely in the field of MEMS-based devices, allowed for a shift in the way human motion data is captured, changing from in-lab environments to the natural daily contexts, from short-time acquisition to long-period monitoring. MEMS inertial sensing is a highly mature technology in terms of both commercial viability and reliability (Rocha, 2010). Beyond the well-known use cases in mobile devices and gaming, significantly more challenging needs exist in the medical and industrial fields. Accelerometers and gyroscopes became common resources to capture human movement and to estimate kinematic parameters; however, these systems still introduce some drawbacks, such as ergonomy, electric insulation or lack of accuracy when estimating segments position (Esfandyari, Bendiscioli, & Xu, 2011). Commercial inertial systems still have a niche market due to the high cost, particularly for multiple module systems. In addition, although providing a good level of performance in terms of accuracy, solutions provided by these commercial systems are closed and many times do not allow for further research besides their own.

A fairly new concept that is proving popular is the use of fiber optic sensors (FOS) to measure body segments displacements. Besides the advantages of small size, weight and electromagnetic immunity, fiber optic

sensors have high sensibility, accuracy and allow the measurement of different variables in a single fiber (i.e. multiplexing capabilities) (Krohn, 2000).

The combination of different wearable sensors will allow the investigation of new quantitative biomechanical models capable of describing movement, which will aid swimmers, coaches, patients and physiotherapists improving their performance, either by optimizing techniques and preventing injuries or by assisting with their recovery and clinical reasoning processes.

1.2. Thesis Objectives

The main objective of this thesis is to conceive, design and develop an electronic wearable prototype with embedded sensors for the assessment of human motion parameters. The idea is to create a new device that overcomes some of the limitations of current acquisition systems, presented in the section above, and that is based on a modular approach, which allows the integration of different sensors according to the requirements of each particular application. Therefore, the main outcomes expected from this research will be the integration of electrical inertial sensors, and ultimately fiber optic sensors, in a functional wearable device and its proof-of-concept and implementation in different applications for the analysis, classification and extraction of meaningful kinematic parameters through proposed algorithms.

In this thesis, the applications chosen for analysis were sports and rehabilitation since both represent major areas of interest in motion analysis, sharing some similarities such as monitoring subject's performance, keeping them healthy and preventing future injuries.

In this manner, the development of the proposed wearable devices will allow the estimation of performance and kinematic parameters that could be used in:

- swimming to characterize swimmer's movements, allowing for the comparison of different experience level swimmers and to differentiate between swimming techniques; and

- rehabilitation as an alternative tool for rehabilitation monitoring, by giving means to quantitatively assess the upper-limb movement of post-stroke patients and by providing timely feedback.

1.3. Work Description

The first approach to accomplish the proposed goals was the utilization of a MEMS-based inertial unit (usually known as IMU) for linear acceleration and position and orientation estimation, and its integration with a transmitting and data-logging sections. This device was named as WIMU – Wearable Inertial Measurement Unit. With the knowledge provided during the design and utilization of the first prototype, a new wearable device based on a modular approach was developed, called W2M2 – Wireless Wearable Modular Monitor. The modular feature allows the integration of different analog and digital sensors, from touch sensors to surface electrodes. In parallel with the inertial measurement units, a new fiber optic sensor was developed and tested, as a proof-of-concept, for the measurement of body segments angular displacements. The ultimate goal will be the integration and combination of both systems, electrical and optical.

The WIMU and the W2M2 were used to monitor swimming athletes during training and to quantify upper-limb movement of stroke patients. Naturally several questions arise from the implementation of the system, both in swimming and rehabilitation:

- In swimming:
  - Evaluate swimmers performance through kinematical variables;
  - Characterize swimmers movement;
  - Differentiate between swimming techniques.

- In rehabilitation:
    - Monitor upper-limb movement of stroke patients;
    - Extraction of meaningful variables to characterize the movement;
    - Identify compensatory strategies while performing functional tasks.

The diagram presented in Figure 1 shows this thesis' roadmap and the main research questions that led the investigation.

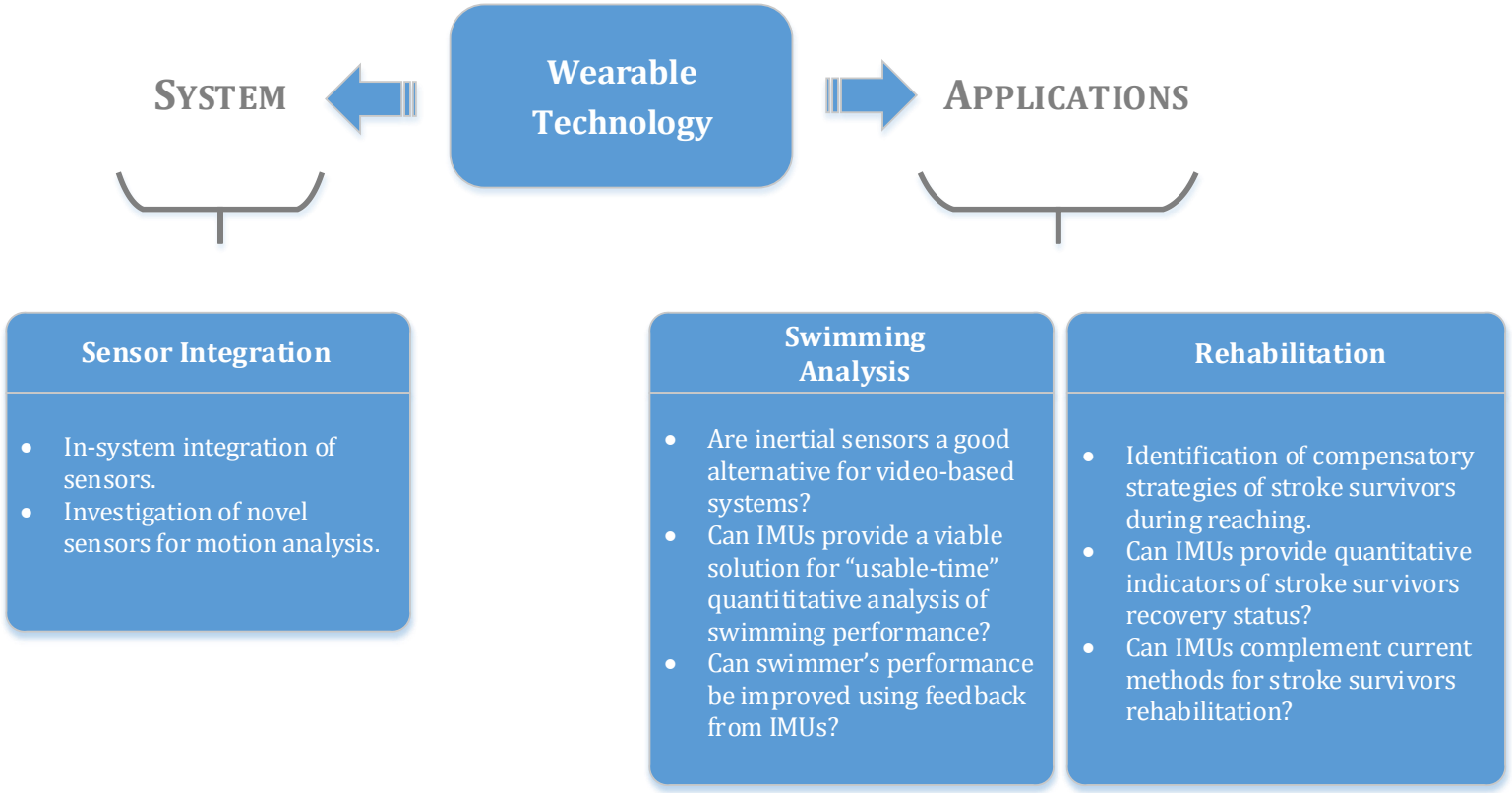

Figure 1: Thesis description: main questions and challenges that led the investigation.

1.4. Main Contributions

The research work completed under this thesis yielded the following outcomes:

- Design and development of wearable inertial measurement units, the first named as WIMU, for swimming performance analysis and the second, based on a modular approach, designated W2M2, for human motion analysis. The modular approach introduced functionality and versatility, since it allowed different sensor modules to be connected to the device and its application in several areas from sports to rehabilitation;
- Design and characterization of a novel fiber optic sensor to measure elbow flexion. The sensing principle was based on macrobending effect, and a customized piece of garment was specifically designed and built to integrate the optical fiber as the sensing element;
- Method for quantification of swimming athletes' performance parameters, such as stroke frequency, stroke duration, number of laps and lap-time, from accelerometry data, obtained by using the WIMU;
- Characterization of different swimming techniques from pitch and roll angles estimation;
- Method for data collection and analysis of upper-limb movement of healthy or impaired subjects during specific functional tasks using the W2M2;
- Identification of upper-limb compensatory strategies adopted by post-stroke patients while performing reaching functional task;

In addition, during the research work several outcomes were submitted to scientific evaluation with success and published:

- **Journal articles:**

Salazar, A. J., Silva, A. S., Silva, C., Borges, C. M., Correia, M. V., Santos, R. S., & Vilas-Boas, J. P. (2014). Low-cost wearable data acquisition for stroke rehabilitation: a proof of concept study on accelerometry for functional task assessment. Topics in Stroke Rehabilitation, 21(1), 12-22.

Silva, A. S., Catarino, A., Correia, M. V., & Frazão, O. (2013). Design and characterization of a wearable macrobending fiber optic sensor for human joint angle determination. Optical Engineering, 52(12), 126106-126106.

Silva, A. S., Salazar, A. J., Borges, C. M., & Correia, M. V. (2013) Wearable Monitoring Unit for Swimming Performance Analysis. Vol. 273. CCIS Lecture Notes in Computer Science (pp. 80-93). Heidelberg: Springer.

Silva, C., Silva, A., Sousa, A., Pinheiro, R., Bourlinova, C., Silva, A. S., A. J. Salazar, C. M. Borges, C. Crasto, M. V. Correia, J. P. Vilas-Boas & Santos, R. S. (2014). Co-Activation Study of Upper Limb Muscles During Reaching in Post-Stroke Subjects: an Analysis of Ipsilesional vs Contralesional Limb. Journal of Electromyography and Kinesiology. (accepted)

- **Conference papers:**

Silva, A. S., Casanova, O. E., Zambrano, A., Borges, C. M., & Salazar, A. J. (2012). Experiencias en Tecnología Portable para Comunicacíon y Monitoreo Personal de Bajo Costo. Paper presented at the IV Congreso Venezolano de Bioingeniería (BIOVEN 2012), San Cristobal, Venezuela.

Salazar, A. J., Silva, A. S., Silva, C., Borges, C. M., Correia, M. V., Santos, R. S., & Vilas-Boas, J. P. (2012). W2M2: Wireless wearable modular monitor. A multifunctional monitoring system for rehabilitation. Paper presented at the International Conference on Biomedical Electronics and Devices (BIODEVICES2012), Vilamoura, Portugal.

Borges, C. M., Silva, C., Salazar, A. J., Silva, A. S., Correia, M. V., Santos, R. S., & Vilas-Boas, J. P. (2012). Compensatory movement detection through inertial sensor positioning for post-stroke rehabilitation. Paper presented at the International Conference on Bio-inspired Systems and Signal Processing (BIOSIGNALS2012), Vilamoura. Portugal.

Borges, C. M., Salazar, A. J., Silva, A. S., Bravo, R. J., & Correia, M. V. (2012). Estudio de factibilidad del uso de acelerometría para Análisis de Movimientos Compensatorios del Miembro Superior en Pacientes Post ACV. Paper presented at the 8th International Seminar on Medical Information Processing and Analysis (SIPAIM 2012), San Cristobal, Venezuela.

Silva, A. S., Salazar, A. J., Borges, C. M., & Correia, M. V. (2011). WIMU: Wearable Inertial Mmonitoring Unit - A MEMS-based device for swimming performance analysis. Paper presented at the International Conference on Biomedical Electronics and Devices (BIODEVICES 2011), Rome, Italy.

Salazar, A. J., Silva, A. S., Borges, C. M., & Correia, M. V. (2010). An initial experience in wearable monitoring sport systems. Paper presented at the 10th IEEE International Conference on Information Technology and Applications in Biomedicine (ITAB).

- **Conference abstracts:**

Salazar, A. J., Silva, A. S., & Correia, M. V. (2011). Sensor characterization for portable and wearable applications. Paper presented at the 17th edition of the Portuguese Conference on Pattern Recognition (RecPad2011), Porto, Portugal.

Silva, C., Borges, C. M., Salazar, A. J., Silva, A. S., Correia, M. V., & Santos, R. S. (2011). Post-stroke patients functional task characterization through accelerometry data for rehabilitation intervention and monitoring. Paper presented at the 17th edition of the Portuguese Conference on Pattern Recognition (RecPad2011), Porto, Portugal.

1.5. Thesis Organisation

This thesis is organised in six chapters and two main parts. After this introductory chapter, Part I is dedicated to wearable sensor systems, with chapters 2 and 3, and Part II, with chapters 4 and 5, focus on the applications of wearable systems to quantitatively assess human movements. Chapter 6 closes the thesis.

Part I – Wearable Sensor System, starting in Chapter 2, presents inertial systems, its main concepts and the state-of-the-art on the application of these systems as wearable devices. In addition, the design and the main features of the wearable inertial units referred to as WIMU and W2M2 is reported. Chapter 3 will focus on fiber optic sensors. The main concepts behind fiber optic technology and its application for wearable purposes will be discussed. Additionally, the development and outcomes of a new intensity-modulated fiber optic sensor for the measurement of human joint angles is presented.

Part II – Human Motion Analysis: sports and rehabilitation, initiates with a chapter dedicated to swimming performance analysis (Chapter 4). The main features and results obtained from WIMU are presented and discussed. Chapter 5 focus on the analysis of stroke survivor movements during the performance of specific functional tasks. Three different studies on the analysis of upper-limb movement during reaching, either in post-stroke and healthy subjects, are presented.

The final chapter includes an overall discussion of the developed wearable systems, the challenges and difficulties experienced and the main outcomes of the application of such systems in sports and rehabilitation. Moreover, the main conclusions, final remarks and future work provide the closure for this thesis.

Figure 2 shows a schematic that illustrates this thesis structure. The reader interested in technological features related with the wearable system will find all the details in chapters 2 and 3, whether its interest is in inertial sensors or fiber optic sensors, respectively. The reader most interested in sports

analysis, namely swimming performance analysis, can consult the outcomes provided by the WIMU for the analysis of swimming techniques in Chapter 4, while the reader concerned with post-stroke rehabilitation matters can focus on Chapter 5 in which the results of using inertial systems to quantify upper-limb movement performance during reaching are described.

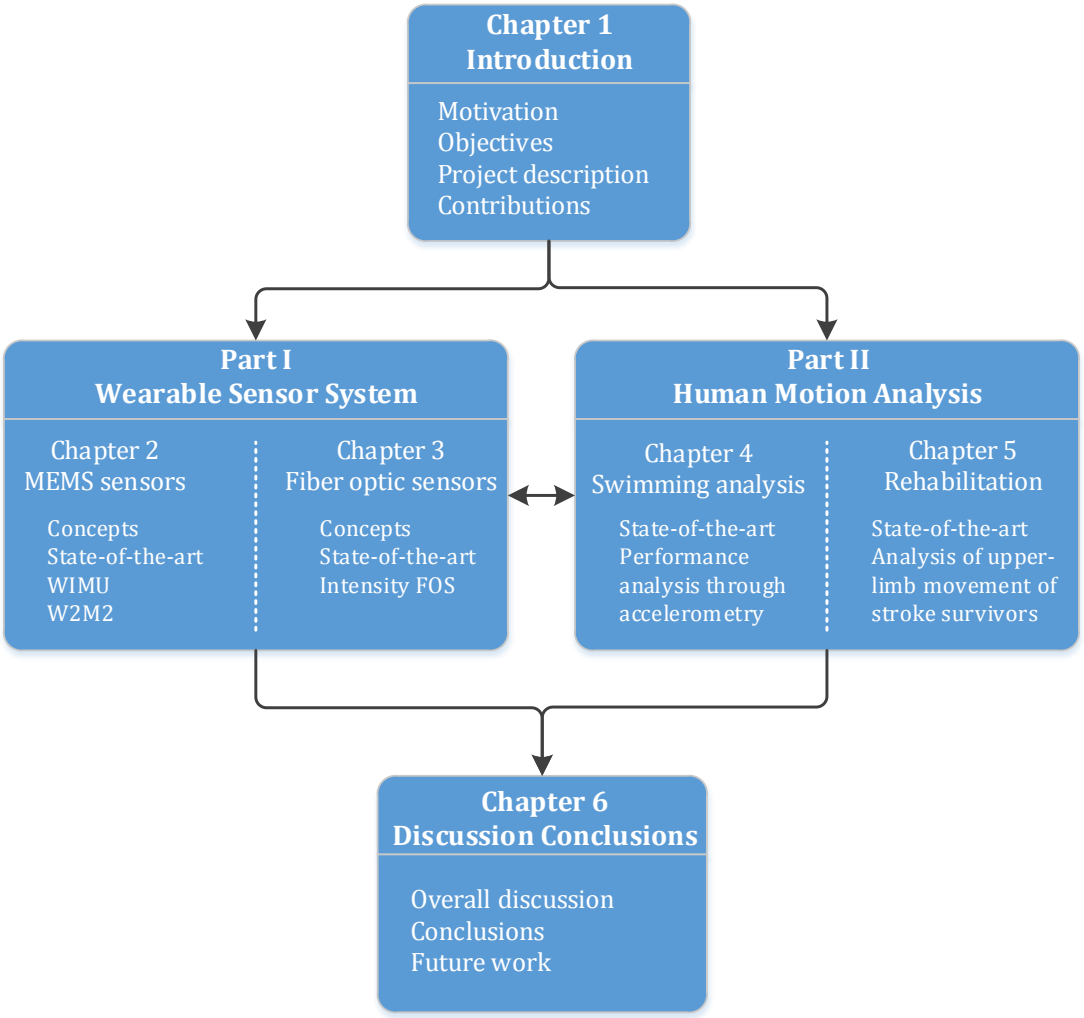

Figure 2: Thesis structure.

PART I

WEARABLE SENSOR SYSTEM

Primarily influenced by healthcare monitoring and supported by recent advances in microtechnologies, sensor miniaturization and smart fabrics, the evolution on wearable systems will progressively influence the landscape of human motion monitoring by allowing continuous evaluation of individual's status.

Concepts such as wearable technology and wireless sensor networks (WSN) have become well established in the scientific community and industry as well. Wireless sensor network, textile integrated circuitry and other achievements have allowed for designs that require less energy and remain on-site for longer periods of time.

Consisting of various devices and components, ranging from sensors and actuators to multimedia devices, these systems support complex monitoring applications and enable low-cost wearable, non-invasive alternatives for monitoring of health, activity and mobility, both indoors and outdoors. The area of personal monitoring is witnessing a set of paradigms shifts:

- the **single moment** data capture is being replace by continuous **long-term data** gathering: instead of a punctual measurement/appointment, individuals' data can be gathered for days or weeks;
- the **laboratory** or controlled environments is being replaced by **real-life scenarios**: individuals can interact with their everyday surroundings;
- **offline database** analysis is being replaced by **real-time** analysis: data gathering can change an individual's performance.

Wearable technology, in general, can serve four main areas: Sports, Healthcare, Entertainment and Science and Industry. Most of them share some

purposes, such as performance analysis, sports assistance, injury prevention or control applications (see Figure 3).

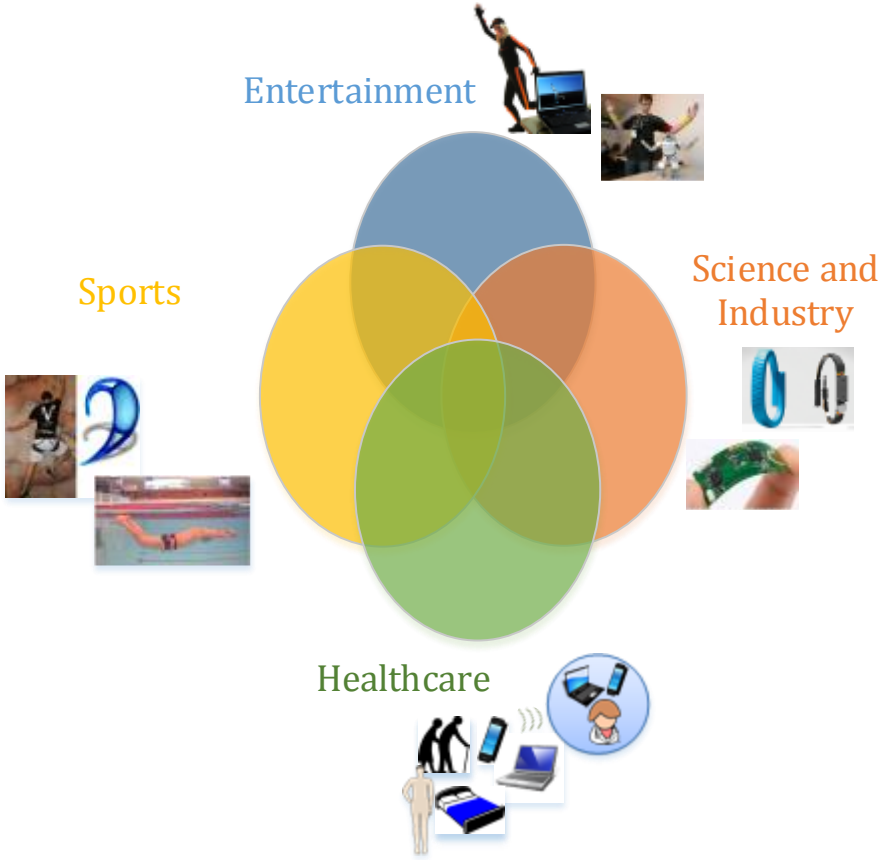

Figure 3: Wearable technology applications.

For monitoring a wide range of physiological, biomechanical and chemical parameters, wearable systems include an extensive variety of components, including sensors, actuators, smart fabrics, power supplies, memory storage, wireless communication protocols and networks, processing units, software and data algorithms for data capture and decision support. An ideal sensor-system would be able to continuously measure, process, transmit wirelessly to a remote station or provide immediate feedback; it would not constrain or affect in any way and it would need few maintenance. Until now, complete systems like these are still not a reality, since one or more than one requirement might be absent or not fully optimized. Nevertheless, taking into account the technological advances of the last decades it seems clear that in the not too distant future complete systems like those will be feasible.

As mentioned before wearable systems are designed to be minimally invasive and based on flexible and smart technologies conformable to the human body. Typically, these systems may be distinguished in two different categories: non-textile wearable systems and intelligent bio-clothing. The first group includes wearable systems which integrate sensors (electrical, chemical, optical, etc.) in a functional piece of garment; the second one consists of truly smart fabrics, where the textile works itself as the sensor (Lymberis & Dittmar, 2007). Most of the research is today focused on developing textile sensors, taking advantage of certain properties of fabrics to measure physiological variables. Textile dry electrodes or piezoresistive fabrics are some examples of such sensors (Chan, Estève, Fourniols, Escriba, & Campo, 2012). Currently, there is a variety of wearable systems developed for healthcare applications. Projects such as Wealthy (Paradiso, Belloc, Loriga, & Taccini, 2005), VTAMN (Noury et al., 2004), MagIC (Rienzo et al., 2005), SmartVest (Pandian et al., 2008), MyHeart (Luprano, Sola, Dasen, Koller, & Chetelat, 2006), BIOTEX (Coyle et al., 2010) and more recently PROLIMB (Zambrano et al., 2012) are just some examples where textile sensors were used to remotely monitor health parameters like electrocardiography (ECG), electromyography (EMG), respiration and physical activity. In the field of sports, some projects exist focused on developing wearable systems to monitor athlete's performance, such as the BIOSWIM (A. S. Silva, Salazar, Borges, & Correia, 2012) and the ClimBSN (Pansiot, King, McIlwraith, Lo, & Guang-Zhong, 2008). Table 1 presents the most relevant research made in wearable systems in the last decade.

This first part of the thesis will focus on presenting the state-of-the-art and concepts behind wearable systems, specifically those related with inertial sensors and fiber optic sensors. Additionally, the features and outcomes of the wearable system proposed hereby will be presented and discussed, namely the inertial measurement units developed and the fiber optic sensor designed.

Table 1: Relevant research on wearable monitoring systems.

Project	Application	Purpose	Sensor Elements	Sensor Location	Feature Extraction	Reference
WEALTHY	Physiological monitoring	Monitoring ECG and respiration during daily activities	Strain fabric sensors (piezoresistive yarns)	Torso and arms	ECG, respiration, upper-limb activity.	(Paradiso et al., 2005)
VTAMN	Physiological monitoring	Ambulatory remote monitoring of physiological parameters	Fabric sensors	Torso	Cardiac frequency, breathing, temperature	(Noury et al., 2004)
SmartVest	Physiological monitoring	Remote monitoring of soldiers' physiological parameters	Silicon rubber + silver electrodes, PPG sensor, platinum thermistor, Ag-AgCl electrodes	Torso and ear	ECG, blood pressure, heart rate, PPG, temperature, galvanic skin response	(Pandian et al., 2008)
PROLIMB	Lower-limb monitoring	Electronic sensing for the prophylaxis of lower-limb pathologies	Textile electrodes, 3-axis accelerometers and gyroscopes	Lower-limbs	EMG, activity	(Zambrano et al., 2012)
OFSETH	MRI scanning	Assessment of vital parameters of sedated patients MRI exams	Silica and polymer optical fibers; Fiber Bragg gratings	Torso	Respiration	(De Jonckheere et al., 2009)
MagIC	Physiological monitoring	Vital signs monitoring during daily life activities	Textile electrodes, conductive fibers	Torso	ECG, respiration	(Rienzo et al., 2005)
BIOTEX	Physiological monitoring	Health monitoring through textile technology for medical and sports physiology	Textile sensors and electrodes, gold electrodes, humidity sensor, pulse oximeters	Waist and chest	pH, sodium concentration, conductivity, sweat rate, oximetry, ECG, respiration	(Coyle et al., 2010)
BIOSWIM	Swimming analysis	Wearable integrated monitorization of swimmers' performance	3-axis accelerometer, 2-axis gyroscope, textile electrodes, textile pressure sensor	Torso, lower-limbs, hands	EMG, activity, heart rate, pressure	(A. S. Silva et al., 2012)
VitalJacket	Physiological monitoring	Vital signs monitor for cardiology and sports	Textile electrodes and sensors, 3-axis accelerometers	Torso	ECG, respiration, activity	(Cunha et al., 2010)
ClimBSN	Climbing	Assess climbing performance during training	3-axis accelerometers	Ears	Motion fluidity, endurance	(Pansiot et al., 2008)

Chapter 2

MEMS-BASED INERTIAL SENSORS

Micro-Electro-Mechanical-Systems can be defined as "mechanical devices that have a characteristic in length of less than 1 mm but more than 1 μm, combining electric and mechanical components" (Maluf, 2004). The name itself establishes a dimensional scale (Micro), suggests either electricity or electronics (Electro) and moving parts (Mechanical). The transduction mechanisms behind these sensors have different sources: mechanical effects (piezoresistivity, piezoelectricity, capacitive techniques), thermal effects (Seebeck, Peltier and Thomson effects) and magnetic effects (Hall effect, magnetoresistivity) (Rocha, 2010); hence the large number of applications of such devices, ranging from inertial to pressure and microfluidics sensors.

Micro-machined inertial sensors are a very versatile group of MEMS-based sensors with applications in many areas. Primarily, the use of medium to high performance inertial sensors was restricted to areas in which the cost was not a critical aspect, such as military and aerospace systems. Nowadays, the development of miniaturized low-power accelerometers and gyroscopes allowed the successful application of these systems in cost-sensitive areas, from rehabilitation to sports, entertainment and automotive industries, either in laboratory environments or daily-life activities, sports events, interactive games, consumer electronics, etc.

The typical inertial sensors used for human tracking are accelerometers, for linear acceleration, and gyroscopes, that measure angular velocity. The information from those sensors can be combined and correlated in order to evaluate human movement and/or posture.

2.1. Accelerometers and Gyroscopes

MEMS accelerometers have become an attractive tool for use in wearable systems for detecting and measuring aspects of human movement. To extract the acceleration value, typically the accelerometer has a movable mass which is connected to a fixed frame via spring structures (see Figure 4). An external acceleration will displace the mass from its rest position. The magnitude of this displacement is proportional to the magnitude of the acceleration and inversely proportional to the stiffness of the spring structures.

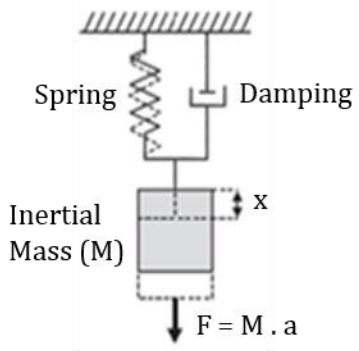

Figure 4: Accelerometer model.

The principle for converting the displacement of the proof mass into an electrical signal can be fulfilled by different mechanisms, such as capacitive, piezoresistive, piezoelectric, optical or tunnelling current (Maluf, 2004). The most commonly used and versatile operation mode is the differential capacitive measurement. Measuring capacitance changes caused by displacement provides a large output signal, good steady-state response, and better sensitivity due to low noise performance. The main drawback is that capacitive sensors are susceptible to electromagnetic fields. The principle of operation is based on two parallel capacitor plates that are fixed while the third one in the middle moves. This movement will increase one capacitance and will decrease the other. Differential capacitors provide a signal that is zero at the balance point and carries a sign which indicates the direction of motion.

Accelerometers are gravity sensitive. This means that their orientation affects their output. If they are oriented with the active element perpendicular to the axis of gravity, they will register the effect of gravity on the mass mounted on the beam and so give an accelerometer reading of 9.81 m/s^2 or 1 g. If the accelerometer is rotated 90º, the axis of gravity will run parallel to the mass and so it will not deform the beam on which it is mounted. In this case the accelerometer will give an output reading of 0 g. The accelerometer output then

represents the vector sum of the gravity (static) and kinematic (dynamic) accelerations of self-movement.

Micro-machined gyroscopes usually rely on a mechanical structure that is driven into resonance and excites a secondary oscillation in either the same structure or in a second one, due to the *Coriolis* force. The amplitude of this secondary oscillation is directly proportional to the angular rate signal to be measured. The *Coriolis* force is a virtual force that depends on the inertial frame of the observer. The effect of this force is the apparent deflection of moving objects from a straight path when they are viewed from a rotating frame reference (Maluf, 2004).

A model of a micro-machined gyroscope is illustrated in Figure 5. The proof mass is excited to oscillate along the *x*-axis with a constant amplitude and frequency. Rotation about the *z*-axis couples energy into an oscillation along the *y*-axis whose amplitude is proportional to the rotational velocity. Any motion along the sense axis is measured and a force is applied to counterbalance this sense motion. The magnitude of the required force is then a measure of the angular rate signal. Thus, the *Coriolis* force induces a motion in a third direction, perpendicular to both the direction of rotation and the driven motion (Lapadatu, 2009).

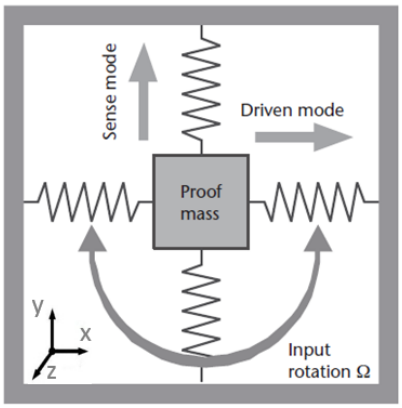

Figure 5: Gyroscope model.

There are some problems concerning the fabrication of those structures. For example, the amplitude of the *Coriolis* is very small which results in a small displacement. It is also very difficult to design structures for an exact resonant frequency, and since these structures need to be continuously excited the power consumption is usually higher than other micro-machined devices. Also, gyroscopes can present some drift problems, which means they do not return to zero-rate when rotation stops. (Baluta, 2009) Nevertheless, micro-machined gyroscopes are still one of the best commercially available solutions for angular

rate measurements and combined with other inertial sensors present a viable solution to monitor displacement rates.

These inertial sensors detect and measure motion, with minimal power and size, and are valuable to nearly any application where movement is involved. Table 2 outlines some of the basic pertinent healthcare and sports applications by motion type.

Table 2: Relevant healthcare and sports applications of MEMS-based inertial sensors.

	Motion Type				
	Acceleration/ Position	*Tilt*	*Angular Rate/ Angle*	*Vibration*	*Sensor Fusion*
Healthcare	CPR Assist	Bed-patient Positioning	Scanning Instruments	Tremor Control	Precision Surgical Navigation
	Activity Monitors	Blood Pressure Monitors	Basic Surgical Tools		Remote Diagnostics
	Biofeedback Monitors	Imaging Equipment	Prosthetics		Rehabilitation Assistance
					Gait Analysis
Sports	Activity Monitors	Control Applications	Rate Monitors	Referee Assistance	Biofeedback
	Equipment Accessories		Pedometers		Performance Improvement
					Injury Prevention

Table 3 presents a comparison between some popular MEMS-based accelerometers, gyroscopes and inertial measurement units currently used as wearable monitoring sensors.

Table 3: Comparison between popular accelerometers, gyroscopes and inertial measurement units.

		Manufacturer	Sensing Axes	Output Type	Dynamic Range	Sensitivity	Operating Voltage	Current Consumption
Accelerometers	MMA7361	Freescale Semiconductor	3-axis	Analog	± 1.5/6g	from 200 mV/g	2.2V – 3.6V	400 µA
	BMA180	Bosch	3-axis	Digital (4-Wire, SPI, I2C)	±1/1.5/2/3/4/ 8/16 g	from 512 LSB/g	1.6V – 3.6V	650 µA
	ADXL345	Analog Devices	3-axis	Digital (SPI, I2C)	± 2/4/8/16 g	from 256 LSB/g	1.7V – 2.75V	145 µA
Gyroscopes	IDG300	InvenSense	2-axis (x,y)	Analog	± 500 º/s	2 mV/º/s	3V – 3.3V	Not Specified
	ITG3200	InvenSense	3-axis	Digital (I2C)	± 2000 º/s	14.375 LSB/º/s	2.1V – 3.6V	6.5 mA
	ADXRS450	Analog Devices	3-axis	Digital (SPI)	± 300 º/s	80 LSB/º/s	3V – 5.25V	6 mA
Sensor Fusion	SCC1300	muRata	3-axis acc 3-axis gyro	Digital (SPI)	± 6g ± 300 º/s	650 LSB/g 18 LSB/º/s	3V – 3.6V	10 mA
	MPU9150	InvenSense	3-axis acc 3-axis gyro 3-axis compass	Digital (I2C)	±2/4/8/16g ±250/500/ 1000/2000 º/s ± 1200 µT	from 2048 LSB/g 16.4 LSB/º/s 0.3 µT/LSB	2.4V – 3.6V	4 mA
	ADIS16300	Analog Devices	3-axis acc 3-axis gyro	Digital (SPI)	± 3g ± 300º/s	0.6 mg/LSB 0.05 º/s/LSB	4.75V – 5.3V	42 mA

2.2. Inertial Systems Concepts

While simple motion detection (linear movement along one axis, for example) is valuable to a number of applications, such as detecting whether an elderly person has fallen, a majority of applications involve multiple types and multiple axes of motion. Being able to capture this complex, multi-dimensional motion can enable new benefits while maintaining accuracy in the most critical of environments.

In many cases, it is necessary to combine multiple sensor types – linear and rotational, for instance – in order to precisely determine the motion an object has experienced. As an example, accelerometers are sensitive to the Earth's gravity, so they can be used to determine inclination angle. As a MEMS accelerometer is rotated through a 1 g field (90º), it is able to translate that motion into an angle representation. However, the accelerometer cannot distinguish static acceleration (gravity) from dynamic acceleration. In the last case, an accelerometer can be combined with a gyroscope and post-processing of both devices can discern the linear acceleration from the tilt, based upon known motion dynamics models. This process of sensor fusion obviously becomes more complex as the system dynamics (number of axes of motion, types, and degrees of freedom of motion) also increases complexity.

The two primary challenges found in any high-performance motion capture implementation are the conversion of raw sensor data to calibrated and stable sensor data, and the translation of precision sensor data into actual position/tracking information, as depicted in Figure 6. Overcoming the first hurdle involves motion calibration, which is based on intimate knowledge of motion dynamics. The second hurdle requires merging an understanding of motion dynamics with a deep knowledge of the peculiarities of the application at hand. Fortunately, many of the principles required for solving these challenges are based on proven approaches from classical industrial navigation problems, including sensor calibration, fusion and processing techniques.

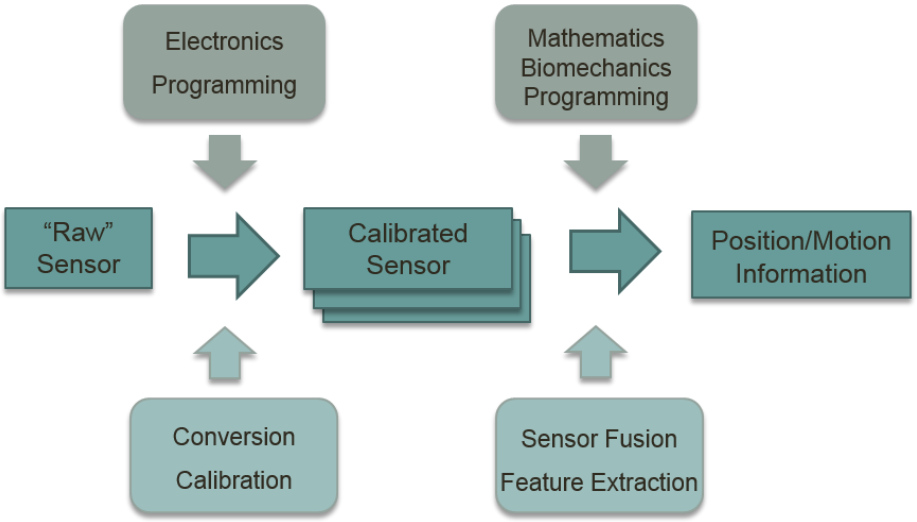

Figure 6: Motion capture implementation steps.

Analysis of accelerometer and gyroscope data to determine position, velocity and attitude, can be derived from inertial navigation systems (INS). In an inertial navigation system the principle is to determine navigation parameters through acceleration and velocity integrations. The first integration provides velocity and the second gives displacement with respect to an initial point. To determine the navigation parameters in a certain frame, the acceleration projections on that frame must be provided. In addition, gyroscopes are needed to reference the sensitive axes of the accelerometers with a certain reference frame. Usually, the algorithm used to perform such operations is called *strapdown inertial navigation system* and uses both information of accelerometers and gyroscopes to estimate position and velocity (Salychev, 2004).

A strapdown navigation system usually contains three accelerometers and three gyroscopes (or three-axis versions of them), which measure the projections of acceleration and angular velocity on their sensitive axes. In order to re-calculate the above projections into the navigation frame, the *direction cosine matrix* (DCM) between the body (*b*) and the navigation (*n*) frame is needed (Titterton, 2007):

$$a^n = C_b^n a^b \quad (1)$$

where a^n and a^b are the acceleration projections in n-frame and b-frame, respectively, and C_b^n is a 3x3 matrix which defines the attitude of the body frame with respect to the n-frame.

The direction cosine matrix, C_b^n, may be calculated from the angular rate measurements provided by the gyroscopes using the following differential equation (Titterton, 2007):

$$\dot{C}_b^n = C_b^n \Omega_{nb}^b \tag{2}$$

where Ω_{nb}^b is the skew symmetric matrix (Titterton, 2007):

$$\Omega_{nb}^b = \begin{bmatrix} 0 & -\omega_z & \omega_y \\ \omega_z & 0 & -\omega_x \\ -\omega_y & \omega_x & 0 \end{bmatrix} \tag{3}$$

where $\omega^b = [\omega_x \quad \omega_y \quad \omega_z]^T$ is the vector which represents the angular rate of the body as measured by the gyroscopes.

The diagram shown in Figure 7 presents the main functions to be implemented within a strapdown inertial system. The processing of the rate measurements to generate body attitude, the resolution of the accelerations into the inertial reference frame, gravity compensation and the integration of the resulting acceleration, are the steps to estimate velocity and position.

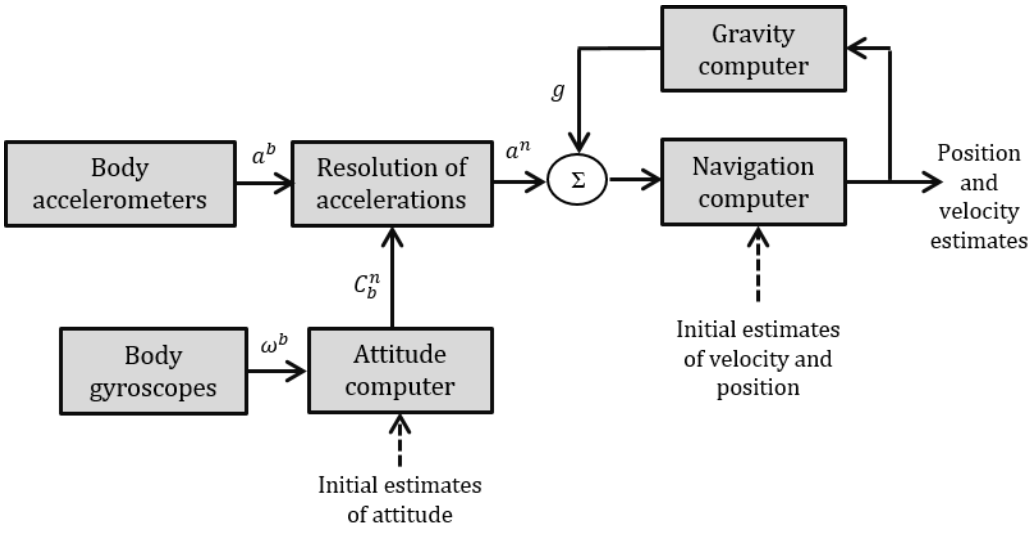

Figure 7: Strapdown inertial navigation system. (Adapted from (Titterton, 2007))

In order to start the computation, the initial coincidence between the accelerometer sensitive axes and the reference frame is needed; this is called alignment of the INS. In a strapdown INS this procedure is done to estimate the initial value of the direction cosine matrix. DCM is usually computed through the Euler angles. These angles are three independent quantities able of defining the position of one coordinate frame with respect to another. Let's coincide $x_n\, y_n\, z_n$ coordinate frame with $x_b\, y_b\, z_b$ coordinate frame and consider three right-handed rotations on the Euler angles (see Figure 8):

- yaw (ψ), rotation about the z-axis;
- roll (φ), rotation about the x-axis;
- pitch (θ), rotation about the y-axis.

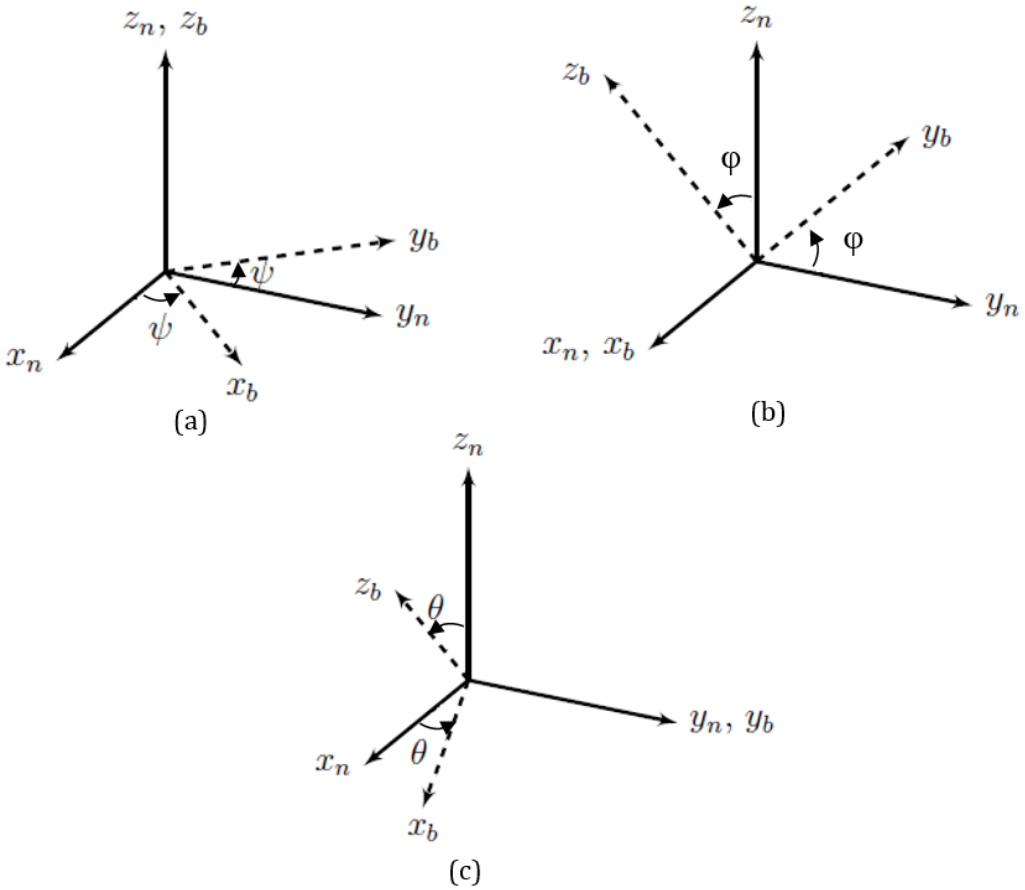

Figure 8: Coordinate transformation from navigation frame to body frame. (a) Yaw – rotation about the z-axis; (b) Roll - rotation about the x-axis and (c) Pitch - rotation about the y-axis.

The first rotation is made about the z-axis by angle ψ. A position vector in the new system can be expressed in terms of the original coordinates as:

$$\begin{aligned} x_b &= x_n \cos\psi + y_n \sin\psi \\ y_b &= -x_n \sin\psi + y_n \cos\psi \\ z_b &= z_n \end{aligned} \tag{4}$$

Or, in matrix form:

$$\begin{bmatrix} x_b \\ y_b \\ z_b \end{bmatrix} = \begin{bmatrix} \cos\psi & \sin\psi & 0 \\ -\sin\psi & \cos\psi & 0 \\ 0 & 0 & 1 \end{bmatrix} \begin{bmatrix} x_n \\ y_n \\ z_n \end{bmatrix} = C_1 \begin{bmatrix} x_n \\ y_n \\ z_n \end{bmatrix} \tag{5}$$

Similarly, the transformation due to second rotation, around x-axis can be described as:

$$\begin{bmatrix} x_b \\ y_b \\ z_b \end{bmatrix} = \begin{bmatrix} 1 & 0 & 0 \\ 0 & \cos\varphi & \sin\varphi \\ 0 & -\sin\varphi & \cos\varphi \end{bmatrix} \begin{bmatrix} x_n \\ y_n \\ z_n \end{bmatrix} = C_2 \begin{bmatrix} x_n \\ y_n \\ z_n \end{bmatrix} \tag{6}$$

And finally, third rotation about the y-axis has a transformation in the form:

$$\begin{bmatrix} x_b \\ y_b \\ z_b \end{bmatrix} = \begin{bmatrix} \cos\theta & 0 & -\sin\theta \\ 0 & 1 & 0 \\ \sin\theta & 0 & \cos\theta \end{bmatrix} \begin{bmatrix} x_n \\ y_n \\ z_n \end{bmatrix} = C_3 \begin{bmatrix} x_n \\ y_n \\ z_n \end{bmatrix} \tag{7}$$

The total transformation matrix can be defined using multiplication of C_3, C_2 and C_1 matrices. Thus the transformation due to all three rotations, from navigation frame to body frame is given by:

$$\begin{bmatrix} x_b \\ y_b \\ z_b \end{bmatrix} = C_3 C_2 C_1 \begin{bmatrix} x_n \\ y_n \\ z_n \end{bmatrix} = C_n^b \begin{bmatrix} x_n \\ y_n \\ z_n \end{bmatrix} =$$

$$\begin{bmatrix} \cos\theta\cos\psi - \sin\varphi\sin\theta\sin\psi & \cos\theta\sin\psi + \sin\varphi\sin\theta\cos\psi & -\cos\varphi\sin\theta \\ -\cos\varphi\sin\psi & \cos\varphi\cos\psi & \sin\varphi \\ \sin\theta\cos\psi + \sin\varphi\cos\theta\sin\psi & \sin\theta\sin\psi - \sin\varphi\cos\theta\cos\psi & \cos\varphi\cos\theta \end{bmatrix} \begin{bmatrix} x_n \\ y_n \\ z_n \end{bmatrix} \tag{8}$$

There is no standardized definition of the Euler angles, thus if the order of the rotations is interchanged, different direction cosine matrix is defined. So, it is important to define right at the beginning the rotation order.

The direction cosine matrix is an orthogonal matrix, which means $C^{-1}=C^T$. This is an important property since it makes easy the transformation from one coordinate system to another and backwards (Titterton, 2007). Following the example above, the transformation matrix from body frame to navigation frame is given by:

$$C_b^n = C_n^{b^T} = C_1^T C_2^T C_3^T \tag{9}$$

After the coordinate transformation, the position and velocity of the body can be estimated.

2.3. Wearable Applications of Inertial Systems

A very promising frontier for wearable and reliable motion capture systems is based on inertial measurement units (IMUs) that can be used virtually anywhere. In the last few years, the use of MEMS-based inertial sensors has noticed an exponential growth, especially due to the perception of their potential compared with traditional monitoring systems, such as video-based systems, and more competitive costs. From simple accelerometers and gyroscopes modules to complete sensor networks, IMUs have become widely accepted for the analysis of human motion.

Commercial systems have also recently been introduced, such as Xsens modules[1], Biosyn FAB (Functional Assessment of Biomechanics)[2], or the Animazoo series[3] (Figure 9). The main limitations of commercial systems are related to the size and weight of the single module. In addition, these solutions require a long calibration routine, which may not be possible for individuals who have difficulty moving. Commercial systems, although providing a high level of performance in terms of accuracy, still have only a niche market due to the high cost, particularly for multiple module systems. Many research centers have developed prototypes that have sought to reduce the main limitations of commercial systems, particularly in terms of size and weight (Pansiot et al., 2008; Zhou, Stone, Hu, & Harris, 2008). Other researchers have tried to customize the design to specific applications by integrating, for example, the sensors in shoes (Morris, 2004; Scapellato, Cavallo, Martelloni, & Sabatini, 2005), or by developing miniaturized solutions for specific joints (Brigante, Abbate, Basile, Faulisi, & Sessa, 2011; Minami et al., 2010).

[1] http://www.xsens.com/
[2] http://www.biosynsystems.net/
[3] http://www.animazoo.com/

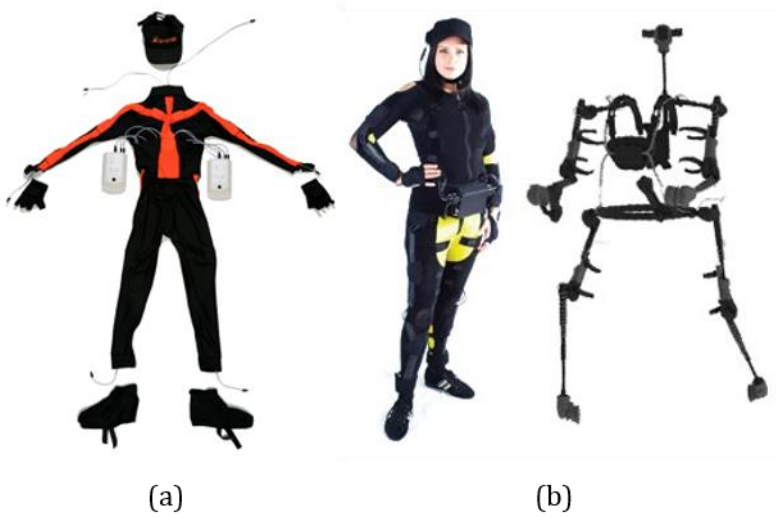

Figure 9: Commercial inertial monitoring systems: (a) Xsens and (b) Animazoo complete suits.

In the gaming industry, the market trend is toward active gaming platforms, where a smart wearable motion capture suite could expand the capability of this type of game and open total virtual reality scenarios, at the edge of the augmented reality. Efforts are being made in order to improve inertial sensing of specific human segments, such as head pitch and roll angles (Keir, Hann, Chase, & Chen, 2007) or hands movement (Oh et al., 2004), in a highly dynamic environment using minimal numbers of low-cost sensors. In parallel, improved algorithms are appearing that compensate for indoor positioning errors, which is one of the major challenges of inertial tracking for augmented reality applications (Esfandyari et al., 2011; Esfandyari, Mascotto, & Xu, 2010).

In medical applications one of the major topics of interest for researches is the use of inertial measurement units for gait analysis. Gait analysis is the study of the biomechanics of human movement aimed at quantifying factors governing the functionality of the lower extremities. This is crucial for the detection of gait disorders, identification of balance factors, and assessment of clinical gait interventions and rehabilitation programs.

Many of the existing works in the field utilize accelerometers as inclinometers to measure knee angles. Often, the operational space is simplified, and movements are only examined in a 2D sagittal plane (Bamberg, Benbasat, Scarborough, Krebs, & Paradiso, 2008). For slow motions, the acceleration contributed by the subject's motion is assumed to be negligible compared to gravity. Trigonometry is applied to the acceleration signal to obtain the tilt of the accelerometer. Bergmann et al. (2010) used accelerometers in this manner to obtain the tilt of the knee and ankle. They showed that this algorithm produces comparable accuracy to joint angles determined by a motion capture system (Figure 10). However, when the motion is fast, it is difficult to determine which component of the acceleration is caused by motion, and which is caused by gravity.

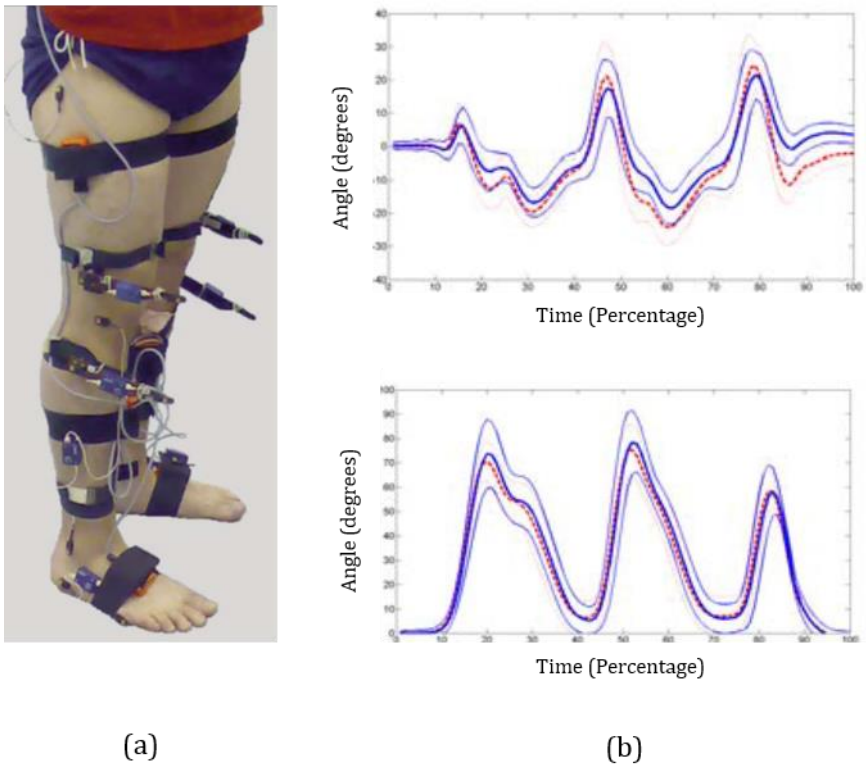

Figure 10: Gait analysis through IMUs: (a) experimental setup with IMUs attached to subject joints and (b) mean angles and standard deviation of ankle (top) and knee (bottom) in sagittal plane acquired with IMUs (red) and video-based system (blue). (Adapted from (Bergmann et al., 2010))

Other researches use inertial measurement units in gait analysis to differentiate between typical and pathological gait patterns (Lai, Begg, & Palaniswami, 2009; Sant'Anna, Wickstro, x, & m, 2009). Clinical gait disorders may appear from different sources, such as Parkinson's disease (Shancang, Jue, & Xinheng, 2010; Titterton, 2007), Huntington's disease (Dalton et al., 2013) or stroke (Mizuike, Ohgi, & Morita, 2009; Yang, Zhang, Novak, Brouwer, & Li, 2013), and IMUs have proven to be a good alternative to conventional video-based systems for detecting abnormal gait parameters.

Also for healthcare purposes, tracking systems are being used in order to build remote monitoring networks for patients and the elderly in hospitals and in their own homes (Bae & Tomizuka, 2013). In the field of rehabilitation, inertial measurement units can also be used as a complementary tool which can guide physiotherapists in their clinical reasoning process. (Lin & Kulić, 2012; H. R. Silva et al., 2007; Veluvolu & Ang, 2011; Zhou, Hu, & Tao, 2006).

In the field of sports one has noticed an increasing number of commercially available wearable sensors that assist athletes. The most well-known wearable sport systems are probably the heart rate monitors widely used in many sports, either by highly-trained athletes and amateurs, such as the Polar®[4] or the Suunto®[5] products. Performance analysis and enhancement has traditionally been performed in the laboratory where the required instrumentation is available and environmental conditions can be easily controlled. In this environment dynamic characteristics of athletes are assessed using treadmills, rowing and cycling machines and even flumes for swimmers. In general these machines allow for the monitoring of athletes using instrumentation that cannot be used in the training environment but instead requires the athlete to remain quasi-static thus enabling a constant field of view for optical devices and relatively constant proximity for tethered electronic sensors, breath gas analysis, etc. Today however by taking advantage of the advances in inertial sensors it is possible to build instrumentation that is small

[4] Polar, http://www.polar.fi
[5] Suunto, http://www.suunto.com

enough to be unobtrusive for a number of sporting applications (D. A. James, Davey, & Rice, 2004).

2.4. Inertial Measurement Units: WIMU and W2M2

The first inertial measurement unit developed under this thesis was the WIMU – Wearable Inertial Measurement Unit. This unit was firstly intended to analyse swimmers' performance, but its characteristics made it also suitable for other applications rather than sports. Some of the challenges and difficulties experienced with the WIMU led to the development of a more robust inertial unit, called the W2M2 (Wireless Wearable Modular Monitor). This unit is based on a modular approach, which allows the customisation of the device according to the specifications of any particular application.

The design considerations, either hardware and software, and overall functioning of these two inertial units will be presented and discussed in the next sections dedicated to WIMU and W2M2.

2.4.1. WIMU – Wearable Inertial Measurement Unit

The WIMU - Wearable Inertial Measurement Unit - was designed as a MEMS-based wearable device for assessing biomechanical parameters of a swimming athlete. The inertial unit comprises a tri-axial accelerometer for linear acceleration and a bi-axial gyroscope for angular velocity measurements; managed by a microcontroller for signal acquisition and wireless transmission. A picture of the system can be observed in Figure 11.

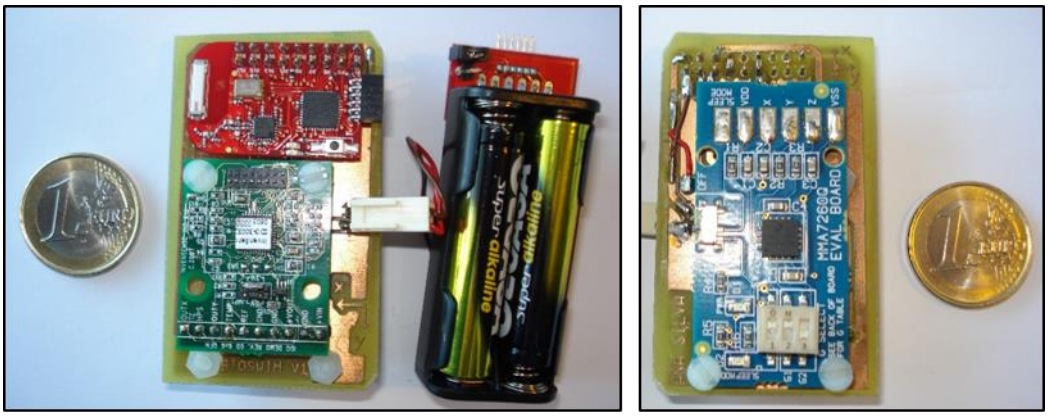

(a) (b)

Figure 11: (a) Top and (b) bottom view of the system.

The mechanical structure of the WIMU consists of a double-sided printed circuit board (PCB) and a battery case. The top side of the PCB comprises the microcontroller with RF transmitter and the gyroscope board while the bottom side contains the accelerometer evaluation board. The WIMU weights approximately 65.6 grams and measures 57x90.5x24 mm. The data collection was achieved at distances of up to 20 meters. Two standard alkaline AA batteries insured the system can operate continuously during approximately one day without any noticeable degradation in performance or signal intensity loss.

Commercially available evaluations boards were used to integrate the MEMS sensors into the WIMU. The accelerometer evaluation board consists of a small setup intended for evaluating the MMA7260QT Freescale Semiconductor accelerometer (see Figure 12 (a)), adequate for fast prototype developing without the need of custom printed circuit boards designs. It also provides means for understanding the best mounting position and location of this accelerometer.

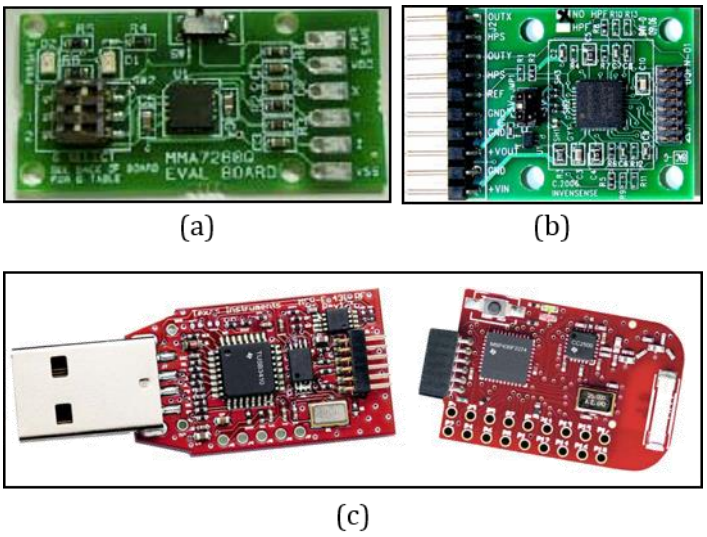

Figure 12: WIMU components: (a) MMA7260QT accelerometer board; (b) IDG-300 gyroscope board and (c) eZ430-RF2500 debugging board (left) and target board (right).

The MMA7260QT is a capacitive micromachined accelerometer with on-chip signal conditioning, temperature compensation and g-select pins which allow the selection of four different dynamic ranges (Table 4) ("±1.5g - 6g Three Axis Low-g Micromachined Accelerometer ", 2008).

Table 4: MMA7260QT accelerometer dynamic ranges.

Dynamic Range	Sensitivity
± 1.5 g	800 mV/g
± 2 g	600 mV/g
± 4 g	300 mV/g
± 6 g	200 mV/g

Similarly, the IDG-300 Invensense gyroscope can be found integrated in an evaluation board (see Figure 12 (b)) along with the components necessary for application-ready functionality. The IDG-300 gyro uses two sensor elements with a vibrating dual-mass bulk silicon configuration that sense the rate of rotation about the X- and Y-axis ("IDG-300 Dual-Axis Gyroscope Evaluation Board Specification ", 2007).

In order to integrate both the accelerometer and the gyroscope into the inertial unit, the Texas Instrument microcontroller based board, eZ430-RF2500, was selected from the many commercially available devices. The eZ430-RF2500 uses the MSP430F2274 microcontroller which combines 200 Ksps 10-bit analog-to-digital converter (ADC) with the CC2500 multi-channel radio-frequency (RF) transceiver, designed for low-power wireless applications. This board offers a combination of hardware and software appropriate for fast prototyping of wireless projects, while offering low-power consumption. The development tool includes two target boards and a USB debugging interface (see Figure 12 (c)). The eZ430-RF2500 uses the IAR Embedded Workbench Integrated Development Environment (IDE) to write, download and debug an application.

The eZ430-RF2500 can readily use the SimpliciTI wireless communication protocol, a low-power RF (2.4 GHz) protocol aimed for simple and small RF networks (proprietary of Texas Instruments). The SimpliciTI protocol claims to use a minimal set of microcontroller requirements, which in theory lowers the associated system cost. In this case, the network topology was configured so that the WIMU behaved as an end device (ED), transmitting data packets to a remote or base station referred to as application point (AP). The protocol permits multiple end devices, therefore multiple WIMUs can be allocated at different body segments, in a truly body sensor network scheme. The WIMU architecture can be seen on Figure 13.

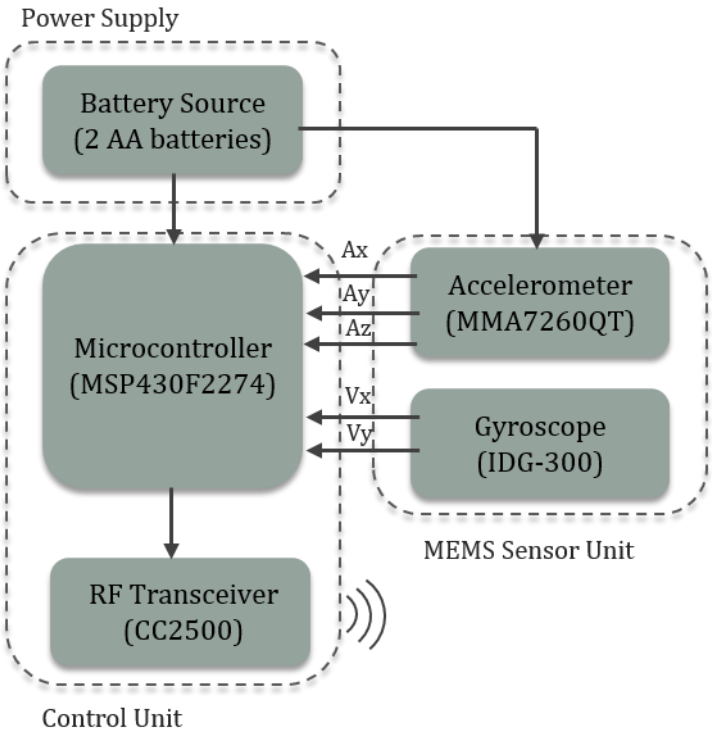

Figure 13: WIMU architecture.

On the WIMU side, minimal pre-processing of the gathered data occurs, just enough to prepare the data for adequate transmission. The microcontroller embedded code performs no complex algorithms: the acceleration and angular velocity signals are acquired and converted sequentially by the 10-bit ADC integrated in the MSP430F2274 micro-controller at a sampling rate of approximately 50 Ksps. The ADC is kept in a continuous loop, converting sequentially all sensor inputs. A simple broadcasting scheme was used for the data gathering: the WIMU acquires and transmits while the receiver station behaves unique as a listener. Although this strategy introduces reduced timing errors and is not applicable for faster transmission rates or for multi-location sensors synchronization, it proved to be effective during the experimental acquisitions stages, providing a modest rate of approximately 7 packets/sec. Additional data processing operations at the WIMU level were left for post-processing analysis, in order to alleviate microcontroller resources and speed up the communication process.

Figure 14 shows the flowchart of the application developed for the AP, i.e., the remote base station. The first thing the AP does is to initialize both the communication between the MSP430 and the CC2500 radio and the LEDs on the board that are to be used. After initialization, a random 4-byte address is created and written in flash memory for reuse on system reset.

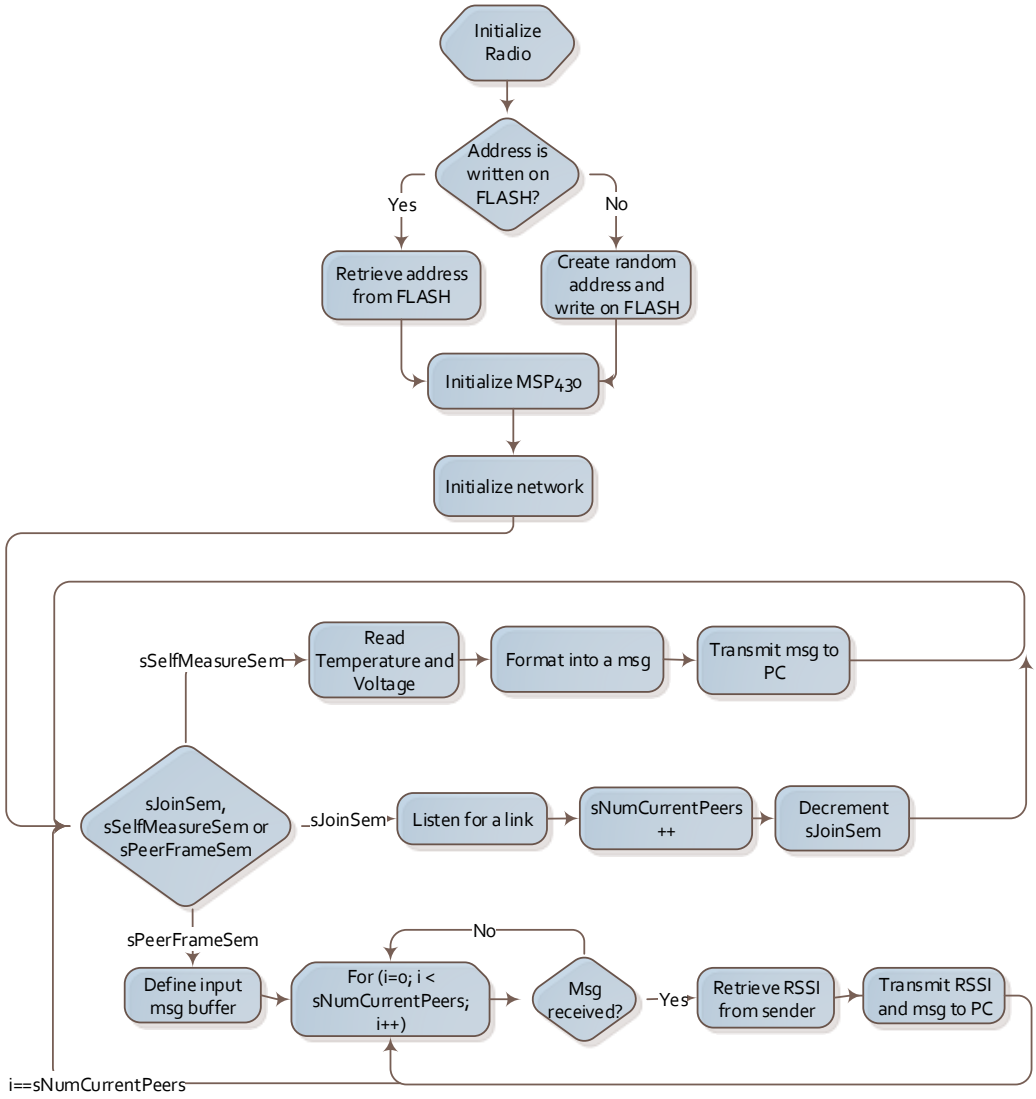

Figure 14: Code flowchart for the Application Point (remote station).

The MSP430 is then initialized: the main clock is set to run at 8 MHz and the UART (Universal Asynchronous Receiver Transmitter) is initialized to communicate with the PC COM port with Baud Rate of 9600 bits/second. Once

the hardware is initialize, the AP enters in a while loop waiting for three different events to occur. The events are identified by three semaphores:

- *sJoinSem*: this semaphore is set when an ED request a network join. This is actually a side effect of an ED initialization procedure. On a successful link creation, the sJoinSem increases the number of devices that the AP recognizes as part of the network;
- *sPeerFrameSem*: this semaphore is incremented every time the AP receives a message from an ED. In this case, the AP first defines a message buffer to store the incoming frame and then searches for messages until it has processed all waiting frames. The messages are formatted containing the sensors data, the ED identification (its address) and the Received Signal Strength Indicator (RSSI) value, and are transmitted to the PC via COM Port;
- *sSelfMeasureSem*: it is an AP specific semaphore that is set at a defined time interval and executes a particular routine. This routine uses the temperature sensor integrated in the ADC to measure self-temperature and transmits it to the PC.

The ED (sensing node) code flowchart is depicted in Figure 15. The initialization procedure is similar to the one AP uses. Once ED's hardware is initialized, a join is requested and the link to the AP is created. The ED enters then in a loop dedicated for converting sensors data and transmits messages to the AP. All the five sensor inputs (three accelerations, Ax, Ay and Az, and two angular velocities, Vx and Vy) are acquired and converted sequentially. After correct conversion an ADC flag is triggered indicating the end of conversion. The time-stamp is then retrieved from TIMER A and all the data is ready to be formatted into a message and to be transmitted to the AP. The complete microcontroller code either for the AP and ED is found in Appendix A.

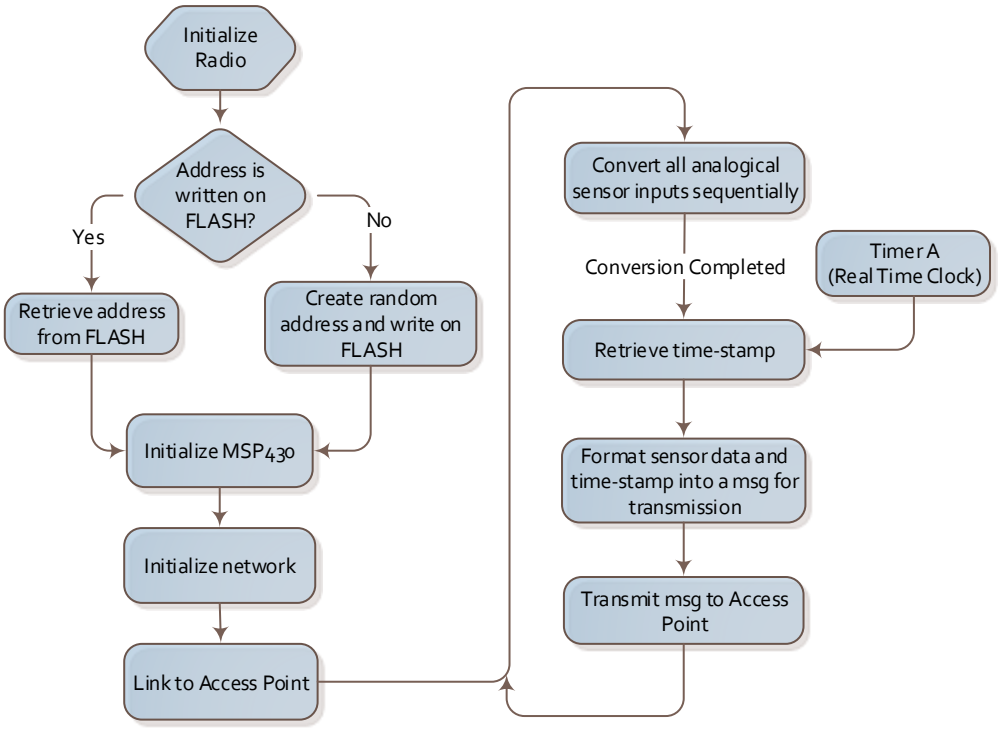

Figure 15: Code flowchart for the End Device (sensor node).

A custom software application for the acquisition, processing and visualisation of the sensor packets coming from the WIMU was developed using National Instruments´ LabVIEW platform for the computer interface. The programing was based on a single state-machine architecture, which allows the program to change the way it executes based on user inputs/actions and results of the application, i.e., it responds intelligently to a stimulus. A diagram of the global software architecture is shown in Figure 16.

The LabVIEW's general user interfaces (GUI) for the configuration stage and data visualisation are shown in Figure 17 and Figure 18, respectively.

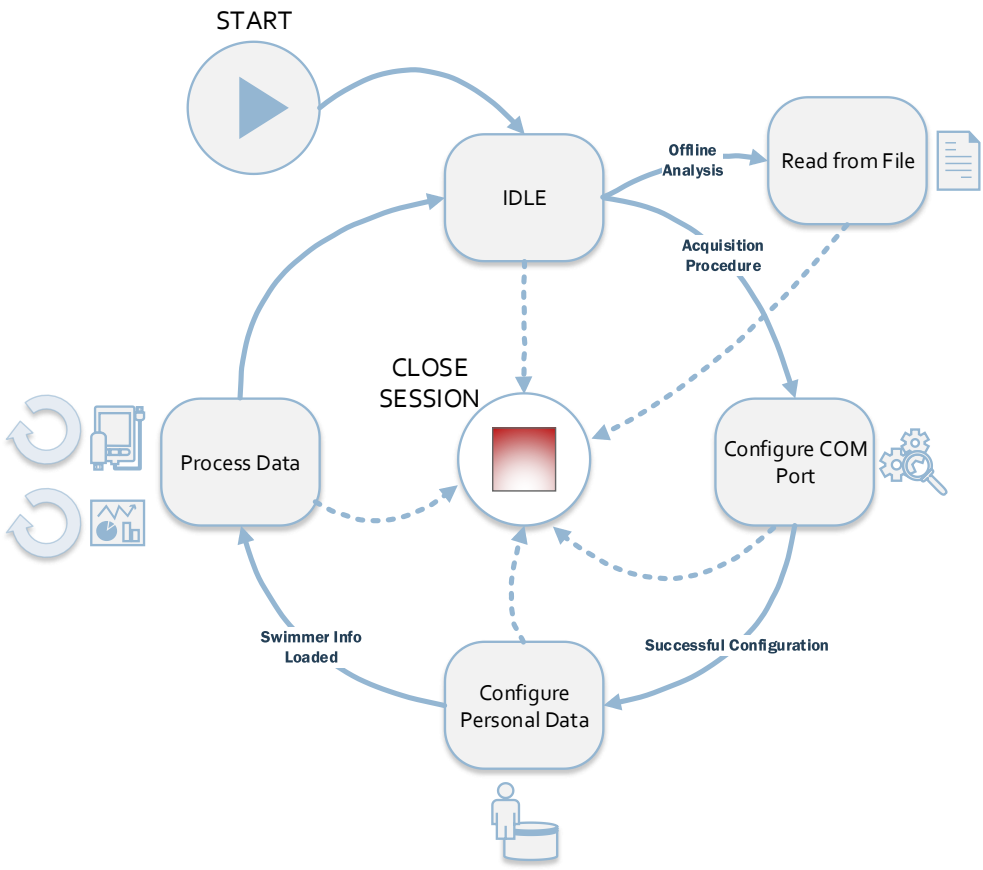

Figure 16: Global diagram of the LabVIEW's program for managing WIMU acquisitions.

The user can either start an experimental acquisition or perform an offline analysis by reading saved data from a previous measurement. The acquisition routine starts with COM port parameters configuration and swimmer's personal information retrieval (the application allows this information to be store in a database). During the acquisition itself, the program enters a producer/consumer loop, which enhances data sharing between loops running at different rates. The data produced in one loop can be buffered for posterior processing in the consumer loop by creating queues, ensuring that no message received from the WIMU is lost during the processing stage. The consumer loop is responsible for extracting data from the sensor packet, convert it to a proper format and display it in real-time graphs.

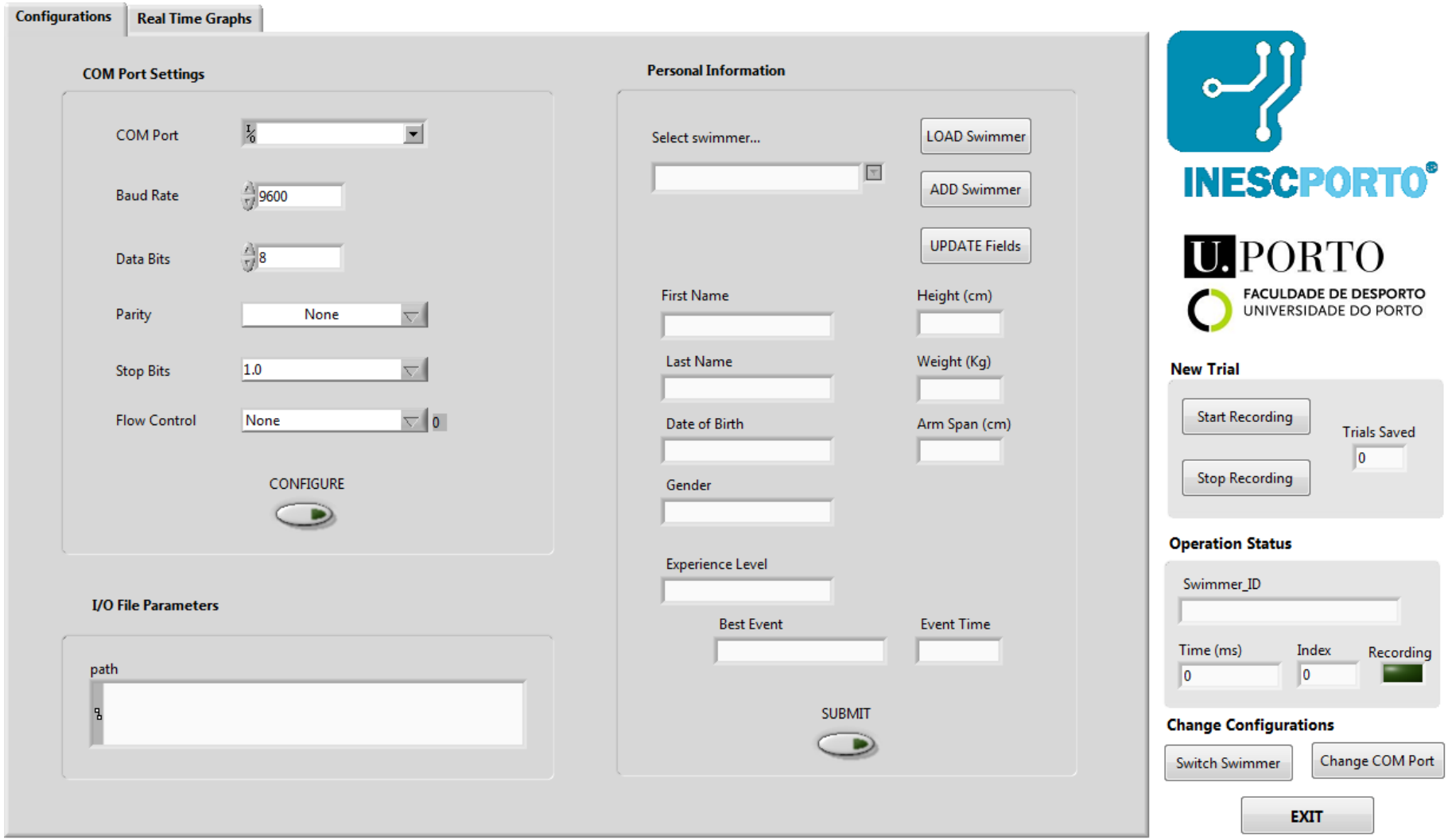

Figure 17: LabVIEW GUI for COM Port configuration and swimmer´s personal data insertion.

Figure 18: LabVIEW GUI with real-time graphs of the captured data.

The WIMU was firstly intended for swimming performance analysis. Nonetheless, due to its architecture, small size and weight it can be placed in different parts of the human body and used for a variety of applications. Two examples of data collected at different body segments, namely at right frontal leg and lower-back, during walking is presented in Figure 19 (a) and (b), respectively.

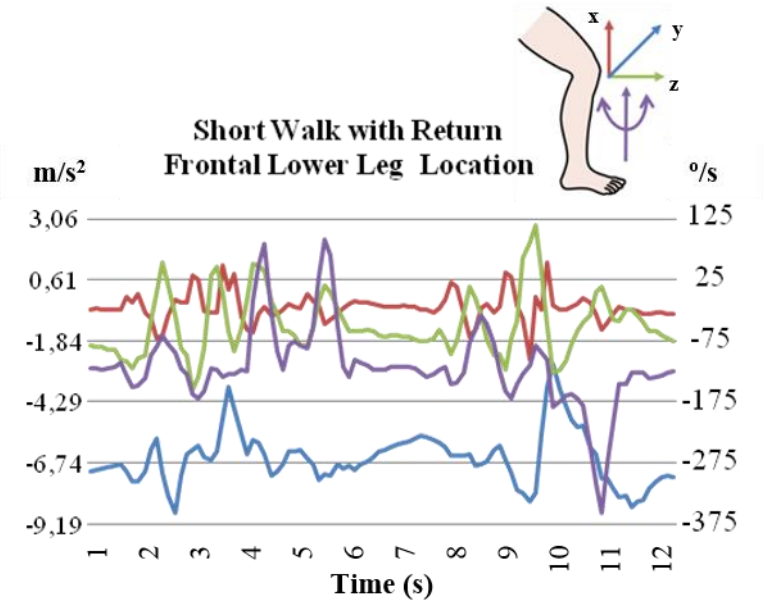

(a)

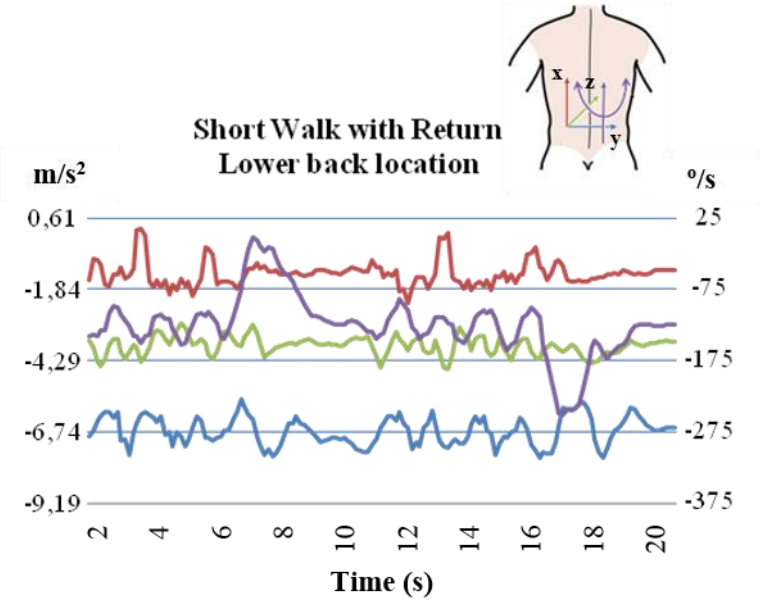

(b)

Figure 19: Walking and return with WIMU located at (a) right front lower leg and (b) lower back.

The X-axis can be considered vertical and together with the Y axis forms the frontal plane of the subject; while the Z-axis points forward, for the lower back location (same as for the lower leg case), with respect to the direction of movement.. Although the data does not produce the traditional analysis graphs, such as for gait analysis, they do provide insight in the local and global actions and reactions of the site were the WIMU was located.

2.4.2. W2M2 – Wireless Wearable Modular Monitor

Following the initial tests and acquisitions with the WIMU, a new simple wearable monitoring device named W2M2 – Wireless Wearable Modular Monitoring, was design and implemented for inertial data capturing and to overcome some of the gaps introduced by the first inertial measurement unit.

Similar to WIMU, this device was based on commercially available components that could be assembled in a fast manner, without extensive knowledge of electronics. The system is based on a modular approach which means different sensor modules can be added to the main component (control unit) according to the application specifications. By default, the W2M2 is composed by a main control unit (MCU) with an accelerometer and different sensor modules connected through I2C, namely an accelerometer board (Acc Board), a combined gyroscope and accelerometer board (COMBO Board), and a magnetometer board, as seen on Figure 20. The MCU unit weights 77 grams and measures 9 x 5.8 x 2.3 cm; the sensor boards are encased in 5.5 x 3 x 2.5 cm standard project boxes which weight 16 grams each.

Figure 20: Component view of W2M2.

The MCU's main component, Arduino FIO[6], is accessible at low-cost and can be used with a reduced learning curve. Arduino is an open-source electronics prototyping platform based on flexible, easy-to-use hardware and software and proved to be an extremely powerful tool to create devices for a numerous type of applications. The Arduino Fio is a microcontroller board based on the ATmega328P and runs at 3.3 V and 8 MHz. It has 14 digital input/output pins (of which 6 can be used as PWM outputs), 8 analog inputs and reset button, among other features. It has connections for a lithium polymer battery and includes a charge circuit over USB. The Arduino Fio is intended for wireless applications since an XBee[7] socket is available on the top of the board and a large number of open-source resources are available to easily integrate the wireless communication with the microcontroller. XBee devices are a series of embedded RF modules based on ZigBee communication protocol. The technology defined by the ZigBee specification is intended to be simpler and less expensive than other wireless personal area networks (WPAN), such as Bluetooth or Wi-Fi. The XBee modules operate within the 2.4 GHz frequency band and ensure serial data rates between 1200 and 250 Kbps. A retry and acknowledgment based approaches guarantee a reliable packet delivery. The

[6] http://www.arduino.cc/
[7] http://www.digi.com/xbee/

W2M2 unit can capture data at a frequency ranging from approximately 100 Hz to 500 Hz, depending on which modules are connected to the MCU.

For the acquisitions made under this thesis research, namely for rehabilitation purposes, two Analog Devices ADXL345 3-axis accelerometer break-out boards were used for acceleration detection. In addition, a combined accelerometer (ADXL345) plus gyroscope (InvenSense ITG-3200) board and the InvenSense MPU-6050 breakout board were used as sensing nodes. The MPU-6050 combines a 3-axis gyroscope and a 3-axis accelerometer on the same silicon die together with an onboard Digital Motion Processor™ capable of processing motion fusion algorithms. In order to sense touch (to indicate start of movement, for instance) the Freescale Semiconductor MPR121 capacitive sensor was used. This chip can control up to twelve individual electrodes. The complete system architecture can be seen in Figure 21.

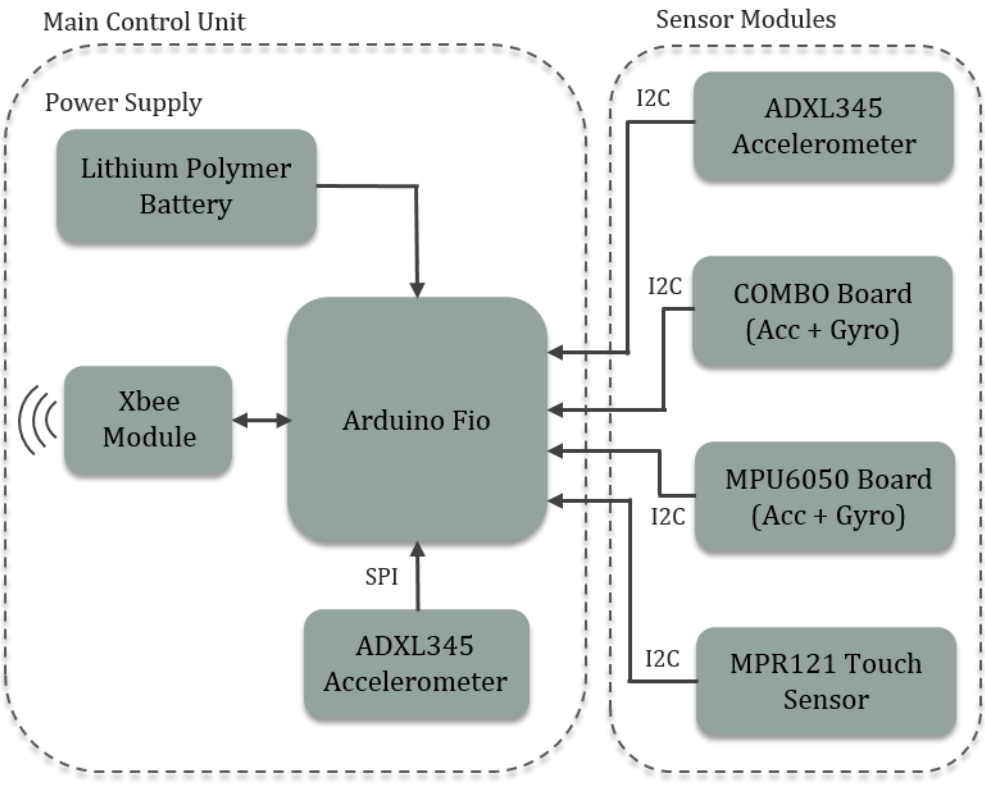

Figure 21: W2M2 architecture.

The sensors on each module of the W2M2 device were properly calibrated in order to compensate for alignment errors during the assembling process. To avoid misinterpretations, the ADXL345 accelerometer present in the main control unit was designated simply as MCU Board, whereas the same sensor which was added as a module to the system was designated as Acc Board.

The original factory calibration for the gyroscopes was taken as the scaling factor (S) to determine angular rate from the anlog-to-digital converter (ADC) output. In addition to this parameter, a zero-offset value was calculated during the experiments. The scaling factor S varies between sensors and different configurations of a single sensor, since:

$$S = \frac{2^n}{r} \tag{10}$$

where, n is the ADC resolution in bits and r represents the dynamic range of the sensor.

Therefore, the angular velocity for each channel in units of degrees per second (º/s) can be obtained using the following equation:

$$\omega = \frac{x_{ADC}}{S} + O \tag{11}$$

where ω is the effective angular rate, x_{ADC} and O are the ADC integer output value and offset, respectively, and S is the sensor scaling factor.

The zero-offset parameter was estimated by reading ADC outputs in a stationary condition. The scaling factors and offsets values for each gyroscope board utilized in this project are presented in Table 5.

Table 5: Scaling factors and zero-offset values for each module's gyroscope.

	Scaling Factor (S)	**Zero-Offset (º/s)**		
		x-channel	*y-channel*	*z-channel*
COMBO Board	131.072	-43	11	12
MPU Board	16.384	475	55	201

The factory accelerometer calibration however can become less accurate once the accelerometer is soldered onto a circuit board, either due to misalignments and thermal stress during soldering (Pedley, 2013). Therefore, a recalibration procedure might be necessary to compensate for such errors.

The standard model used for calibration of a digital accelerometer relates the calibrated accelerometer output *SAcc* (in units of bit counts) to the outputs of the internal ADC using a simple linear model with a total of six parameters, comprising new three-channel gains S'_x, S'_y and S'_z and three zero-g offsets O'_x, O'_y and O'_z (Pedley, 2013):

$$SAcc = S \begin{bmatrix} Acc_x \\ Acc_y \\ Acc_z \end{bmatrix} \Rightarrow \begin{bmatrix} S'_x & 0 & 0 \\ 0 & S'_y & 0 \\ 0 & 0 & S'_z \end{bmatrix} \begin{bmatrix} x_{ADC} \\ y_{ADC} \\ z_{ADC} \end{bmatrix} + \begin{bmatrix} O'_x \\ O'_y \\ O'_z \end{bmatrix} \quad (12)$$

As mentioned before, the scaling factor differs from sensor; for a particular case of an accelerometer operating in a ±2 g full-scale with a 14-bits resolution ADC, $S = 4096$.

A minimum of two-measurement orientations (in opposite directions) for each channel, giving a total of six measured data points, are required to solve Equation 12. A simple approach to perform the measurements is to have the circuit boards on a structure with faces at right angles to each other and make the six measurements with the structure aligned on its top (Position 1), bottom (Position 2), front (Position 3), back (Position 4), left (Position 5) and right (Position 6) faces (see Figure 22). This leads to *1 g* and *-1 g* in each channel and zero in the other channels, as presented in Table 6.

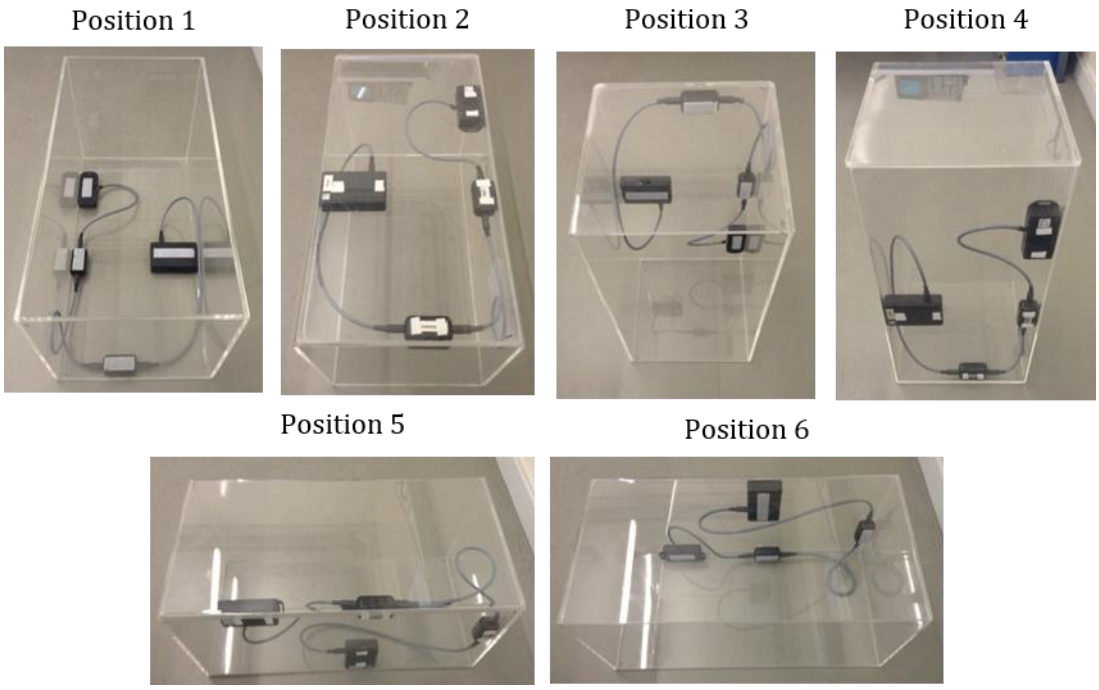

Figure 22: Experimental procedure for the six-parameter calibration.

Table 6: Acceleration values for each accelerometers' channels for the six positions.

		Position					
		1	*2*	*3*	*4*	*5*	*6*
MCU Board	X	0	0	0	0	+1 g	-1 g
	Y	0	0	+1 g	-1 g	0	0
	Z	-1 g	+1 g	0	0	0	0
Acc Board	X	0	0	0	0	-1 g	+1 g
	Y	0	0	-1 g	+1 g	0	0
	Z	-1 g	+1 g	0	0	0	0
COMBO Board	X	0	0	0	0	+1 g	-1 g
	Y	0	0	-1 g	+1 g	0	0
	Z	+1 g	-1 g	0	0	0	0
MPU6050 Board	X	0	0	-1 g	+1 g	0	0
	Y	0	0	0	0	+1 g	-1 g
	Z	+1 g	-1 g	0	0	0	0

For the case of the x-channel, if $x_{ADC}[0]$ is the first measurement when aligned for *+1 g* and $x_{ADC}[1]$ is the second measurement when aligned for *-1 g*, then Equation 12 gives:

$$\begin{cases} S = S'_x \, x_{ADC}[0] + O'_x \\ -S = S'_x \, x_{ADC}[1] + O'_x \end{cases} \tag{13}$$

Solving the above equations, the gain and offset for x-channel can be easily obtained:

$$\begin{cases} S'_x = \dfrac{2S}{x_{ADC}[0] - x_{ADC}[1]} \\ O'_x = \dfrac{-S\,(x_{ADC}[0] + x_{ADC}[1])}{x_{ADC}[0] - x_{ADC}[1]} \end{cases} \tag{14}$$

The y and z-channel calibration parameters are similarly given as:

$$\begin{cases} S'_y = \dfrac{2S}{y_{ADC}[0] - y_{ADC}[1]} \\ O'_y = \dfrac{-S\,(y_{ADC}[0] + y_{ADC}[1])}{y_{ADC}[0] - y_{ADC}[1]} \end{cases} \tag{15}$$

$$\begin{cases} S'_z = \dfrac{2S}{z_{ADC}[0] - z_{ADC}[1]} \\ O'_z = \dfrac{-S\,(z_{ADC}[0] + z_{ADC}[1])}{z_{ADC}[0] - z_{ADC}[1]} \end{cases} \tag{16}$$

These six-parameter computed with this method can then be applied to the accelerometer output using Equation 12.

This calibration method was applied for each accelerometer on each board utilized during the experimental acquisitions. The correspondent gains and offsets for each board's accelerometers are presented in Table 7.

Table 7: Gains and offsets for each accelerometer in each board calculated using the six-parameter method.

	Gain, S'			**Offset, O' (bits)**		
	x-channel	*y-channel*	*z-channel*	*x-channel*	*y-channel*	*z-channel*
MCU Board	-29.037	-28.621	-1.018	-3590.203	-3664.015	-3.253
Acc Board	-0.979	-0.968	-1.019	12.691	0.476	-4.887
COMBO Board	-0.981	-0.976	-1.001	1.103	-0.762	-8.767
MPU6050 Board	-1.000	-0.994	0.985	107.742	377.565	516.155

The microcontroller on the Arduino Fio board (MCU board) was programmed using the Arduino programming language (based on Wiring[8]). The control unit is responsible for initializing all modules and communications. Afterwards, the microcontroller enters in an idle mode where it waits for user commands. There are four commands available:

- *Start Acquisition*: this command initiates data sending, by reading all sensor outputs and format sensor packet to be wirelessly transmitted;
- *Stop Acquisition*: the program interrupts data sending and returns to idle mode;
- *Data Format Raw*: the data from sensor outputs is kept in units per bits count;
- *Data Format Scaled*: data from sensors outputs is converted to proper units according to the measure being read.

The Arduino Fio code flowchart is depicted in Figure 23. The complete microcontroller code is found in Appendix A.

[8] http://wiring.org.co/

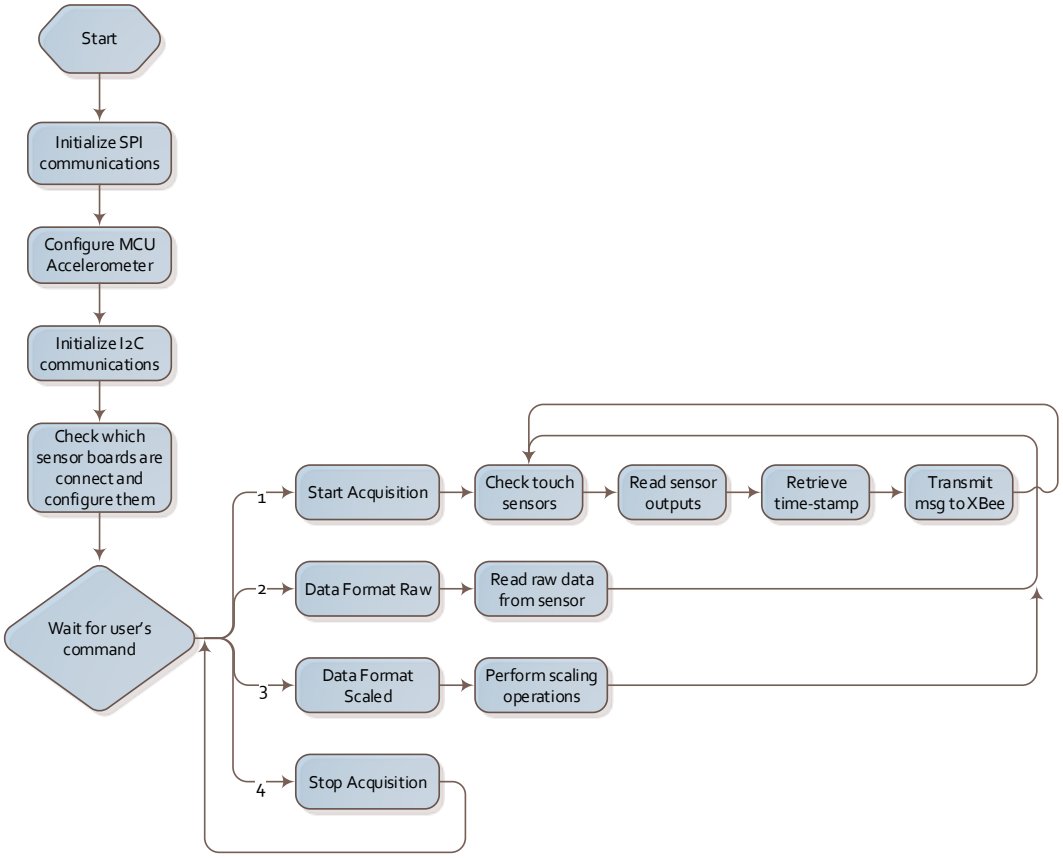

Figure 23: Arduino Fio microcontroller program flowchart.

To handle data coming from the W2M2 a simple and easy-to-use GUI was developed in Processing[9]. Processing is an open-source programming language and integrated development environment (IDE) built for the electronic arts and visual design communities. It uses simplified syntax and graphics programming model, and it has more than one hundred libraries. As mentioned before, the concept behind the W2M2 was to make a functional device where no relevant expertise in electronics and programming is necessary in order to use it and perform acquisitions. This feature is crucial given the potential users of such device, i.e., physicians, patients, athletes or coaches. The user interface developed using Processing was created in line with this principle.

[9] http://processing.org

Figure 24 shows the user interface developed for the W2M2. It allows for hardware configuration, synchronization with video system, storing patient information and data acquisition to file.

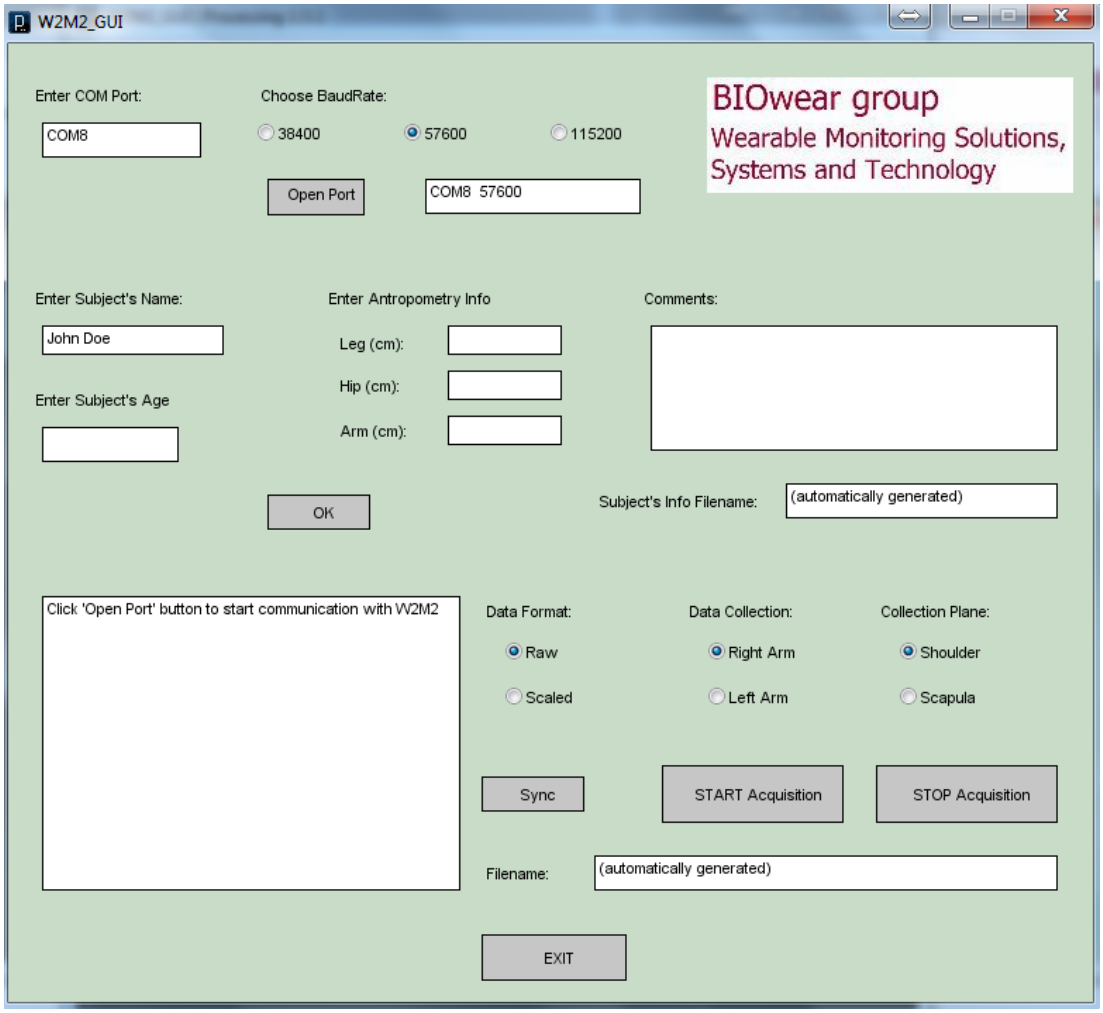

Figure 24: W2M2 GUI developed in Processing.

An example of accelerometry data collected with W2M2 during experiments with post-stroke patients for rehabilitation purposes can be seen in Figure 25. The inertial data illustrates the difference between three independent reach-press-return trials performed by a typical subject (Figure 25 (a)), with no neural nor musculoskeletal pathologies, and a stroke survivor (Figure 25 (b)). The 3-axis accelerometers data was captured at a frequency of approximately 100 Hz, which was then buffered and transmitted wirelessly.

After package format verification, the data was processed in Matlab[10] by applying a simple moving average smoothing filter.

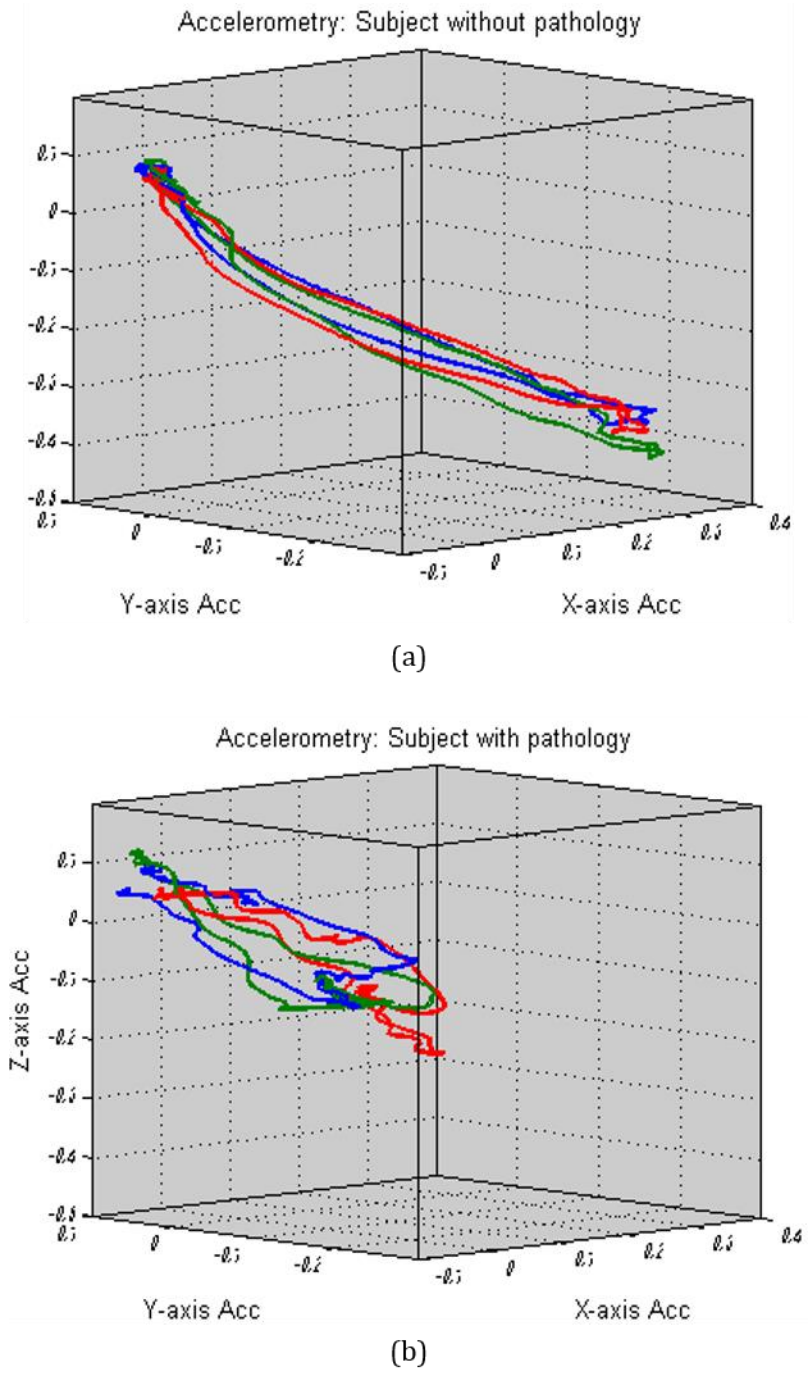

Figure 25: W2M2 inertial data of three independent reach-press-return movement: (a) subject without pathology and (b) subject with pathology.

[10] http://www.mathworks.com/

Looking at these figures, clear differences are observed between movement path of typical vs. post-stroke individuals, namely the smoothness and the consistency of the reach and return movements.

2.5. Summary

Recent advances in MEMS-based sensors, such as miniaturization and power consumption, have allowed their presence in today's wearable solutions. Accelerometers and gyroscopes dominate the movement/position category and are becoming each day more accessible for numerous research opportunities.

The first inertial prototype developed under this thesis was called WIMU, and was primarily intended for swimming performance analysis. It comprised an accelerometer and a gyroscope as sensing elements, a microcontroller for data packaging and wireless transmission. The experimental tests made with this system revealed some drawbacks: it provided a low packet transmission rate, did not allowed for sensor expansion and integration with other acquisition systems and lacked of memory storage for measurements in which wireless transmission could not be possible.

The W2M2 was based on a modular approach, where several sensor modules can be assembled and used together to extract meaningful information according to the application requirements. Instead of a complex sensor system, the key aspect of this system was to combine functionality and usability in a simple wearable solution. Along with simplicity comes small size and weight, which are crucial features when referring to wearable technology and sensor integration.

The biggest improvement of W2M2 with respect to WIMU was the concept of modular device: multiple modules, connected through digital communication (although analog connection could be also possible), which could be linked to the processing unit, transforming the device into a multi-purpose monitoring system. The W2M2 allows the interconnection of accelerometer, magnetometer and gyroscope boards, electrodes for surface

electromyography (sEMG) and also On/Off sensor; nonetheless the use of standard communication protocols such as I2C and SPI allow interconnecting to a wide variety of commercially available sensors which may be added to address particular purposes. In addition, data transmission rate was significantly improved, from roughly 10 packets/s with the WIMU device to a maximum of 500 packets/s with the W2M2.

Chapter 3

FIBER OPTIC SENSORS

Fiber optic technology emerged in the 60s with the description of an optical waveguide fiber (Snitzer, 1961) and was later boosted by the demands on optical communications. Since then, a rapid evolution on optical devices and fibers technology has been noticed, especially concerning fiber fusion splicing devices, fiber coupling and intensity losses measuring equipments, such as the Optical Time Domain Reflectomer (OTDR) (Frazao, 2009). In parallel, an increasing interest on using optical fibers in different areas rather than communications has triggered the fiber optic sensor technology. The initial idea of using these fibers only for communication purposes was replaced by the perception that the optical fiber could also be used as a sensing element to monitor several physical and chemical quantities. Later, the concept of using fibers as both sensing element and communication channel has demonstrated the huge potential of fiber optic sensors which made them a strong competitor among sensors technology. Even so, fiber optic sensors (FOS) still remain apart from most engineers and researches, perhaps due to the more conventional use of non-optical (mostly electrical) technologies and also given the limited number of available turn-key solutions.

FOS represent a technology base that can be applied to a multitude of sensing applications, since most physical properties can be sensed optically with fibers. Light intensity, displacement, temperature, pressure, strain or flow are just some of the phenomena that can be measured (Krohn, 2000). Nowadays, technology can challenge traditional sensors in a large number of innovative applications. Figure 26 shows the distribution of papers presented at the 22nd International Conference on Optical Fiber Sensors in 2012 according to

measurands of interest. This conference is a major event in the field of fiber optic sensors. The most highly reported developments are found in the field of chemical and gas sensors, followed by strain and temperature optical fiber sensors. Biosensors have suffered a substantial growth compared with past conferences (from 2.4% to 12.63%) (Lee, 2003).

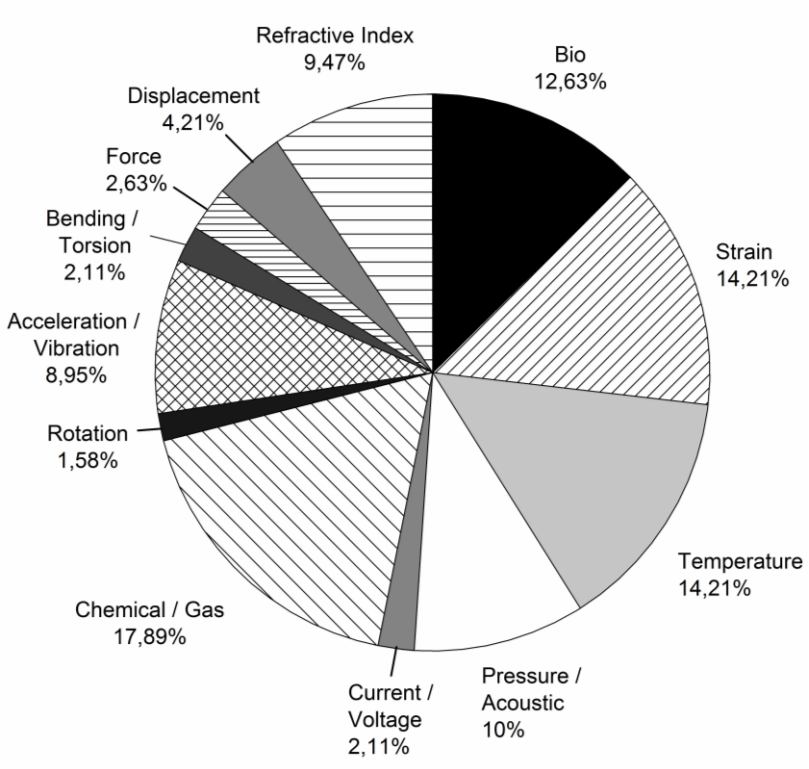

Figure 26: Paper distribution under the 22nd International Conference on Fiber Optic Sensors (2012) according to measurands of interest.

A huge number of fiber optic sensors for biomedical applications has been reported in the last years. The most referenced optical sensing devices are for biomechanical, biological and physiological measurands. In the field of biomechanics, FOS based on different sensing principles are described to measure force and pressure (Roriz, Frazão, Lobo-Ribeiro, Santos, & Simões, 2013), as well as to monitor different joint angle (Kwang Yong et al., 2008). For biological purposes, several optical devices have been developed to target cells and proteins (Velasco-Garcia, 2009), identify DNA (Deoxyribo-Nucleic Acid) markers (Leung, Shankar, & Mutharasan, 2007) or to measure humidity/moisture (Yeo, Sun, & Grattan, 2008). In addition, physiological

parameters such as temperature, pH (Shao, Yin, Tam, & Albert, 2012) or heart beat (Kreber, 2013) can be sensed with fiber optic devices.

3.1. Fiber Optic Sensor Concepts

Light propagation inside fibers is due to the phenomenon of total internal reflection. It is common sense that refraction occurs when light passes from one homogeneous medium to another, according to the Snell's Law:

$$n_1 \sin\theta_1 = n_2 \sin\theta_2 \tag{17}$$

where n_1 and n_2 are the refractive indices of the two mediums and θ_1 and θ_2 are the angles of the incident and refractive light rays, respectively.

Therefore, when the light passes from a high-index of refraction medium to a lower-index medium, a certain portion of the incident light is reflected (Figure 27 (a)). If the incident ray hits the boundary with an angle equal to the angle between the refracted ray and the normal to the interface, no refraction will occur (Figure 27 (b)). This angle is known as the critical angle. Incident ray with angles greater than the critical angle will be entirely reflected at the interface and no refraction takes place (Figure 27 (c)). This is the total internal reflection phenomenon.

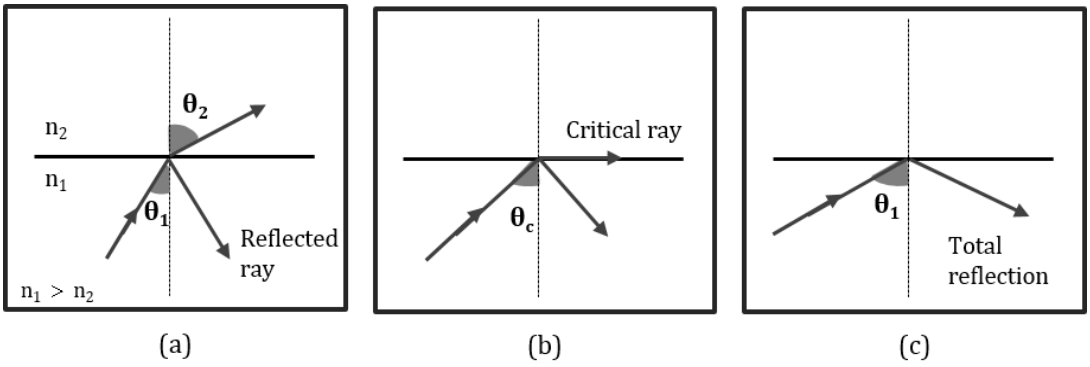

Figure 27: Total internal reflection phenomenon: (a) reflection of some light portion; (b) no refraction (critical angle) and (c).total reflection (Adapted from (Krohn, 2000)).

Traditionally, optical fibers have been used for telecommunications, due to their intrinsic properties of integrity (low attenuation when compared with electrical cables) and transmission rate. Now, their use has been spreading and optical fibers are more often being reported by their sensing capabilities.

Some of the advantages of fiber optics that make their use attractive as sensors are: small size and weight; no electrical hazard; remotable; easy to install; immune to radio-frequency interference and electromagnetic interference; high accuracy; high sensitivity; multiplexing capabilities (Krohn, 2000).

The simplest partition of optical sensors is into so called *intrinsic* devices, where the interaction occurs actually within an element of the optical fiber itself, and *extrinsic* devices, where the optical fiber is used to couple light, usually to and from the region where the light beam is influenced by the quantity being measured (Z. Zhang & Grattan, 1998).

Traditionally, fiber optic sensors can be divided into three basic categories (Davis, 1995): *intensity-modulated*, *phase-modulated* and *wavelength-modulated* sensors. Figure 28 shows three different examples of such sensors.

Intensity-modulated sensors are generally associated with displacement or some other disturbance that interacts with the fiber causing a change in received light intensity, which is a function of the variable being measured. The light loss can be associated with transmission or reflection, and the attenuation mechanisms can be based on microbending, macrobending, or other phenomena such as absorption or scattering which can be incorporated in the fiber (Krohn, 2000).

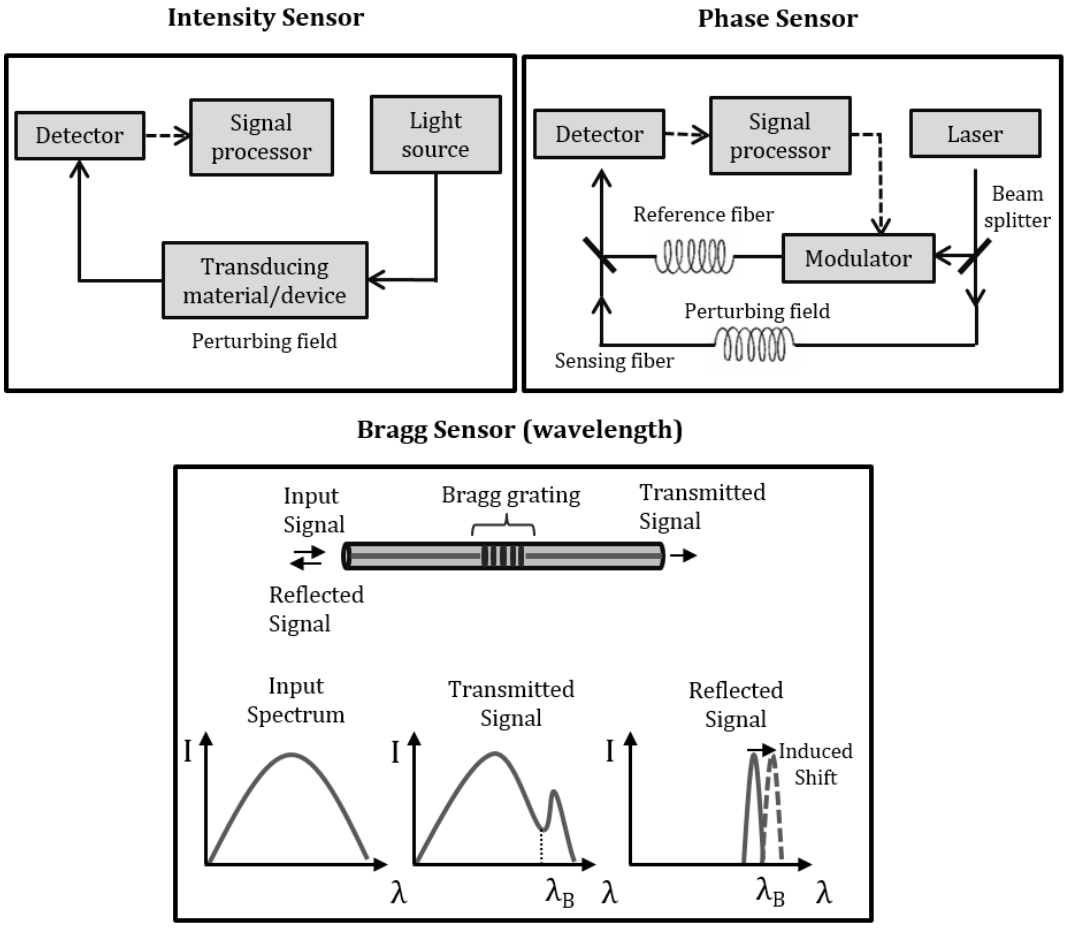

Figure 28: Fiber optic sensors. (Adapted from (Krohn, 2000))

Wavelength-modulated sensors, as the name indicates, use changes in wavelength to implement the sensing function. The wavelength modulation can be a result of fluorescence; however, the broad concept is accomplished with Bragg gratings. The Bragg grating has a resonance condition at a specific wavelength, in which incident light is reflected. If a change in strain or temperature occurs, a perturbation in the grating will cause a wavelength shift in the reflected light, which is a direct function of the change in strain and/or temperature (Raman, 2010). Bragg grating sensors have several advantages: the wavelength shift is independent on the light source intensity; high accuracy and sensitivity; and multiplexing capabilities (Mishra, Singh, Tiwari, & Kapur, 2011), just to mention a few.

Phase-modulated sensors compare the phase of the light in a sensing fiber to a reference fiber known as interferometer. The sensors are much more accurate than intensity-modulated sensors and can be used in a larger dynamic range. However, they are often more expensive and less appropriated to be integrated in a wearable piece of garment, since they are much more complex than simple intensity-modulated sensors (Krohn, 2000; Rantala, Hannikainen, & Vanhala, 2011). Generally, the sensors employ a coherent laser light source and two fibers in which previously splitted light is injected; if the environment perturbs one fiber relative to the other, a phase shift occurs that can be detected very precisely by an interferometer (Grattan & Sun, 2000). All interferometers have a sensing fiber and an isolated reference fiber. There are four basic interferometric techniques: the Mach-Zehnder, the Michelson, the Fabry-Perot and the Sagnac. The interferometric techniques are generally used to detect physical parameters with high resolution.

The sensing principle and examples how these fiber optic sensors (intensity, wavelength and phase -modulated sensors) can be used to detect position, displacement, relative rotation for human motion analysis and other biomedical applications will be discussed in detail in subsequent sections.

3.1.1. Intensity-modulated Sensors

As introduced before, concepts associated with intensity-modulated sensors include transmission, reflection, microbending and macrobending. For the purpose of motion analysis the most popular and attractive sensors are transmission sensors based on the microbending and macrobending phenomena (Krohn, 2000). If a fiber is bent, small amounts of light are lost through the wall of the fiber. If a transducer bends the fiber due a change in a physical property, the amount of received light is related to the value of this physical property. The attenuation, or intensity loss, is defined by the following equation (Krohn, 2000):

$$A = -10 \log {}^{P_i}/_{P_o} \tag{18}$$

where A is the attenuation and P_i and P_o are the input power and output power, respectively. The negative sign arises from the convention that attenuation is negative (Krohn, 2000). Attenuation is measured in decibels (dB) per unit of length.

Microbending sensors are inherently very similar to macrobending sensors, difference lies in the sensor geometry and bending scale. Microbending sensors are used in applications where the measurands such as strain, pressure, force, position or acceleration, can be mechanically coupled to a device movement that deforms the fiber (Xuejin, Yuanlong, Yongqin, Xinyi, & Jingxian, 2008). To activate the microbending loss in the sensing applications, the fiber is usually placed in between teeth-like deformers (Figure 29). As the selected measurand is sensed by the sensing head, the distance between the upper and the lower teeth is reduced and causes a series of bending along the fiber (Gardner, 1975). Continuous movement of the deformer is linearly dependent on the light-intensity measured at the end of the fiber (Zawawi, O'Keefe, & Lewis, 2013).

Figure 29: Schematic drawing of a microbending sensor.

Microbending losses in the fiber leads present a problem only if the leads move while the sensor is in operation. Studies made with different cable coatings revealed that the sensitivity of the leads to bending loss can be reduced if a protective cable surrounds the fiber (Krohn, 2000).

Macrobending sensors can be considered one of the simplest in terms of operating principle and instrumentation (Zawawi et al., 2013). Macrobending sensors are both accurate and low cost, and, since they have a closed optical

path, they are immune to dirty environments (Krohn, 2000). As compared to microbending, these sensors do not require any deformers to cause changes in the light output. Instead, different fiber geometry configurations are used to allow light attenuation. Usually, the fiber is placed onto elastic elements and as the fabric is stretched the bending radius of the fiber changes and causes attenuation in light output (Zawawi et al., 2013). Several approaches have been described using different fiber bending configurations, including single loops, U-shape, sinusoidal and figure-of-eight shapes, as can be seen in Figure 30.

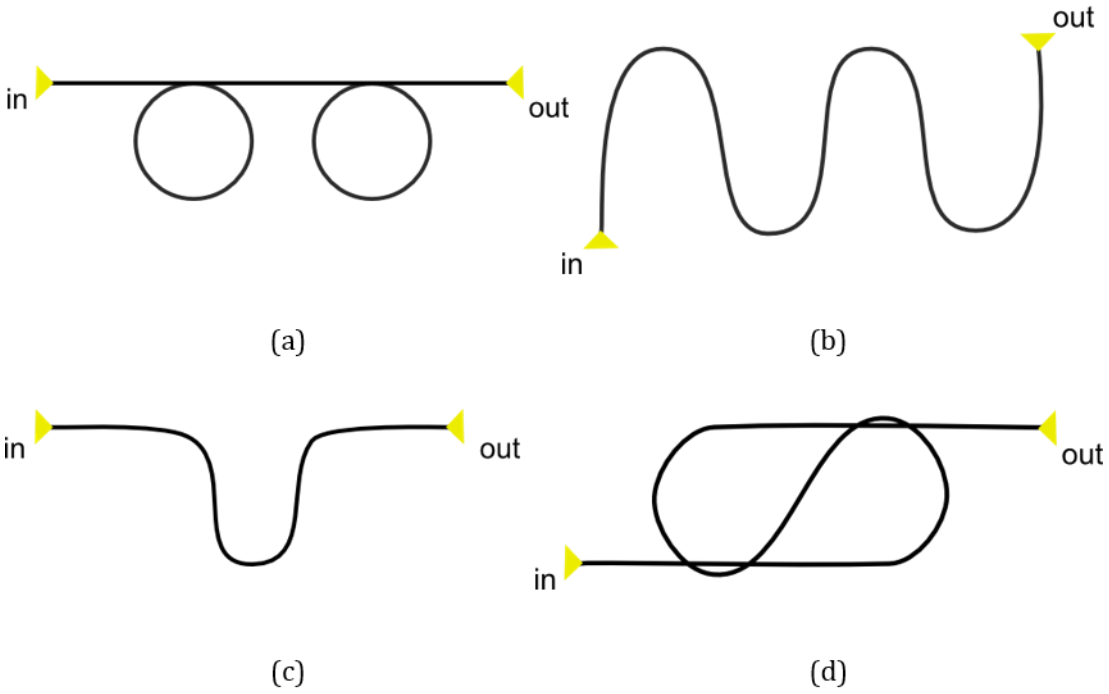

Figure 30: Schematic of different configurations used for intensity-modulated fiber optic sensors: (a) single loops; (b) sinusoidal, (c) U-shape and (d) figure-of-eight shape.

Fiber bending losses due to sinusoidal shapes have some limitations, such as uneven force distribution along the curves, which may cause a light attenuation not directly dependent on the number of curves and bending radius (Zendehnam, Mirzaei, Farashiani, & Farahani, 2010). To overcome this hurdle, the figure-of-eight scheme has been proposed as a different fiber geometry (Augousti, Maletras, & Mason, 2005).

Most of the intensity-modulated sensors are analog and problems associated with variations in light source intensity can affect the sensor output,

as well as microbending in the leads to and from the sensing region. Typically, the light source is a light-emitting diode (LED) which can vary in intensity; to resolve this problem, a reference can be used that detects the intensity variations and corrects the LED output (Krohn, 2000).

The bending effect can be used in the biomedical field to monitor a variety of physical and physiological variables. Some classic examples are the use of simple silica fibers to recognize breathing movements (D'Angelo et al., 2008) and to determine angular movements of human joints (Munoz, Leija, Diaz, & Alvarez, 1995). A project supported by the EU under FP6 and called *Optical Fiber Sensors Embedded into Technical Textiles for Healthcare* (OFSETH) was launched with the goal of taking advantage of pure optical sensing technologies for wearable health monitoring, especially in magnetic resonance imaging (MRI) environments (Grillet et al., 2008). For many applications where electromagnetic immunity is needed, optical fibers have proven advantages compared with standard technologies. By analysing attenuation of the ray which is driven in the optical fiber, placed at the patient's upper body, when it is bend, it was possible to recognize the breathing movements of the subject. However, when using bending loss sensors attention must be given to its placement and configuration. Within the OFSETH project, researches have analysed different configurations in order to investigate the optimal sensor which maximizes sensitivity. The best results accomplished were with distributed fibers placed at the thorax in a sinewave configuration, with a 6 mm radius. In addition, a two times better detection was achieved using a belt with one part elastic (correspondent to the sensor area) and the rest non-elastic (D'Angelo et al., 2008). Some of the results obtained so far under the OFSETH project are shown in Figure 31.

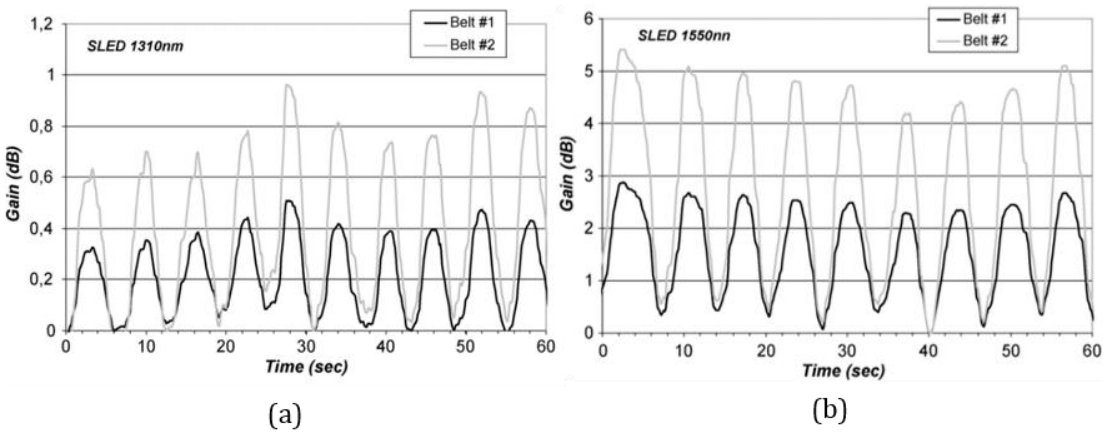

Figure 31: Respiratory abdominal movements recorded simultaneously by two belts, one completely elastic (Belt #1) and other semi-elastic (Belt #2), embedding a bending sensor, at (a) 1310 nm and (b) 1550 nm. (Adapted from (Grillet et al., 2008))

A different application of an optical sensor that uses the microbending concept is the case of a plantar pressure monitor device, used to control and prevent the plant ulcers (that can lead to infection and subsequent amputation) associated with complications caused by diabetes disease. In this study, a fiber optic sensor array was built, which consists of an array of optical fibers lying in perpendicular rows and columns separated by elastomeric pads. Intensity attenuation is caused by the physical deformation of two adjacent perpendicular fibers (Wang, Ledoux, Sangeorzan, & Reinall, 2005). Nonetheless, this new sensor still lacks calibration optimization, especially for fibers located near the periphery of the array, and needs improvements related to repeatability.

When considering silica fibers as the tool to build bend-loss sensors, one issue that immediately appears is the problem of fiber breakage. If no special attention is given to the bending limit of the fiber, the sensor functionality can be compromised. In order to overcome such limitation, polymer-based optical fibers, also known as POF, can be used. Besides the advantages of elasticity and easy-handling, this type of fibers suffer from higher attenuation and distortion compared with traditional silica fibers; where this represents a drawback for telecommunication purposes, it also means increased detection capabilities when considering macrobending sensors. In addition, since POF usually have larger diameters, they permit the use of plastic connectors with lower precision.

POF macrobending sensors have been reported for monitoring seated spinal posture (Dunne, Walsh, Smyth, & Caulfield, 2006) and for monitoring rescuers' heart rate and respiratory rate wearing a smart fabric suitable to be used in high-risk and complex environments (i-Protect project) (Witt, Krebber, Demuth, & Sasek, 2011). These sensors have also been utilized to detect the flexion angles of finger joints for commercial sensing gloves (Zimmerman & Lanier, 1987). Still, POF sensors alone have low sensitivity and there are some error sources in power losses measurements (Kyoobin & Dong-Soo, 2001). One method that improves the sensitivity of a bent optical fiber based sensor is side-polishing (L. Bilro, Pinto, Oliveira, & Nogueira, 2008; Lomer, Quintela, López-Amo, Zubia, & López-Higuera, 2007). The side-polishing is accomplished by removing a portion of the jacket, cladding and core of the fiber, bringing a polished elliptical surface out into the open. This polished region of the fiber core is in direct contact with the external medium, with a specific refraction index. If one combines this method with a loop configuration, a sensor with twice the sensitivity is obtained (see Figure 32). In this case, the input rays suffer refraction from the curved region and a subsequent refraction due to the polishing area (Lúcia Bilro, Alberto, Pinto, & Nogueira, 2012).

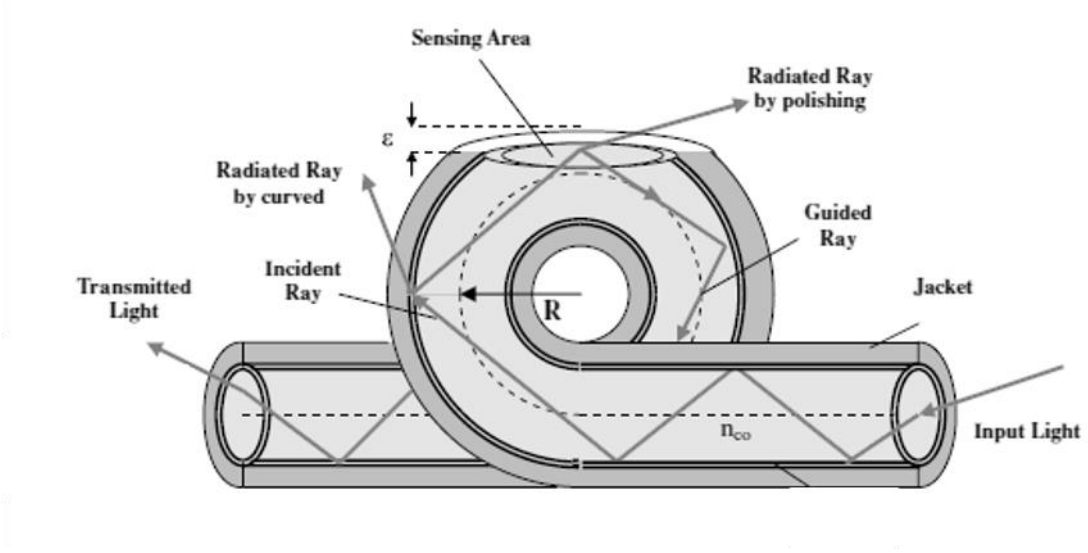

Figure 32: Example of a side-polished POF cable loop. (Adapted from (Lomer et al., 2007))

This sensor configuration was proposed as a liquid-level sensor, using the changes of the refraction index in the sensing area to promote variations in the optical power (Lomer et al., 2007). Also similar sensor configurations have been reported for gait analysis, by measuring human joints angles, with good results when compared with simultaneous video analysis (see Figure 33)(L. Bilro et al., 2008).

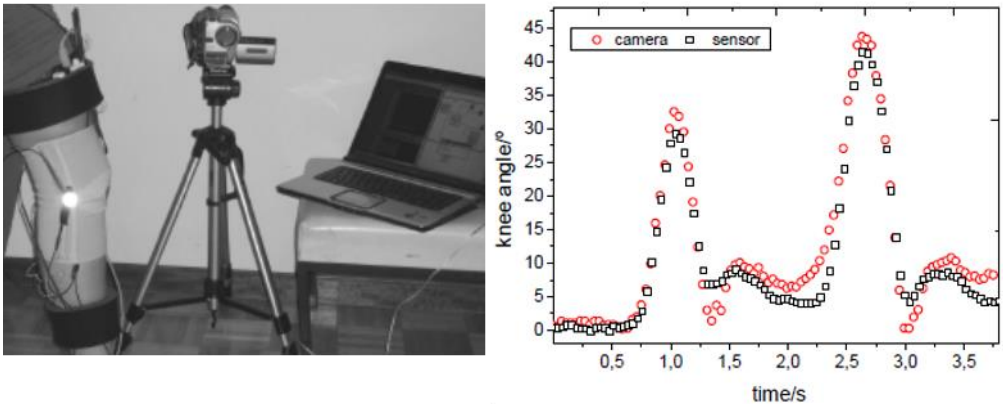

Figure 33: Experimental setup to validate optical sensor for gait analysis: (a) sensor attached to knee joint and video-based system for simultaneous acquisition; (b) optical sensors and video's knee angle of a complete gait cycle. (Adapted from (L. Bilro et al., 2008))

Another referred concept, based on macrobending losses, that has intrinsically more sensitivity than silica fibers to measure intensity variations is the use of hetero-core fiber optic sensors. Hetero-core optical fibers are fabricated by inserting a small portion of fiber with a smaller core diameter into two identical fibers with larger core diameters. The cladding diameters of the fibers should be the same. Hetero-core fiber optic sensors have large sensitivity because of the power coupling that takes place at the interface, which makes leakage easier when an external deformation occurs (Efendioglu, Sahin, Yildirim, & Fidanboylu, 2011). This way, hetero-core sensors have been found to have highly sensitive and reproducible performance in response to macrobending based on optical intensity variations and, additionally, are unaffected by temperature fluctuations (Nishiyama, Sasaki, & Watanabe, 2006).

Some researchers have developed a wearable sensing glove with embedded hetero-core fiber-optic sensors capable of detecting finger flexion for hand motion monitoring (see Figure 34) (Nishiyama & Watanabe, 2009). However, the sensors used in the glove cannot discriminate between different joint flexion, and different sensors are needed to detect each particular joint movement. Another study reports the use of sensing clothes with embedded hetero-core fibers to measure a joint angle ranging from 0-90º during human walking (Nishijima, Sasaki, & Watanabe, 2007).

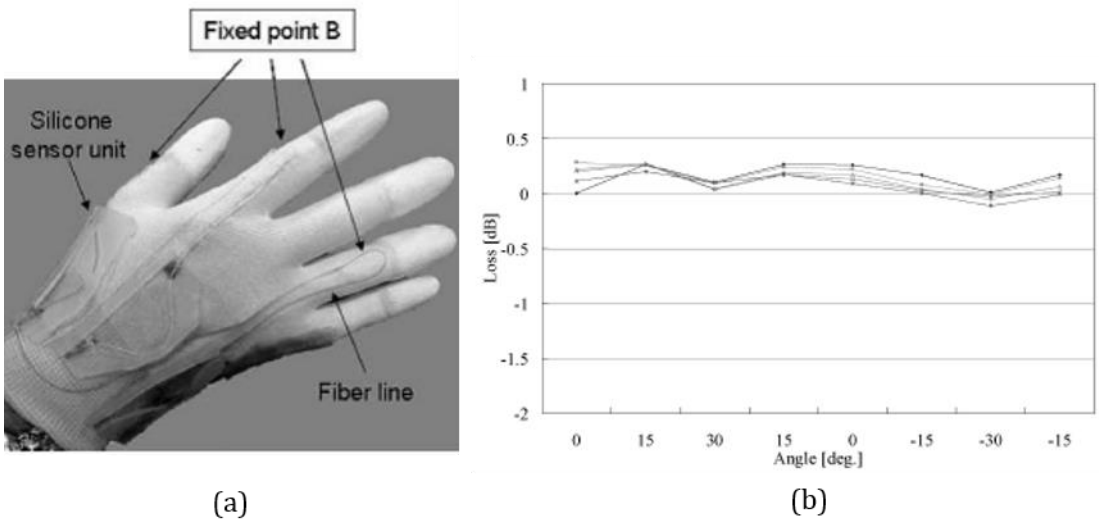

Figure 34: (a) Photo of the sensing glove and (b) experimental data acquired during hand waving. (Adapted from (Nishiyama & Watanabe, 2009))

3.1.2. Wavelength-modulated Sensors

Fiber Bragg Gratings (FBG) are truly wavelength-modulated sensors. The parameter being measured is a direct function of the wavelength shift associated with the Bragg resonance condition (Krohn, 2000). Bragg grating sensors have several advantages: high sensitivity and accuracy, and because they are small, they are excellent point sensors, which means a single fiber may have several sensors written in sequence, each at a different wavelength (multiplexing capabilities), measuring different physical variables (multi-parameter sensor). Bragg gratings are intrinsic elements of a fiber where the

index of refraction in the fiber core is periodically modulated after illuminating it with ultraviolet light. As light propagates through the modulated region, some with a specific wavelength (resonant Bragg grating wavelength, λ) will be reflected. The resonant Bragg grating wavelength depends on the refraction index, n, and the spacing between grating periods, Λ, as follows (Krohn, 2000):

$$\lambda = 2n\Lambda \tag{19}$$

At wavelengths that do not satisfy the Bragg condition, the light passes through without being affected; however, at the Bragg wavelength, the signal is reflected. An example of a reflection spectrum of a standard FBG sensor is shown in Figure 35.

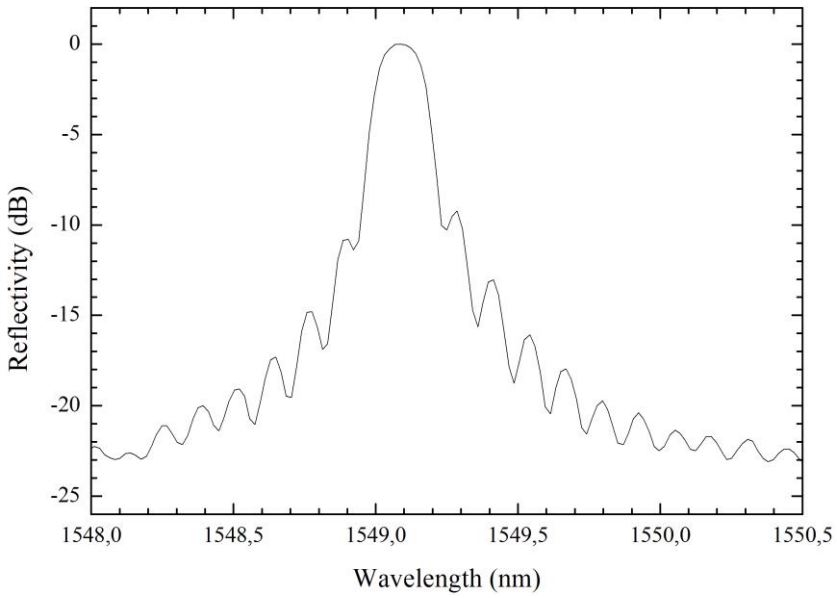

Figure 35: Reflected spectrum of a standard FBG sensor.

The Bragg grating responds to both strain and temperature. Strain effects the elongation of the fiber, changing the grating spacing, and thus affecting the transmitted wavelength. Also, the index of refraction is affected due to Poisson's effect (photoelasticity). Temperature causes thermal expansion, which also changes the grating spacing. The refractive index itself is temperature dependent. Usually, to discriminate temperature from strain effects, a reference grating is used in the sensing head.

Another grating approach uses long-period gratings (LPG): when the grating spacing is in the 500 μm range (typically ten times larger than FBGs) the resonant condition couples light from the core to the cladding (Krohn, 2000). LPGs have specific properties that make them possible to differentiate between strain and temperature, twist and bending (Raman, 2010).

As both FBGs and LPGs can directly sense variations in temperature and strain and, indirectly, a variety of physical properties such as pressure, rotation and curvature, they can be useful for many applications in the field of healthcare and, more specifically, human motion analysis.

An embedded array of FBGs can be used for pressure mapping at different human segments and joints. A temperature independent grating with the proper configuration can be used as pressure sensor for biomechanics or rehabilitation. The EU FP7 IASiS project addresses pressure ulcer incidence and treatment and aims to develop and demonstrate an Intelligent Adaptable Surface for serving as the skin/machine interface in therapy beds and wheelchair seating systems (Pleros, Kanellos, & Papaioannou, 2009). The system integrates FBG sensor arrays in a 2D mesh structure, providing an effective way of monitoring pressure and strain along the entire surface. Another similar system was built that monitors the patient continuously, registering the amount and frequency of movement over a given time, generating a report that alerts the nursing staff if the patient stays unmoved for a long period of time (Hao et al., 2010).

Chest strain can be used for monitoring patients, as breathing is difficult to monitor. A temperature independent FBG can be designed for monitoring ventilator movements and to determine the respiratory frequency spectrum. In (Wehrle, Nohama, Kalinowski, Torres, & Valente, 2001), a FBG was attached to an elastic belt, which was held in position just above the breast. As the patient breathes, the thorax cage distends and deflates rhythmically. In addition, the frequency of the signal can be used to trigger corrective action should the patient be under stress. Figure 36 shows two respiratory signals recorded with this system: the first reveals a normal inhaling and exhaling movement of a 26

year old man, in sitting position; the second represents the respiratory movement when the subject is turning his arms.

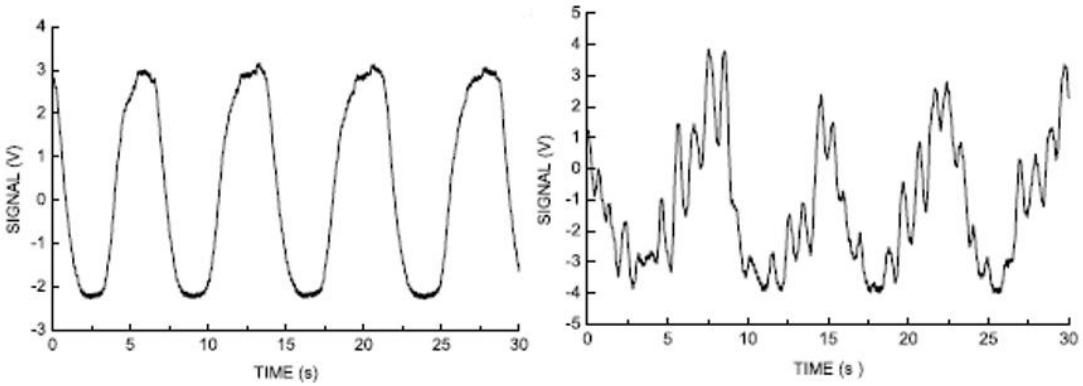

(a) (b)

Figure 36: Respiratory signal captured through a FBG sensor of (a) a normal subject in sitting position and (b) a subject turning his arms. (Adapted from (Wehrle et al., 2001))

Using the same concept and taking advantage of the FBG linear sensitivity to longitudinal mechanical stress, a system comprising a FBG sensor was developed to investigate the capabilities of optical sensors for healthcare monitoring in magnetic resonance imaging (MRI) environments (De Jonckheere et al., 2010; De Jonckheere et al., 2009). Due to the well-known immunity of fiber optics against electromagnetic radiations, FBG sensors are suitable for MRI environments. The sensors were placed at abdominal and thoracic levels to continuously monitor ventilation motion. Detecting these movements can be useful to monitor anaesthetized patients during MRI scans, especially for infants who are susceptible to the Sudden Infant Death Syndrome (De Jonckheere et al., 2010). The developed system was able to precisely detect respiratory movements; however, due to the variability of age, size and weight of the patients, this wearable solution needs to be adapted to different groups.

There are many other different examples of using FBG and LPG sensors to monitor respiration (Allsop et al., 2007; Allsop et al., 2005; Xiaobin, Chunxi, Kun Mean, Hao, & Xunming, 2008). All these systems are based in the same sensing principle described above and differ in the specific purpose for which they were built.

For a proof-of-concept demonstration, an FBG sensor was placed in a vibrating membrane of a subwoofer. Using recordings of various heartbeat sounds, the vibrations felt by the membrane would induce stretching and/or contraction of the FBG. Some relevant features such as strength of the heartbeat or heart rate can be extracted from the wavelength signal. The researchers predicted that in real-life scenario a FBG sensor could be used as a simple stethoscope (Gurkan, Starodubov, & Xiaojing, 2005). Another example of how to use an FBG sensor to measure cardiac activity was proposed by Witt et al. (2011). The sensor was placed at the wrist of the patient and the small elongations produced by heartbeat were detected by means of wavelength shifts.

FBG sensors can also be used in biomechanics to measure human joint angles. The system proposed in (da Silva, Goncalves, Mendes, & Correia, 2011) is a simple sensing glove which uses FBGs to measure the angle between the finger phalanges. The method consists in measuring the elongation of the upper side of the finger joints when stretching out or in the finger. Since the purpose is to detect the flexion/extension of the finger, sensor positioning and disposition is crucial. The sensors must be placed in order to maximize elongation and minimize wrinkles that could lead to fiber breakage. In this system, the fiber was positioned in a curvilinear layout and a sensor was placed over each phalanx joint, performing a total of 14 FBGs sensors in the glove (see Figure 37). Due to FBGs multiplexing capabilities and high sensitivity, a single fiber is enough to accurately measure the angles. The sensing glove revealed a linear response while the hand was opening and closing, and a good agreement with real angles was achieved. However, the integration of the fiber into the textiles revealed some problems and the systems lacks portability.

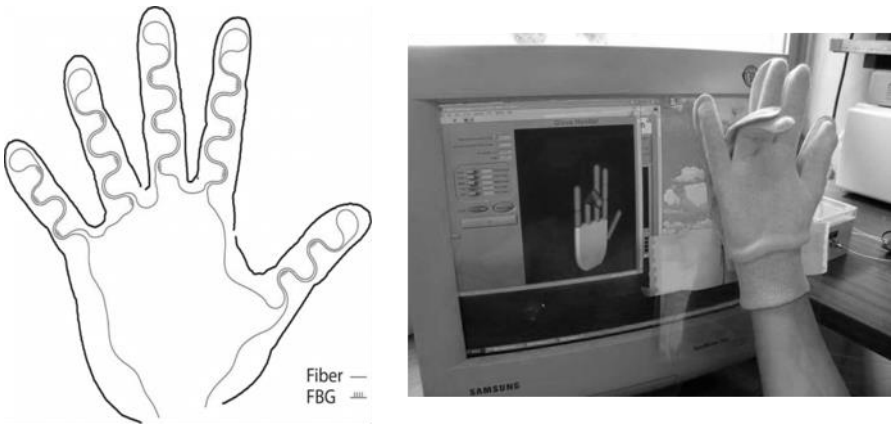

Figure 37: FBG sensing glove. (a) FGB sensor positioning; (b) Real-time monitoring of hand posture. (Adapted from (da Silva et al., 2011))

3.1.3. Phase-modulated Sensors

The use of interferometers in optical measurement has been well established for many decades. Because of their extreme sensitivity, phase-modulated sensors are the most publicized of all fiber optic sensors (Krohn, 2000). Typically, these sensors use a coherent laser lightsource and two single-mode fibers. The light is split and injected in each fiber. Therefore, if the environment perturbs one fiber relative to the other, a phase shift occurs that can be detected very precisely (Krohn, 2000). This phase shift is detected by an interferometer. As mentioned before, there are four interferometric configurations: the Mach-Zehnder, the Michelson, the Fabry-Perot and the Sagnac.

The Mach-Zehnder interferometer configuration can be seen in Figure 38 (a). It uses a laser beam that is split using a 3 dB coupler, which means 50% of the light is injected into the sensing fiber and 50% into the reference fiber. The light beams are recombined using another 3 dB coupler and the phase shift is measured. This shift results from changes in the length and the refractive index of the sensing fiber (Krohn, 2000).

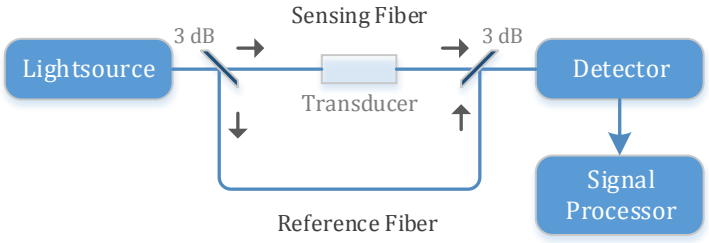

(a)

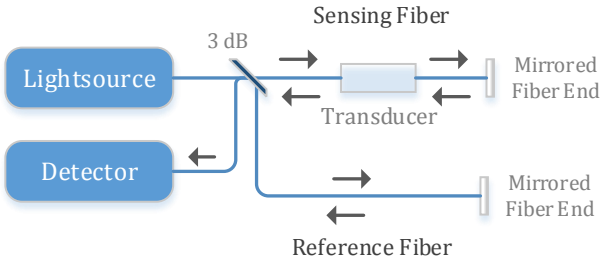

(b)

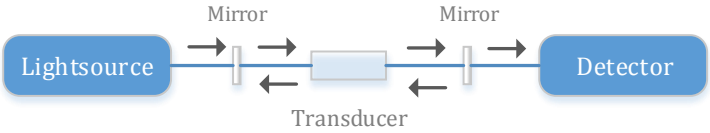

(c)

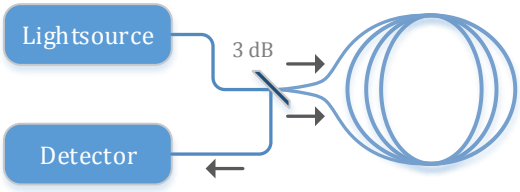

(d)

Figure 38: Fiber optic interferometers: (a) Mach-Zehnder configuration; (b) Michelson interferometer; (c) Fabry-Perot scheme and (d) Sagnac interferometer. (Adapted from (Krohn, 2000))

The Michelson interferometer approach is depicted in Figure 38 (b). It employs a configuration very similar to the Mach-Zehnder interferometer, but it uses back reflection due to the fibers having mirrors at its ends. The initial beam is split and injected in the reference and sensing fibers. Since both fibers have end mirrors, the light is reflected and re-coupled to a shift detector. The sensitivity of such configuration is higher but it has the disadvantage of feeding light both into the detector and the laser, which causes noise (Krohn, 2000).

Fabry-Perot interferometers are different from the ones mentioned so far, since they do not require a reference fiber. Instead, the interference results from successive reflections of the initial beam (see Figure 38 (c)). The multiple passes along the fiber will magnify the phase shifts, which results in high sensitivity (Krohn, 2000).

Finally, the Sagnac configuration is shown in Figure 38 (d). This approach requires a coupler that injects light into two ends of a single-mode fiber in a coiled configuration. The injection of light is such that light propagates in both clockwise and counter-clockwise directions. In this case, both fibers work as sensing fibers. If the coil rotates, one propagation time will be longer than the other and when recombined the beams will be out of phase (Krohn, 2000). These sensors do not require a change in refraction index or length to originate a phase shift. Devices of this type have been developed and applied principally, but not exclusively, to develop fiber optic gyroscopes (Grattan & Sun, 2000).

As mentioned before, due to its characteristics, fiber optic interferometers are used to sense measurands with high resolution and sensitivity. For biomedical purposes, the majority of these sensors are utilized to measure physiological and biological parameters.

Recent studies describe the use of fiber-based interferometers breathing sensors. In the study developed by Favero et al (2012) the device sensing head consisted of a simple photonic crystal fiber (PCF) which was fusion spliced at the distal end of a standard single mode fiber. The reflection spectrum of the device exhibited a sinusoidal interference pattern that instantly shifted when water molecules, present in exhaled air, were adsorbed on or desorbed from the PCF surface. This way, the device could be used to monitor a person's breathing whatever the respiration rate (see Figure 39). Similarly, another study reported an interferometric sensor which detected the variation in relative humidity that occurs between inhaled and exhaled breath, making possible the determination of breath rate and status (Mathew, Semenova, & Farrell, 2012). Several other sensors have been described to detect physiological parameters. The

mechanical and acoustic activity of cardiac muscle and respiration reflects in the interferometric signal which enables the monitoring of heartbeat and respiration (Podbreznik, Đonlagić, Lešnik, Cigale, & Zazula, 2013; Sprager & Zazula, 2012).

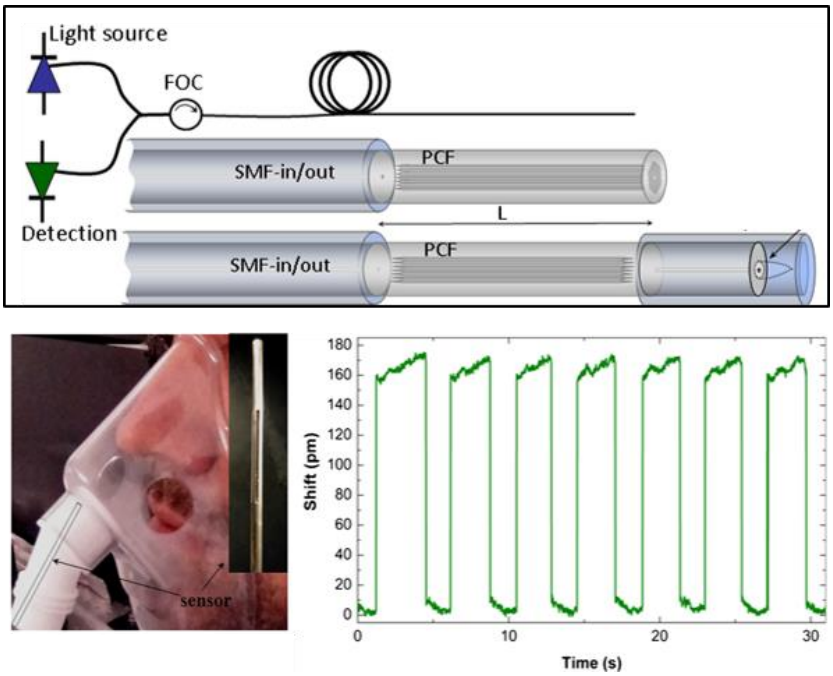

Figure 39: Interferometer sensor for monitoring breathing. Top: sensor scheme; Bottom Left: sensor integration on a medical device; Bottom Right: phase shifts due to breathing pattern. (Adapted from (Mathew et al., 2012))

For biological applications, the most common interferometric sensors are based on integrated optical waveguide structures with Mach-Zehnder, Fabry-Perot (Y. Zhang, Shibru, Cooper, & Wang, 2005) or Young (Schmitt, Schirmer, Hoffmann, Brandenburg, & Meyrueis, 2007; Ymeti, Subramaniam, Beumer, & Kanger, 2007) interferometer configurations. Usually, these sensors are used to detect specific molecules which bind to the optical path resulting in a phase shift (Davé, 2009). Interferometers can also be used to monitor biochemical parameters, such as pH and other chemical substances (Gu, Yin, Zhang, Qian, & He, 2009; T. Zhang et al., 2010).

For biomechanical purposes, namely for measuring human joint angles, a variety of other fiber-optic-based devices are described in the literature, based on operation principles different from those presented in the above sections. Optical linear encoders (OLE) can be used to substitute electrogoniometers. Electrogoniometers are used to measure joint angles, but they need careful sensor alignment and may restrict movements if many of them are used. An OLE has already been described as a distance-measurement device: the emitter light is reflected off a reflective code strip; the encoder counts the number of lines that have passed upon the strip and which can be converted to travel distance with direction index (Kim Doang, Chen, Zhiqiang, Song Huat, & Duh, 2011). Nevertheless, similarly to electrogoniometers, these sensors still lack of ergonomy. Recently, a fiber optic sensor based on polarization effects was described as an optical goniometer (Donno, Palange, Di Nicola, Bucci, & Ciancetta, 2008). The sensor uses a single mode fiber with two polarizers and three paddles: when a relative rotation of the paddles planes occurs, a change in the polarization of the light is achieved; since the polarizers allow the determination on the initial polarization status, it is possible to estimate the real rotation of the joint. Finally, a device utilizing the light refraction characteristics of optical fibers was built in order to measure angular displacement of the human joints (Jeong-Whan et al., 2006). An asymmetric beam profile was done by cutting one end of the fiber tips at a certain angle and, as the angle between the optical fiber tip and the phototransistor changes, the collector voltage varies accordingly. Thus the sensed signal represents an indirect measure of the curvature angle. The results showed that asymmetrical beam profile provide wider linear relationship than the symmetrical one.

3.2. Wearable Intensity-modulated Fiber Optic Sensor

A simple intensity-modulated fiber optic sensor was designed and characterized with the purpose to measure elbow flexion. The ultimate goal of this device was to be integrated in the wearable system and combined with the inertial units described in the previous sections.

The standard method to determine human joint angles is based on electrogoniometers. These devices are commonly used by physiotherapists to evaluate and score the performance of their patients while doing typical functional tasks, such as the reach movement. The elbow flexion is the primary phase of the reach sequence (Paten et al., 2010), thus one can understand the great amount of interest devoted to its analysis, since a crucial aspect guiding physiotherapist's clinical reasoning, and thus design of rehabilitation intervention, is the assessment of patients' motor performance. The typical functional range of motion of elbow flexion on an adult is between 10º and 130º (Morrey, Askew, & Chao, 1981). For the reach functional task, with the subject seated at a height corresponding to the alignment of the iliac crests and next to a table aligned with the distal border of the subject's thigh (so as not to interfere with the arm trajectory), the typical range of motion varies from 15º to 60º (Salazar et al., 2014). Despite its wide spread usage, electrogoniometers need careful sensor alignment, still lack of ergonomy and may restrict movements (Shiratsu & Coury, 2003).

According to the American Medical Association (AMA), the mean error limit accepted for the evaluation of movement impairments in clinical contexts, to consider a measurement as reliable, is established as 5 degrees (Nitschke, Nattrass, Disler, Chou, & Ooi, 1999). Standard commercial electrogoniometers used for these purposes stand below, or are equal, to this limit (Shiratsu & Coury, 2003). However, when it comes to sensitivity, research studies report fiber optic sensors as better alternatives to standard devices, since they are more sensitive to angular changes. Moreover, these sensors can provide repeatable results and allow to simultaneously measure multiple joints and store them directly in a database (Bell & Stigant, 2008; Wise et al., 1990).

Therefore, in order to overcome some of the hurdles of standard measure devices, a fiber optic sensor based on macrobending design was characterized and integrated in a customized piece of garment specifically designed and built to integrate the optical fiber as sensing element (Figure 40 (a)).

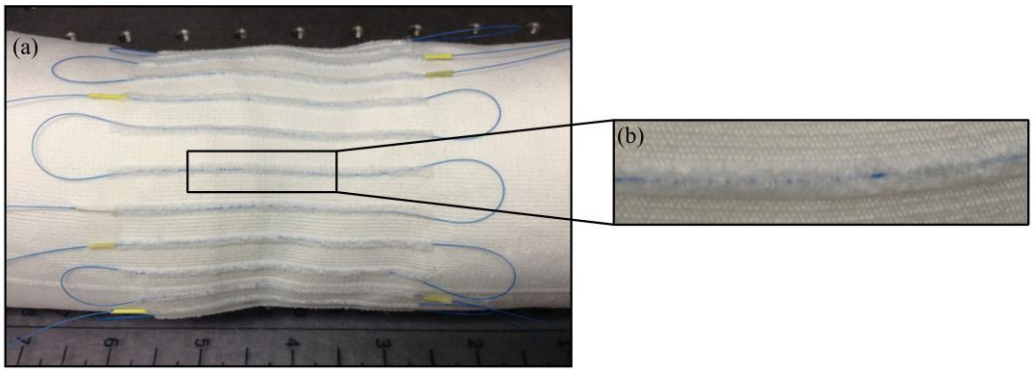

Figure 40: Fiber optic sensor: (a) customized piece of garment with different sensor configurations; (b) optical fiber channel detail on the fabric.

Experimental Procedure

A MBS seamless knitting machine model from MERZ company[11] was used to fabricate the piece of garment, mounted with a single needles system in a cylinder. The disk comprises transferring jacks, knives and springs which allow the control of the yarn in terms of going in or out the knitting zone. This machine is also a jacquard machine, with which it is possible to obtain complex structures with localized variations. These features have been used to produce a particularly voluminous structure at the area used for the optical fiber channels (see Figure 40 (b)). In this way, the channels protrude from the rest of the fabric, making simple the integration of the fiber onto the garment. Also, the feeding head of the machine comprising seven yarn guides allows to produce a customized fabric tube, with different compression effects and drawings based on the yarns characteristics.

[11] http://www.merz-maschinenfabrik.de/

The optical sensing device consists of a simple intensity-modulated sensor in which the light loss is associated with transmission and occurs due to bending effect, namely through the decrease of the curvature radius. As the flexion angle increases the loops radius decrease accordingly and hence the light loss inside the fiber for a single-mode fiber (SMF) is usually obtained by (Zendehnam et al., 2010):

$$L = 10\log\left(e^{2\alpha l}\right) \tag{20}$$

where L is the bending light loss, l is the fiber length and α is the bending loss coefficient, which is a function of bending radius, light wavelength and also optical fiber material and structure. Initial experimental results obtained from the optical fiber sensor with a single loop revealed an almost linear relationship between the curvature radius of the fiber and the flexion angle, as depicted in Figure 41.

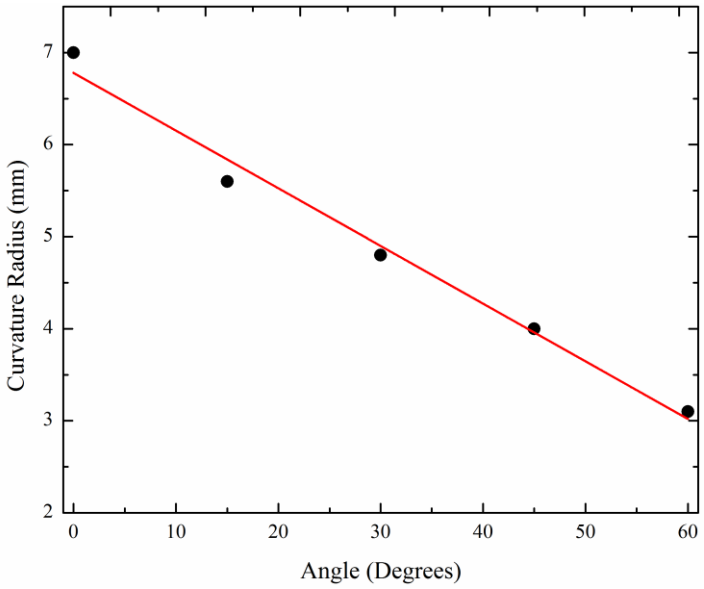

Figure 41: Relationship between curvature radius and flexion angle.

A standard single-mode fiber (SMF 28) was introduced in the specifically designed optical fiber channels with curvature radius with approximately 7 mm and 10 mm distance separated. The optical fiber coating and its integration into the fabric channels provides the fibers protection and stability, and,

consequently, increases sensor lifetime. Four different configurations were tested in order to investigate the sensor behaviour in terms of sensitivity and repeatability with increasing number of turns. The schemes studied covered sensors with a single, two, three and four loops (Figure 42).

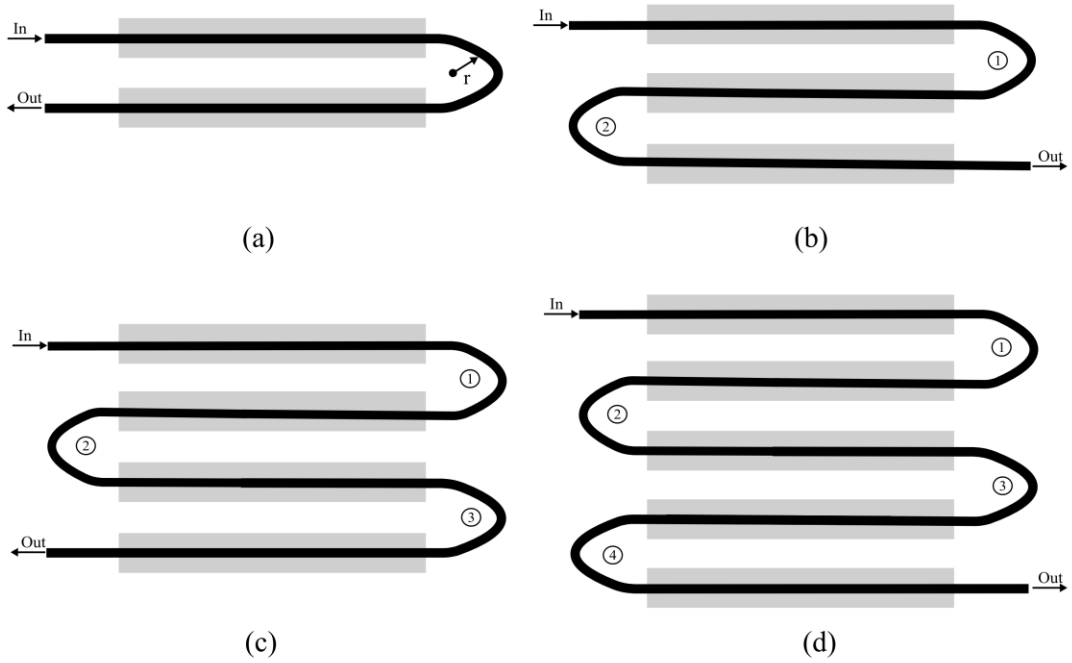

Figure 42: Schematic of sensor configurations studied: (a) single loop, (b) two loops, (c) three loops and (d) four loops.

The first scheme studied, shown in Figure 42 (a), has only one curvature and the light input and output are on the same side, while in the second case (Figure 42 (b)) the sensor has two curvatures and the light input and output are opposite to each other. Figure 42 (c) represents a situation similar to the single loop configuration and Figure 42 (d) is analogous to the two loops configurations; in both cases the number of loops increases relatively to the previous case.

Figure 43 (a) presents the experimental setup used to measure flexion angle. Light from a broadband source centered at 1550 nm and with width 100 μm was guided into the fiber. A photodetector (Agilent Technologies 8163B Lightwave Multimeter) in the telecommunications window of 1550 nm was

used to measure the optical power at a sample frequency of approximately 10 Hz. A Matlab script was used to acquire and visualize the output signal in real-time (the complete code can be found in Appendix C. For each sensor configuration, ten repetitions were performed at a fixed angle. The flexion angle ranged from 0º, equivalent to rest position (Figure 43 (b)), to 60º, which corresponded to the maximum elbow flexion (Figure 43 (c)), with increments of 3 degrees. As mentioned before, the range chosen for the flexion angle was based on the typical range of motion observed while performing the reach task, which is one of the most important upper-limb functional tasks that are in the basis of most daily-life routines. During the experiments, no degradation in-use of the fiber was observed.

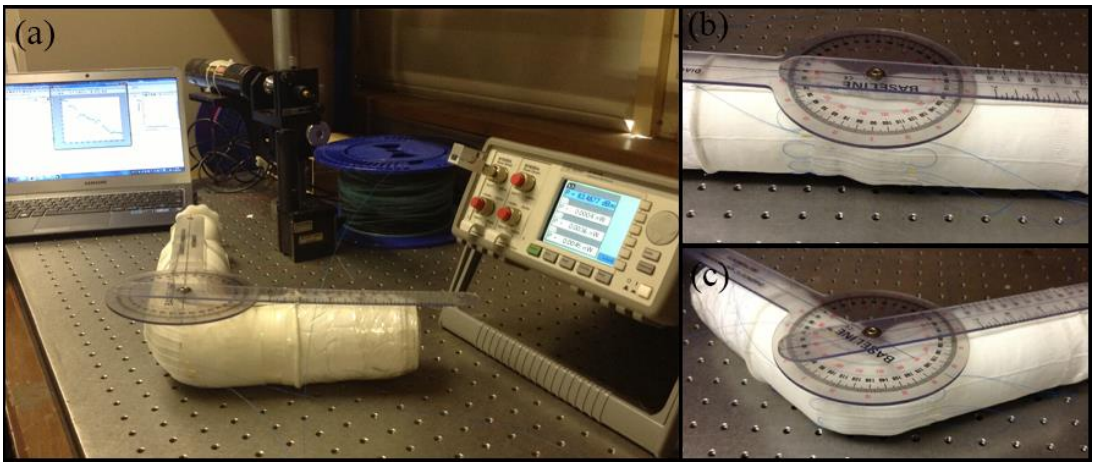

Figure 43: (a) Experimental setup; (b) sensor at rest position (0º) and (c) sensor at maximum elbow flexion (60º).

Results and Discussion

The results of the measurements for each sensor configuration are shown in Figure 44.

Each graph shows the output light power for all ten measurements (small circles) for a given angle, the corresponding average (large circles) and standard deviation, as well as a linear fit (shown in red) between the light power and the flexion angle.

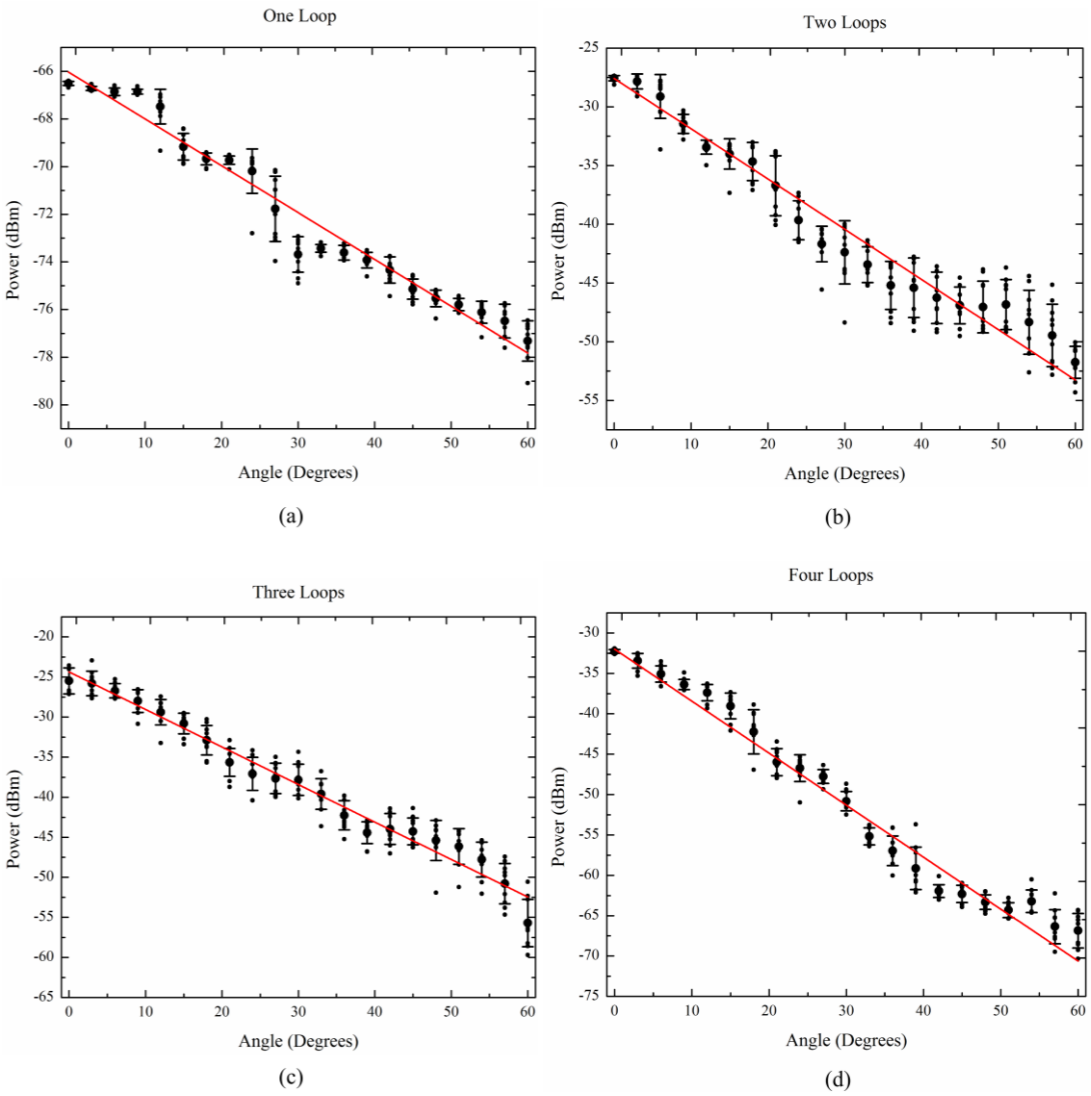

Figure 44: Light output power variation with increasing elbow flexion angle for (a) single loop, (b) two loops, (c) three loops and (d) four loops configurations.

Overall, all configurations show losses in optical power as the angle increases, as expected. Concerning sensor response, the way the optical fiber behaved inside the channels on the fabric as the flexion angle increased changed between configurations and, consequently, influenced the sensitivity of the sensor device. For the single loop scheme, the sensitivity is dictated by the decrease on the curvature radius of the only loop present and, as one can see on Figure 44 (a) the light losses due to bending do not change uniformly as the flexion angle increases. In fact, it is possible to note that the sensitivity is smaller for smaller angles (until approximately 15º) and likewise the variability

between repetitions increases. One can also observe a lack of resolution on the sensor response; however this limitation is caused by the resolution of the acquisition equipment used for this experiment.

For the second case, i.e., two loops configuration, the sensor response is a consequence of a symmetric decrease of both curvature radius. Thus, the sensitivity of this configuration is approximately the double of the single loop scheme. It should be noted the high variability between samples for this sensor (see Figure 44 (b)).

Concerning the three loops scheme, shown on Figure 44 (c), one should assume a higher sensitivity when compared with the two loops configuration. In fact, there is a slight increase of the sensitivity, but the difference is not as high as it should, theoretically, be expected. This behaviour can be explained by the way the curvature radius decreased as the flexion angle increased: the inner loop (referred as number 2 in Figure 42 (c)) has a different behavior from the outer loops (1 and 3), which translates into a behaviour similar to the one seen on the two loops configuration. Therefore, the sensitivity of this scheme is very close to the two loops sensor. However, the dispersion between the ten repetitions for this configuration is smaller than the previous case.

Finally, during the experiments with the four loops scheme (Figure 44 (d)) it was possible to see that the decrease on the curvature radius of the outer loops (referred as numbers 1 and 4 of Figure 42 (d)) and the inner loops (2 and 4) was different from each other, which reflected in an increase of the sensitivity of approximately the triple of the sensor with a single loop. Additionally, this configuration provided the best approximation to a linear response.

A comparison between the sensitivity of all configurations is shown in Figure 45. Table 8 presents the values of sensitivity, correspondent standard deviation and R-squared of the linear fit for all configurations.

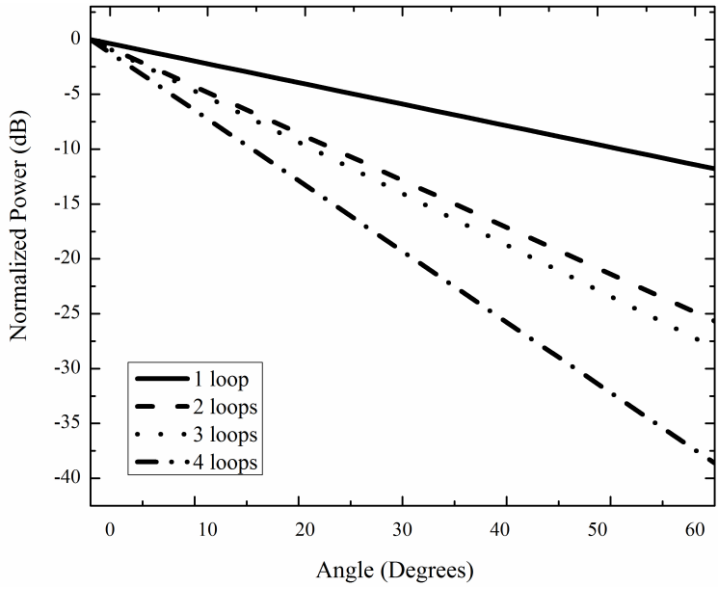

Figure 45: Comparison of sensor response for the four configurations studied.

Table 8: Sensitivity, standard deviation and R-squared values for each sensor configuration.

Sensor Scheme	**Sensitivity** (dBm/degree)	**Standard Deviation**	**R-squared**
1 Loop	0.197	0.008	0.963
2 Loops	0.42	0.01	0.985
3 Loops	0.46	0.01	0.982
4 Loops	0.64	0.01	0.989

Looking at these values it is clear that the configuration that assures a higher sensitivity, i.e. 0.64 dBm/degree, is the one with four loops, as expected. In fact, this sensor has a sensitivity 3 times higher than the single loop configuration and almost 1.5 times higher than the two and three loops schemes. Additionally, this configuration provided the best approximation to a linear response.

3.3. Summary

Fiber optic sensors are a relatively new concept for the measurement of biomechanical variables. Besides the advantages of small size and weight, electromagnetism and radio-frequency immunity, these sensors have high sensitivity and accuracy which makes them a good alternative for conventional electrical sensors.

In the previous section a simple intensity-modulated fiber optic sensor was designed and characterized to determine elbow flexion. This movement is the first phase of the reach task and one of the most important features physiotherapist evaluate in order to score stroke survivors performance.

A customized piece of garment was specifically designed to integrate the optical fiber sensor making it truly wearable. Different sensor configurations were studied and light loss resulting from bending was measured with an elbow angle ranging from 0º to 60º. Results showed that, when compared to other sensor configurations, the four loops scheme had a good sensor response in what concerns linearity, sensitivity and repeatability. The sensitivity for this configuration (0.64 dBm/degree) was 3 times higher than the single loop scheme and approximately 1.5 times higher than the three loops configuration. This wearable sensor has demonstrated a good response to elbow flexion and, when compared with traditional sensors, such as electrogoniometers, it can overcome some hurdles such as sensor alignment and ergonomy, and can also provide automatic means for monitoring human movement without the dependency on therapists or other end-users.

Since the proposed system revealed good performance for the determination of elbow flexion, it is simple to handle and comfortable for the user, it has a great potential for rehabilitation, especially to monitor upper-limb intervention progress of stroke patients, identify relevant compensatory movement strategies and help physicians with their clinical reasoning process. For swimming analysis, the proposed sensor represents a breakthrough for determining human segments angles in real-time, although some efforts need to

be done in order to insulate the electrical part of the system (light emitter, photodetector, etc.).

PART II

HUMAN MOTION ANALYSIS

SPORTS AND REHABILITATION

Chapter 4

SWIMMING PERFORMANCE ANALYSIS

Swimming is a technically challenging sport. The forward displacement during swimming results from the ratio between propulsive and resistive forces. From the biomechanical point of view, swimming performance depends on the mechanical interaction between water and the dynamical actions of a swimmer's body.

Swimmer's propulsion results from angular movements of the superior and inferior limbs and their synchronization. The mechanics behind propulsion were first considered as an application of Newton's Third Law: the hand and the forearm push dense masses of water backwards in a straight line to propel the swimmer's body (Lauer, Figueiredo, Vilas-Boas, Fernandes, & Rouard, 2013). In fact, to generate high propulsive forces, a swimmer must perform a complex cyclic motion. However, swimmer's body and movements do not generate exclusively propulsive forces. In truth, it is well-known that body orientation and volume contribute significantly for motion resistance. Whereas some factors are more difficult to be changed in order to reduce resistance forces, since they are intrinsic to body characteristics or swimming style, other factors such as body orientation in the water or angular adjustments of specific segments can be easily improved to reduce some of the resistance forces and the production of waves. Several studies report that the angle formed between the swimmer's body and the horizontal plays and important role in swimmers' forward displacement: if the legs are deep into the water than the drag coefficient increases (Bächlin, Förster, & Tröster, 2009). Also, the body and head rotations contribute to increase resistive forces. It can be said that the

generation of resistance forces is inherent to self-body locomotion inside the water.

At a constant speed, the total body drag, representing the resistive force, is equal to the propulsive force. If the swimmer needs to increase speed, i.e. accelerate, then propulsive forces need to be greater than the total drag. Speed fluctuations are quite visible in breaststroke technique, due to the intermittent propulsive movement of the limbs and the drag of the underwater recovery movements. Less evident speed fluctuations occur in butterfly technique, since the over-water arm recovery eliminates the drag caused by the underwater recovery in the conventional breaststroke, and the wave-like movement provides more or less a continuous propulsion. A more constant body speed is observed in the crawl technique because the limbs operate to generate propulsion forces throughout the total stroke cycle (Soares, 2000).

In the field of swimming, specifically when considering high level swimmers, the analysis of swimmers performance plays a crucial role. Monitoring physiological and biomechanical parameters of athletes during training allows analyzing and describing phenomena through which is possible to establish explanations for some movements and postures and thus hydrodynamic consequences. Moreover, the analysis of such parameters can allow the optimization of swimmers technique in order to increase their performance and decrease the risk of injuries. The relevance of biomechanical swimming performance analysis is systematized in the diagram shown in Figure 46.

Commonly used assessment techniques can be separated into different areas, such as performance, kinematics and physiology, although there is considerable overlap between them. Performance monitoring contains measurable movements of the swimmer during the monitoring period and typically times related to their movement. Kinematic monitoring, a detailed part of performance analysis, uses direct and indirect measurement methods to quantify the movement of the swimmer, often to map them to theoretical models. Physiological investigations mainly look at the energy systems of the

athlete during training, competition and recovery (Daniel A. James, Burkett, & Thiel, 2011).

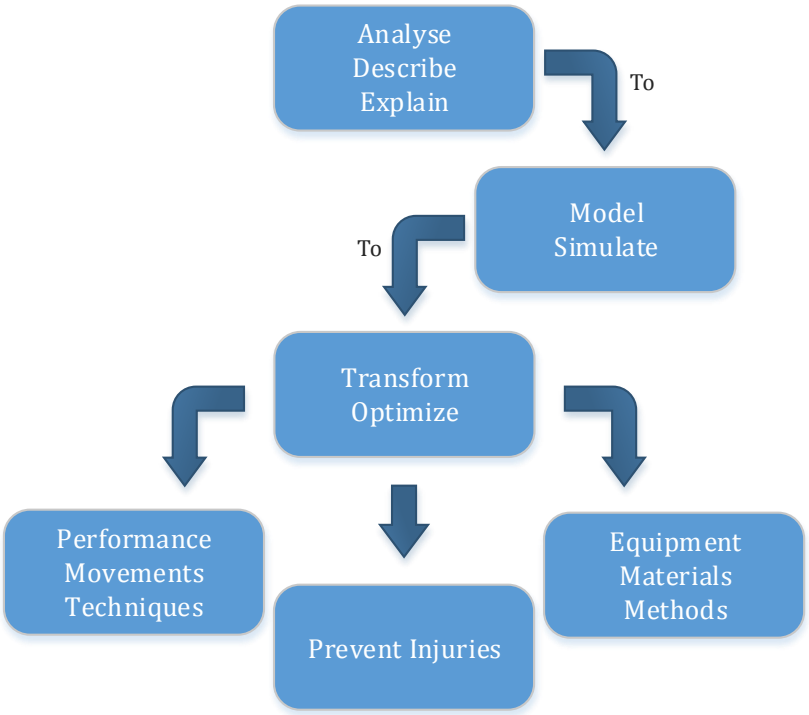

Figure 46: Biomechanical relevance in swimming analysis.

4.1. Wearable Systems for Swimming Analysis

Nowadays we know more about the best and most efficient swim techniques than several years ago, but the swimming performance evaluation methods are still basic the same. There are three main observation methods (Bächlin & Tröster, 2011):

- Self-perception: the swimmer ‘‘feels the water’’ and can react to perceived forces;
- Supervision by the coach: is the most frequently used observation method. The coach can give direct instructions to the swimmer but he can only observe one swimmer at a time. Observation by the coach also has its limitations, as movements below the water surface are difficult to observe;

- Video analysis: is the most objective evaluation method. However, video analysis can only be done offline, it is time-consuming, and the swimmer cannot correct his errors instantly.

Analysis of swimmers' kinematics through video-based systems is a challenging problem because of the difficult experimental conditions that affect the cameras setup. 2D analyses require a single camera; points of interest are digitized on each video and analysis of movement on the sagittal plane is performed (Holthe & McLean, 2001). Since the motion in front-crawl swimming occurs on different planes (Schleihauf, Gray, & DeRose, 1983), for a descriptive analysis of three-dimensional (3D) motion a multi-camera setup is needed, which requires not only calibration, but also synchronization of the cameras (Figure 47).

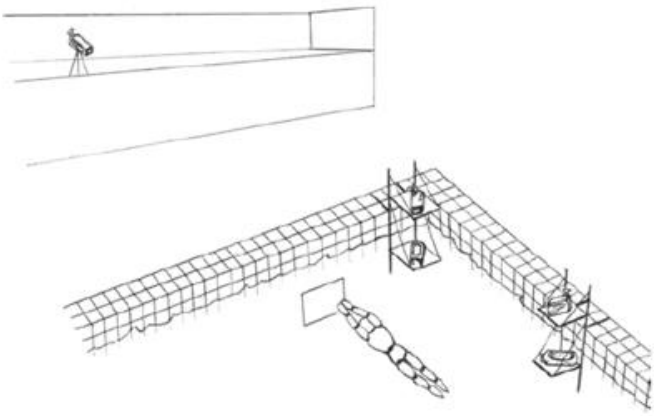

Figure 47: Multi-camera experimental setup used to determine to swimmer's instantaneous velocity (adapted from (Barbosa, Fernandes, Morouco, & Vilas-boas, 2008)).

These procedures are hindered by the underwater experimental environment: refraction of light rays causes image deformations, yielding to lower accuracy, and the equipment must comply with safety regulations (Gourgoulis et al., 2008). Furthermore, videos are analyzed by manual digitization of feature points on all images, which may correspond to either visual markers drawn on the subject or crucial points, such as joint centers, identified by the operator. This procedure has two main drawbacks: it is time-consuming and can easily lead to misidentification of features, especially when a

large number of points are involved. The adoption of markers constituted of LEDs has allowed to automate the tracking process, but investigation so far has mainly regarded identification of areas instead of single points, and motion on the sagittal plane (Slawson, Conway, Justham, & West, 2010). Recently, markerless analysis of swimming performance has been introduced (Aguiló, Martinez, Buades, Perales, & Gonzaléz, 2004). This approach uses a semi-automatic method to synthesize underwater motion by adjusting a ‘‘virtual human’’ model to the morphology of the subject. Nevertheless, no biomechanical validation of the model has been carried out. The approach proposed by Ceseracciu et al. (2011) adapted the markerless video method described by Corazza et al. (2010) to determine arms movement during crawl swimming. Nevertheless, information from out-of-water cameras could not be easily integrated with the underwater views because of the issues related to the water–air interface, such as waves and foam.

For swimmers there are only a few commercial swim-timer devices available, which can be used to measure lane times and to count the number of lanes swum. There are devices to be placed on the pool wall, e.g. the Finis Lap Track 5[12] or worn on the swimmers finger, e.g. SportCount Chrono[13]. They are based on push buttons and displays.

In-stroke variations of swimming velocity is an important feature for athletes and coaches. Traditionally, swimming velocity is estimated using video-based systems (Takagi, Nishijima, Sugimoto, & Wilson, 2004; Tella et al., 2008) or tethered methods (Geiser, 1999). Dopsaj et al. (2000) used tethered methods to determine swimming force and velocity while Mouroço et al. (2006) developed a cable speedometer to investigate butterfly swimming techniques through changes of velocity profiles. Tethered methods have some drawbacks due to its complicated setup and the cabling attached to the swimmer (Khoo, Lee, Senanayake, & Wilson, 2009).

[12] http://www.finisinc.com/
[13] http://sportcount.com/

In 2008, Justham et al. published a critical evaluation of existing analysis techniques in swimming, and concluded that more thorough feedback could be provided through the use of inertial sensor technology (Ride, Ringuet, Rowlands, Lee, & James, 2013).

The last decade has noticed an increasingly number of inertial-based systems for swimming performance analysis. Estimation of velocity is one of the most investigated feature of swimming. Most of the existing systems use offline post-processing algorithms to determine velocity and acceleration profiles of different swimming techniques (Seifert, Chollet, & Bardy, 2004; Siirtola, Laurinen, Roning, & Kinnunen, 2011; Stamm, Thiel, Burkett, & James, 2011). Ohgi (2002) described a wrist-mounted tri-axial accelerometer that was used to discriminate stroke phases in front crawl and breaststroke techniques. Khoo et al. (2009) used a combined system of underwater cameras and head-mounted accelerometers to compare left and right handed stroke acceleration values. Le Sage et al. (2010) proclaimed a system comprising vision analysis with real-time image processing, a Body Sensor Network (BSN) of inertial units and force transducers at the end of the pool for real-time monitoring of swimmers' performance. So far, the results have allowed to extract in real-time the stroke rate, stroke duration and lap count. Pansiot & Guang-Zhong (2010) used a modified ear-worn activity recognition (e-AR) sensor mounted on swimmer's goggles to analyse stroke phases in front crawl (see Figure 48).

(a)

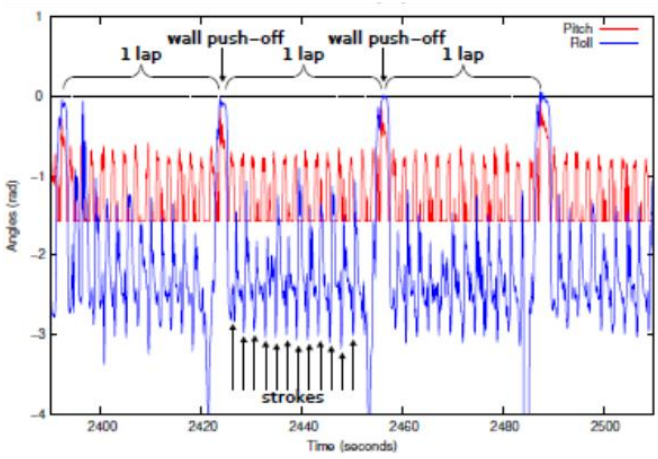

(b)

Figure 48: Swimming analysis using accelerometers: (a) sensor placed on swimmer's goggles; (b) pitch and roll angles in front crawl swimming.

Several comparison studies between video-based systems and inertial wearable technology have been reported (Daukantas, Marozas, Lukosevicius, Jegelevicius, & Kybartas, 2011; Davey, Anderson, & James, 2008). These studies focus on validating inertial measurement units as reliable instruments to analyse swimming performance. Results have shown that accelerometer-derived features can be as good as or even better than collected video data (Davey et al., 2008).

One aspect that is crucial in swimming analysis is feedback. Video-based systems fail to provide swimming features in a time-frame that is useful for athletes and their coaches. Real-time feedback can be delivered through wearable technology, specifically inertial units, since important swimming characteristic can be extracted with embedded algorithms and be wirelessly

transmitted to a remote station for visualisation. Nevertheless, wireless transmission is not as trivial as it seems at the beginning. The water-air interface represents a barrier which is difficult to overcome using standard wireless protocols, such as ZigBee or Bluetooth. In fact, studies have demonstrated that significant data can be lost if air transmission path overcomes 1 meter distance (Hagem, Thiel, O'Keefe, Wixted, & Fickenscher, 2011; Daniel A. James, Galehar, & Thiel, 2010). As an alternative, transmission antennas operating in different frequency bands can be used, but its size and limited data rate are prohibitive (Abbosh, James, & Thiel, 2010). Different strategies for providing feedback to swimmers can be adopted, as the one described by Hagema et al. (2013) which consists of a wrist-mounted accelerometer which calculates time difference between strokes and activates a LED which makes swimmer react according to light colour.

4.2. Swimming Analysis through WIMU

In swimming analysis some of the most important parameters to be monitored can be divided in two groups:

- Performance parameters:
    - Time and distance;
    - Average velocity;
    - Number of laps;
    - Number of strokes, stroke length and frequency.
- Kinematic parameters:
    - Angular positions of body segments;
    - Linear velocity and acceleration profiles;
    - Angular velocities.

The above mentioned parameters can be obtained through inertial sensors, either directly from sensors outputs or indirectly by applying the principles described in Chapter 2. The estimation of such parameters can be used to characterize swimmer’s movements and allow for the comparison of

different experience level swimmers and to differentiate between swimming styles.

When analyzing swimmer's performance through accelerometers, some of the equations presented in Chapter 2 for angles estimation can be simplified. This is because of the nature of swimming movements. Typically, the inertial units are placed at the upper back or at the lower back, which is expected to better correspond to the center of mass of the swimmer. The upper back location is often preferable since it is more accurate when detecting strokes, turns and styles (Siirtola et al., 2011). Movements at this region are very slow and body (dynamic) acceleration is small when compared with gravity (static acceleration). Thus, swimmer's movements can be considered as non-accelerated movements and a quasi-static condition can be adopted. The application of this assumption has revealed very good results when compared with video-based systems (Bächlin & Tröster, 2011; Daukantas et al., 2011; Pansiot et al., 2010). In this case the extraction of some angular positions can be done using only the information given by the accelerometer. The acceleration measured by the accelerometer, a^b, depends on the actual acceleration of the system, a^n, the orientation (given by the Direction Cosine Matrix, Equation 8 of Chapter 2) and gravity, g:

$$\begin{bmatrix} a_x \\ a_y \\ a_z \end{bmatrix}^b = C_n^b \left(\begin{bmatrix} a_x \\ a_y \\ a_z \end{bmatrix}^n + \begin{bmatrix} 0 \\ 0 \\ -g \end{bmatrix} \right) \tag{21}$$

Considering that $\|a^n\| \ll g$, Equation 21 can be simplified to estimate:

$$\begin{bmatrix} a_x \\ a_y \\ a_z \end{bmatrix}^b = -g \begin{bmatrix} \cos\varphi \sin\theta \\ \sin\varphi \\ \cos\varphi \cos\theta \end{bmatrix} \tag{22}$$

Therefore, the pitch and roll angles can be derived from the measured acceleration as follows:

$$\theta = -\tan^{-1}\left(\frac{a_x^b}{a_z^b}\right) \tag{23}$$

$$\varphi = -\sin^{-1}\left(\frac{a_y^b}{g}\right) \tag{24}$$

The estimation of such angles can give information about alignment of the body. Vertical alignment, also referred to as body balance, is associated with the angle between the swimmer's body and the water surface (pitch angle); Horizontal alignment, or body rotation, refers to the swimmer's body rotation along his own longitudinal body axis (roll angle) (see Figure 49).

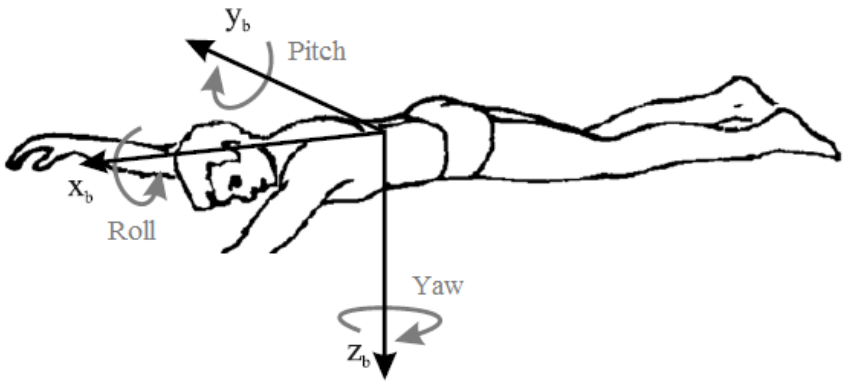

Figure 49: Body coordinate system. Body balance and body rotation can be estimated from the pitch and roll angles, respectively.

A good body balance is important for efficient swimming as drag forces are reduced. There are several possible reasons for a bad body balance, for example weak leg kicks, a weak body tension or a bad posture of the head due to looking upwards instead of aligning spine and head. Body rotation is efficient in crawl and backstroke swimming because the stroke length can be increased and the side-lying gliding position is the body position with the least water resistance. The body rotation can be initiated by the leg kicks. The upper and the lower body part should rotate together, because a synchronized rotation leads to a fluent motion (Bächlin, Förster, & Tröster, 2009). The roll angle information is also useful for breathing studies and to determine the number of strokes (Siirtola et al., 2011).

The study described in this section presents the main outcomes accomplished with the inertial measurement unit referred to as WIMU in the first part of this thesis, to measure the performance of a swimming athlete.

Experimental Procedure

During the experimental tests the WIMU was located at the dorsal zone of the coronal plane of the swimmer, within the vertebral region at the inferior scapular section, as can be seen on Figure 50. This location was chosen in order to measure, in addition to the accelerations on the three axes, the longitudinal rotation of the trunk and body balance. As mentioned before, these parameters can be considered a useful factor when evaluating swimming performance, due to its correlation to the displacement velocity. Another important consideration was the comfort of the swimmer and avoiding restricting or modifying their average sequence of movements.

Figure 50: WIMU positioned at the upper back of the athlete.

A female athlete in her late teens served as the main tester. Before entering the pool, the swimmer was required to perform a number of flexibility related routines, in order to determine movement constraints. Once in the pool, she was asked to swim, submerge and perform various movements in order to determine if the WIMU's presence represented an obstruction to her movements. In both cases (outside and inside the pool) the swimmer reported that the unit did not affect her movements. Finally, the swimmer was told to

complete several sets of laps using the crawl technique, then a number of laps with, butterfly and finally breaststroke. For all styles indicated, the turn at the end of the pool was perform through a vertical turnaround (i.e., stop-touch wall turnaround), reversing direction without flipping under water.

Although data gathering for the crawl techniques laps did not required signal compensation strategies, the butterfly and breaststroke techniques did present some data gaps. The recorded data was later processed applying compensation techniques (interpolation).

Results and Discussion

The acceleration signals (in units of g's) for two laps crawl technique are shown in Figure 51. Considering these signals, the X-axis points opposite to the direction of displacement and together with the Y-axis form the coronal plane of the subject; while the Z-axis is pointing inwards to the subject, forming the sagittal plane with the X-axis and the transversal plane with the Y-axis.

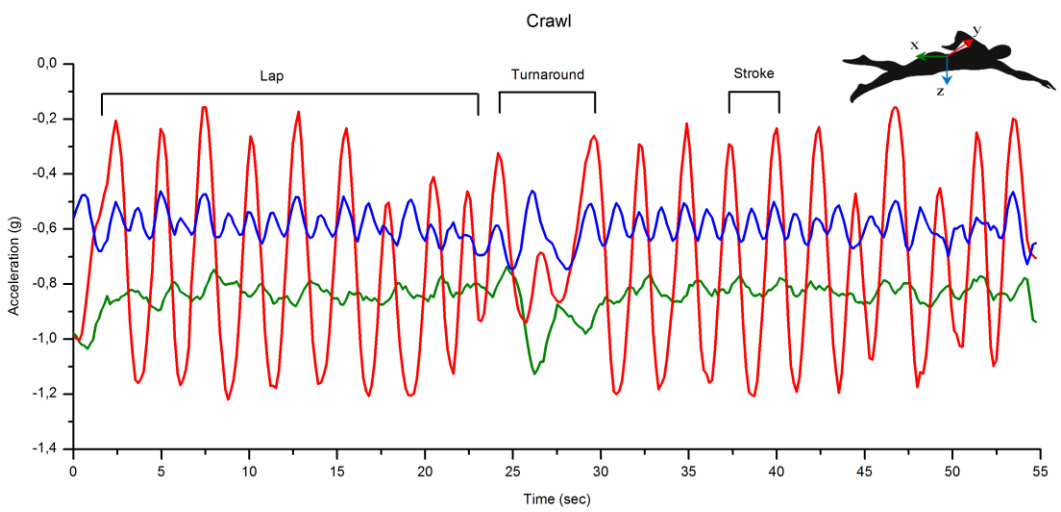

Figure 51: Acceleration in all three axes (X-axis: green; Y-axis: red; Z-axis: blue) for two laps crawl technique.

As mentioned before, performance parameters such as the number of strokes, number of laps or start/end of lap can be directly taken from the accelerometry profiles. As expected for crawl technique, higher acceleration amplitudes occur in the Y-axis, which relates to rotation movements around the

X-axis, corresponding to arms strokes. A direct analysis also allows to quantify the time between each arm stroke and its evolution along each lap, as shown in Figure 52.

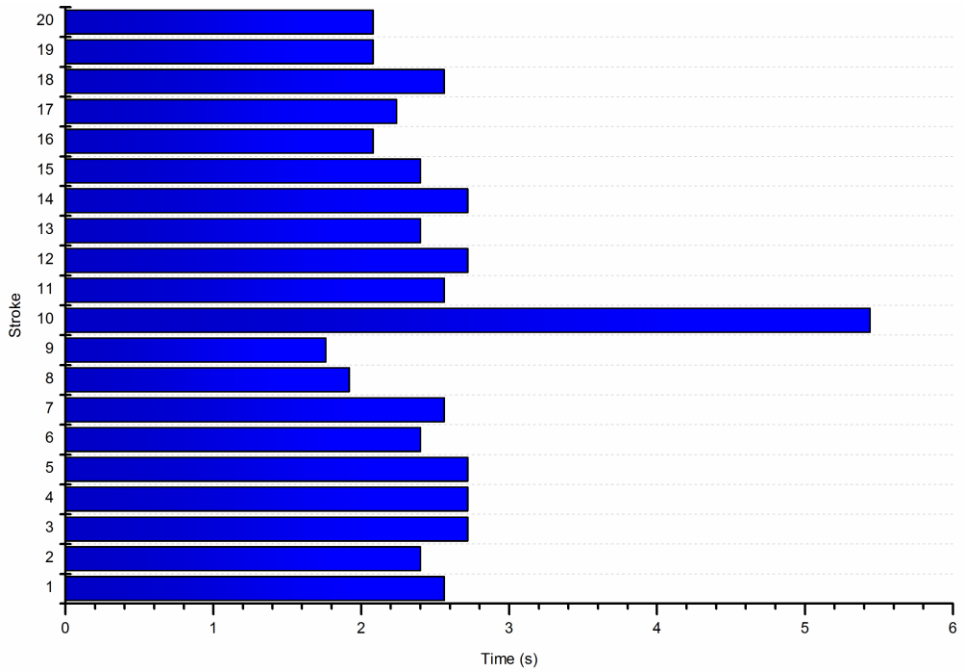

Figure 52: Elapsed time between each stroke for two laps. The 10th stroke corresponds to lap end, i.e. vertical turnaround.

Table 9 summarizes some relevant performance features extracted from the accelerometry profile.

Table 9: Some relevant performance parameters extracted from accelerometry data for crawl technique.

	Lap 1	**Lap 2**
Duration (s)	24.16	23.84
Number of strokes	9	10
Stroke frequency (Hz)	2.68	2.38
Average stroke duration (s)	2.41±0.33	2.38±0.24

Equivalent lap sections acceleration signals (in units of g's) for different swimming techniques are presented in Figure 53.

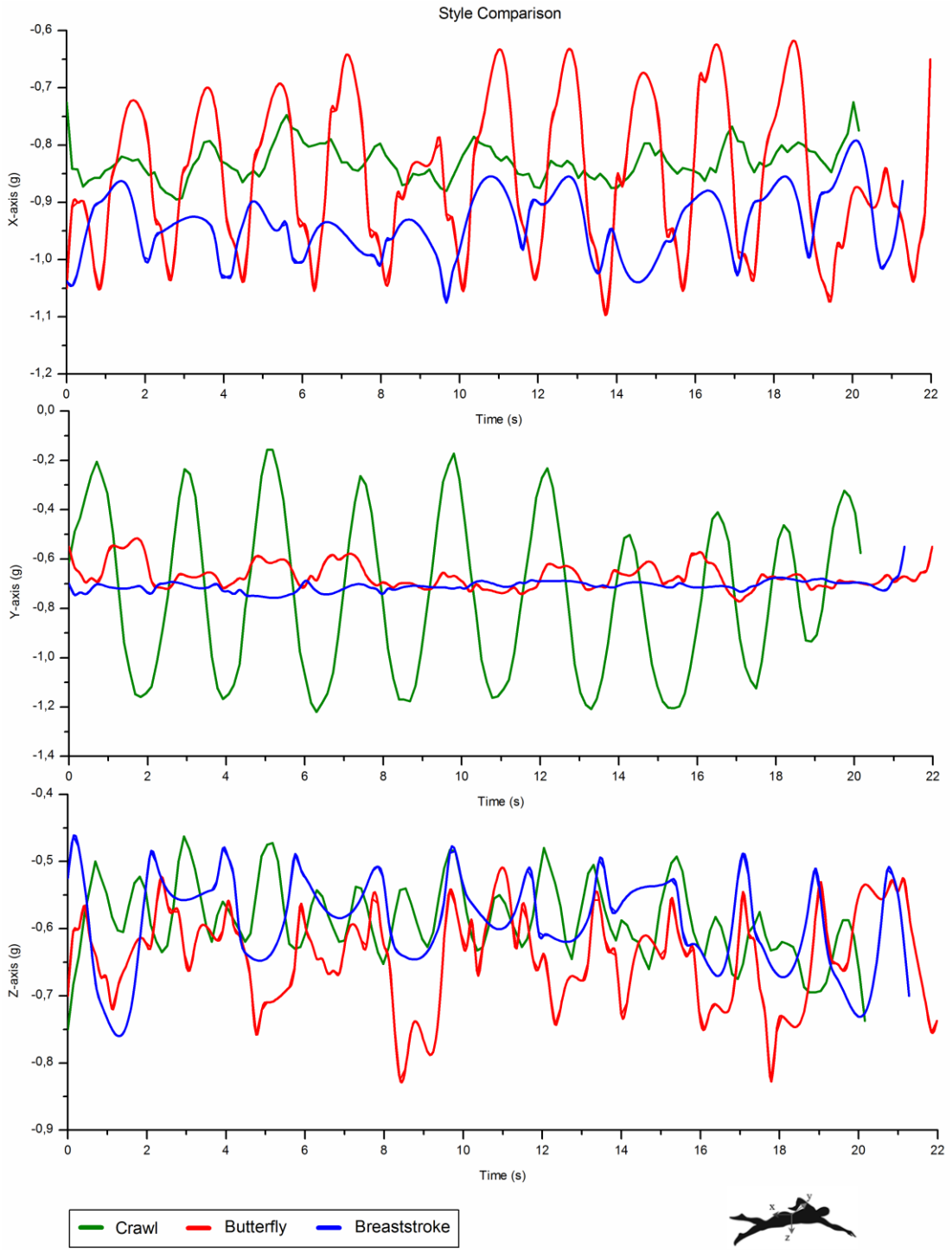

Figure 53: Equivalent lap section acceleration signals for each performed technique.

Crawl, butterfly and breaststroke styles were evaluated for each movement axis. Observing the graphs concerning each swimming technique, it was possible to differentiate between styles. For example, crawl technique can be readily distinguish from breaststroke and butterfly by the signal provided by

the accelerometer in Y-axis. This signal presents large variations for the crawl technique, while for the other styles these variations are comparatively small. Alternatively, the butterfly and breaststroke technique can be differentiated from each other from the data produced by the accelerometers in the X-axis, or the longitudinal axis.

As mentioned in the beginning of this section, pitch and roll angles can be estimated from acceleration signals. These values provide a better understanding about the swimmer's movements to progress in the water and to minimize drag.

The pitch angle, which is related with the angle formed with the horizontal, for one lap crawl, butterfly and breaststroke techniques is presented in Figure 54.

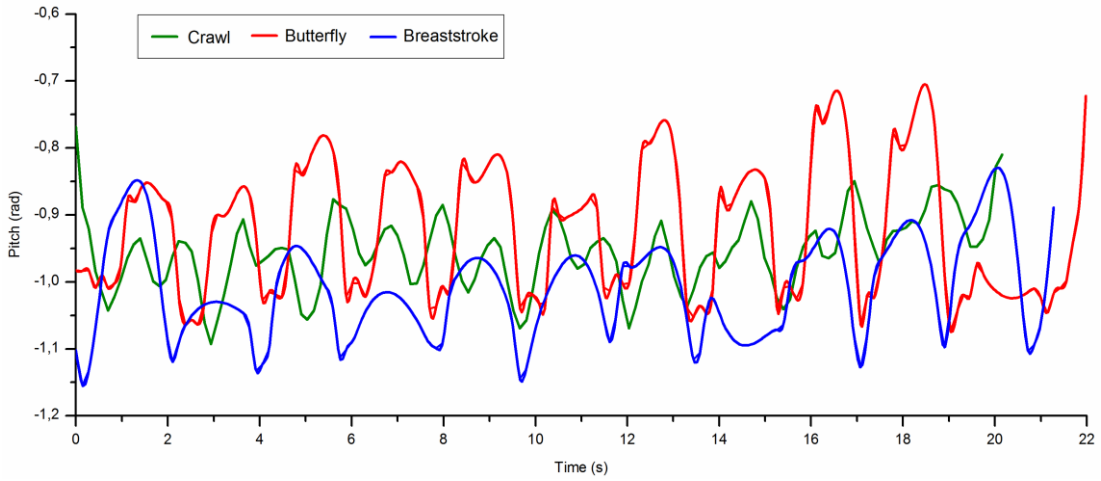

Figure 54: Pitch angle for one lap crawl, butterfly and breaststroke techniques.

As expected, variations in the pitch angle for the butterfly technique are higher when compared with the other styles. In addition, it is clear to observe double-bell shapes of this signal, each corresponding to a single stroke. This behaviour is strongly related with this swimming technique pattern, which is characterized by two leg movements (the first when entering the water and the second at water exit) in each cycle or stroke (Soares, 2000).

The roll angle for all the evaluated techniques, i.e. crawl, butterfly and breaststroke, is shown in Figure 55. As one should deduce, the crawl technique exhibits roll angles with a higher amplitude, due to the swimmers' rotation along the longitudinal axis. It is expected that both butterfly and breaststroke techniques have small body rotations.

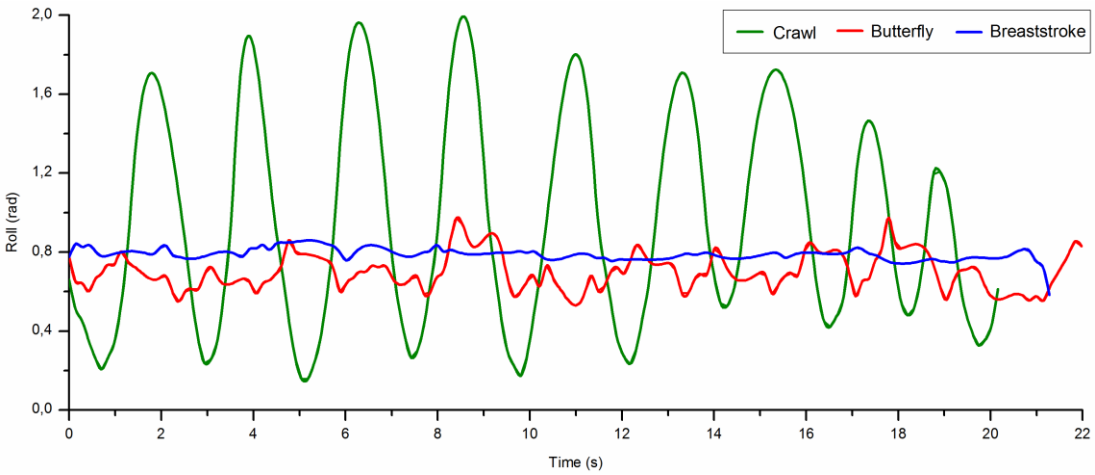

Figure 55: Roll angle for one lap crawl, butterfly and breaststroke techniques.

4.3. Summary

The leading method for swimming analysis is based on image processing of video data. Nonetheless, there are some hurdles to overcome due to time-consuming setup and data processing procedures and also due to water interference at the air-water interface (waves and bubbles, for instance). The use of wearable technology, such as inertial measurement units, allow the extraction of meaningful features that can be transmitted to the swimmer or coach, providing real-time feedback of swimmer's performance. In addition, the information from these systems can be combined with other systems in order to overcome some of the obstacles mentioned before.

In this chapter, results from accelerometry data acquired with the WIMU device are presented. The WIMU was placed at swimmers' backs and

movements were acquired for different swimming techniques. It was possible to obtain acceleration profiles for each style, allowing the identification of the number of laps swam, lap turnaround, number of strokes, stroke frequency and duration. The pitch and roll angles for each swimming technique were estimated and differences between each technique were identified from these profiles.

Chapter 5

POST-STROKE PATIENTS MOVEMENT ANALYSIS

Stroke is defined as an acute neurological dysfunction of vascular origin with rapid onset of signs and symptoms according to the committed areas of the brain (World Health Organization, 2011). Generically, it can be understood as an acute interruption of blood flow caused by vessel blockage (thrombosis, arterial embolism), or a rupture on the blood artery (A. O. Silva, 2007).

Strokes can be classified into two major categories: ischemic and hemorrhagic. Ischemic strokes are those that are caused by interruption of the blood supply, while hemorrhagic strokes are the ones which result from rupture of a blood vessel or an abnormal vascular structure (A. O. Silva, 2007). About 87% of strokes are caused by ischemia, and the remainder by hemorrhage (World Health Organization, 2011).

Risk factors for stroke include old age, high blood pressure, previous stroke or transient ischemic attack (TIA), diabetes, high cholesterol, tobacco smoking and atrial fibrillation. High blood pressure is the most important modifiable risk factor of stroke.

In post-stroke subjects, the ability to efficiently perform functional tasks can be substantially modified (Achache et al., 2010; Milot, Nadeau, Gravel, & Requiao, 2006). Difficulties in these functional tasks are mainly attributed to impairments resulting from central nervous system (CNS) lesion, being the middle cerebral artery (MCA) territory the most common affected area after stroke (Ng, Stein, Ning, & Black-Schaffer, 2007). Neuro-motor dysfunctions after MCA stroke affect predominantly the upper-limb and face, and less the lower-limb (Shelton & Reding, 2001).

Considering that stroke is the most important cause of morbidity and long-term disability in Europe, this clinical condition represents a major burden on healthcare system.

5.1. Rehabilitation Protocols and Procedures

An in depth understanding of the human body in everyday scenarios and advanced skills in physical assessment, allow physiotherapists to manage a broad range of conditions, with the fundamental goal of promoting wellness, mobility and independent function (Tate, 2006). Despite these well stated skills, most current evaluation procedures still lack some objectiveness since they rely mostly in clinical assessment scales, which, although very useful, are influenced by a certain degree of subjectivity. The development and implementation of objective measures within rehabilitation evaluation procedures may contribute to enhance clinical reasoning and potentiate rehabilitation efficiency.

Modern technological developments for rehabilitation must consider low-cost adaptable solutions, which can be integrated in everyday scenarios as opposed to rigid strategies meant for limited usability. Rehabilitation interventions should specifically address the individual's impairment; present sufficient difficult as to challenge the motor system and integrate strategies to develop transfer of performance gains from the training situation to everyday life (Strong, Mathers, & Bonita, 2007). Post-stroke rehabilitation reality is far from being ideal, from both a clinical and economical points of view. Considering that there were an estimated 10.3 million first-ever stroke survivors worldwide in 2005 (Strong, Mathers, & Bonita, 2007) and stroke is projected to remain a leading cause of disability-adjusted life years through 2030 (Lopez, Mathers, Ezzati, Jamison & Murray, 2006), stroke care represents a major burden on global healthcare expenditures, representing about 3% of healthcare costs (Evers et al., 2004). Despite the elevated related cost, there is a general agreement on the importance of addressing the sequels of stroke. Although there are well establish beneficial effects of timely and continuous

managed rehabilitation (Tate, 2006), there is a clear need to improve its quantity, quality and overall effectiveness.

A crucial aspect guiding physiotherapist's clinical reasoning, and thus design of rehabilitation intervention, is the assessment of motor performance. According to some authors (Evers et al., 2004), implementing therapeutical programs requires accurate clinical and field measurements based on motor pattern identification not readily available from traditional tools. Standardized clinical motor assessments rely on physiotherapists observational skills, which as necessary as it may be considered, remains insufficient for reliable measurement of certain quantitative features (e.g., intersegment coordination, quality of movement and smoothness). Moreover, observation-based assessment is subject to observer error and personal bias and is limited to the human visual perception, just to mention some of the most common handicaps. The Rivermead Motor Assessment (RMA) (Adams, Pickering, Ashburn, & Lincoln, 1997), Fugl-Meyer Motor Assessment (FMA) (Fugl-Meyer, Jaasko, Leyman, Olsson, & Steglind, 1975), Postural Assessment Scale for Stroke patient (PASS) (Benaim, Pérennou, Villy, Rousseaux, & Pelissier, 1999) and Reaching Performance Scale (RPS) (Levin, Desrosiers, Beauchemin, Bergeron, & Roschette, 2004) are examples of viable and considered reliable instruments commonly used in physiotherapy.

The FMA evaluates 33 items related to movements of the proximal and distal parts of the arm and the total score ranges from 0 to 66. A maximum score of 66 corresponds to typical motor function and clinical subdivision; while cases that score between 50–63 correspond to mild-to-moderate motor impairment; between 46-50 to a moderate (gross and some fine movement) to severe (gross motor function only) motor impairment (Fugl-Meyer et al., 1975). The RPS focuses on visual assessment of compensatory movements used during the transport phase of reaching, defined as the beginning of the movement until the object is grasped (Levin et al., 2004). Each component can be scored between 0 and 3, where 0 refers to maximum compensation and 3 to complete absence of compensation. The scores of the trunk displacement, movement smoothness, shoulder movements, elbow movements and quality of prehension components

allow for the identification of deficiencies in aspects specific to movement and these scores in conjunction with a global score can be added for a total score that can vary from 0 to 18, for each of the subcategories: close target and far target (Levin et al., 2004).

In what refers to evaluation instrumentation encountered in the laboratory environment, relevant to the field at hand, one can refer to electromyography scans, force platforms and complex image/video analysis systems, that introduce a degree of objectivity in the interpretation of events, augmenting the therapist/physician perspectives in what refers to functional and motor characterization (Gilmore & Spaulding, 2007; Lucca, 2009; Paten et al., 2010). However, such resources accessibility in clinical environment is scarce or null, restricting their routinely usage from clinical rehabilitation practices.

Physiotherapists clinical practice reality, concerning data gathering and recording, is far from being optimally effective, despite the World Confederation for Physical Therapy guidelines and other established protocols (Bury, 2003). In fact, this important step of the overall rehabilitation process is sometimes neglected and when present tends to be mainly subjective and qualitative, based on the therapist opinions and patient's provided information regarding movement restoration and overall progress (Bury, 2003). Such record-keeping varies from institution to institution, from therapist to therapist, and are not necessarily updated at each session; therefore a progressive evaluation based on such records remains subjective to the experience and interpretation of the reader, which clearly contributes to compromise results, both in progress and outcomes. Quantitative data records provide means for efficient and expedient analysis of the effectiveness of a therapy on a patient's progress, which provide a safeguard from negative activities that can go unnoted and unrecorded. Such an approach strengthens and streamlines internal technological platforms, expanding their coverage and added value and promoting the formulation of standards and protocols for monitoring patient progress, thus augmenting current guidelines.

5.2. Upper-Limb Movement Analysis during Reaching

The reaching gesture constitutes the most evident example of upper-limb's ability to organize itself in space, with specific goals, always related with a motor concretization (Shumway-Cook et al., 2007a; Shumway-Cook et al., 2007b). In fact, numerous daily-living activities require the coordinated action of the upper-limb segments, in order to successfully reach the target (Bernhardt et al., 1998; de los Reyes-Guzman et al., 2010). It is clear the importance of this functional tasks for post-stroke patients, for restoring independence and autonomy.

Commonly, reaching is divided in two components, the transport phase, which involves the translation of the hand from a starting position to the desired location; and the grasp phase, which involves hand shaping and the manipulation of the target, according to its characteristics (Jeannerod, 1984). Some researchers have divided the reaching movement according to postural control demands, as follows (see Figure 56) (Cláudia Silva et al., 2014):

- the first sub-phase, named as the elbow flexion phase, which includes the period since movement initiation till the maximum of elbow flexion; this phase requires a highly demanding proximal postural control; and
- the second sub-phase, here named as the shoulder flexion phase, starts when the elbow reaches its maximum flexion and ends when the target is reached; this phase is predominantly movement demanding, especially in the shoulder joint.

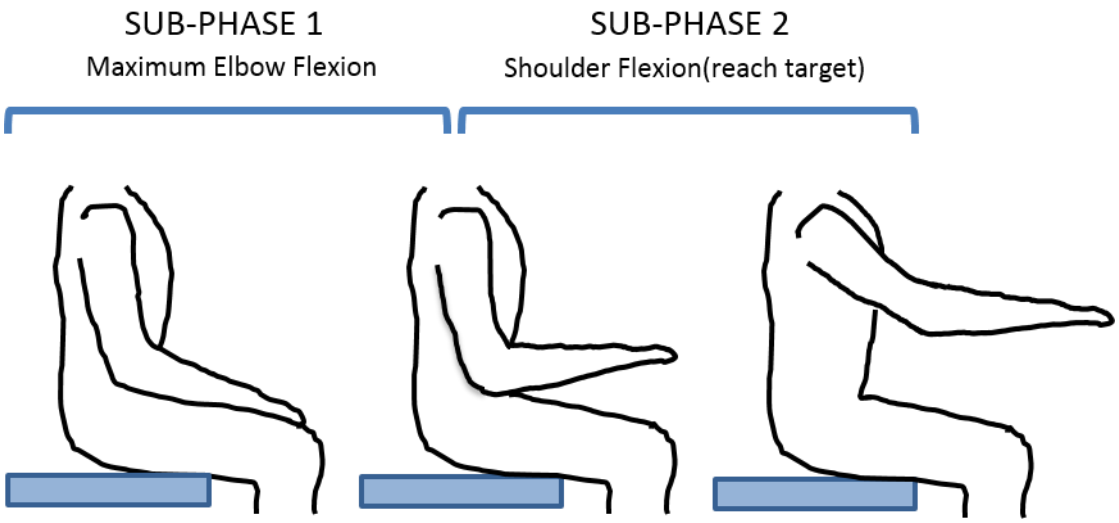

Figure 56: Reaching sub-phases according to postural control demands.

The upper-limb analysis is becoming an increasingly topic of interest among scientists and physiotherapists. Although most of the studies rely on image-based data acquisition and analysis systems (Mendonça, Santos, & López-Moliner, 2011; Teasell, Foley, Bhogal, & Speechley, 2003; Vandenberghe, Levin, De Schutter, Swinnen, & Jonkers, 2010), several research is starting to be conducted based on wearable sensors, more specifically through inertial measurement units (Paten et al., 2010; Pérez et al., 2010; Zhou et al., 2008). Some studies report classification algorithms of upper-limb performance (Patel et al., 2010; Zhe, Qiang, & Ferry, 2011) while others are focus on estimating qualitative scales scores, such as the FMA score, from accelerometry data (Del Din, Patel, Cobelli, & Bonato, 2011).

The analysis of the reaching movement in post-stroke patients and in healthy subjects was performed with the wearable system described previously as W2M2. Several studies were performed in order to establish a systematic protocol for the acquisition of inertial data and more important, to understand the mechanisms underlined in the execution of the reaching movement, both for post-stroke and healthy subjects. Therefore, the next sub-sections describe the experimental procedures and results achieved in these studies. All the participants of the studies were informed of the experimental procedures and provided written consent in accordance with policies of the institution's Ethics

Committee (see the Experimental Protocol approved by Ethics Committee in Appendix D).

5.2.1. Inertial Measurement Units Positioning

The presence of compensatory strategies is often observed in post-stroke subjects when attempting to reach an object. Although some controversy remains regarding the functional benefits of compensatory movements as a way of accomplishing a given task, studies suggest that such maladaptive strategies may limit the plasticity of the nervous system to enhance neuro-motor recovery. The study presented in the current section intends to aid in the development of a system for compensatory movement detection in post-stroke patients through accelerometry data, by analyzing the best sensor positioning for the identification of such strategies.

Participants

The sample was composed by two post-stroke patients receiving physiotherapy care at a rehabilitation center. Participants had to meet the following inclusion criteria:

- Confirmatory neuroimaging results of a single, unilateral stroke in the Medial Cerebral Artery (MCA) territory, sustained at least 3 months prior;
- Absence of hemispatial neglect;
- Absence of major visual, perceptual or cognitive deficits, confirmed by the mini-mental state examination (MMSE);
- Active range of motion in the compromised arm of at least 15 in the shoulder (flexion/extension; abduction/adduction and internal/external rotation) and elbow (flexion/extension) (Sveistrup, 2004).

Explicit exclusion criteria included cerebellar or brain stem lesions and pain/sub-luxation in the upper-limb. Arm motor impairment was evaluated prior to measurements, as seen on Table 10, with the arm subsection of the Fugl-Meyer scale and the Reach Performance Scale (close target). This clinical evaluation was performed by a team of three experienced physiotherapists with more than 10 years of clinical practice in neurological field.

At the time of the experiment, the post-stroke patients were following the conventional rehabilitation procedures associated with their condition, based on the Bobath Concept principles (Raine, 2009). This is a problem-solving approach for the assessment and treatment of individuals with disturbances of function, movement and postural control due to a lesion of the central nervous system (Raine, 2009) Although sitting balance was not measured directly, all subjects were ambulatory without aids and had no difficulty in maintaining a stable sitting posture during data collection.

Table 10: Demographic data and clinical scores of post-stroke subjects.

	Subjects	
	A	**B**
Age	49	47
Gender	Male	Female
Location of lesion	LMCA	RMCA
Months post-stroke	66	20
RPS score	5/18	12/18
FMA (shoulder, elbow, forearm)	4/36	20/36
FMA (wrist)	0/10	2/10
FMA (hand)	2/14	12/14
FMA (coordination)	0/6	3/6

LMCA/RMCA: Left/Right Medial Cerebral Artery
RPS: Reach Performance Scale
FMA: Fugl-Meyer Motor Assessment

Experimental Procedure

Each subject was assessed in the sitting position, with a table placed in front of him/her, at a height corresponding to the alignment of the iliac crests. The proximal table limit was coincident with the distal border of the subject's knees, so as not to interfere with the arm trajectory. The subjects started the task with approximately 0º of flexion/extension/internal rotation at the shoulder; approximately 100º of flexion at the elbow with forearm in pronation and the palm of the hand resting on the thigh. The subjects were instructed to reach a target placed ipsilaterally to the upper-limb in study, in groups of three repetitions (as to avoid variations due to fatigue) separated by one minute rest period.

The target's placement reference was the anatomical reaching distance of the hand, using the measured distance from the acromion to the metacarpophalangeal joint of the thumb (Vandenberghe et al., 2010). The individual was instructed, after verbal command, to perform reaching. Performance was video recorded for posterior visual cross-reference.

In order to insure sensor placement repeatability, precise bone landmarks were required. After a physiological study of the target area and experimental trial of sensor positioning for assured subject upper-limb mobility and comfort, the following positions were considered (see Figure 57):

- P1, placed under the acromion, following the line that connects the lateral epicondyle and the acromion;
- P2, placed on the middle point between lateral epicondyle and the acromion;
- P3, immediately above lateral epicondyle, in alignment with acromion;
- P4, immediately below the lateral epicondyle, after elbow articulation;
- P5 in the trunk over the T12 vertebra.

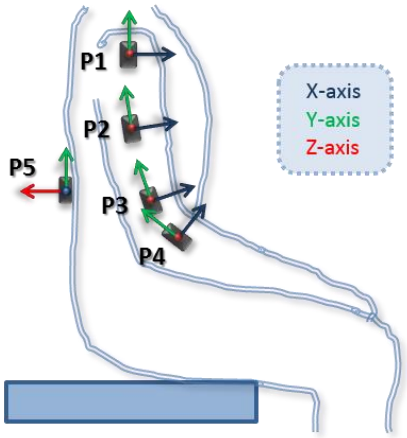

Figure 57: Sensor positioning under consideration.

Results and Discussion

A set of accelerometry data for subjects A and P is presented in Figure 58. The different colors represent a set of three different trials performed.

The inherent difference in acceleration amplitudes shown especially in X-axis between subjects is related to the fact they present opposite compromise limbs (LMCA vs. RMCA). The discussion that follows is based on the multiple data collected from both subjects and their correspondent video records.

In relation with sensor position P1, post-stroke patients present on the collected data, elevation and abduction of the shoulder, at the initial phase of the movement, corroborating the visual analysis.

Position P2 exhibits an increased displacement in the anterior direction (X-axis) when compared with P1; however there is a lack of marked differences observed on the global pattern of the movement. Such could suggest that P2 offers more movement detection sensitivity when compared to P1. In reference to the Y-axis, the opposite seems to occur, i.e., there is a reduced sensitivity for such detection when compared with P1, in both cases.

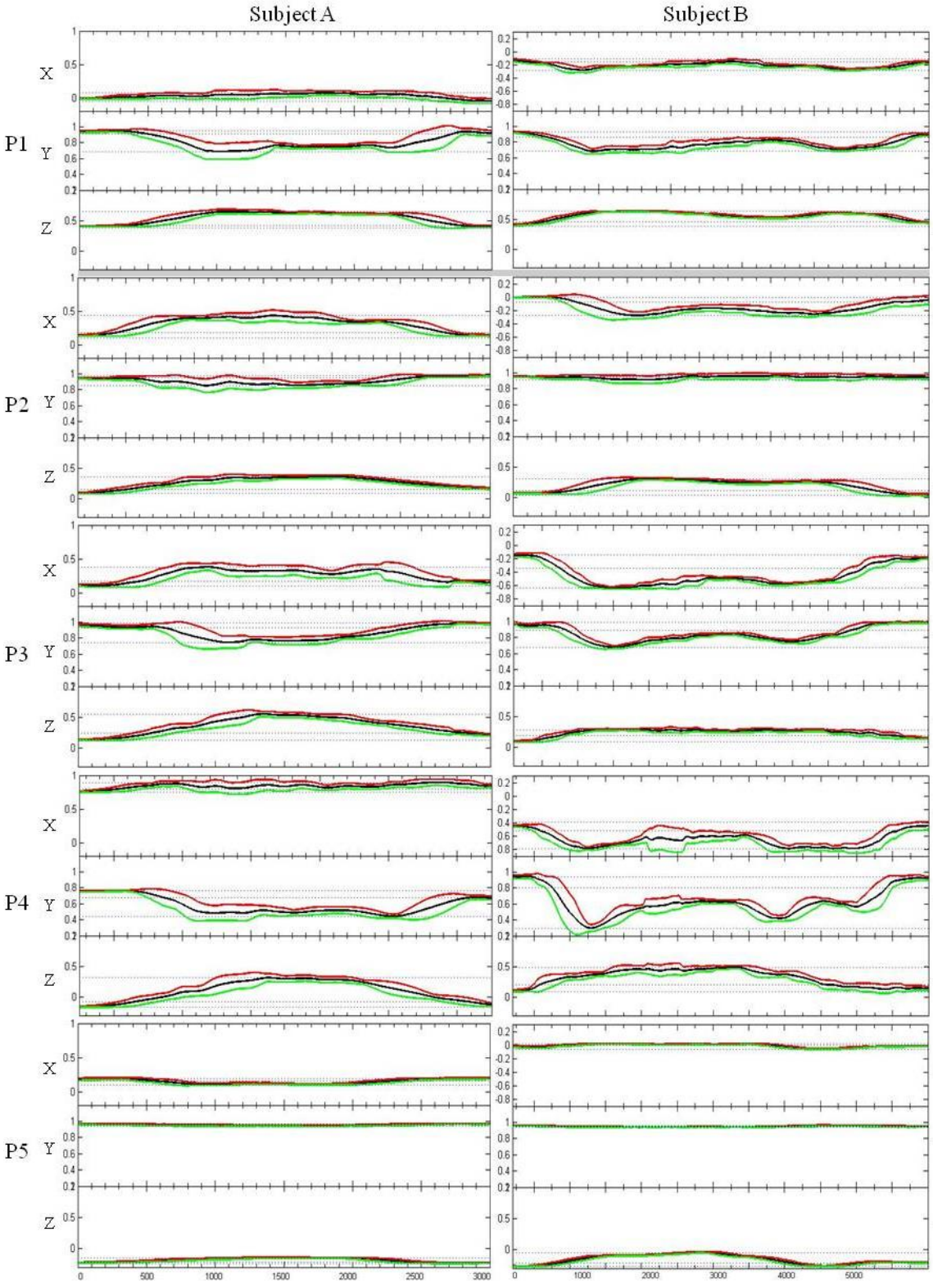

Figure 58: Accelerometry data for Subject A and B for locations P1, P2, P3, P4 and P5.

Sensor position P3 shows some variability among the patients. The movement in the anterior direction (X-axis), performed by subject A is more pronounced when compared with P1; in turn, for subject B this movement is better detected when compared to both P1 and P2. A similar situation occurs in the remaining movements, i.e. superior direction (Y-axis) and lateral direction (Z-axis). Subject B presents no pronounced differences among the sensor position P1, P2 and P3 for the lateral direction. This could be explained by lack of evident movement component recruitment as compensation during the functional task.

Given the localization of position P4, there exists a need for redefining the detected movement components by each of the axis. Thus, the movement in the anterior-posterior direction is now captured by the Y-axis, and the superior-inferior direction by the X-axis, remaining the Z-axis capturing the lateral movements. Subject A, does not present a significant elevation component (X-axis), which could be related with the deficit to enlist selective flexion of the elbow. Subject B presents an increase elevation component, resulting from an improved shoulder-elbow interjoint coordination, being able to perform selective flexion of the elbow as an integrating part of the movement pattern.

Some evidences exist thus, that sensor position P1 presents increased commitment between movement detection in the superior direction (identification of shoulder elevation as compensation) and an inter-patient variability; however a larger number of measurements and varied sample size would be required for such validation.

Finally, as for sensor position P5, one verifies that such position offers increased reproducibility among trials, while presenting reduced acceleration variations (less than 0.1 g in most cases), translating into a reduced movement of the trunk, especially in the superior-inferior direction (Y-axis). Some anterior-posterior movement (Z-axis) and rotation (X-axis) are present, which behave as compensations, given the reduced capacity of enlisting shoulder flexion with elbow extension (extensor synergy); implying a displacement of the trunk as attempting to reach the target. Subject B presents increased anterior-

posterior displacement of the trunk when compared to subject A. The presence of a larger compensation at this level, in a clinically less affected individual, could be related to its fully completion of the functional task.

Data analysis seems to suggest that the P1 position is advantageous for compensatory movement detection at the shoulder level, being however necessary to complement with information provided by P5, in order to discriminate between shoulder or trunk elevation. The information provided by sensor locations P2 and P3 do not seem to add relevant knowledge to that provided by sensor position P1. The P4 position seems the most appropriate for detecting the abduction component of the limb; however, in relation with the superior-inferior movement, this particular sensor position is insufficient for determination of the corporal segment where the elevation occurs (shoulder/elbow/trunk), limiting its reliability for compensatory movement identification in this direction. Finally, sensor position P5 presents a good sensitivity for anterior-posterior movement and rotation detection. Table 11 summarizes the sensitivity of each position for the detection of compensatory movements: anterior-posterior (A-P), superior-inferior (S-I) and medial-lateral (M-L). A growing sensitivity scale ranging from 1 to 3 was used for the characterization by a team of physiotherapists.

Table 11: Sensitivity descriptive analysis of movement components for sensor locations.

	Subject A			**Subject B**		
	A-P	S-I	M-L	A-P	S-I	M-L
P1	1	3	1	1	3	2
P2	2	1	1	2	2	2
P3	2	2	2	2	2	2
P4	2	2	3	2	2	3
P5	3	3	3	3	3	3

A-P: Anterior-Posterior; S-I: Superior-Inferior; M-L: Medial-Lateral

5.2.2. Compensatory Movements Detection in Post-Stroke Subjects

Following the initial results described above, an in-depth analysis of upper-limb movement of post-stroke patients during reaching was performed, in order to identify compensatory strategies and to extract quantitative parameters that allow describing the behaviour of such movements.

Participants

The sample was composed by four post-stroke patients receiving physiotherapy care at a rehabilitation center. Participants had to meet the same inclusion criteria as the ones described in the previous study. In addition, exclusion criteria included cerebellar or brain stem lesions and pain/sub-luxation in the upper-limb.

Arm motor impairment was evaluated prior to measurements, as seen on Table 12, with the arm subsection of the Fugl-Meyer scale and the Reach Performance Scale (close target).

Experimental Procedure

The experimental procedure followed the protocol described in the previous study: each subject was assessed in the sitting position, with a table placed in front of them; the table limit was coincident with the distal border of the subject's thigh, so as not to interfere with the arm trajectory. The individual was instructed, after verbal command, to perform the functional task.

Table 12: Demographic data and clinical scores of post-stroke patients.

	Subjects			
	A	**B**	**C**	**D**
Age	64	47	53	49
Gender	Male	Female	Female	Male
Location of lesion	LMCA	RMCA	LMCA	LMCA
Months post-stroke	19	20	34	66
RPS score	7/18	12/18	8/18	5/18
FMA (shoulder, elbow, forearm)	8/36	20/36	17/36	4/36
FMA (wrist)	1/10	2/10	2/10	0/10
FMA (hand)	6/14	12/14	10/14	2/14
FMA (coordination)	1/6	3/6	4/6	0/6

LMCA/RMCA: Left/Right Medial Cerebral Artery
RPS: Reach Performance Scale
FMA: Fugl-Meyer Motor Assessment

Following the results described in the previous study, the positions chosen for the present study were as follows (Figure 59):

- P1, placed under the acromion, following the line that connects the lateral epicondyle and the acromion;
- P2, immediately below the lateral epicondyle, after elbow articulation;
- P3, in the trunk over the T12 vertebra.

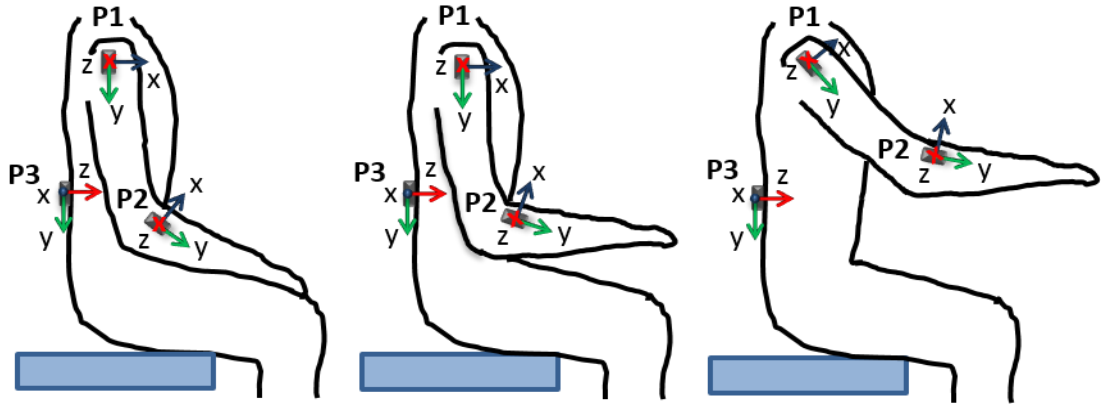

Figure 59: Sensor positioning.

Results and Discussion

The data collected from the inertial units was post-processed using a 50-point symmetrical moving average filter in order to attenuate dynamic acceleration and artifacts. The generated accelerometry profile provided a visual representation of the completed functional task, which can be associated with angular displacement using the same principles defined for swimming performance analysis (Section 4.2), i.e. assuming a low-acceleration patterns.

A set of signals from the accelerometers positioned at positions P1, P2, and P3 for a reference subject are presented in Figure 60. Similarly, accelerometry data were recorded from post-stroke patients referred to as A (Figure 61), B (Figure 62), C (Figure 63), and D (Figure 64) for all mentioned positions. In Figures 60-64, the solid lines represent the processed signal, the black dashed lines represent the plus/minus envelope signals, and the gray dashed lines represent the maximum, minimum, and mean values of the processed signal. Each position has its corresponding acceleration graphs (measured in g) presenting information for all 3 axes. In general, the subjects present a proximal to distal sequence of muscular requirement, varying degrees of deficit of elbow extension, and trunk recruitment for task completion.

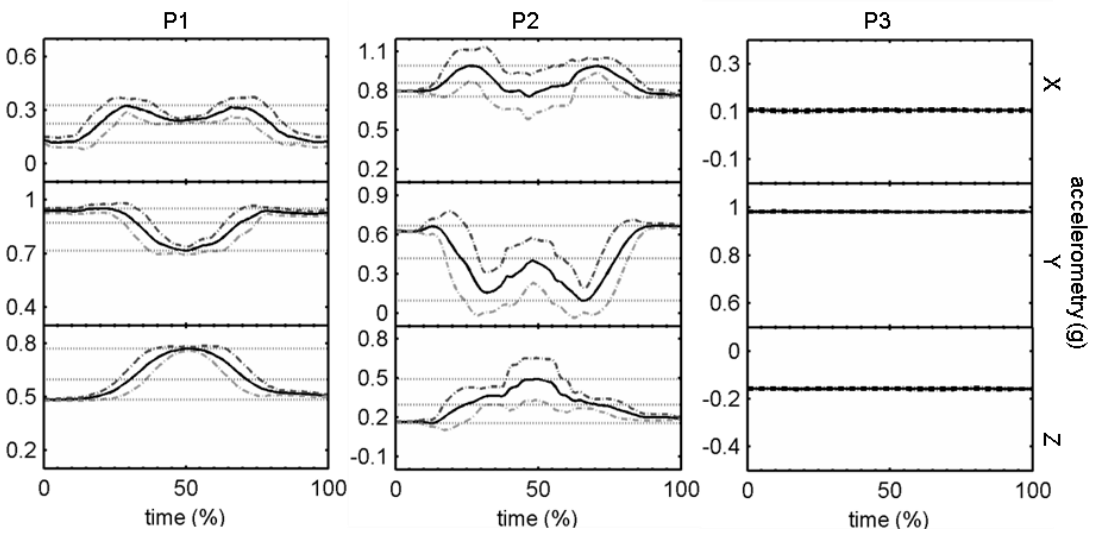

Figure 60: Accelerometry data for subject without pathology in positions P1, P2 and P3.

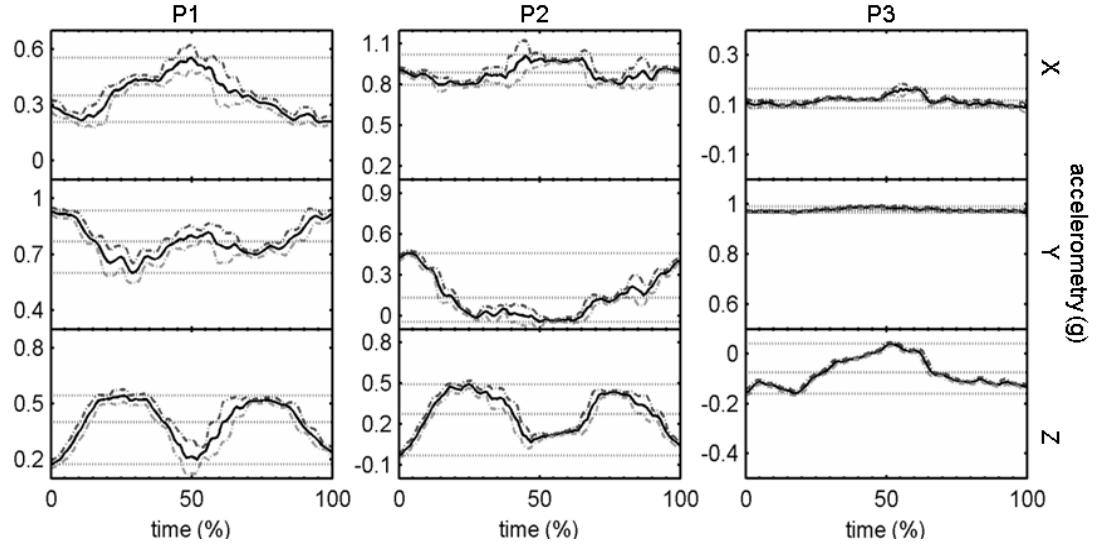

Figure 61: Accelerometry data for subject A in positions P1, P2 and P3.

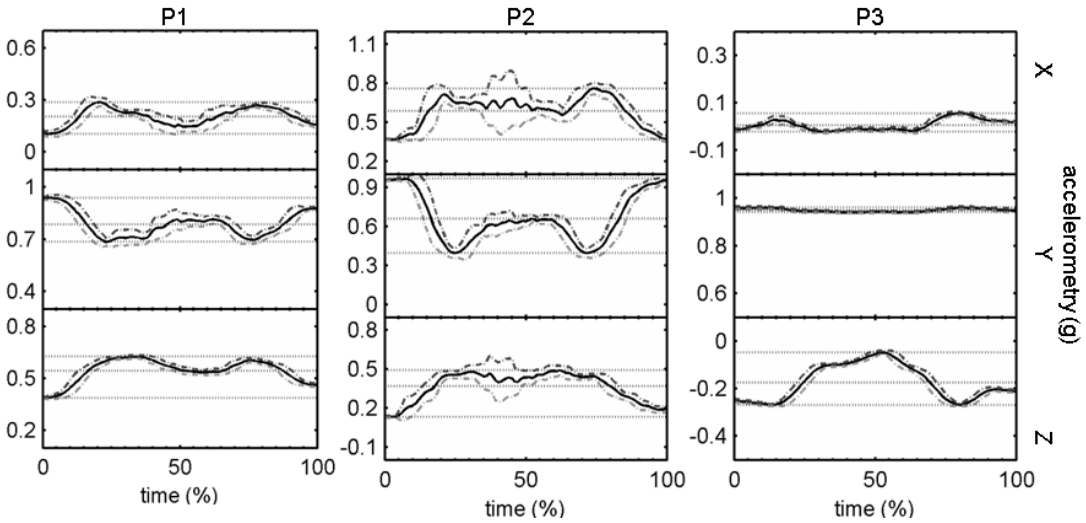

Figure 62: Accelerometry data for subject B in positions P1, P2 and P3.

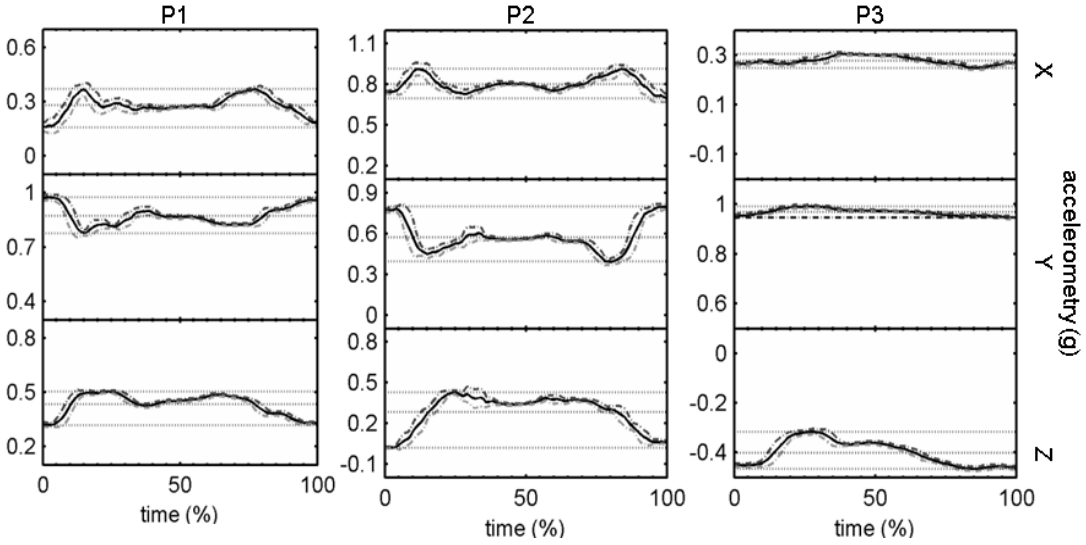

Figure 63: Accelerometry data for subject C in positions P1, P2 and P3.

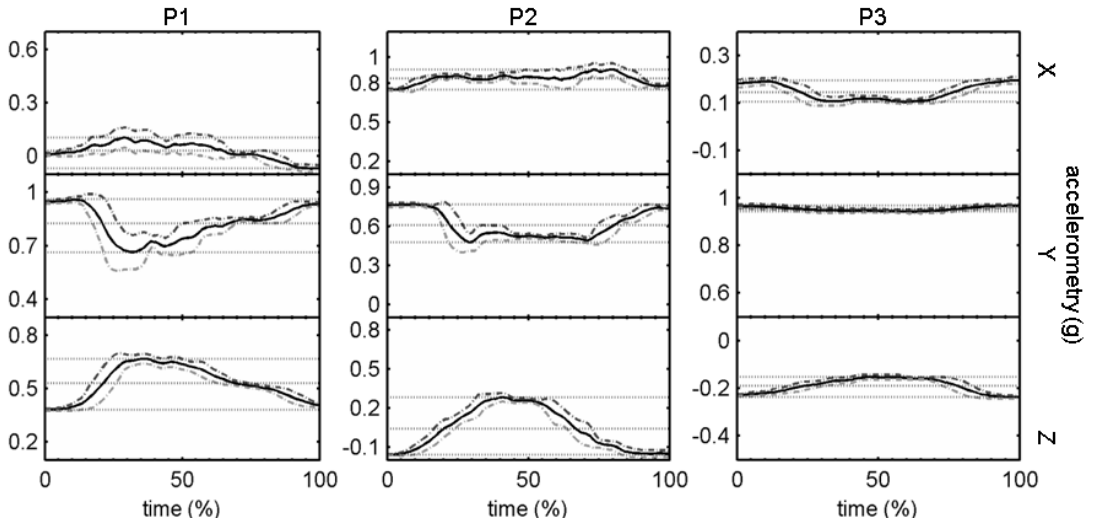

Figure 64: Accelerometry data for subject D in positions P1, P2 and P3.

Table 13 summarizes the observations extracted from the data collected, direct observation, and corresponding video records.

Table 13: Summary of accelerometry profiles observations.

	X-axis	Y-axis	Z-axis	Movement Compensations
P1	Shoulder angular displacement on the anterior/ posterior direction	Shoulder angular displacement on the superior/ inferior direction	Shoulder angular displacement on the medial/lateral direction	Shoulder abduction and elevation*
P2	Forearm angular displacement information on the superior-inferior direction	Forearm angular displacement information on the anterior-posterior direction	Forearm angular displacement information lateral movement	Lack of elbow extension and shoulder abduction
P3	Trunk rotation	Trunk angular displacement on the superior/ inferior direction	Trunk angular displacement on the anterior/ posterior direction	Forward dislocation and trunk rotation

* Needs confirmation with additional information from P3

For instance, trunk compensation, either through forward displacement or rotation, can be well detected by data collected from accelerometers at position P3. At this location, the reference subject's accelerometry data reveal small variations during the entire movement, caused by small shifts in the center of mass. In contrast, stroke patients show a perceived displacement of the trunk: an upper movement to assist with the forearm elevation and a forward displacement and rotation to compensate for lack of full elbow extension.

In general, the differences observed in the accelerometry profiles can be related to the presence of compensatory movements. For instance, stroke survivor subjects' Y-axis profiles at position P1 (which are clearly dissimilar from the corresponding reference profile because of the presence of a double bell shape for subjects A, B, and C and an asymmetrical bell shape for subject D) can be attributed to a shoulder and possible trunk compensatory elevation. Care must be taken when extracting quantifiers, because they could ignore specific maladaptive behaviors. For instance, subject B presented a strong tremor when approaching the press target, which can be observed by a noticeable pseudo-envelope deviation near the 40% mark for the X- and Z-axes of position P2. Such tremor is indicative of a lack of proper muscular organization to complete the task and can be monitored by measuring the magnitude of the deviation.

Table 14 summarizes some quantifiers extracted from the generated accelerometry profiles, including variations on the different axes (relatable to maximum angular displacement), mean comparability factor, repeatability factor, and average execution time.

The mean comparability factor was obtained, for position P1 and P2, through a standard normalized zero-lag cross-correlation between a reference vector and vectors generated by the grouping of centered (offset removed) accelerometry data of all axes. Because of the reduced variations of the signals for position P3, the offset removal was not performed prior to the cross-correlation calculation.

The repeatability factor, presented in Table 14, represents a measure of consistency of the subject's movement components while performing the functional task. This measure was calculated based on a repeatability index applied in gait analysis (Bravo, Salazar, Basso, & Borges, 2012), analogous to the American National Standards Institute procedure for obtaining a repeatability index for industrial robots (Jeswiet & Helferty, 1995). Equation 28 was used for the factor calculation where n = 100 (representing the length of the data that was time normalized) and i = 3 (representing the number of repetitions), for the present cases.

$$\text{Repeatability} = \frac{1}{n}\sqrt{\sum_{k}^{\{x,y,z\}}\left(\int_0^n \left[\max_{\forall i} F_k^i(l) - \min_{\forall i} F_k^i(l)\right] dl\right)^2} \tag{28}$$

where F_k^i is the k component of the i^{th} repetition and k ∈ {x, y, z}.

Overall analysis of the acceleration variations shows that for certain scenarios, post-stroke subjects recruit additional degrees of freedom for task completion when compared with the reference signals. For instance, the Y-axis delta values at P1 and Z-axis delta values at P2 are consistent with observed excessive elevation and abduction of the shoulder performed by the patients. The mean comparability and repeatability factors for P1 are consistent with the FMA and RPS overall scores; however, positions P2 and P3 are more sensitive to the specific recruited strategies of each individual and permit some insight on the performance of the elbow and trunk regions, respectively.

As with most indicators, the presented quantifiers should be analyzed in context, because the data obtained from a subject could be misconstrued as being associated with a process of motor refinement when, in reality, it may represent a maladaptive behavior. A particular case occurred for subject D. Although his FMA and RPS scores showed that subject D was the most impaired patient, he presented high comparability and consistency compared with the rest of the group. A possible explanation is the extension of his post-stroke period (the patient experienced his stroke almost 6 years before study) and his severe biomechanical impairments at the arm's joints and at soft tissues levels,

which compromised his ability to successfully accomplish the task. The anticipation of task failure had accustomed the patient to avoid recruiting additional degrees of freedom (observed on the delta information for positions P1 and P2), thus forcing him to incorporate a maladaptive behavior to his reaching approach (which with time has become consistent).

Table 14: Extracted quantifiers from accelerometry profiles.

		Subjects				
		A	**B**	**C**	**D**	**Ref**
P1	**Avg. ΔX-axis (g)**	0.39	0.17	0.21	0.14	0.21
	Avg. ΔY-axis (g)	0.42	0.25	0.20	0.26	0.22
	Avg. ΔZ-axis (g)	0.42	0.24	0.20	0.25	0.28
	Mean Comparability Factor	0.13	0.27	0.26	0.72	0.98
	Repeatability Factor	13.89	3.63	6.54	3.83	2.47
P2	**Avg. ΔX-axis (g)**	0.23	0.45	0.32	0.17	0.23
	Avg. ΔY-axis (g)	0.50	0.62	0.35	0.31	0.57
	Avg. ΔZ-axis (g)	0.53	0.37	0.45	0.45	0.33
	Mean Comparability Factor	0.47	0.60	0.34	0.69	0.98
	Repeatability Factor	5.85	10.65	11.36	6.34	6.34
P3	**Avg. ΔX-axis (g)**	0.09	0.08	0.11	0.09	0.04
	Avg. ΔY-axis (g)	0.03	0.02	0.17	0.02	0.01
	Avg. ΔZ-axis (g)	0.23	0.22	0.23	0.09	0.01
	Mean Comparability Factor	0.99	0.99	0.96	0.99	0.99
	Repeatability Factor	4.76	5.57	2.59	1.83	1.27
Average Time (sec)		12.60	5.62	7.02	3.15	3.56

5.2.3. Analysis of Postural Control during Reaching in Healthy vs. Post-Stroke Subjects through Inertial Data

For a proper performance during the reaching task, it is crucial to have an adequate trunk stability in order to ensure a proper control and coordination all the segments involved in the task. Therefore, it is of paramount importance to understand the biomechanical mechanisms behind the trunk motor control, since a good relationship between postural control and movement control leads to a smooth interaction among all the segments (Bartolo, Don, Ranavolo, Serrao, & Sandrini, 2009). During the reaching task, and when the target is properly distant from the subject, it is expected that the trunk does not contribute with additional degrees of freedom to accomplish the task with success (Archambault, Pigeon, Feldman, & Levin, 1999). After a lesion of the MCA not only the movement of the subject might be affect but also the postural control can be compromised (Robertson & Roby-Brami, 2011).

In order to study the trunk behaviour during the reaching task, the W2M2 system was used to perform a quantitative comparison of trunk movement between healthy subjects and post-stroke patients. Kinematic parameters were extracted from accelerometry data, namely movement duration and trunk displacement, both the anterior-posterior and the medial-lateral movements. These parameters were chosen following the results obtained in the previous studies, specifically the compensatory strategies at trunk level, observed in stroke survivors when executing the reaching task.

Participants

The sample was composed by a group of eight post-stroke patients receiving physiotherapy care at a rehabilitation center and a group of ten healthy subjects. For the healthy group inclusion, subjects were above 45 years old. Exclusion criteria comprised musculoskeletal pathology, neck and/or upper-limb pain, cerebellar, basal ganglia or brain stem lesions, and a Mini Mental State Examination score below 25. The sample characterization is shown in Table 15.

Table 15: Study sample characterization.

		Healthy Subjects	Post-Stroke Subjects
n	**Female**	5	4
	Male	5	4
Average Age		49.30±4.24	55.38±4.63
Average Body Mass Index		24.6±3.62	26.52±3.52

Post-stroke patients had to meet the following inclusion criteria:

- Confirmatory neuroimaging results of a single, unilateral stroke in the MCA territory, sustained at least 6 months prior;
- Absence of hemispatial neglect;
- Score between 30 and 50 of the Fugl-Meyer Assessment Scale (moderately impaired) (Scheidt & Stoeckmann, 2007);
- Absence of major visual, perceptual or cognitive deficits, confirmed by the mini-mental state examination (MMSE);
- Active range of motion in the compromised arm of at least 15 in the shoulder (flexion/extension; abduction/adduction and internal/external rotation) and elbow (flexion/extension) (Sveistrup, 2004).

Explicit exclusion criteria included cerebellar or brain stem lesions and pain/sub-luxation in the upper-limb. Post-stroke group characterization, namely age, gender, body mass index (BMI) location of lesion and FMA score, can be seen on Table 16.

Table 16: Post-stroke group characterization

Subjects	Age/ Gender	BMI	Location of lesion	FMA score
A	57/Female	19.48	RMCA	32
B	54/Male	23.81	LMCA	32
C	55/Female	27.41	LMCA	35
D	54/Male	30.12	LMCA	45
F	66/Male	28.37	LMCA	32
G	53/Male	25.28	LMCA	42
H	53/Female	28.91	LMCA	43
I	51/Female	28.80	RMCA	45

BMI: Body Mass Index
LMCA/RMCA: Left/Right Medial Cerebral Artery
FMA: Fugl-Meyer Motor Assessment

Experimental Procedure

The acquisition method followed the protocol described in the previous studies: each subject was assessed in the sitting position, with a table placed in front of them; the table limit was coincident with the distal border of the subject's thigh, so as not to interfere with the arm trajectory (see Figure 65). The individual was instructed, after verbal command, to perform the functional task.

In order to investigate the upper-trunk movement, the W2M2 device was placed over the T3 vertebra. At this point, trunk displacements, either in the anterior-posterior or medial-lateral directions are maximized (Lima, 2013). Both contralesional and ipsilesional movements were studied in comparison with the performance of typical subjects, since there are evidences that lesions of the MCA at sub-cortical levels can interfere bilaterally (A. Silva et al., 2012; C. Silva et al., 2014). Moreover, the movement was investigated in two different

movement planes, namely in the shoulder plane and the scapula plane, as both planes represent the typical scenarios for the reaching task to occur in daily-life activities (C. Silva et al., 2014).

A module with a capacitive touch sensor module was added to the W2M2 device, in order to determine automatically the movement duration: one touch pad was placed at the subject's thigh while the other was located at the target.

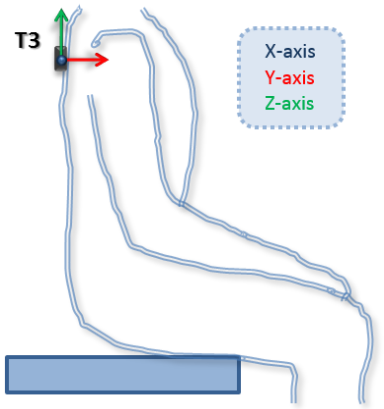

Figure 65: Sensor location for the study of postural control.

Results and Discussion

The data collected from the inertial unit was post-processed using a 50-point symmetrical moving average filter in order to attenuate dynamic acceleration and artifacts. The movement duration for post-stroke subjects, both for the ipsilesional and contralesional limbs, and for healthy subjects, specifically for the dominant limb, on the two planes of movement studied, is present in Figure 66.

As expected, post-stroke subjects perform a longer reaching movement with the contralesional limb when compared with the dominant limb of healthy subjects, both in the shoulder and scapula planes. Moreover, the movement time of the ipsilesional side was also longer than the dominant side, suggesting poorer performance.

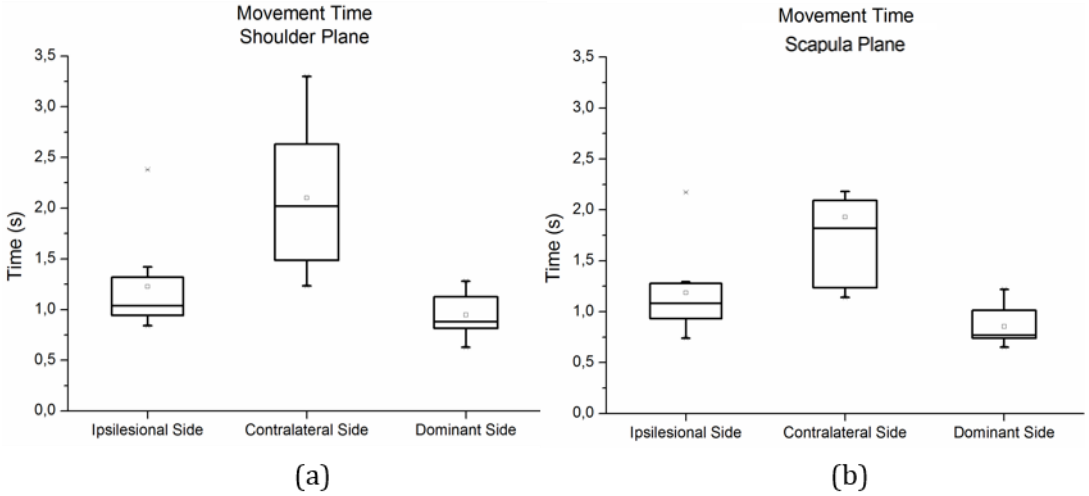

Figure 66: Movement duration for the ipsilesional and contralesional limbs of post-stroke subjects and for the dominant limb of healthy subjects in the (a) shoulder plane and (b) scapula plane.

According to the reference frame presented in Figure 65, the angular displacements around the Y-axis, representing the pitch angle, correspond to medial-lateral movements of the trunk. The results of pitch variation during the reaching movement for post-stroke subjects (ipsilesional and contralesional limbs) and healthy subjects (dominant limb) on the shoulder and scapula planes are shown in Figure 67.

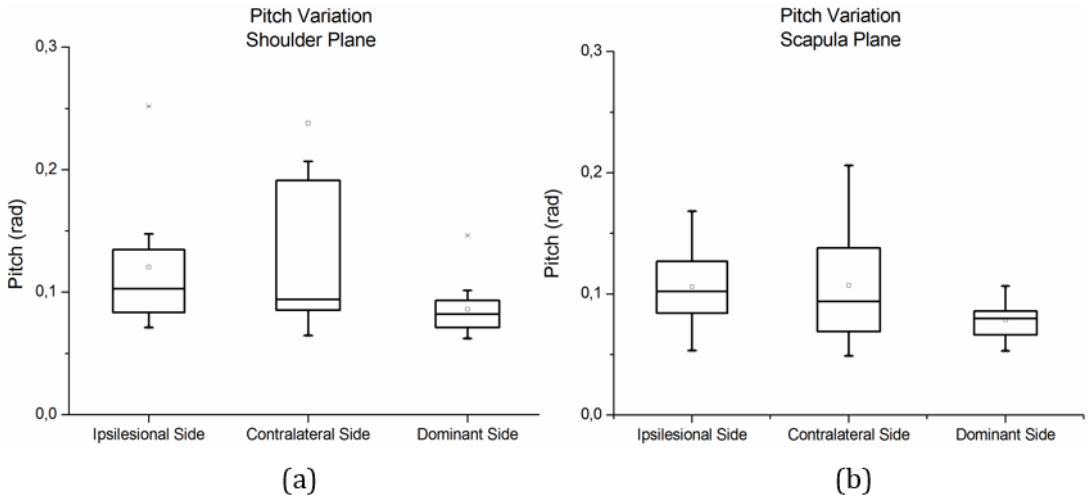

Figure 67: Pitch variation for the ipsilesional and contralesional limbs of post-stroke subjects and for the dominant limb of healthy subjects in the (a) shoulder plane and (b) scapula plane.

It can be clearly seen that in post-stroke subjects the trunk displacement in the medial-lateral direction is higher when the movement is performed with the contralesional limb, as other studies report (Michaelsen, Luta, Roby-Brami, & Levin, 2001; Robertson & Roby-Brami, 2011). In addition, the movement variability is significantly higher in post-stroke subjects than in healthy subjects. It should be mentioned that the movement at this location (upper-trunk) is also associated with shoulder elevation. In fact, the differences shown in Figure 67 reveal the excessive trunk and shoulder movements performed by the post-stroke subjects when attempting to reach the target, which is directly related with strategies adopted by the patients to compensate the lack of movement, specially the elbow extension. It can also be noted that, similarly to the results presented above, the ipsilesional limb shows a higher trunk movement when compared to healthy subjects. This reinforces the hypothesis that this limb might be also compromised in terms of performance.

The information about the roll angle (around the X-axis) can be associated with movements in the anterior-posterior direction. The variations of the roll angle during the reaching movement for post-stroke subjects (ipsilesional and contralesional limbs) and healthy subjects (dominant limb) on the shoulder and scapula planes are shown in Figure 68.

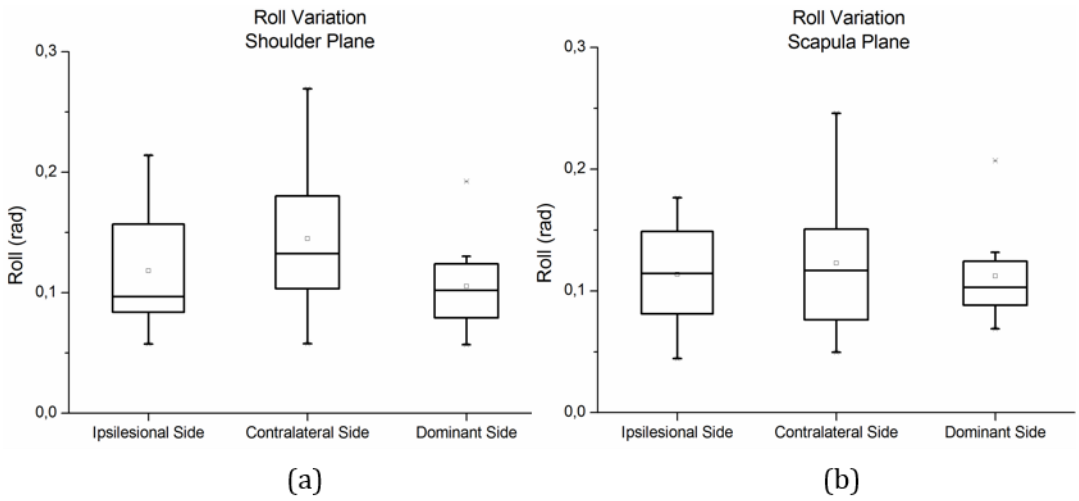

Figure 68: Roll variation for the ipsilesional and contralesional limbs of post-stroke subjects and for the dominant limb of healthy subjects in the (a) shoulder plane and (b) scapula plane.

The trunk displacement in the anterior-posterior direction is higher in post-stroke subjects than healthy subjects. Nevertheless, this difference is not as higher when compared to the medial-lateral displacement. In fact, although post-stroke subjects exhibit a higher variability than healthy subjects, the amplitude of movement is not significantly different. This can might be related with some sloppiness showed by healthy subjects when performing the task. In truth, the called "healthy" subjects sometimes also demonstrate a poor postural control and post-stroke subjects can sometimes reveal better trunk stabilization (especially those moderately impaired) than healthy subjects due to their rehabilitation intervention.

When looking at the two planes of movement studied, it can be seen that there is an increased trunk displacement, both in the medial-lateral and anterior-posterior directions, when the movement is performed in the shoulder plane. This indicates that in this plane, the demands in terms of postural control represent a higher challenge for the subjects.

At this point, it seems pertinent to question the pre-conceived idea that only the contralesional limb of post-stroke subjects is affected by the lesion. The results seem to reveal that the performance of the ipsilesional limb is worst when compared to the dominant limb of healthy subjects. Some recent studies have reported results that corroborate this hypothesis, either for the upper-limb movement or lower-limb movement (A. Silva et al., 2012; C. Silva et al., 2014).

5.3. Summary

The leading method for the acquisition and analysis of motor behavior of post-stroke subjects, namely through kinematic parameters, is based on video systems. Nevertheless, the need for a portable, easy-to-use and functional device that allows for a continuous monitoring of human movement has placed wearable inertial sensors at the top of the solutions.

The use of wearable systems allowed to bring together physiotherapist, engineers and technology. Currently, these devices can be relatively easy to incorporate in physiotherapists' activities and helping them with their clinical reasoning process. In this way, an objective quantitative analysis can be done about the motor performance of post-stroke subjects and their evolution.

In order to create new quantitative scales, it is important to understand how the information from inertial sensors can be useful. The studies described in the previous sections attempted to establish methods to analyze upper-limb performance during the reaching task, provide quantifiers to characterize the movement and better understand specific behaviors of post-stroke subjects, namely the study of their postural control.

The results of the first study allowed the definition of a method/protocol for the acquisition and analysis of upper-limb movement during reaching, specifically the optimal placement of sensor units for the identification of compensatory movements. With this previous knowledge, it was possible to identify compensatory strategies adopted by post-stroke subjects that allowed them to accomplish the task. In addition, movement quantifiers, such as repeatability and comparability factor, were extracted from accelerometry profiles. Finally, it was possible to compare the postural control of post-stroke subjects with healthy subjects by studying the trunk displacement during the reaching task. The excessive trunk displacement observed is post-stroke subjects can be associated with a compensation for the lack of their motor functions resulting from the lesion, such as elbow extension. Moreover, it could be noted that also the ipsilesional limb of post-stroke subjects showed evidences of a poorer performance when compared with healthy subjects, suggesting that the ipsilesional side might also be affected. Nevertheless, it should be taken into account that the studies described in the previous sections are limited by the small number of participants. Given the deviations found for some movement parameters, it would be desirable to have studies with a larger sample, or perform a higher number of repetitions among each subject, since variability among post-stroke subjects is expected to be large.

CHAPTER 6

DISCUSSION, CONCLUSIONS AND FUTURE WORK

6.1. Overall Discussion

Until recent years most research involving the capture and analysis of biomechanical or physiological signals have been limited to a laboratory or otherwise controlled environment. Wearable technologies introduced a refinement to personal signal capturing by permitting a long-term on-person approach. Long-term, objective measurements under daily-life unsupervised conditions are the key benefits of wearable sensor systems.

Inertial sensors are suitable sensors for wearable systems since current enhancements in MEMS technology have made possible the manufacture of miniaturized, low power, low cost devices which are useful for logging human motion data for long periods of time in uncontrolled environments. Therefore, wearable systems comprising inertial sensors can clearly introduce a very good trade-off between mobility and ease-of-use in terms of power consumption, autonomy, placement, patient compliance and data analysis. The ultimate wearable system proposed hereby, named W2M2, was based on a modular approach, where several sensor modules can be assembled and used together to extract meaningful information according to the application requirements. Instead of a complex sensor system, the key aspect of this system was to combine functionality and usability in a simple wearable solution. Along with simplicity comes small size and weight, which are crucial features when referring to wearable technology and sensor integration. This system has introduced a significant improvement with respect to the first one, called WIMU. In fact, its versatility, robustness and higher sampling rate have allowed to overcome some hurdles experienced during the acquisitions with the WIMU prototype.

With respect to fiber optic sensors, at the moment, very few research and scarce industrial efforts were found on wearable applications of fiber optic components, whereas wearable electronics have been studied for some years and some industry is developing. Through a development of all the components required for fiber optic sensor systems, some of sensors could become more

suitable for wearable applications. Especially, size and weight of the components could be reduced and connection methods improved. In the simplest example, a macrobending sensor should sense straight bending of a fabric, and in this case, it could be easily integrated into fabric. The proof-of-concept study on fiber optic sensor based on macrobending effect presented in this thesis has introduced a new thinking about wearable sensors and their functionality. Tough it might be an initial prototype, it has revealed the potentialities of such sensors to monitor human motion in real-time by means of angular displacements. The extraction of this direct measure could represent an important contribution for data fusion algorithms, since it can be combined with the information retrieved from inertial sensors, for instance, to optimize their readings and reduce inherent drift errors. There are a couple of fabric manufacturing processes compatible with optical fibers. However, the special strategy adopted for the integration of the macrobending sensor into the fabric has ensured a controlled movement for the optical fiber, improving reliability, repeatability and functionality of the sensor.

An increasingly important aspect of a wearable system is to have an intelligent monitoring device capable of providing real-time (or "valuable-time") processing and feedback to patients, clinicians, athletes and healthy subjects. However, there are a number of obstacles that must be overcome to fully implement such wearable systems, including high-costs for end-users, energy consumption, sensors integration and connectivity, autonomy, reliability, security and, ultimately, ethics, laws and privacy issues.

Wearability and power consumption are fundamental parameters to take into account in the design. A low-power design becomes relevant in order to obtain sufficient battery life and to reduce both battery size and weight. Wireless connectivity represents a significant improvement on wearability, but it would also represent a significant increase in power consumption. Even so, the ZigBee protocol used in this research has proven to provide a reliable low-power connection with a great deal of flexibility in network connection. Although low-power strategies should be adopted, the design of the device should not be a reflection of obsessive power consumption pursue, but instead

should represent a good compromise between functionality, size, usability and autonomy.

The leading method for swimming analysis is based on image processing of video data. Nonetheless, there are some hurdles to overcome due to time-consuming setup and data processing procedures and also due to water interference at the air-water interface. The wearable system proposed here can be the solution for such drawbacks. The experiences developed with swimming athletes have demonstrated that inertial sensors can provide meaningful information about swimmers' performance through the extraction of angular displacements (pitch and roll) and temporal parameters (lap time, stroke duration and frequency). Moreover, different swimming styles can be differentiated by analyzing acceleration profiles.

Nonetheless, the system and algorithms for the extraction of biomechanical parameters in swimming can be improved in order to overcome some of the difficulties encountered. Specifically, when referring to feedback for the swimmer, it is of paramount importance that the system is capable of providing noteworthy information in "valuable-time" that permits the athlete to correct or maintain chosen strategies. In addition, the ability to obtain performance measures for every training session, creating an electronic training diary, could be used to assess training loads or the effectiveness of an intervention. This has significant potential benefits for athletes where detailed performance assessment may be restricted because of distance, cost, or resource accessibility.

While fiber optic sensors are being reported as sensing tools in healthcare, namely to measure human joint angles and physiological parameters, no literature exists regarding its use in swimming analysis. Curiously, the underwater environment, with its special conditions, is one of the scenarios where the use of optical sensors would have more advantages.

Post-stroke rehabilitation is dictated by subjective analysis based on the therapist's personal experience and patients' needs, leading to a biased and sometimes incomplete perception. During the rehabilitation process, therapists

analyze patient's movements, motor learning processes and evaluate motor-control neurophysiology. Such is achieved through visual observation, patient provided information and personal handling capabilities, which can introduce misreading and affect the patient's potential for recovering. Qualitative scales can be replaced by quantifiable measurements, which can be stored, shared and processed, in order to extend the current understanding of human response and adaptation to physical compromise.

The use of wearable systems such as the one proposed in this thesis can allow the extraction of key parameters that can help therapists and physicians with their clinical reasoning process. The pilot-studies described in the previous chapter have introduced systematic means for the assessment of such measures. The information extracted from inertial sensors can in fact be used to create new quantitative scales, based on objective kinematic measures. Moreover, the capability to identify compensatory movements performed by post-stroke patients is of paramount importance for the therapist to understand the strategies adopted by their patients.

Wearable systems may not only be used to aid directly in the rehabilitation process. In fact, the information retrieved from inertial sensors can be used by academics to unveil and clarify some hypothesis concerning stroke survivors' movements. For instance, it has been hypothesized by some researches (A. Silva et al., 2012; C. Silva et al., 2014) that post-stroke subjects present a postural control dysfunction also in the ipsilesional body side. The results of accelerometry data of the study presented in the previous chapter have strengthened this hypothesis.

However, it is still early to establish a simple and straightforward comparison between accelerometry profiles, because a large number of subjects, both pathological as nonpathological, would need to be assessed before proper validation is achieved. Despite this, it is important to be aware that gathering a sample as homogeneous as possible within post-stroke population is clearly a challenge. Moreover, a larger sample might not solve the large deviations, since variability is a common feature of post-stroke population. Nevertheless, the data extracted from the wearable system revealed the potential to

quantitatively characterize the functional movement and establish parameters that complement observations from physiotherapists to determine compensatory behavior and proper behavioral progression.

6.2. Conclusions and Future Work

Wearable sensors are an integral part of future pervasive, ubiquitous and individual-centered motion analysis.

The inertial wearable system proposed in this research was based on a modular approach, which allows the integration of multiple sensors, both electrical and optical, in a truly functional device. Although this system was primarily used for swimming performance analysis and post-stroke upper-limb rehabilitation monitoring, its flexibility and adaptability allow its usage in a number of monitoring purposes. The development of a new fiber optic sensor based on macrobending effect has introduced a breakthrough in wearable sensor technology. The initial results have demonstrated its potential to complement, and even replace, traditional electrical sensors with a more robust solution. Not only the fiber optic sensor could be used as a sensing element, but it could also serve as data transmission channel.

The results obtained during the experiments in swimming and rehabilitation have demonstrated that this system represents a good alternative to conventional motion acquisition systems. Moreover, in applications where traditional methods, such as video-based systems, are not able to provide exact and reliable data (due to markers loss or interferences, for instance) this wearable systems can act as a complement to fill such gaps.

Though some advances may take place in the field of sensors technology (textile, electrical or optical) and actuators, future challenges include the integration of wearable systems into sensor-enhanced information systems and evaluation studies involving measures of patients/athletes acceptance.

In the field of swimming performance analysis, the outcomes achieved during the research initiated a new era of movement analysis based on

wearable inertial data acquisition. Nonetheless, there is room for future expansion in the wearable system proposed, given the transmission losses due to water interference. In fact, wireless transmission could be improved by adopting strategies such as new antennas operating at different frequency bands or floating transmission modules. In addition, feedback strategies can be introduced in the wearable system to assist swimmers to define proper movements.

The presented accelerometry profiles and quantifiers obtained for post-stroke patients will facilitate establishing quantifiable methodologies and protocols to assess patients' evolution and status. In addition, the data gathering outside clinical environment can give therapists useful information for their clinical reasoning process. In this manner, the wearable system could be used as a part of a home-based rehabilitation monitoring platform, assisting therapists to establish effective and efficient rehabilitation methodologies.

As with most thesis, the research work seems to never end and, although the wide scope of this investigation demands for a large number of topics to be studied, there are main key aspects that are relevant to highlight as future work:

- Development of data fusion algorithms to integrate data from fiber optic sensors;
- Feedback system, either through visual markers or auditive signals, about performance status and progression;
- Method to automatically differentiate between swimming athletes' level and swimming techniques;
- Definition of a typical pattern of the reaching functional task;
- Development of quantitative scales based on the quantifiers extracted from the wearable system to characterize post-stroke subjects' motor performance.

REFERENCES

. ±1.5g - 6g Three Axis Low-g Micromachined Accelerometer (2008). In F. S. Inc. (Ed.), (pp. 8).

Abbosh, A. M., James, D., & Thiel, D. V. (2010, 11-17 July 2010). *Compact UHF antenna in aquatic environments for mobile sporting applications.* Paper presented at the IEEE Antennas and Propagation Society International Symposium (APSURSI).

Achache, V., Mazevet, D., Iglesias, C., Lackmy, A., Nielsen, J. B., Katz, R., & Marchand-Pauvert, V. (2010). Enhanced spinal excitation from ankle flexors to knee extensors during walking in stroke patients. *Clin Neurophysiol, 121*(6), 930-938. doi: 10.1016/j.clinph.2009.12.037

Adams, S. A., Pickering, R. M., Ashburn, A., & Lincoln, N. B. (1997). The scalability of the Rivermead Motor Assessment in nonacute stroke patients. *Clin Rehabil, 11*(1), 52-59.

Aguiló, A., Martinez, P., Buades, J. M., Perales, F. J., & Gonzaléz, M. (2004). *Human motion analysis and synthesis using graphical biomechanics models applied to disable swimming people.* Paper presented at the 3rd International Workshop on Virtual Rehabilitation, Lausanne, Switzerland.

Allsop, T., Carroll, K., Lloyd, G., Webb, D. J., Miller, M., & Bennion, I. (2007). Application of long-period-grating sensors to respiratory plethysmography. *J. Biomed Opt, 12*(6).

Allsop, T., Reeves, R., Webb, D. J., Bennion, I., Earthrowl, T., Jones, B., & Miller, M. (2005). *Respiratory monitoring using fibre long period grating sensors*. Paper presented at the Proc. SPIE

Archambault, P., Pigeon, P., Feldman, A. G., & Levin, M. F. (1999). Recruitment and sequencing of different degrees of freedom during pointing movements involving the trunk in healthy and hemiparetic subjects. *Exp Brain Res, 126*(1), 55-67.

Augousti, A. T., Maletras, F.-X., & Mason, J. (2005). The use of a figure-of-eight coil for fibre optic respiratory plethysmography: geometrical analysis and experimental characterisation. *Optical Fiber Technology, 11*(4), 246-360.

Bächlin, M., Förster, K., & Tröster, G. (2009). *SwimMaster: a wearable assistant for swimmer.* Paper presented at the 11th International Conference on Ubiquitous Computing, Orlando, USA.

Bächlin, M., & Tröster, G. (2011). Swimming performance and technique evaluation with wearable acceleration sensors. *Pervasive and Mobile Computing*. doi: 10.1016/j.pmcj.2011.05.003

Bae, J., & Tomizuka, M. (2013). A tele-monitoring system for gait rehabilitation with an inertial measurement unit and a shoe-type ground reaction force sensor. *Mechatronics, 23*(6), 646-651. doi: http://dx.doi.org/10.1016/j.mechatronics.2013.06.007

Baluta, S. (2009). A Guide to using IMU (Accelerometer and Gyroscope Devices) in Embedded Applications. 2011, from http://www.starlino.com/imu_guide.html

Bamberg, S. M., Benbasat, A. Y., Scarborough, D. M., Krebs, D. E., & Paradiso, J. A. (2008). Gait Analysis Using a Shoe-Integrated Wireless Sensor System. *IEEE Transactions on Information Technology in Biomedicine, 12*(4), 413-423. doi: 10.1109/titb.2007.899493

Barbosa, T., Fernandes, R., Morouco, P., & Vilas-boas, J. (2008). Predicting the intra-cyclic variation of the velocity of the centre of mass from segmental velocities in butterfly stroke: a pilot study. *Journal of Sports Science & Medicine, 7*, 201-209.

Bartolo, M., Don, R., Ranavolo, A., Serrao, M., & Sandrini, G. (2009). Kinematic and neurophysiological models: future applications in neurorehabilitation. *J Rehabil Med, 41*(12), 986-987. doi: 10.2340/16501977-0413

Bell, J. A., & Stigant, M. (2008). Validation of a fibre-optic goniometer system to investigate the relationship between sedentary work and low back pain. *International Journal of Industrial Ergonomics, 38*(11–12), 934-941. doi: http://dx.doi.org/10.1016/j.ergon.2008.02.005

Benaim, C., Pérennou, D. A., Villy, J., Rousseaux, M., & Pelissier, J. Y. (1999). Validation of a Standardized Assessment of Postural Control in Stroke Patients: The Postural Assessment Scale for Stroke Patients (PASS). *Stroke, 30*(9), 1862-1868. doi: 10.1161/01.str.30.9.1862

Bergmann, J. H. M., Mayagoitia, R. E., & Smith, I. C. H. (2010). A portable system for collecting anatomical joint angles during stair ascent: a comparison with an optical tracking device. *Journal for the motion-capture community,* (1).

Bilro, L., Alberto, N., Pinto, J. L., & Nogueira, R. (2012). Optical Sensors Based on Plastic Fibers. *Sensors, 12*(9), 12184-12207.

Bilro, L., Pinto, J. L., Oliveira, J., & Nogueira, R. (2008, 26-29 Oct. 2008). *Gait monitoring with a wearable plastic optical sensor.* Paper presented at the 2008 IEEE Sensors.

Bravo, R. J., Salazar, A. J., Basso, D. M., & Borges, C. M. (2012). *Propuesta preliminary de un índice de consistencia para patrones de cinemática de marcha humana.* Paper presented at the Cong. Vzla. Bioeng. BIOVEN, Venezuela.

Brigante, C. M. N., Abbate, N., Basile, A., Faulisi, A. C., & Sessa, S. (2011). Towards Miniaturization of a MEMS-Based Wearable Motion Capture System. *IEEE Transactions on Industrial Electronics, 58*(8), 3234-3241.

Bury, T. (2003). Primary Health Care and Comunity Based Rehabilitation (pp. 12-16): World Confederation for Physical Therapy.

Ceseracciu, E., Sawacha, Z., Fantozzi, S., Cortesi, M., Gatta, G., Corazza, S., & Cobelli, C. (2011). Markerless analysis of front crawl swimming. *Journal of Biomechanics, 44*(12), 2236-2242. doi: 10.1016/j.jbiomech. 2011.06.003

Chan, M., Estève, D., Fourniols, J.-Y., Escriba, C., & Campo, E. (2012). Smart wearable systems: Current status and future challenges. *Artificial Intelligence in Medicine, 56*(3), 137-156. doi: http://dx.doi.org/ 10.1016/j.artmed.2012.09.003

Corazza, S., Gambaretto, E., Mundermann, L., & Andriacchi, T. P. (2010). Automatic Generation of a Subject-Specific Model for Accurate Markerless Motion Capture and Biomechanical Applications. *Biomedical Engineering, IEEE Transactions on, 57*(4), 806-812. doi: 10.1109/TBME.2008.2002103

Coyle, S., King-Tong, L., Moyna, N., O'Gorman, D., Diamond, D., Di Francesco, F., . . . Bini, C. (2010). BIOTEX: Biosensing Textiles for Personalised Healthcare Management. *IEEE Transactions on Information Technology in Biomedicine, 14*(2), 364-370.

Cunha, J. P. S., Cunha, B., Pereira, A. S., Xavier, W., Ferreira, N., & Meireles, L. (2010, 22-25 March 2010). *Vital-Jacket®: A wearable wireless vital signs monitor for patients' mobility in cardiology and sports.* Paper presented at the 4th International Conference on Pervasive Computing Technologies for Healthcare.

D'Angelo, L. T., Weber, S., Honda, Y., Thiel, T., Narbonneau, F., & Luth, T. C. (2008, 20-25 Aug. 2008). *A system for respiratory motion detection using optical fibers embedded into textiles.* Paper presented at the 30th Annual International Conference of the IEEE Engineering in Medicine and Biology Society, EMBS 2008.

da Silva, A. F., Goncalves, A. F., Mendes, P. M., & Correia, J. H. (2011). FBG Sensing Glove for Monitoring Hand Posture. *IEEE Sensors Journal, 11*(10), 2442-2448.

Dalton, A., Khalil, H., Busse, M., Rosser, A., van Deursen, R., & ÓLaighin, G. (2013). Analysis of gait and balance through a single triaxial accelerometer in presymptomatic and symptomatic Huntington's disease. *Gait & Posture, 37*(1), 49-54. doi: http://dx.doi.org/10.1016/j.gaitpost.2012.05.028

Daukantas, S., Marozas, V., Lukosevicius, A., Jegelevicius, D., & Kybartas, D. (2011, 15-17 Sept. 2011). *Video and inertial sensors based estimation of kinematical parameters in swimming sport.* Paper presented at the IEEE 6th International Conference on Intelligent Data Acquisition and Advanced Computing Systems (IDAACS).

Davé, D. (2009). Phase Sensitive Interferometry for Biosensing Applications. In A. Rasooly & K. Herold (Eds.), *Biosensors and Biodetection* (Vol. 503, pp. 179-187): Humana Press.

Davey, N., Anderson, M., & James, D. A. (2008). Validation trial of an accelerometer-based sensor platform for swimming. *Sports Technology, 1*(4-5), 202-207.

Davis, C. M. (1995). Fiber Optic Sensing: An Overview. *SPIE MS108*, 12-16.

De Jonckheere, J., Narbonneau, F., D'Angelo, L. T., Witt, J., Paquet, B., Kinet, D., . . . Logier, R. (2010, 1-3 July 2010). *FBG-based smart textiles for continuous monitoring of respiratory movements for healthcare applications.* Paper presented at the 12th IEEE International Conference on e-Health Networking Applications and Services (Healthcom).

De Jonckheere, J., Narbonneau, F., Jeanne, M., Kinet, D., Witt, J., Krebber, K., . . . Logier, R. (2009, 3-6 Sept. 2009). *OFSETH: Smart medical textile for continuous monitoring of respiratory motions under magnetic resonance imaging.* Paper presented at the Annual International Conference of the IEEE Engineering in Medicine and Biology Society, EMBC 2009.

Del Din, S., Patel, S., Cobelli, C., & Bonato, P. (2011). Estimating Fugl-Meyer clinical scores in stroke survivors using wearable sensors. *Conf Proc IEEE Eng Med Biol Soc, 2011*, 5839-5842. doi: 10.1109/iembs.2011.6091444

Dobkin, B. (2004). Strategies for stroke rehabilitation. *Lancet Neurol, 3*, 528-536.

Donno, M., Palange, E., Di Nicola, F., Bucci, G., & Ciancetta, F. (2008). A New Flexible Optical Fiber Goniometer for Dynamic Angular Measurements: Application to Human Joint Movement Monitoring. *IEEE Transactions on Instrumentation and Measurement, 57*(8), 1614-1620.

Dopsaj, M., Matkovic, I., & Zdravkovic, I. (2000). The relationship between 50m-freestyle results and characteristics of tethered forces in male sprint swimmers: a new approach to tethered swimming test. *Physical Education and Sport, 1*(7), 15-22.

Dunne, L. E., Walsh, P., Smyth, B., & Caulfield, B. (2006, 11-14 Oct. 2006). *Design and Evaluation of a Wearable Optical Sensor for Monitoring Seated Spinal Posture.* Paper presented at the 10th IEEE International Symposium on Wearable Computers.

Efendioglu, H. S., Sahin, A. K., Yildirim, T., & Fidanboylu, K. (2011, 15-18 June 2011). *Design of a hetero-core smart fiber optic microbend sensor.* Paper presented at the International Symposium on Innovations in Intelligent Systems and Applications (INISTA).

Esfandyari, J., Bendiscioli, P., & Xu, G. (2011). MEMS sensors for advance mobile applications - An overview. *Communications DesignLine*.

Esfandyari, J., Mascotto, M., & Xu, G. (2010). MEMS Pressure Sensors in Pedestrian Navigation. *Sensors*.

Evers, S. M., Struijs, J. N., Ament, A. J., van Genugten, M. L., Jager, J. H., & van den Bos, G. A. (2004). International comparison of stroke cost studies. *Stroke, 35*(5), 1209-1215. doi: 10.1161/01.str.0000125860.48180.48

Favero, F. C., Villatoro, J., & Pruneri, V. (2012). Microstructured optical fiber interferometric breathing sensor. *Journal of Biomedical Optics, 17*(3), 0370061-0370065. doi: 10.1117/1.JBO.17.3.037006

Frazao, O. (2009). *Sensores em Fibra Óptica Baseados em Interferometria e Efeitos Não-Lineares.* (PhD), Universidade do Porto, Porto.

Fugl-Meyer, A. R., Jaasko, L., Leyman, I., Olsson, S., & Steglind, S. (1975). The post-stroke hemiplegic patient. A method for evaluation of physical performance. . *Scand J Rehab Med, 7*, 13-31.

Gardner, W. B. (1975). Microbending loss in optical fibers *The Bell System Technical Journal, 54*(2), 457-465.

Geiser, W. P. (1999). USA Patent No. Free Patents Online.

Gilmore, P., & Spaulding, S. (2007). Motor learning and the use of videotape feedback after stroke. *Top stroke rehabil, 14*(5), 28-36.

Gourgoulis, V., Aggeloussis, N., Kasimatis, P., Vezos, N., Boli, A., & Mavromatis, G. (2008). Reconstruction accuracy in underwater three-dimensional kinematic analysis. *J Sci Med Sport, 11*(2), 90-95. doi: 10.1016/j.jsams.2007.02.010

Grattan, K. T. V., & Sun, T. (2000). Fiber optic sensor technology: an overview. *Sensors and Actuators A: Physical, 82*(1–3), 40-61. doi: http://dx.doi.org/10.1016/S0924-4247(99)00368-4

Grillet, A., Kinet, D., Witt, J., Schukar, M., Krebber, K., Pirotte, F., & Depre, A. (2008). Optical Fiber Sensors Embedded Into Medical Textiles for Healthcare Monitoring. *IEEE Sensors Journal, 8*(7), 1215-1222.

Gu, B., Yin, M.-J., Zhang, A. P., Qian, J.-W., & He, S. (2009). Low-cost high-performance fiber-optic pH sensor based on thin-core fiber modal interferometer. *Optics Express, 17*(25), 22296-22302. doi: 10.1364/OE.17.022296

Gurkan, D., Starodubov, D., & Xiaojing, Y. (2005, Oct. 30 2005-Nov. 3 2005). *Monitoring of the heartbeat sounds using an optical fiber Bragg grating sensor.* Paper presented at the IEEE Sensors Journal.

Hagem, R. M., Thiel, D. V., O'Keefe, S. G., Wixted, A., & Fickenscher, T. (2011, 28-31 Oct. 2011). *Low-cost short -range wireless optical FSK modem for swimmers feedback.* Paper presented at the 2011 IEEE Sensors.

Hagema, R. M., Haelsig, T., O'Keefe, S. G., Stamm, A., Fickenscher, T., & Thiel, D. V. (2013). Second Generation Swimming Feedback Device Using a Wearable Data Processing System based on Underwater Visible Light Communication. *Procedia Engineering, 60*(0), 34-39. doi: http://dx.doi.org/10.1016/j.proeng.2013.07.065

Hao, J., Jayachandran, M., Kng, P., Foo, S., Aung Aung, P., & Cai, Z. (2010). FBG-based smart bed system for healthcare applications. *Frontiers of Optoelectronics in China, 3*(1), 78-83. doi: 10.1007/s12200-009-0066-0

Holthe, M. J., & McLean, S. P. (2001). *Kinematic comparison of grab and track starts in swimming.* Paper presented at the XIX International Society of Biomechanics in Sport Symposium, San Francisco, USA.

. IDG-300 Dual-Axis Gyroscope Evaluation Board Specification (2007). In I. InvenSense (Ed.).

James, D. A., Burkett, B., & Thiel, D. V. (2011). An unobtrusive swimming monitoring system for recreational and elite performance monitoring. *Procedia Engineering, 13*(0), 113-119. doi: 10.1016/j.proeng.2011.05.060

James, D. A., Davey, N., & Rice, T. (2004). *An accelerometer based sensor platform for insitu elite athlete performance analysis.* Paper presented at the Proceedings of IEEE Sensors, 2004.

James, D. A., Galehar, A., & Thiel, D. V. (2010). Mobile sensor communications in aquatic environments for sporting applications. *Procedia Engineering, 2*(2), 3017-3022. doi: 10.1016/j.proeng.2010.04.104

Jeannerod, M. (1984). The timing of natural prehension movements. *J Mot Behav, 16*(3), 235-254.

Jeong-Whan, L., Lee-Yon, H., Jae-Hoon, J., Kang-Hwi, L., Kyeong-Seop, K., Dong-Jun, K., & Kyung-Ho, K. (2006). *A Simple Optical Angular Sensors to Measure the Human Joint Angle.* Paper presented at the International Joint Conference SICE-ICASE.

Jeswiet, J., & Helferty, R. (1995). Measuring robot repeatability an application of ISO and ANSI standards. *Advanced Robotics, 10*(5), 503-520.

Keir, M. S., Hann, C. E., Chase, J. G., & Chen, X. Q. (2007). *A New Approach to Accelerometer-based Head Tracking for Augmented Reality.* Paper presented at the IEEE International Conference on Automation Science and Engineering, CASE 2007.

Khoo, B. H., Lee, B. K. J., Senanayake, S. M. N. A., & Wilson, B. D. (2009, 14-17 July 2009). *System for determining within-stroke variations of speed in swimming (SWiSS).* Paper presented at the IEEE/ASME International Conference on Advanced Intelligent Mechatronics 2009.

Kim Doang, N., Chen, I. M., Zhiqiang, L., Song Huat, Y., & Duh, H. B. L. (2011). A Wearable Sensing System for Tracking and Monitoring of Functional Arm Movement. *IEEE/ASME Transactions on Mechatronics, 16*(2), 213-220.

Knorr, B., Hughes, R., Sherrill, D., Stein, J., Akay, M., & Bonato, P. (2005). *Quantitative Measures of Functional Upper Limb Movement in Persons after Stroke.* Paper presented at the 2nd International IEEE EMBS Conference on Neural Engineering.

Kreber, K. (2013). Smart Technical Textiles Based on Fiber Optic Sensors. In S. W. Harun & H. Arof (Eds.), *Current Developments in Optical Fiber Technology* (pp. 319-344).

Krohn, D. A. (2000). *Fiber Optic Sensors: Fundamentals and Applications* (Third ed.). USA: Instrument Society of America.

Kwang Yong, L., Goh, F. Y. K., Wei, D., Kim Doang, N., Chen, I. M., Song Huat, Y., . . . Chung Gon, K. (2008, 19-23 May 2008). *A wearable, self-calibrating, wireless sensor network for body motion processing.* Paper presented at the IEEE International Conference on Robotics and Automation, ICRA 2008.

Kyoobin, L., & Dong-Soo, K. (2001, 2001). *Wearable master device using optical fiber curvature sensors for the disabled.* Paper presented at the Proceedings of the IEEE International Conference on Robotics and Automation.

Lai, D. T. H., Begg, R. K., & Palaniswami, M. (2009). Computational Intelligence in Gait Research: A Perspective on Current Applications and Future Challenges. *IEEE Transactions on Information Technology in Biomedicine, 13*(5), 687-702.

Lapadatu, D. (2009). *Microsensors*. Paper presented at the Third STIMESI Workshop on MEMS and Microsystems, Prague, Czech Republic.

Lauer, J., Figueiredo, P., Vilas-Boas, J. P., Fernandes, R. J., & Rouard, A. H. (2013). Phase-dependence of elbow muscle coactivation in front crawl swimming. *Journal of Electromyography and Kinesiology, 23*(4), 820-825.

Le Sage, T., Bindel, A., Conway, P., Justham, L., Slawson, S., & West, A. (2010). Development of a real time system for monitoring of swimming performance. *Procedia Engineering, 2*(2), 2707-2712. doi: 10.1016/j.proeng.2010.04.055

Lee, B. (2003). Review of the present status of optical fiber sensors. *Optical Fiber Technology, 9*(2), 57-79. doi: http://dx.doi.org/10.1016/S1068-5200(02)00527-8

Leung, A., Shankar, P. M., & Mutharasan, R. (2007). A review of fiber-optic biosensors. *Sensors and Actuators B: Chemical, 125*(2), 688-703. doi: http://dx.doi.org/10.1016/j.snb.2007.03.010

Levin, M. F., Desrosiers, J., Beauchemin, D., Bergeron, N., & Roschette, A. (2004). Development and Validation of a Scale for Rating Motor Compensations Used for Reaching Patients With Hemiparesis: The Reaching Performance Scale. *Physical Therapy, 84*(1), 8-22.

Lima, S. O. (2013). *Controlo postural do tronco durante o gesto de alcance - análise do deslocamento tri-dimensional em indivíduos saudáveis e pós-AVE.* (Master Thesis), Instituto Politécnico do Porto, Porto.

Lin, J. F. S., & Kulić, D. (2012). Human pose recovery using wireless inertial measurement units. *Physiological Measurement, 33*(12), 2099.

Lomer, M., Quintela, A., López-Amo, M., Zubia, J., & López-Higuera, J. M. (2007). A quasi-distributed level sensor based on a bent side-polished plastic optical fibre cable. *Measurement Science and Technology, 18*, 2261-2267.

Lopez, A. D., Mathers, C. D., Ezzati, M., Jamison, D. T., & Murray, C. J. (2006). Global and regional burden of disease and risk factors, 2001: systematic analysis of population health data. *Lancet, 367*(9524), 1747-1757. doi: 10.1016/s0140-6736(06)68770-9

Lucca, L. (2009). Virtual reality and motor rehabilitation of the upper limb after stroke: a generation of progress? *J Rehabili Med, 41*, 1003-1006.

Luprano, J., Sola, J., Dasen, S., Koller, J. M., & Chetelat, O. (2006). *Combination of body sensor networks and on-body signal processing algorithms: the practical case of MyHeart project.* Paper presented at the International Workshop on Wearable and Implantable Body Sensor Networks, BSN 2006.

Lymberis, A., & Dittmar, A. (2007). Advanced Wearable Health Systems and Applications - Research and Development Efforts in the European Union. *IEEE Engineering in Medicine and Biology Magazine, 26*(3), 29-33.

Maluf, N. (2004). *An Introduction to Microelectromechanical Systems Engineering*. Norwood, USA: Artech House, Inc.

Mathew, J., Semenova, Y., & Farrell, G. (2012). A miniature optical breathing sensor. *Biomedical Optics Express, 3*(12), 3325-3331.

Mendonça, C., Santos, J., & López-Moliner, J. (2011). The benefit of multisensory integration with biological motion signals. *Experimental Brain Research, 213*(2-3), 185-192. doi: 10.1007/s00221-011-2620-4

Michaelsen, S. A., Luta, A., Roby-Brami, A., & Levin, M. F. (2001). Effect of trunk restraint on the recovery of reaching movements in hemiparetic patients. *Stroke, 32*, 1875-1883.

Milot, M. H., Nadeau, S., Gravel, D., & Requiao, L. F. (2006). Bilateral level of effort of the plantar flexors, hip flexors, and extensors during gait in hemiparetic and healthy individuals. *Stroke, 37*(8), 2070-2075. doi: 10.1161/01.STR.0000229900.88186.1a

Minami, A., Horikawa, T., Ohkubo, T., Kobayashi, K., Watanabe, K., & Kurihara, Y. (2010, 18-21 Aug. 2010). *A study on gait analysis by measuring axis rotation based on 3D magnetic and acceleration sensors.* Paper presented at the Proceedings of SICE Annual Conference 2010.

Mishra, V., Singh, N., Tiwari, U., & Kapur, P. (2011). Fiber grating sensors in medicine: Current and emerging applications. *Sensors and Actuators A: Physical, 167*(2), 279-290. doi: 10.1016/j.sna.2011.02.045

Mizuike, C., Ohgi, S., & Morita, S. (2009). Analysis of stroke patient walking dynamics using a tri-axial accelerometer. *Gait & Posture, 30*(1), 60-64. doi: http://dx.doi.org/10.1016/j.gaitpost.2009.02.017

Morouço, P., Lima, A. B., Semblano, P., Fernandes, D., Sousa, F., Fernandes, R., Vilas-Boas, J. P. (2006). Validation of a cable speedometer for butterfly evaluation. *Revista Portuguesa de Ciências do Desporto, 6*, 236-239.

Morrey, B. F., Askew, L. J., & Chao, E. Y. (1981). A biomechanical study of normal functional elbow motion. *The Journal of Bone & Joint Surgery, 63*(6), 872-877.

Morris, S. J. (2004). *A Shoe-Integrated Sensor System for Wireless Gait Analysis and Real-Time Therapeutic Feedback.* (Doctor of Science in Medical Engineering), Massachussetts Institute of Technology (MIT).

Munoz, R., Leija, L., Diaz, F., & Alvarez, J. (1995, 20-23 Sep 1995). *3D continuous monitoring system for localization of upper limb based on optical fiber.* Paper presented at the IEEE 17th Annual Conference Engineering in Medicine and Biology Society.

Ng, Y. S., Stein, J., Ning, M., & Black-Schaffer, R. M. (2007). Comparison of Clinical Characteristics and Functional Outcomes of Ischemic Stroke in Different Vascular Territories. *Stroke, 38*(8), 2309-2314. doi: 10.1161/strokeaha.106.475483

Nishijima, M., Sasaki, H., & Watanabe, K. (2007). *Restraint-free wearable sensing clothes using a hetero-core optic fiber for measurements of arm motion and walking action.* Paper presented at the Sensors and Smart Structures Technologies for Civil, Mechanical, and Aerospace Systems, San Diego, California.

Nishiyama, M., Sasaki, H., & Watanabe, K. (2006, 22-25 Oct. 2006). *Wearable Sensing Clothes Embedding a Hetero-core Optic Fiber for Recognizing Arm Segment Posture and Motion.* Paper presented at the 5th IEEE Conference on Sensors.

Nishiyama, M., & Watanabe, K. (2009). Wearable Sensing Glove With Embedded Hetero-Core Fiber-Optic Nerves for Unconstrained Hand Motion Capture. *IEEE Transactions on Instrumentation and Measurement, 58*(12), 3995-4000.

Nitschke, J. E., Nattrass, C. L., Disler, P. B., Chou, M. J., & Ooi, K. T. (1999). Reliability of the American Medical Association guides' model for measuring spinal range of motion. Its implication for whole-person impairment rating. *Spine (Phila Pa 1976), 24*(3), 262-268.

Noury, N., Dittmar, A., Corroy, C., Baghai, R., Weber, J. L., Blanc, D., . . . Comet, B. (2004). *VTAMN - A Smart Clothe for Ambulatory Remote Monitoring of Physiological Parameters and Activity.* Paper presented at the Engineering in Medicine and Biology Society, 2004. IEMBS '04. 26th Annual International Conference of the IEEE.

Oh, J. K., Sung-Jung, C., Won-Chul, B., Wook, C., Eunseok, C., Jing, Y., . . . Dong Yoon, K. (2004). *Inertial sensor based recognition of 3-D character gestures with an ensemble classifiers.* Paper presented at the Ninth International Workshop on Frontiers in Handwriting Recognition.

Ohgi, Y. (2002, 2002). *Microcomputer-based acceleration sensor device for sports biomechanics -stroke evaluation by using swimmer's wrist acceleration.* Paper presented at the Proceedings of IEEE Sensors.

Pandian, P. S., Mohanavelu, K., Safeer, K. P., Kotresh, T. M., Shakunthala, D. T., Gopal, P., & Padaki, V. C. (2008). Smart Vest: Wearable multi-parameter remote physiological monitoring system. *Medical Engineering & Physics, 30*(4), 466-477.

Pansiot, J., King, R. C., McIlwraith, D. G., Lo, B., & Guang-Zhong, Y. (2008, 1-3 June 2008). *ClimBSN: Climber performance monitoring with BSN.* Paper presented at the Medical Devices and Biosensors, 2008. ISSS-MDBS 2008. 5th International Summer School and Symposium on.

Pansiot, J., Lo, B., & Guang-Zhong, Y. (2010, 7-9 June 2010). *Swimming Stroke Kinematic Analysis with BSN.* Paper presented at the International Conference on Body Sensor Networks (BSN).

Paradiso, R., Belloc, C., Loriga, G., & Taccini, N. (2005). Wearable HealthCare Systems: New Frontiers of e-Textile. *Studies in Health Technology and Informatics, 117*, 9-16.

Patel, S., Hughes, R., Hester, T., Stein, J., Akay, M., Dy, J. G., & Bonato, P. (2010). A Novel Approach to Monitor Rehabilitation Outcomes in Stroke Survivors Using Wearable Technology. *Proceedings of the IEEE, 98*(3), 450-461. doi: 10.1109/JPROC.2009.2038727

Paten, S., Hughes, R., Hester, T., Stein, J., Akay, M., Dy, J., & Bonato, P. (2010). *Tracking Motor Recovery in Stroke Survivors Undergoing Rehabilitation Using Wearable Technology*. Paper presented at the 32nd Annual International Conference of the IEEE EMBS, Buenos Aires, Argentina.

Pedley, M. (2013). High Precision Calibration of a Three-Axis Accelerometer (pp. 4-15): Freescale Semiconductor.

Pendergast, D., Termin, A., & Zaharkin, J. (1999). USA Patent No. Free patents online: WIPO.

Pérez, R., Costa, Ú., Torrent, M., Solana, J., Opisso, E., Cáceres, C., . . . Gómez, E. J. (2010). Upper Limb Portable Motion Analysis System Based on Inertial Technology for Neurorehabilitation Purposes. *Sensors, 10*(12), 10733-10751.

Pleros, N., Kanellos, G. T., & Papaioannou, G. (2009, 4-7 Nov. 2009). *Optical fiber sensors in orthopedic biomechanics and rehabilitation.* Paper presented at the 9th International Conference on Information Technology and Applications in Biomedicine, ITAB 2009.

Podbreznik, P., Đonlagić, D., Lešnik, D., Cigale, B., & Zazula, D. (2013). Cost-efficient speckle interferometry with plastic optical fiber for unobtrusive monitoring of human vital signs. *Journal of Biomedical Optics, 18*(10), 107001-107001. doi: 10.1117/1.JBO.18.10.107001

Raine, S. (2009). The Bobath concept: developments and current theoretical underpinning. In Raine, Meadows & Lynch-Ellerington (Eds.), *Bobath Concept – Theory and clinical practice in neurological rehabilitation*: Wiley-Blackwell.

Raman, K. (2010). Chapter 10 - Principles of Optical Fiber Grating Sensors *Fiber Bragg Gratings (Second Edition)* (pp. 441-502). Boston: Academic Press.

Rantala, J., Hannikainen, J., & Vanhala, J. (2011). Fiber optic sensors for wearable applications. *Personal Ubiquitous Comput., 15*(1), 85-96. doi: 10.1007/s00779-010-0303-y

Ride, J., Ringuet, C., Rowlands, D., Lee, J., & James, D. (2013). A Sports Technology Needs Assessment for Performance Monitoring in Swimming. *Procedia Engineering, 60*(0), 442-447. doi: http://dx.doi.org/10.1016/j.proeng.2013.07.072

Rienzo, M. D., Rizzo, F., Parati, G., Brambilla, G., Ferratini, M., & Castiglioni, P. (2005). *MagIC System: a New Textile-Based Wearable Device for Biological Signal Monitoring. Applicability in Daily Life and Clinical Setting.* Paper presented at the 27th Annual International Conference of the Engineering in Medicine and Biology Society, IEEE-EMBS 2005.

Robertson, J. V., & Roby-Brami, A. (2011). The trunk as a part of the kinematic chain for reaching movements in healthy subjects and hemiparetic patients. *Brain Res, 1382*, 137-146. doi: 10.1016/j.brainres.2011.01.043

Rocha, L. A. (2010). MEMS Sensors and Actuators: Silicon Transduction Techniques (pp. 79). Porto, Portugal: Faculdade de Engenharia, Universidade do Porto.

Roriz, P., Frazão, O., Lobo-Ribeiro, A. B., Santos, J. L., & Simões, J. A. (2013). Review of fiber-optic pressure sensors for biomedical and biomechanical applications. *Journal of Biomedical Optics, 18*(5), 050903-050903. doi: 10.1117/1.JBO.18.5.050903

Salazar, A. J., Silva, A. S., Silva, C., Borges, C. M., Correia, M. V., Santos, R. S., & Vilas-Boas, J. P. (2014). Low-cost wearable data acquisition for stroke rehabilitation: a proof of concept study on accelerometry for functional task assessment. *Topics in Stroke Rehabilitation, 21*(1), 12-22.

Salychev, O. S. (2004). *Applied Inertial Navigation: Problems and Solutions*. Moscow, Russia: BMSTU Press.

Sant'Anna, A., Wickstro, x, & m, N. (2009, 1-3 April 2009). *Developing a motion language: Gait analysis from accelerometer sensor systems.* Paper presented at the 3rd International Conference on Pervasive Computing Technologies for Healthcare.

Scapellato, S., Cavallo, F., Martelloni, C., & Sabatini, A. M. (2005). In-use calibration of body-mounted gyroscopes for applications in gait analysis. *Sensors and Actuators A: Physical, 123-124*, 418-422. doi: 10.1016/j.sna.2005.03.052

Scheidt, R. A., & Stoeckmann, T. (2007). Reach adaptation and final position control amid environmental uncertainty after stroke. *J Neurophysiol, 97*(4), 2824-2836. doi: 10.1152/jn.00870.2006

Schleihauf, R. E., Gray, L., & DeRose, J. (1983). Three-dimensional analysis of hand propulsion in the sprint front crawl stroke. In A. P. Hollander, P. A. Huijing & G. De Groot (Eds.), *Biomechanics and medicine in swimming* (pp. 173-183). Campaign: Human Kinetics Publishers.

Schmitt, K., Schirmer, B., Hoffmann, C., Brandenburg, A., & Meyrueis, P. (2007). Interferometric biosensor based on planar optical waveguide sensor chips for label-free detection of surface bound bioreactions. *Biosensors and Bioelectronics, 22*(11), 2591-2597. doi: http://dx.doi.org/10.1016/j.bios.2006.10.016

Seifert, L., Chollet, D., & Bardy, B. G. (2004). Effect of swimming velocity on arm coordination in the front crawl: a dynamic analysis. *Journal of Sports Sciences, 22*(7), 651-660. doi: 10.1080/02640410310001655787

Shancang, L., Jue, W., & Xinheng, W. (2010, 6-10 Dec. 2010). *A novel gait recognition analysis system based on body sensor networks for patients with parkinson's disease.* Paper presented at the GLOBECOM Workshops (GC Wkshps), 2010 IEEE.

Shao, L. Y., Yin, M. J., Tam, H. Y., & Albert, J. (2012). *Fiber optic pH sensor with self-assembled multilayer nanocoatings on tilted FBG*.

Shelton, F. N., & Reding, M. J. (2001). Effect of lesion location on upper limb motor recovery after stroke. *Stroke, 32*(1), 107-112.

Shiratsu, A., & Coury, H. J. C. G. (2003). Reliability and accuracy of different sensors of a flexible electrogoniometer. *Clinical Biomechanics, 18*(7), 682-684. doi: http://dx.doi.org/10.1016/S0268-0033(03)00110-4

Siirtola, P., Laurinen, P., Roning, J., & Kinnunen, H. (2011, 11-15 April 2011). *Efficient accelerometer-based swimming exercise tracking.* Paper presented at the 2011 IEEE Symposium on Computational Intelligence and Data Mining (CIDM).

Silva, A., Sousa, A. S., Pinheiro, R., Tavares, J. M., Santos, R., & Sousa, F. (2012). Soleus activity in post-stroke subjects: movement sequence from standing to sitting. *Somatosens Mot Res, 29*(3), 71-76. doi: 10.3109/08990220.2012.686935

Silva, A. O. (2007). AVC. In Cofina (Ed.), *O essencial da saúde* (Vol. 10, pp. 5-10). Porto: Faculdade de Medicina da Universidade do Porto.

Silva, A. S., Salazar, A. J., Borges, C. M., & Correia, M. V. (2012) Wearable Monitoring Unit for Swimming Performance Analysis. *Vol. 273. CCIS Lecture Notes in Computer Science* (pp. 80-93). Heidelberg: Springer.

Silva, C., Silva, A., Sousa, A., Pinheiro, R., Bourlinova, C., Silva, A. S., . . . Santos, R. (2014). Co-Activation Study of Upper-Limb Muscles During Reaching in Post-Stroke Subjects. *Journal of Electromyography and Kinesiology*.

Silva, C., Silva, A., Sousa, A., Pinheiro, R., Bourlinova, C., Silva, A. S., . . . Santos, R. S. (2014). Co-Activation Study of Upper Limb Muscles During Reaching in Post-Stroke Subjects: an Analysis of Ipsilesional vs Contralesional Limb. *Journal of Electromyography and Kinesiology*. (in press)

Silva, H. R., Afonso, J. A., Morim, P. C., Oliveira, P. M., Correia, J. H., & Rocha, L. A. (2007). *Wireless Hydrotherapy Smart-Suit Network for Posture Monitoring.* Paper presented at the IEEE International Symposium on Industrial Electronics.

Slawson, S. E., Conway, P. P., Justham, L. M., & West, A. A. (2010). The development of an inexpensive passive marker system for the analysis of starts and turns in swimming. *Procedia Engineering, 2*(2), 2727-2733. doi: http://dx.doi.org/10.1016/j.proeng.2010.04.058

Snitzer, E. (1961). Cylindrical Dielectric Waveguide Modes. *Journal of the Optical Society of America, 51*(5), 491-498. doi: 10.1364/JOSA.51.000491

Soares, S. (2000). Natação. In F.-U. CMP (Ed.), *Educação Física no 1º Ciclo* (pp. 154-173).

Sprager, S., & Zazula, D. (2012). Heartbeat and Respiration Detection From Optical Interferometric Signals by Using a Multimethod Approach. *Biomedical Engineering, IEEE Transactions on, 59*(10), 2922-2929. doi: 10.1109/TBME.2012.2213302

Stamm, A., Thiel, D. V., Burkett, B., & James, D. A. (2011). Towards determining absolute velocity of freestyle swimming using 3-axis accelerometers. *Procedia Engineering, 13*(0), 120-125. doi: 10.1016/ j.proeng.2011.05.061

Strong, K., Mathers, C., & Bonita, R. (2007). Preventing stroke: saving lives around the world. *Lancet Neurol, 6*(2), 182-187. doi: 10.1016/s1474-4422(07)70031-5

Sveistrup, H. (2004). Motor rehabilitation using virtual reality. *Journal of NeuroEngineering and Rehabilitation, 1*(10), 1-8.

Takagi, H., Nishijima, N., Sugimoto, S., & Wilson, B. (2004). Differences in Stroke Phases, Arm-Leg Coordination and Velocity Fluctuation due to Event, Gender and Performance level in Breaststroke. *Sports Biomechanics, 3*(1), 15-27.

Tate, D. (2006). The state of rehabilitation research:art or science? *Arch Phys Med Rehabil, 87*, 160-166.

Teasell, R., Foley, N. C., Bhogal, S. K., & Speechley, M. R. (2003). An evidence-based review of stroke rehabilitation. *Top stroke rehabil, 10*(1), 29-58.

Tella, V., Toca-Herrera, J. L., Gallach, J. E., Benavent, J., González, L. M., & Arellano, R. (2008). Effect of fatigue on the intra-cycle acceleration in front crawl swimming: A time-frequency analysis. *Journal of Biomechanics, 41*(1), 86-92.

Thompson, K. G., MacLaren, D. P. M., Lees, A., & Atkinson, G. (2004). The effects of changing pace on metabolism and stroke characteristics during high-speed breaststroke swimming. *Journal of Sports Sciences, 22*(2), 149-157. doi: 10.1080/02640410310001641467

Titterton, D. H. (2007). Basic Principles of Strapdown Inertial Navegation Systems. In J. L. Weston (Ed.), Strapdown inertial navigation technology (pp. 17-57): Stevenage: Institution of Electrical Engineers.

Vandenberghe, A., Levin, O., De Schutter, D., Swinnen, S., & Jonkers, I. (2010). Three-dimensional reaching tasks: effect of reaching height and width on upper limb kinematics and muscle activity. *Gait \& Posture, 32*(4), 500-507.

Velasco-Garcia, M. N. (2009). Optical biosensors for probing at the cellular level: A review of recent progress and future prospects. *Seminars in Cell & Developmental Biology, 20*(1), 27-33. doi: http://dx.doi.org/10.1016/j.semcdb.2009.01.013

Veluvolu, K. C., & Ang, W. T. (2011). Estimation of Physiological Tremor from Accelerometers for Real-Time Applications. *Sensors, 11*(3), 3020-3036.

Wang, W.-C., Ledoux, W. R., Sangeorzan, B. J., & Reinall, P. G. (2005). A shear and plantar pressure sensor based on fiber-optic bend loss. *Journal of Rehabilitation Research and Development, 42*(3), 315-326.

Wehrle, G., Nohama, P., Kalinowski, H., Torres, P., & Valente, L. (2001). A fibre optic Bragg grating strain sensor for monitoring ventilatory movements. *Measurement Science and Technology, 12*, 805-809.

Wise, S., Gardner, W., Sabelman, E., Valainis, E., Wong, Y., Glass, K., . . . Rose, J. M. (1990). Evaluation of a fiber optic glove for semi-automated goniometer measurements. *Journal of Rehabilitation Research and Development, 27*(4), 411-424.

Witt, J., Krebber, K., Demuth, J., & Sasek, L. (2011, 8-10 June 2011). *Fiber optic heart rate sensor for integration into personal protective equipment.* Paper presented at the 2011 International Workshop on BioPhotonics.

World Health Organization. (2011). Stroke, Cerebrovascular accident. from http://www.who.int/topics/cerebrovascular_accident/en/

Xiaobin, X., Chunxi, Z., Kun Mean, H., Hao, D., & Xunming, D. (2008, 5-7 Nov. 2008). *A New Wireless Fiber Optic Sensor for Monitoring Breath Motion.* Paper presented at the New Technologies, Mobility and Security, 2008. NTMS '08.

Xuejin, L., Yuanlong, D., Yongqin, Y., Xinyi, W., & Jingxian, L. (2008). *Microbending optical fiber sensors and their applications.* Paper presented at the International Conference on Advanced Infocomm Technology, New York, USA.

Yang, S., Zhang, J.-T., Novak, A. C., Brouwer, B., & Li, Q. (2013). Estimation of spatio-temporal parameters for post-stroke hemiparetic gait using inertial sensors. *Gait & Posture, 37*(3), 354-358. doi: http://dx.doi.org/10.1016/j.gaitpost.2012.07.032

Yeo, T. L., Sun, T., & Grattan, K. T. V. (2008). Fibre-optic sensor technologies for humidity and moisture measurement. *Sensors and Actuators A: Physical, 144*(2), 280-295. doi: http://dx.doi.org/10.1016/j.sna.2008.01.017

Ymeti, A., Subramaniam, V., Beumer, T. A. M., & Kanger, J. S. (2007). An ultrasensitive Young interferometer handheld sensor for rapid virus detection. *Expert Review of Medical Devices, 4*(4), 447-454. doi: 10.1586/17434440.4.4.447

Zambrano, A., Derogarian, F., Dias, R., Abreu, M. J., Catarino, A., Rocha, A. M., . . . Velhote Correia, M. (2012). A wearable sensor network for human locomotion data capture. *Stud Health Technol Inform, 177*, 216-223.

Zawawi, M. A., O'Keefe, S. G., & Lewis, E. (2013). Intensity-modulated fiber optic sensor for health monitoring applications: a comparative review. *Sensor Review, 33*(1), 57-67.

Zendehnam, A., Mirzaei, M., Farashiani, A., & Farahani, L. H. (2010). Investigation of bending loss in a single-mode optical fibre. *PRAMANA - Journal of Physics, 74*(4), 591-603.

Zhang, T., Talla, S., Gong, Z., Karandikar, S., Giorno, R., & Que, L. (2010). Biochemical sensing with a polymer-based micromachined Fabry-Perot sensor. *Optics Express, 18*(17), 18394-18400. doi: 10.1364/OE.18.018394

Zhang, Y., Shibru, H., Cooper, K. L., & Wang, A. (2005). Miniature fiber-optic multicavity Fabry-Perot interferometric biosensor. *Optics Letters, 30*(9), 1021-1023. doi: 10.1364/OL.30.001021

Zhang, Z., & Grattan, K. T. V. (1998). *Survey of U.S. patent activity in optical fibre sensors*.

Zhe, Z., Qiang, F., & Ferry, F. (2011, 7-10 Nov. 2011). *Upper limb motion capturing and classification for unsupervised stroke rehabilitation.* Paper presented at the IECON 2011 - 37th Annual Conference on IEEE Industrial Electronics Society.

Zhou, H., Hu, H., & Tao, Y. (2006). Inertial measurements of upper limb motion. *Medical and Biological Engineering and Computing, 44*(6), 479-487. doi: 10.1007/s11517-006-0063-z

Zhou, H., Stone, T., Hu, H., & Harris, N. (2008). Use of multiple wearable inertial sensors in upper limb motion tracking. *Medical Engineering & Physics, 30*(1), 123-133. doi: http://dx.doi.org/10.1016/j.medengphy.2006.11.010

Zimmerman, T. G., & Lanier, J. (1987). A hand gesture interface device. *Proc. Human Factors Comput. Syst. Graph. Interface*, 189–192.

APPENDIXES

Appendix A: Microcontroller Embedded Code

WIMU AP Board

```
//*************************************************
//  eZ430-RF2500 Sensor Access Point
//
//      Description: This is the Access Point
software for the eZ430-2500RF Sensing
//
//*************************************************

#include "bsp.h"
#include "mrfi.h"
#include "bsp_leds.h"
#include "bsp_buttons.h"
#include "nwk_types.h"
#include "nwk_api.h"
#include "nwk_frame.h"
#include "nwk.h"

#include "msp430x22x4.h"
#include "vlo_rand.h"

#define MESSAGE_LENGTH 9
void TXString( char* string, int length );
void MCU_Init(void);
void transmitData(int addr, signed char rssi,
char msg[MESSAGE_LENGTH] );
void createRandomAddress();

// Temperature offset set at production
__no_init volatile int tempOffset @ 0x10F4;
// Flash address set randomly
__no_init volatile char Flash_Addr[4] @ 0x10F0;

//reserve space for the maximum possible peer
Link IDs
static linkID_t sLID[NUM_CONNECTIONS];
static uint8_t  sNumCurrentPeers;

// callback handler
static uint8_t sCB(linkID_t);

// work loop semaphores
static uint8_t sPeerFrameSem;
static uint8_t sJoinSem;
static uint8_t sSelfMeasureSem;


void main (void)
{
  addr_t lAddr;
  bspIState_t intState;

  // Stop WDT
WDTCTL = WDTPW + WDTHOLD;
  {
  // delay loop to ensure proper startup before
SimpliciTI increases DCO
  // This is typically tailored to the power supply
used, and in this case
  // is overkill for safety due to wide distribution.
    volatile int i;
    for(i = 0; i < 0xFFFF; i++){}
  }
  if( CALBC1_8MHZ == 0xFF )          // Do not run
if cal values are erased
  {
    volatile int i;
    P1DIR |= 0x03;
    BSP_TURN_ON_LED1();
    BSP_TURN_OFF_LED2();
    while(1)
    {
      for(i = 0; i < 0x5FFF; i++){}
      BSP_TOGGLE_LED2();
      BSP_TOGGLE_LED1();
    }
  }

  BSP_Init();

  if( Flash_Addr[0] == 0xFF &&
      Flash_Addr[1] == 0xFF &&
      Flash_Addr[2] == 0xFF &&
      Flash_Addr[3] == 0xFF )
  {
    createRandomAddress();                  // set
Random device address at initial startup
  }
  lAddr.addr[0]=Flash_Addr[0];
  lAddr.addr[1]=Flash_Addr[1];
  lAddr.addr[2]=Flash_Addr[2];
  lAddr.addr[3]=Flash_Addr[3];
  SMPL_Ioctl(IOCTL_OBJ_ADDR,  IOCTL_ACT_SET,
&lAddr);

  MCU_Init();
  //Transmit  splash  screen  and  network  init
notification
 // TXString( (char*)splash, sizeof splash);
  TXString( "\r\nInitializing Network....", 26 );

  SMPL_Init(sCB);

  // network initialized
  TXString( "Done\r\n", 6);

  // main work loop
  while (1)
  {
```

```
  // Wait for the Join semaphore to be set by the receipt of a Join frame from a
  // device that supports and End Device.

  if (sJoinSem && (sNumCurrentPeers < NUM_CONNECTIONS))
  {
   // listen for a new connection

SMPL_LinkListen(&sLID[sNumCurrentPeers]);
    sNumCurrentPeers++;
    BSP_ENTER_CRITICAL_SECTION(intState);
    if (sJoinSem)
    {
     sJoinSem--;
    }
    BSP_EXIT_CRITICAL_SECTION(intState);
  }

  // if it is time to measure our own temperature...
  if(sSelfMeasureSem)
  {
    char msg [6];
    char addr[] = {"HUB0"};
    int degC, volt;
    volatile long temp;
    int results[2];

    ADC10CTL1 = INCH_10 + ADC10DIV_4;     // Temp Sensor ADC10CLK/5
    ADC10CTL0 = SREF_1 + ADC10SHT_3 + REFON + ADC10ON + ADC10IE + ADC10SR;
    for( degC = 240; degC > 0; degC-- );  // delay to allow reference to settle
    ADC10CTL0 |= ENC + ADC10SC;           // Sampling and conversion start
    __bis_SR_register(CPUOFF + GIE);      // LPM0 with interrupts enabled
    results[0] = ADC10MEM;

    ADC10CTL0 &= ~ENC;

    ADC10CTL1 = INCH_11;                  // AVcc/2
    ADC10CTL0 = SREF_1 + ADC10SHT_2 + REFON + ADC10ON + ADC10IE + REF2_5V;
    for( degC = 240; degC > 0; degC-- );  // delay to allow reference to settle
    ADC10CTL0 |= ENC + ADC10SC;           // Sampling and conversion start
    __bis_SR_register(CPUOFF + GIE);      // LPM0 with interrupts enabled
    results[1] = ADC10MEM;
    ADC10CTL0 &= ~ENC;
    ADC10CTL0 &= ~(REFON + ADC10ON);      // turn off A/D to save power

    // oC = ((A10/1024)*1500mV)-986mV)*1/3.55mV = A10*423/1024 - 278
    // the temperature is transmitted as an integer where 32.1 = 321
    // hence 4230 instead of 423
    temp = results[0];
    degC = (((temp - 673) * 4230) / 1024);
    if( tempOffset != 0xFFFF )
    {
     degC += tempOffset;
    }

    temp = results[1];
    volt = (temp*25)/512;

    msg[0] = degC&0xFF;
    msg[1] = (degC>>8)&0xFF;
    msg[2] = volt;

    char temp_string[] = {" XX.XC"};
    int aux = msg[0] + (msg[1]<<8);

  if( aux < 0 )
  {
   temp_string[0] = '-';
   aux = aux * -1;
  }
  else if( ((aux/1000)%10) != 0 )
  {
   temp_string[0] = '0'+((aux/1000)%10);
  }
  temp_string[4] = '0'+(aux%10);
  temp_string[2] = '0'+((aux/10)%10);
  temp_string[1] = '0'+((aux/100)%10);

   char output_temperature[] = {"\r\nNode:XXXX,Temp:-XX.XC,Battery:X.XV"};

   output_temperature[17] = temp_string[0];
   output_temperature[18] = temp_string[1];
   output_temperature[19] = temp_string[2];
   output_temperature[20] = temp_string[3];
   output_temperature[21] = temp_string[4];
   output_temperature[22] = temp_string[5];

   output_temperature[32] = '0'+(msg[2]/10)%10;
   output_temperature[34] = '0'+(msg[2]%10);
   output_temperature[7] = addr[0];
   output_temperature[8] = addr[1];
   output_temperature[9] = addr[2];
   output_temperature[10] = addr[3];
   TXString(output_temperature, sizeof output_temperature );

    BSP_TOGGLE_LED1();
    sSelfMeasureSem = 0;
   }

   // Have we received a frame on one of the ED connections?
   // No critical section -- it doesn't really matter much if we miss a poll
   if (sPeerFrameSem)
   {
    uint8_t    msg[MAX_APP_PAYLOAD], len, i;

    // process all frames waiting
    for (i=0; i<sNumCurrentPeers; ++i)
    {
     if (SMPL_Receive(sLID[i], msg, &len) == SMPL_SUCCESS)
     {
```

```
        ioctlRadioSiginfo_t sigInfo;
        sigInfo.lid = sLID[i];
        SMPL_Ioctl(IOCTL_OBJ_RADIO,
IOCTL_ACT_RADIO_SIGINFO, (void *)&sigInfo);
        transmitData(          i,          (signed
char)sigInfo.sigInfo[0], (char*)msg );
        BSP_TOGGLE_LED2();
        BSP_ENTER_CRITICAL_SECTION(intState);
        sPeerFrameSem--;
        BSP_EXIT_CRITICAL_SECTION(intState);
      }
    }
   }
  }
}

/*-------------------------------------------------------*/
void createRandomAddress()
{
 unsigned int rand, rand2;
 do
 {
  rand = TI_getRandomIntegerFromVLO();    //
first byte can not be 0x00 of 0xFF
 }
 while( (rand & 0xFF00)==0xFF00 || (rand &
0xFF00)==0x0000 );
 rand2 = TI_getRandomIntegerFromVLO();

 BCSCTL1 = CALBC1_1MHZ;                  // Set
DCO to 1MHz
 DCOCTL = CALDCO_1MHZ;
 FCTL2 = FWKEY + FSSEL0 + FN1;           //
MCLK/3 for Flash Timing Generator
 FCTL3 = FWKEY + LOCKA;                  // Clear
LOCK & LOCKA bits
 FCTL1 = FWKEY + WRT;                    // Set WRT
bit for write operation

 Flash_Addr[0]=(rand>>8) & 0xFF;
 Flash_Addr[1]=rand & 0xFF;
 Flash_Addr[2]=(rand2>>8) & 0xFF;
 Flash_Addr[3]=rand2 & 0xFF;

 FCTL1 = FWKEY;                          // Clear WRT
bit
 FCTL3 = FWKEY + LOCKA + LOCK;           // Set
LOCK & LOCKA bit
}

/*-------------------------------------------------------*/
void transmitData(int addr, signed char rssi,
char msg[MESSAGE_LENGTH] )
{
 char addrString[4];
 char rssiString[3];
 volatile signed int rssi_int;

 addrString[0] = '0';
 addrString[1] = '0';
 addrString[2] = '0'+(((addr+1)/10)%10);
 addrString[3] = '0'+((addr+1)%10);

 rssi_int = (signed int) rssi;
 rssi_int = rssi_int+128;
 rssi_int = (rssi_int*100)/256;
 rssiString[0] = '0'+(rssi_int%10);
 rssiString[1] = '0'+((rssi_int/10)%10);
 rssiString[2] = '0'+((rssi_int/100)%10);


 int AccX = msg[0];
 int AccY = msg[1];
 int AccZ = msg[2];
 int VelX = msg[3];
 int VelY = msg[4];

 char output[] = {"\r\nNode:XXXX, AccX:x.xxV,
AccY:x.xxV, AccZ:x.xxV, VelX:x.xxV, VelY:x.xxV,
Time:00:00:00:000, Strength:XXX%"};

 output[7] = addrString[0];
 output[8] = addrString[1];
 output[9] = addrString[2];
 output[10] = addrString[3];

 output[18] = '0' + (AccX/100)%10;
 output[20] = '0' + (AccX/10)%10;
 output[21] = '0' + (AccX%10);

 output[30] = '0' + (AccY/100)%10;
 output[32] = '0' + (AccY/10)%10;
 output[33] = '0' + (AccY%10);

 output[42] = '0' + (AccZ/100)%10;
 output[44] = '0' + (AccZ/10)%10;
 output[45] = '0' + (AccZ%10);

 output[54] = '0' + (VelX/100)%10;
 output[56] = '0' + (VelX/10)%10;
 output[57] = '0' + (VelX%10);

 output[66] = '0' + (VelY/100)%10;
 output[68] = '0' + (VelY/10)%10;
 output[69] = '0' + (VelY%10);

 output[78] = '0'+(msg[5]/10)%10;
 output[79] = '0'+(msg[5]%10);
 output[81] = '0'+(msg[6]/10)%10;
 output[82] = '0'+(msg[6]%10);
 output[84] = '0'+(msg[7]/10)%10;
 output[85] = '0'+(msg[7]%10);
 output[87] = '0'+(msg[8]/100)%10;
 output[88] = '0'+(msg[8]/10)%10;
 output[89] = '0'+(msg[8]%10);

 output[101] = rssiString[2];
 output[102] = rssiString[1];
 output[103] = rssiString[0];

 TXString(output, sizeof output );

}

/*-------------------------------------------------*/
void TXString( char* string, int length )
{
 int pointer;
 for( pointer = 0; pointer < length; pointer++)
 {
```

```
   volatile int i;
   UCA0TXBUF = string[pointer];
   while  (!(IFG2&UCA0TXIFG));                  //
USCI_A0 TX buffer ready?
  }
}

/*-------------------------------------------------------*/
void MCU_Init()
{
  BCSCTL1 = CALBC1_8MHZ;                    // Set
DCO
  DCOCTL = CALDCO_8MHZ;

  BCSCTL3 |= LFXT1S_2;                    // LFXT1 =
VLO
  TACCTL0 = CCIE;                           // TACCR0
interrupt enabled
  TACCR0 = 65000;                       // ~5 sec
  TACTL = TASSEL_1 + MC_1;                 // ACLK,
upmode

  P3SEL |= 0x30;                            // P3.4,5 =
USCI_A0 TXD/RXD
  UCA0CTL1 = UCSSEL_2;                  // SMCLK
  UCA0BR0 = 0x41;                           // 9600 from
8Mhz
  UCA0BR1 = 0x3;
  UCA0MCTL = UCBRS_2;
  UCA0CTL1 &= ~UCSWRST;                        //
**Initialize USCI state machine**
  IE2 |= UCA0RXIE;                          // Enable
USCI_A0 RX interrupt
  __enable_interrupt();
}

/*-------------------------------------------------------------
* Runs in ISR context. Reading the frame should
be done in the application thread not in the ISR
thread. -----------------*/
static uint8_t sCB(linkID_t lid)
{
  if (lid)
  {
    sPeerFrameSem++;
  }
  else
  {
    sJoinSem++;
  }
  // leave frame to be read by application.
  return 0;
}


/*-------------------------------------------------------------
------ADC10 interrupt service routine------------*/

#pragma vector=ADC10_VECTOR
__interrupt void ADC10_ISR(void)
{
  __bic_SR_register_on_exit(CPUOFF);       // Clear
CPUOFF bit from 0(SR)
}

/*-------------------------------------------------------------
---Timer A0 interrupt service routine----------*/
#pragma vector=TIMERA0_VECTOR
__interrupt void Timer_A (void)
{
  sSelfMeasureSem = 1;
}

/*-------------------------------------------------------------
--------USCIA interrupt service routine--------*/
#pragma vector=USCIAB0RX_VECTOR
__interrupt void USCI0RX_ISR(void)
{
}
```

WIMU ED Board

```
//*************************************************
*******************************
//  eZ430-RF2500  Sensor End Device
//
//    Description: End Device software for the
WIMU
//
//  A. Silva
//  Version   1.00
//  FEUP
//  July 2010
//
//
//  Sensor output   |   ez430-RF2500TG pins   |
Analog input  |  Flash Address
//      Ax              P4              A1          206h
//      Ay              P3              A0          208h
//      Az              P6              A3          202h
//      Vx              P5              A2          204h
//      Vy              P7              A4          200h
//
//*************************************************
*******************************

#include "bsp.h"
#include "mrfi.h"
#include "nwk_types.h"
#include "nwk_api.h"
#include "bsp_leds.h"
#include "bsp_buttons.h"
#include "vlo_rand.h"

void linkTo(void);
void ADC_Init(void);

void createRandomAddress();
int increment_mseconds(void);
int increment_seconds(void);
int increment_minuts(void);
int increment_hour(void);


int msecond, second, minut, hour;

__no_init volatile int tempOffset @ 0x10F4; //
Temperature offset set at production
__no_init volatile char Flash_Addr[4] @ 0x10F0;
// Flash address set randomly
__no_init volatile int result_A4 @ 0x200;
__no_init volatile int result_A3 @ 0x202;
__no_init volatile int result_A2 @ 0x204;
__no_init volatile int result_A1 @ 0x206;
__no_init volatile int result_A0 @ 0x208;



void main (void)
{
 addr_t lAddr;
 WDTCTL = WDTPW + WDTHOLD;                  //
Stop WDT
 {
 // delay loop to ensure proper startup before
SimpliciTI increases DCO
 // This is typically tailored to the power supply
used, and in this case
 // is overkill for safety due to wide distribution.
  volatile int i;
  for(i = 0; i < 0xFFFF; i++){}
 }


 if( CALBC1_8MHZ == 0xFF )                  // Do not
run if cal values are erased
 {
  volatile int i;
  P1DIR |= 0x03;
  BSP_TURN_ON_LED1();
  BSP_TURN_OFF_LED2();
  while(1)
  {
   for(i = 0; i < 0x5FFF; i++){}
   BSP_TOGGLE_LED2();
   BSP_TOGGLE_LED1();
  }
 }

 // SimpliciTI will change port pin settings as
well
 P1DIR = 0xFF;
 P1OUT = 0x00;
 P2DIR = 0x27;
 P2OUT = 0x00;
 P3DIR = 0xC0;
 P3OUT = 0x00;
 P4DIR = 0xFF;
 P4OUT = 0x00;

 BSP_Init();

 if( Flash_Addr[0] == 0xFF &&
    Flash_Addr[1] == 0xFF &&
    Flash_Addr[2] == 0xFF &&
    Flash_Addr[3] == 0xFF )
 {
  createRandomAddress();                    // set
Random device address at initial startup
 }
 lAddr.addr[0]=Flash_Addr[0];
 lAddr.addr[1]=Flash_Addr[1];
 lAddr.addr[2]=Flash_Addr[2];
 lAddr.addr[3]=Flash_Addr[3];


 SMPL_Ioctl(IOCTL_OBJ_ADDR,  IOCTL_ACT_SET,
&lAddr);

 //CLK system configuration
 BCSCTL1 = CALBC1_16MHZ;                    // Set
DCO after random function
```

```
  DCOCTL = CALDCO_16MHZ;

  //Timer B configuration
  BCSCTL3 |= LFXT1S_2;                    // LFXT1 =
VLO
  TBCCTL0 = CCIE;                         // TBCCR0
interrupt enabled
  TBCCR0 = 12;                      // ~ 1 msec
  TBCTL = TBSSEL_1 + MC_1;                // ACLK,
upmode
  msecond=0;
  second = 0;
  minut = 0;
  hour = 0;

  //ADC configuration
  ADC10AE0 |= 0x1F;
  ADC10CTL1 = INCH_4 + ADC10SSEL_3 +
CONSEQ_1;
  ADC10CTL0 = SREF_1 + ADC10SHT_1 +
REF2_5V + REFON + ADC10ON + MSC +
ADC10IE;
  ADC10DTC1 = 0x05;

  // keep trying to join until successful. toggle
LEDS to indicate that
  // joining has not occurred. LED3 is red but
labeled LED 4 on the EXP
  // board silkscreen. LED1 is green.

  while (SMPL_NO_JOIN == SMPL_Init((uint8_t
(*)(linkID_t))0))
  {
    BSP_TOGGLE_LED1();
    BSP_TOGGLE_LED2();;
    //__bis_SR_register(LPM3_bits + GIE);       //
LPM3 with interrupts enabled
  }
  // unconditional link to AP which is listening
due to successful join.


  linkTo();
}


//*************************************************
*******************************

void linkTo()
{
  linkID_t linkID1;
  uint8_t  msg[9];

  // keep trying to link...
  while                (SMPL_SUCCESS                !=
SMPL_Link(&linkID1))
  {
    //__bis_SR_register(LPM3_bits + GIE);       //
LPM3 with interrupts enabled
    BSP_TOGGLE_LED1();
    BSP_TOGGLE_LED2();
  }

  // Turn off all LEDs
  if (BSP_LED1_IS_ON())
  {
    BSP_TOGGLE_LED1();
  }
  if (BSP_LED2_IS_ON())
  {
    BSP_TOGGLE_LED2();
  }

  while (1)
  {

    SMPL_Ioctl(                  IOCTL_OBJ_RADIO,
IOCTL_ACT_RADIO_SLEEP, "" );
    //__bis_SR_register(LPM3_bits+GIE);          //
LPM3 with interrupts enabled
    SMPL_Ioctl(                  IOCTL_OBJ_RADIO,
IOCTL_ACT_RADIO_AWAKE, "" );

    ADC10CTL0 &= ~ENC;
    ADC10SA = 0x200;
    ADC10CTL0 |= ENC + ADC10SC;               //
Sampling and conversion start
    //__bis_SR_register(CPUOFF + GIE);          //
LPM0 with interrupts enabled

    float value4 = ((float) result_A4 * 2.5)/1023;
    int A4 = value4 * 100;

    float value3 = ((float) result_A3 * 2.5)/1023;
    int A3 = value3 * 100;

    float value2 = ((float) result_A2 * 2.5)/1023;
    int A2 = value2 * 100;

    float value1 = ((float) result_A1 * 2.5)/1023;
    int A1 = value1 * 100;

    float value0 = ((float) result_A0 * 2.5)/1023;
    int A0 = value0 * 100;

    /*message format,  UB = upper Byte, LB =
lower Byte
    --------------------------------
    |degC LB | degC UB |  volt LB |
    --------------------------------
      0       1       2
    */

    msg[0] = A1;
    msg[1] = A0;
    msg[2] = A3;
    msg[3] = A2;
    msg[4] = A4;
    msg[5] = hour;
    msg[6] = minut;
    msg[7] = second;
    msg[8] = msecond;

    if (SMPL_SUCCESS == SMPL_Send(linkID1,
msg, sizeof(msg)))
    {
      BSP_TOGGLE_LED2();
    }
    else
```

```
   {
    BSP_TOGGLE_LED2();
    BSP_TOGGLE_LED1();
   }
  }
}

//*********************************************
*****************************

void createRandomAddress()
{
  unsigned int rand, rand2;
  do
  {
    rand = TI_getRandomIntegerFromVLO();     //
first byte can not be 0x00 of 0xFF
  }
  while( (rand & 0xFF00)==0xFF00 || (rand &
0xFF00)==0x0000 );
  rand2 = TI_getRandomIntegerFromVLO();

  BCSCTL1 = CALBC1_1MHZ;                    // Set
DCO to 1MHz
  DCOCTL = CALDCO_1MHZ;
  FCTL2 = FWKEY + FSSEL0 + FN1;             //
MCLK/3 for Flash Timing Generator
  FCTL3 = FWKEY + LOCKA;                    // Clear
LOCK & LOCKA bits
  FCTL1 = FWKEY + WRT;                      // Set WRT
bit for write operation

  Flash_Addr[0]=(rand>>8) & 0xFF;
  Flash_Addr[1]=rand & 0xFF;
  Flash_Addr[2]=(rand2>>8) & 0xFF;
  Flash_Addr[3]=rand2 & 0xFF;

  FCTL1 = FWKEY;                            // Clear WRT
bit
  FCTL3 = FWKEY + LOCKA + LOCK;             // Set
LOCK & LOCKA bit
}

/*-------------------------------------------------------------
------* ADC10 interrupt service routine----*/
#pragma vector=ADC10_VECTOR
__interrupt void ADC10_ISR(void)
{
}

/*-------------------------------------------------------------
-------*Tmer B0 interrupt service routine-------*/
#pragma vector=TIMERB0_VECTOR
__interrupt void Timer_B (void)
{
 increment_mseconds();
}

int increment_mseconds(void)
{
 if (msecond < 999)
 {
  msecond = msecond + 1;
 }
 else
 {
  msecond = 0;
  increment_seconds ();
 }
}

int increment_seconds(void)
{
 if (second < 59)
 {
  second = second + 1;
 }
 else
 {
  second = 0;
  increment_minuts ();
 }
}

int increment_minuts(void)
{
 if (minut < 59)
 {
  minut = minut + 1;
 }
 else
 {
  minut = 0;
  increment_hour();
 }
}

int increment_hour(void)
{
 if (hour < 23)
 {
  hour = hour + 1;
 }
 else
 {
  hour = 0;
 }
}
```

W2M2 MCU Board

```
// Project: Arduino FIO + ADXL345 MCU + ADXL345 remote board + COMBO Board
//        + HMC5883 Magnetometer
// Author: Ana S. Silva
// Date: 03/05/2012

// Description: The system performs simple monitoring of all sensor boards.
//Sample frequencies  min=50Hz max=500Hz

// Version control: v1 03/05/2012 based on example
code:teste_allADXL345_itg3200_HMC5883.ino



//***** LIBRYRIES and VARIABLES *******
#include <Wire.h>
#include <ADXL345.h>
#include <SPI.h>
#include <HMC5883L.h>
#include <mpr121.h>
#include "MPU6050.h"
#include "I2Cdev.h"

// I2C 7bit address of ADXL345 Board(SDO->VDD:0x1D ; SDO->GND:0x53)
#define ADXLBoardAddress 0x1D
// I2C 7bit address of ADXL345 COMBO
#define ADXLCOMBO 0x53
// I2C 7bit address of ITG3200 COMBO
char itgAddress = 0x68;

// class default I2C address is 0x68
// specific I2C addresses may be passed as a parameter here
// AD0 low = 0x68 (default for InvenSense evaluation board)
// AD0 high = 0x69
MPU6050 accelgyro(0x69);

int16_t ax, ay, az;
int16_t gx, gy, gz;

int irqpin = 2;  // Digital 2 for capacitive sensor interrupt
boolean touchStates[3]; //to keep track of the previous touch states

// Declare global instances of the accelerometer boards.
ADXL345 accel_board;
ADXL345 accel_combo;

// Store our compass as a variable.
HMC5883L compass;

//Assign the Chip Select signal to pin 10.
int CS=10;

//variables for commands
int inByte          = 0;    // a variable to read incoming serial data into
int loopans         = 0;    // acknowledgement response to receive command from PC
boolean datasend    = false;
//boolean calibration       = false;
boolean format_raw  = true;  // Reading format: 1 = raw; 0= scaled; (default:raw)
char onsd[6]        = "01010";  // Start
char offsd[6]       = "02020";  // Stop
//char syncsd[6]    = "03030";  // Synchronization
char rawd[6]        = "03030";  // Format raw
char scaled[6]      = "04040";  // Format scaled

//unsigned long SyncTime[2];

//This buffer will hold values read from the ADXL345 MCU registers.
char valuesMCU[10];

//These variables will be used to hold the x,y and z axis accelerometer values from MCU.
int rawX_MCU, rawY_MCU, rawZ_MCU;
float scaledX_MCU, scaledY_MCU, scaledZ_MCU;
//Create variables to hold the output rates.
int xRate, yRate, zRate;

//Time-stamp
unsigned long time;

//This is a list of registers in the ITG-3200. Registers are parameters that determine how the sensor will behave, or they can hold data that represent the
//sensors current status.
//To learn more about the registers on the ITG-3200, download and read the datasheet.
char WHO_AM_I = 0x00;
char SMPLRT_DIV= 0x15;
char DLPF_FS = 0x16;
char GYRO_XOUT_H = 0x1D;
char GYRO_XOUT_L = 0x1E;
char GYRO_YOUT_H = 0x1F;
char GYRO_YOUT_L = 0x20;
char GYRO_ZOUT_H = 0x21;
char GYRO_ZOUT_L = 0x22;

//This is a list of settings that can be loaded into the registers.
//DLPF, Full Scale Register Bits
//FS_SEL must be set to 3 for proper operation
//Set DLPF_CFG to 3 for 1kHz Fint and 42 Hz Low Pass Filter
char DLPF_CFG_0 = 1<<0;
char DLPF_CFG_1 = 1<<1;
char DLPF_CFG_2 = 1<<2;
char DLPF_FS_SEL_0 = 1<<3;
```

```
char DLPF_FS_SEL_1 = 1<<4;

//connection status variables
int ADXL345Board  = 0;
int ComboBoard    = 0;
int HMC5883Board  = 0;
int MPU6050Board  = 0;
int Configuration = 0;

//************ SETUP******************

void setup(){

 //Initiate an SPI communication instance.
 SPI.begin();
 //Configure the SPI connection for the ADXL345 MCU board.
 SPI.setDataMode(SPI_MODE3);
 //Create a serial connection to display the data on the terminal.
 Serial.begin(57600);

 //Set up the Chip Select pin to be an output from the Arduino.
 pinMode(CS, OUTPUT);
 //Before communication starts, the Chip Select pin needs to be set high.
 digitalWrite(CS, HIGH);

 //Put the ADXL345 into +/- 4G range by writing the value 0x01 to the DATA_FORMAT register.
 writeRegister(Register_DataFormat, 0x01);
 //Put the ADXL345 into Measurement Mode by writing 0x08 to the POWER_CTL register.
 writeRegister(Register_PowerControl, 0x08); //Measurement mode

 // Start the I2C Wire library so we can use I2C to talk to the accelerometer board.
 Wire.begin();

 //Set up capacitive sensor
 pinMode(irqpin, INPUT);
 digitalWrite(irqpin, HIGH); //enable pullup resistor
 mpr121_setup();

 // Create an instance of each accelerometer on the given addresses
 accel_board = ADXL345(ADXLBoardAddress);
 accel_combo = ADXL345(ADXLCOMBO);
 // Construct a new HMC5883 compass on the default addresss.
 compass = HMC5883L();

 // Check which boards are infact connected.
 if(accel_board.EnsureConnected())
 {
  Serial.println("Connected to ADXL345 Board.");
  ADXL345Board = true;
  // Set the range of the accelerometer ADXL345 Board 4G.
  accel_board.SetRange(4, false);
  // Tell the accelerometer to start taking measurements.
  accel_board.EnableMeasurements();
 }
 else
 {
  Serial.println("ADXL345 Board not present.");
 }

 if(accel_combo.EnsureConnected())
 {
  Serial.println("Connected to COMBO Board.");
  ComboBoard = true;
  // Set the range of the accelerometer ADXL345 COMBO 4G.
  accel_combo.SetRange(4, false);
  // Tell the accelerometer to start taking measurements.
  accel_combo.EnableMeasurements();

  //Configure the gyroscope
  //Set the gyroscope scale for the outputs to +/-2000 degrees per second
  itgWrite(itgAddress, DLPF_FS, (DLPF_FS_SEL_0|DLPF_FS_SEL_1|DLPF_CFG_0));
  //Set the sample rate to 100 hz
  itgWrite(itgAddress, SMPLRT_DIV, 9);
 }
 else
 {
  Serial.println("COMBO Board not present.");
 }

 if(compass.EnsureConnected())
 {
  Serial.println("Connected to HMC5883L magnetometer.");
  HMC5883Board = true;
  // Set the scale of the compass.
  compass.SetScale(1.3);
  // Set the measurement mode to Continuous

compass.SetMeasurementMode(Measurement_Continuous);
 }
 else
 {
  Serial.println("HMC5883L magnetometer not present.");
 }

 accelgyro.initialize();

 if (accelgyro.testConnection()) {
   Serial.println("Connected to MPU6050 Board.");
   MPU6050Board = true;
 }

 //tell about BSN configuration (which sensors are connected)
 if (ADXL345Board && ComboBoard && HMC5883Board) {
  Configuration = 7;
```

```
  } else if (ADXL345Board && ComboBoard &&
!HMC5883Board) {
   Configuration = 6;
  } else if (ADXL345Board && !ComboBoard &&
HMC5883Board) {
   Configuration = 5;
  } else if (ADXL345Board && !ComboBoard &&
!HMC5883Board) {
   Configuration = 4;
  } else if (!ADXL345Board && ComboBoard &&
HMC5883Board) {
   Configuration = 3;
  } else if (!ADXL345Board && ComboBoard &&
!HMC5883Board) {
   Configuration = 2;
  } else if (!ADXL345Board && !ComboBoard &&
HMC5883Board) {
   Configuration = 1;
  } else {
   Configuration = 0;
  }

  Serial.print("Configuration Code:");
  Serial.println(Configuration);

}

//******* MAIN FUNCTION ********************

void loop()
{
  if (Serial.available() > 0) {
    inByte = Serial.read();
    if (inByte == 35) {
      loopans= ackresp();
      if (loopans == 1){
        Serial.println("Ack Start");
        datasend = true;
      } else if (loopans == 2) {
        Serial.println("Ack Stop");
              datasend = false;
      } else if (loopans == 3){
        Serial.println("Ack Data Format Raw");
        format_raw = true;
      } else if (loopans == 4){
        Serial.println("Ack Data Format Scaled");
        format_raw = false;
      } else {
              Serial.println("Ack "+ loopans);
      }
    } else {}
  } else if (datasend) {
    readData();
    //delay(1000);
  } else {}
}

//********* DECLARED FUNCTIONS ******

//This function will verified command received
by serial and return int based on confirmation
// 0 = unknown, 1 for Ack 1 (start sending data)
and 2 (stop sending data)
//Parameters: NONE
int ackresp() {
  delay(50);
  char mess[6];
  int bufread = Serial.available();
  if (bufread>5) {
    for(int i=0; i<5; i++) {
      mess[i] = Serial.read();
    }
    mess[5] = 0;
    if (strcmp(onsd,mess) == 0) {    //strcmp(x,y)
function looks for x parameter in string y
      return 1;
    } else if (strcmp(offsd,mess) == 0) {
      return 2;
    } else if (strcmp(rawd,mess) == 0) {
      return 3;
    } else if (strcmp(scaled,mess) == 0) {
      return 4;
    } else {
      return 0;
    }
  } else {
    return 0;
  }
}

void readData() {

  //check if any change occured in capacitive
sensor and if so process data
  if(!checkInterrupt()){

    //read the touch state from the MPR121
    Wire.requestFrom(0x5A,2);

    byte LSB = Wire.read();
    byte MSB = Wire.read();

    uint16_t touched = ((MSB << 8) | LSB);
//16bits that make up the touch states

    for (int i=0; i < 3; i++){   // Check what
electrodes were pressed

      if(touched & (1<<i)){

        if(touchStates[i] == 0){
          //pin i was just touched
          Serial.print(i);
          Serial.print(" T:");       // T: touched
          Serial.println(millis());
//          Serial.print("pin ");
//          Serial.print(i);
//          Serial.println(" was just touched");

        }else if(touchStates[i] == 1){
          //pin i is still being touched
        }
        touchStates[i] = 1;
      }
      else{
        if(touchStates[i] == 1){
          Serial.print(i);
          Serial.print(" NLT:");       // NLT: no longer
touching
          Serial.println(millis());
```

```
      //pin i is no longer being touched
    }

     touchStates[i] = 0;
   }  }    }

 if (format_raw) {
  //Reading 6 bytes of data starting at register DATAX0 will retrieve the x,y and z acceleration
  //The results of the read operation will get stored to the valuesMCU[] buffer.
  readRegister(Register_DataX, 6, valuesMCU);

  rawX_MCU = ((int)valuesMCU[1]<<8)|(int)valuesMCU[0];
  rawY_MCU = ((int)valuesMCU[3]<<8)|(int)valuesMCU[2];
  rawZ_MCU = ((int)valuesMCU[5]<<8)|(int)valuesMCU[4];

  //data from ADXL345 MCU
  //Serial.print("ADXL345 MCU:\t");
  Serial.print(rawX_MCU);
  Serial.print("\t");
  Serial.print(rawY_MCU);
  Serial.print("\t");
  Serial.print(rawZ_MCU);
  Serial.print("\t");

   if(ADXL345Board)
   {
    //Read accelerometer data from ADXL345 Board and scales it
    AccelerometerRaw raw_board = accel_board.ReadRawAxis();

    // raw data from the ADXL345 board
    //Serial.print("  \tADXL345 Board:\t");
    Serial.print(raw_board.XAxis);
    Serial.print("\t");
    Serial.print(raw_board.YAxis);
    Serial.print("\t");
    Serial.print(raw_board.ZAxis);
    Serial.print("\t");
   }

   if(ComboBoard)
   {
    //Read raw data from accelerometer COMBO board
    AccelerometerRaw raw_combo = accel_combo.ReadRawAxis();

    //Read the x,y and z output rates from the gyroscope.
    xRate = readX();
    yRate = readY();
    zRate = readZ();

    //data from the ADXL345 combo
    //Serial.print("  \tADXL345 COMBO:\t");
    Serial.print(raw_combo.XAxis);
    Serial.print("\t");
    Serial.print(raw_combo.YAxis);
    Serial.print("\t");
    Serial.print(raw_combo.ZAxis);
    Serial.print("\t");

    //Print the output rates to the terminal, seperated by a TAB character.
    //Serial.print("  \tITG3200:\t");
    Serial.print(xRate);
    Serial.print("\t");
    Serial.print(yRate);
    Serial.print("\t");
    Serial.print(zRate);
    Serial.print("\t");
   }

   if(HMC5883Board)
   {
    MagnetometerRaw raw_compass = compass.ReadRawAxis();
    Serial.print(raw_compass.XAxis);
    Serial.print("\t");
    Serial.print(raw_compass.YAxis);
    Serial.print("\t");
    Serial.print(raw_compass.ZAxis);
    Serial.print("\t");
   }
   if(MPU6050Board) {
    accelgyro.getMotion6(&ax, &ay, &az, &gx, &gy, &gz);
    Serial.print(ax); Serial.print("\t");
    Serial.print(ay); Serial.print("\t");
    Serial.print(az); Serial.print("\t");
    Serial.print(gx); Serial.print("\t");
    Serial.print(gy); Serial.print("\t");
    Serial.print(gz); Serial.print("\t");
   }

   //Retrieve time-stamp
   time = millis();

   // Time-stamp
   //Serial.print("  \tTime:\t");
   Serial.println(time);
  }
 else {
  //Reading 6 bytes of data starting at register DATAX0 will retrieve the x,y and z acceleration
  //The results of the read operation will get stored to the valuesMCU[] buffer.
  readRegister(Register_DataX, 6, valuesMCU);

  rawX_MCU = ((int)valuesMCU[1]<<8)|(int)valuesMCU[0];
  rawY_MCU = ((int)valuesMCU[3]<<8)|(int)valuesMCU[2];
  rawZ_MCU = ((int)valuesMCU[5]<<8)|(int)valuesMCU[4];

  scaledX_MCU = rawX_MCU * ScaleFor4G;
  scaledY_MCU = rawY_MCU * ScaleFor4G;
  scaledZ_MCU = rawZ_MCU * ScaleFor4G;

  //data from ADXL345 MCU
  //Serial.print("ADXL345 MCU:\t");
  Serial.print(scaledX_MCU);
```

```
  Serial.print("\t");
  Serial.print(scaledY_MCU);
  Serial.print("\t");
  Serial.print(scaledZ_MCU);
  Serial.print("\t");

  if(ADXL345Board)
  {
   //Read accelerometer data from ADXL345 Board and scales it
   AccelerometerScaled scaled_board = accel_board.ReadScaledAxis();

   // Scaled data from the ADXL345 board
   //Serial.print("  \tADXL345 Board:\t");
   Serial.print(scaled_board.XAxis);
   Serial.print("\t");
   Serial.print(scaled_board.YAxis);
   Serial.print("\t");
   Serial.print(scaled_board.ZAxis);
   Serial.print("\t");
  }

  if(ComboBoard)
  {
   //Read raw data from accelerometer COMBO board
   AccelerometerScaled scaled_combo = accel_combo.ReadScaledAxis();

 //  scaledX_combo = raw_combo.XAxis * ScaleFor4G;
 //  scaledY_combo = raw_combo.YAxis * ScaleFor4G;
 //  scaledZ_combo = raw_combo.ZAxis * ScaleFor4G;

   //Read the x,y and z output rates from the gyroscope.
   xRate = readX();
   yRate = readY();
   zRate = readZ();

   //data from the ADXL345 combo
   //Serial.print("  \tADXL345 COMBO:\t");
   Serial.print(scaled_combo.XAxis);
   Serial.print("\t");
   Serial.print(scaled_combo.YAxis);
   Serial.print("\t");
   Serial.print(scaled_combo.ZAxis);
   Serial.print("\t");

   //Print the output rates to the terminal, seperated by a TAB character.
   //Serial.print("  \tITG3200:\t");
   Serial.print(xRate);
   Serial.print("\t");
   Serial.print(yRate);
   Serial.print("\t");
   Serial.print(zRate);
   Serial.print("\t");
  }

  if(HMC5883Board)
  {
   MagnetometerScaled scaled_compass = compass.ReadScaledAxis();
   Serial.print(scaled_compass.XAxis);
   Serial.print("\t");
   Serial.print(scaled_compass.YAxis);
   Serial.print("\t");
   Serial.print(scaled_compass.ZAxis);
   Serial.print("\t");
  }


  //Retrieve time-stamp
  time = millis();

  // Time-stamp
  //Serial.print("  \tTime:\t");
  Serial.println(time);
 } }

//This function will write a value to a register on the ADXL345.
void writeRegister(char registerAddress, char value){
 //Set Chip Select pin low to signal the beginning of an SPI packet.
 digitalWrite(CS, LOW);
 //Transfer the register address over SPI.
 SPI.transfer(registerAddress);
 //Transfer the desired register value over SPI.
 SPI.transfer(value);
 //Set the Chip Select pin high to signal the end of an SPI packet.
 digitalWrite(CS, HIGH);
}

//This function will read a certain number of registers starting from a specified
// address and store their values in a buffer.
void readRegister(char registerAddress, int numBytes, char * values)
{
 //Since we're performing a read operation, the most significant bit of the register address should be set.
 char address = 0x80 | registerAddress;
 //If we're doing a multi-byte read, bit 6 needs to be set as well.
 if(numBytes > 1)address = address | 0x40;

 //Set the Chip select pin low to start an SPI packet.
 digitalWrite(CS, LOW);
 //Transfer the starting register address that needs to be read.
 SPI.transfer(address);
 //Continue to read registers until we've read the number specified, storing the results to the input buffer.
 for(int i=0; i<numBytes; i++){
  values[i] = SPI.transfer(0x00);
 }
 //Set the Chips Select pin high to end the SPI packet.
 digitalWrite(CS, HIGH);
}
```

```
//This function will write a value to a register on the itg-3200.
//Parameters:
// char address: The I2C address of the sensor. For the ITG-3200 breakout the address is 0x69.
// char registerAddress: The address of the register on the sensor that should be written to.
// char data: The value to be written to the specified register.
void itgWrite(char address, char registerAddress, char data)
{
 //Initiate a communication sequence with the desired i2c device
 Wire.beginTransmission(address);
 //Tell the I2C address which register we are writing to
 Wire.write(registerAddress);
 //Send the value to write to the specified register
 Wire.write(data);
 //End the communication sequence
 Wire.endTransmission();
}

//This function will read the data from a specified register on the ITG-3200 and return the value.
//Parameters:
// char address: The I2C address of the sensor. For the ITG-3200 breakout the address is 0x69.
// char registerAddress: The address of the register on the sensor that should be read
//Return:
// unsigned char: The value currently residing in the specified register
unsigned char itgRead(char address, char registerAddress)
{
 //This variable will hold the contents read from the i2c device.
 unsigned char data=0;

 //Send the register address to be read.
 Wire.beginTransmission(address);
 //Send the Register Address
 Wire.write(registerAddress);
 //End the communication sequence.
 Wire.endTransmission();

 //Ask the I2C device for data
 Wire.beginTransmission(address);
 Wire.requestFrom(address, 1);

 //Wait for a response from the I2C device
 if(Wire.available()){
  //Save the data sent from the I2C device
  data = Wire.read();
 }

 //End the communication sequence.
 Wire.endTransmission();

 //Return the data read during the operation
 return data;
}

//This function is used to read the X-Axis rate of the gyroscope. The function returns the ADC value from the Gyroscope
//NOTE: This value is NOT in degrees per second.
//Usage: int xRate = readX();
int readX(void)
{
 int data=0;
 data = itgRead(itgAddress, GYRO_XOUT_H)<<8;
 data |= itgRead(itgAddress, GYRO_XOUT_L);

 return data;
}

//This function is used to read the Y-Axis rate of the gyroscope. The function returns the ADC value from the Gyroscope
//NOTE: This value is NOT in degrees per second.
//Usage: int yRate = readY();
int readY(void)
{
 int data=0;
 data = itgRead(itgAddress, GYRO_YOUT_H)<<8;
 data |= itgRead(itgAddress, GYRO_YOUT_L);

 return data;
}

//This function is used to read the Z-Axis rate of the gyroscope. The function returns the ADC value from the Gyroscope
//NOTE: This value is NOT in degrees per second.
//Usage: int zRate = readZ();
int readZ(void)
{
 int data=0;
 data = itgRead(itgAddress, GYRO_ZOUT_H)<<8;
 data |= itgRead(itgAddress, GYRO_ZOUT_L);

 return data;
}
void mpr121_setup(void){

 set_register(0x5A, ELE_CFG, 0x00);

 // Section A - Controls filtering when data is > baseline.
 set_register(0x5A, MHD_R, 0x01);
 set_register(0x5A, NHD_R, 0x01);
 set_register(0x5A, NCL_R, 0x00);
 set_register(0x5A, FDL_R, 0x00);

 // Section B - Controls filtering when data is < baseline.
 set_register(0x5A, MHD_F, 0x01);
 set_register(0x5A, NHD_F, 0x01);
 set_register(0x5A, NCL_F, 0xFF);
 set_register(0x5A, FDL_F, 0x02);
```

```
  // Section C - Sets touch and release thresholds for each electrode
  set_register(0x5A, ELE0_T, TOU_THRESH);
  set_register(0x5A, ELE0_R, REL_THRESH);

  set_register(0x5A, ELE1_T, TOU_THRESH);
  set_register(0x5A, ELE1_R, REL_THRESH);

  set_register(0x5A, ELE2_T, TOU_THRESH);
  set_register(0x5A, ELE2_R, REL_THRESH);

  set_register(0x5A, ELE3_T, TOU_THRESH);
  set_register(0x5A, ELE3_R, REL_THRESH);

  set_register(0x5A, ELE4_T, TOU_THRESH);
  set_register(0x5A, ELE4_R, REL_THRESH);

  set_register(0x5A, ELE5_T, TOU_THRESH);
  set_register(0x5A, ELE5_R, REL_THRESH);

  set_register(0x5A, ELE6_T, TOU_THRESH);
  set_register(0x5A, ELE6_R, REL_THRESH);

  set_register(0x5A, ELE7_T, TOU_THRESH);
  set_register(0x5A, ELE7_R, REL_THRESH);

  set_register(0x5A, ELE8_T, TOU_THRESH);
  set_register(0x5A, ELE8_R, REL_THRESH);

  set_register(0x5A, ELE9_T, TOU_THRESH);
  set_register(0x5A, ELE9_R, REL_THRESH);

  set_register(0x5A, ELE10_T, TOU_THRESH);
  set_register(0x5A, ELE10_R, REL_THRESH);

  set_register(0x5A, ELE11_T, TOU_THRESH);
  set_register(0x5A, ELE11_R, REL_THRESH);

  // Section D
  // Set the Filter Configuration
  // Set ESI2
  set_register(0x5A, FIL_CFG, 0x04);

  // Section E
  // Electrode Configuration
  // Set ELE_CFG to 0x00 to return to standby mode
  set_register(0x5A, ELE_CFG, 0x0C);  // Enables all 12 Electrodes

  // Section F
  // Enable Auto Config and auto Reconfig
  /*set_register(0x5A, ATO_CFG0, 0x0B);
  set_register(0x5A, ATO_CFGU, 0xC9);  // USL = (Vdd-0.7)/vdd*256 = 0xC9 @3.3V
set_register(0x5A, ATO_CFGL, 0x82);  // LSL = 0.65*USL = 0x82 @3.3V
  set_register(0x5A, ATO_CFGT, 0xB5);*/  // Target = 0.9*USL = 0xB5 @3.3V

  set_register(0x5A, ELE_CFG, 0x0C);

}

boolean checkInterrupt(void){
  return digitalRead(irqpin);
}
void set_register(int address, unsigned char r, unsigned char v){
    Wire.beginTransmission(address);
    Wire.write(r);
    Wire.write(v);
    Wire.endTransmission();
}
```

Appendix B: PROCESSING Code

```
------READ DATA FROM W2M2---------

// Need G4P library
import guicomponents.*;
import processing.serial.*;

PFont myFont;
PFont g_font;

Serial myPort;  // The serial port

PrintWriter output_data, Subject_data,
SyncTimes;

int open_port       = 0;
int start_acquisition = 0;
int trial           = 1;
int BaudRate        = 57600;


String inBuffer, inBufferIntro, data_filename,
Info_filename, sync_filename, Subject_name,
Subject_age, Subject_arm;
String Subject_hip, Subject_leg, observations,
COMPORT;
String arm = "Right";
String plane = "Shoulder";

void setup(){
 size(770, 680);
 createGUI();
 customGUI();

}

void draw(){
 background(200,220,200);

 if (open_port == 1){

   while (myPort.available() > 0) {
    inBufferIntro = myPort.readString();
    if (inBufferIntro != null) {
     print(inBufferIntro);
     //txtData.setText(inBufferIntro);
    }
   }
    open_port = 0;
 }

 else if (start_acquisition == 1) {
  while (myPort.available() > 0 ) {
   inBuffer = myPort.readString();
   if (inBuffer != null) {
    print(inBuffer);
    txtData.setText(inBuffer);
    output_data.print(inBuffer);
    }
   }

 } else {

 }

}


// Use this method to add additional statements
// to customise the GUI controls
void customGUI(){

//  btnStop.setFont("Verdana-16.vlw", 20);
//  btnStop.setColorScheme(122);
}


-------------GENERAL USER INTERFACE---------


void eventData(GTextField textfield) {
//_CODE_:txtData:316170:
 println("txtData - GTextField event occured " +
System.currentTimeMillis()%10000000 );
} //_CODE_:txtData:316170:

void eventStartAcq(GButton button) {
//_CODE_:btnStart:605144:
 println("btnStart - GButton event occured " +
System.currentTimeMillis()%10000000 );
 myPort.clear();
 myPort.write("#01010" + 13);
 start_acquisition = 1;
 data_filename = Subject_name + "_" + arm + "_"
+ plane + "_Trial " + trial + ".txt";
 output_data = createWriter(data_filename);
 sync_filename = Subject_name + "_" + arm + "_"
+ plane + "_Trial " + trial + "_SyncTimes.txt";
 SyncTimes = createWriter(sync_filename);
 //output_data.print(inBufferIntro);
 SyncTimes.print("Starting Time: ");

SyncTimes.println(System.currentTimeMillis());
 txtDataFile.setText(data_filename);
 trial++;
} //_CODE_:btnStart:605144:

void eventStopAcq(GButton button) {
//_CODE_:btnStop:992317:
 println("btnStop - GButton event occured " +
System.currentTimeMillis()%10000000 );
 myPort.write("#02020" + 13); //send STOP
command
 output_data.flush(); // Write the remaining
data
```

```
  output_data.close(); // Finish the file
  SyncTimes.close();
  start_acquisition = 0;
} //_CODE_:btnStop:992317:

void eventSerialPort(GTextField textfield) {
//_CODE_:txtSerialPort:637799:
  println("txtSerialPort - GTextField event
occured " +
System.currentTimeMillis()%10000000 );
} //_CODE_:txtSerialPort:637799:

void eventFilename(GTextField textfield) {
//_CODE_:txtDataFile:887671:
  println("txtDataFile - GTextField event occured
" + System.currentTimeMillis()%10000000 );
} //_CODE_:txtDataFile:887671:

void eventImgBiowear(GImageButton
imagebutton) {
//_CODE_:btnImgBiowear:981398:
  println("imgButton1 - GImageButton event
occured " +
System.currentTimeMillis()%10000000 );
  link("http://paginas.fe.up.pt/~biowear/");
} //_CODE_:btnImgBiowear:981398:

void eventExit(GButton button) {
//_CODE_:btnExit:750263:
  println("btnExit - GButton event occured " +
System.currentTimeMillis()%10000000 );
  myPort.clear();
  myPort.stop();
  exit();
} //_CODE_:btnExit:750263:

void eventOpenPort(GButton button) {
//_CODE_:btnOpenPort:414558:
  println("btnOpenPort - GButton event occured
" + System.currentTimeMillis()%10000000 );
  COMPORT = TextComPort.getText();
  myPort = new Serial(this, COMPORT,
BaudRate);
  txtSerialPort.setText(COMPORT + "  " +
BaudRate);
  open_port = 1;
} //_CODE_:btnOpenPort:414558:

void rawData_Click1(GOption opt_selected,
GOption opt_deselected) {
//_CODE_:Raw:938014:
  println("Raw - GOption event occured " +
System.currentTimeMillis()%10000000 );
   myPort.write("#04040" + 13);
} //_CODE_:Raw:938014:

void ScaledData_Click1(GOption opt_selected,
GOption opt_deselected) {
//_CODE_:Scaled:861742:
  println("Scaled - GOption event occured " +
System.currentTimeMillis()%10000000 );
  myPort.write("#05050" + 13);
} //_CODE_:Scaled:861742:

void SubjectName_Enter1(GTextField textfield) {
//_CODE_:SubjectName:680835:
  println("SubjectName - GTextField event
occured " +
System.currentTimeMillis()%10000000 );
} //_CODE_:SubjectName:680835:

void Age_Enter1(GTextField textfield) {
//_CODE_:SubjectAge:575600:
  println("SubjectAge - GTextField event occured
" + System.currentTimeMillis()%10000000 );
} //_CODE_:SubjectAge:575600:

void SubjectInfo_Click1(GButton button) {
//_CODE_:SubmitData:315676:
  println("SubmitData - GButton event occured "
+ System.currentTimeMillis()%10000000 );
  Subject_name = SubjectName.getText();
  Subject_age = SubjectAge.getText();
  Subject_arm = ArmMeasure.getText();
  Subject_hip = HipMeasure.getText();
  Subject_leg = LegMeasure.getText();
  observations = Comments.getText();

  Info_filename = "Info_" + Subject_name + ".txt";
  Subject_data = createWriter(Info_filename);
  Subject_data.println("Subject Name: " +
Subject_name);
  Subject_data.println("Subject Age: " +
Subject_age);
  Subject_data.println("Subject Antropometry: ");
  Subject_data.println("    Arm: " + Subject_arm);
  Subject_data.println("    Hip: " + Subject_hip);
  Subject_data.println("    Leg: " + Subject_leg);
  Subject_data.println("Additional Comments: ");
  Subject_data.println(observations);
  Subject_data.close(); // Finish the file
  InfoFilename.setText(Info_filename);

} //_CODE_:SubmitData:315676:

void arm_Enter1(GTextField textfield) {
//_CODE_:ArmMeasure:217156:
  println("ArmMeasure - GTextField event
occured " +
System.currentTimeMillis()%10000000 );
} //_CODE_:ArmMeasure:217156:

void hip_Enter2(GTextField textfield) {
//_CODE_:HipMeasure:263978:
  println("HipMeasure - GTextField event
occured " +
System.currentTimeMillis()%10000000 );
} //_CODE_:HipMeasure:263978:

void leg_Enter3(GTextField textfield) {
//_CODE_:LegMeasure:421167:
  println("LegMeasure - GTextField event
occured " +
System.currentTimeMillis()%10000000 );
} //_CODE_:LegMeasure:421167:

void InfoFilename_Enter1(GTextField textfield) {
//_CODE_:InfoFilename:899478:
```

```
 println("InfoFilename - GTextField event occured " + System.currentTimeMillis()%10000000 );
} //_CODE_:InfoFilename:899478:

void RightArm_Click1(GOption opt_selected, GOption opt_deselected) {
//_CODE_:RightArm:465554:
 println("RightArm - GOption event occured " + System.currentTimeMillis()%10000000 );
 arm = "Right";
} //_CODE_:RightArm:465554:

void LeftArm_Click1(GOption opt_selected, GOption opt_deselected) {
//_CODE_:LeftArm:960881:
 println("LeftArm - GOption event occured " + System.currentTimeMillis()%10000000 );
 arm = "Left";
} //_CODE_:LeftArm:960881:

void shoulder_Click1(GOption opt_selected, GOption opt_deselected) {
//_CODE_:Shoulder:613941:
 println("option1 - GOption event occured " + System.currentTimeMillis()%10000000 );
 plane = "Shoulder";
} //_CODE_:Shoulder:613941:

void Scapula_Click1(GOption opt_selected, GOption opt_deselected) {
//_CODE_:Scapula:338226:
 println("option2 - GOption event occured " + System.currentTimeMillis()%10000000 );
 plane = "Scapula";
} //_CODE_:Scapula:338226:

void comments_Enter1(GTextField textfield) {
//_CODE_:Comments:211458:
 println("Comments - GTextField event occured " + System.currentTimeMillis()%10000000 );
} //_CODE_:Comments:211458:

void COMPort_Enter1(GTextField textfield) {
//_CODE_:TextComPort:584961:
 println("TextComPort - GTextField event occured " + System.currentTimeMillis()%10000000 );
} //_CODE_:TextComPort:584961:

void BD38400_Click1(GOption opt_selected, GOption opt_deselected) {
//_CODE_:BD38400:916242:
 println("option1 - GOption event occured " + System.currentTimeMillis()%10000000 );
 BaudRate = 38400;
} //_CODE_:BD38400:916242:

void BD57600_Click1(GOption opt_selected, GOption opt_deselected) {
//_CODE_:BD57600:885488:
 println("option2 - GOption event occured " + System.currentTimeMillis()%10000000 );
 BaudRate = 57600;
} //_CODE_:BD57600:885488:

void BD115200_Click1(GOption opt_selected, GOption opt_deselected) {
//_CODE_:BD115200:416920:
 println("option3 - GOption event occured " + System.currentTimeMillis()%10000000 );
 BaudRate = 115200;
} //_CODE_:BD115200:416920:

void SyncQualysis_Click1(GButton button) {
//_CODE_:SyncQualysis:598017:
 println("button1 - GButton event occured " + System.currentTimeMillis()%10000000 );

SyncTimes.println(System.currentTimeMillis());
 //myPort.write("#03030" + 13);
} //_CODE_:SyncQualysis:598017:

void resettrial_Click1(GButton button) {
//_CODE_:ResetButton:293685:
 println("ResetButton - GButton event occured " + System.currentTimeMillis()%10000000 );
 trial = 1;
} //_CODE_:ResetButton:293685:

void MCUGraphs(GWinApplet appc, GWinData data) { //_CODE_:MCUBoard:860613:
 appc.background(200,220,200);

} //_CODE_:MCUBoard:860613:

void AccBoardGraphs(GWinApplet appc, GWinData data) { //_CODE_:AccBoard:225894:
 appc.background(200,220,200);
} //_CODE_:AccBoard:225894:

void ComboBoardGraphs(GWinApplet appc, GWinData data) {
//_CODE_:ComboBoard:896781:
 appc.background(200,220,200);
} //_CODE_:ComboBoard:896781:



// Create all the GUI controls.
// autogenerated do not edit
void createGUI(){
 G4P.setColorScheme(this, GCScheme.GREY_SCHEME);
 G4P.messagesEnabled(false);
 txtData = new GTextField(this, "Click 'Open Port' button to start communication with W2M2", 24, 392, 296, 208, true);
 txtData.addEventHandler(this, "eventData");
 btnStart = new GButton(this, "START Acquisition", 464, 512, 128, 40);
 btnStart.setTextAlign(GAlign.CENTER | GAlign.MIDDLE);
 btnStart.addEventHandler(this, "eventStartAcq");
 btnStop = new GButton(this, "STOP Acquisition", 616, 512, 128, 40);
 btnStop.setTextAlign(GAlign.CENTER | GAlign.MIDDLE);
```

```
 btnStop.addEventHandler(this,
"eventStopAcq");
 txtSerialPort = new GTextField(this, "", 296, 96,
152, 24, false);
 txtSerialPort.addEventHandler(this,
"eventSerialPort");
 txtDataFile = new GTextField(this,
"(automatically generated)", 416, 576, 328, 24,
false);
 txtDataFile.addEventHandler(this,
"eventFilename");
 btnImgBiowear = new GImageButton(this, null,
"BIOwear_small.jpg", 1, 496, 24);
 btnImgBiowear.addEventHandler(this,
"eventImgBiowear");
 btnExit = new GButton(this, "EXIT", 336, 632,
102, 32);
 btnExit.setTextAlign(GAlign.CENTER |
GAlign.MIDDLE);
 btnExit.addEventHandler(this, "eventExit");
 btnOpenPort = new GButton(this, "Open Port",
184, 96, 68, 25);
 btnOpenPort.setTextAlign(GAlign.CENTER |
GAlign.TOP);
 btnOpenPort.addEventHandler(this,
"eventOpenPort");
 optGroup1 = new GOptionGroup();
 Raw = new GOption(this, "Raw", 352, 424, 95);
 optGroup1.addOption(Raw);
 Raw.setSelected(true);
 Raw.addEventHandler(this, "rawData_Click1");
 Scaled = new GOption(this, "Scaled", 352, 456,
96);
 optGroup1.addOption(Scaled);
 Scaled.addEventHandler(this,
"ScaledData_Click1");
 DataFormat = new GLabel(this, "Data Format:",
336, 392, 79, 20);
 filename = new GLabel(this, "Filename:", 336,
576, 80, 24);
 Name = new GLabel(this, "Enter Subject's
Name:", 16, 168, 168, 24);
 SubjectName = new GTextField(this, "John
Doe", 24, 200, 128, 20, false);
 SubjectName.addEventHandler(this,
"SubjectName_Enter1");
 Age = new GLabel(this, "Enter Subject's Age",
16, 240, 168, 24);
 SubjectAge = new GTextField(this, "", 24, 272,
96, 24, false);
 SubjectAge.addEventHandler(this,
"Age_Enter1");
 SubmitData = new GButton(this, "OK", 184,
320, 72, 24);
 SubmitData.setTextAlign(GAlign.CENTER |
GAlign.MIDDLE);
 SubmitData.addEventHandler(this,
"SubjectInfo_Click1");
 Antropometry = new GLabel(this, "Enter
Antropometry Info", 224, 168, 192, 24);
 Leg = new GLabel(this, "Leg (cm):", 232, 200,
64, 24);
 hip = new GLabel(this, "Hip (cm):", 232, 232,
64, 20);
 Arm = new GLabel(this, "Arm (cm):", 232, 264,
64, 20);
 ArmMeasure = new GTextField(this, "", 312,
264, 80, 20, false);
 ArmMeasure.addEventHandler(this,
"arm_Enter1");
 HipMeasure = new GTextField(this, "", 312,
232, 80, 20, false);
 HipMeasure.addEventHandler(this,
"hip_Enter2");
 LegMeasure = new GTextField(this, "", 312,
200, 80, 20, false);
 LegMeasure.addEventHandler(this,
"leg_Enter3");
 SubInfoFilename = new GLabel(this, "Subject's
Info Filename:", 416, 312, 136, 24);
 InfoFilename = new GTextField(this,
"(automatically generated)", 552, 312, 192, 24,
false);
 InfoFilename.addEventHandler(this,
"InfoFilename_Enter1");
 ArmAnalysis = new GLabel(this, "Data
Collection:", 480, 392, 80, 20);
 optGroup2 = new GOptionGroup();
 RightArm = new GOption(this, "Right Arm",
496, 424, 90);
 optGroup2.addOption(RightArm);
 RightArm.setSelected(true);
 RightArm.addEventHandler(this,
"RightArm_Click1");
 LeftArm = new GOption(this, "Left Arm", 496,
456, 90);
 optGroup2.addOption(LeftArm);
 LeftArm.addEventHandler(this,
"LeftArm_Click1");
 CollectionPlane = new GLabel(this, "Collection
Plane:", 616, 392, 80, 20);
 optGroup3 = new GOptionGroup();
 Shoulder = new GOption(this, "Shoulder", 632,
424, 90);
 optGroup3.addOption(Shoulder);
 Shoulder.setSelected(true);
 Shoulder.addEventHandler(this,
"shoulder_Click1");
 Scapula = new GOption(this, "Scapula", 632,
456, 90);
 optGroup3.addOption(Scapula);
 Scapula.addEventHandler(this,
"Scapula_Click1");
 Observations = new GLabel(this, "Comments:",
448, 168, 80, 24);
 Comments = new GTextField(this, "", 456, 200,
288, 88, true);
 Comments.addEventHandler(this,
"comments_Enter1");
 COMPort = new GLabel(this, "Enter COM Port:",
16, 24, 88, 24);
 TextComPort = new GTextField(this, "COM8",
24, 56, 112, 24, false);
 TextComPort.addEventHandler(this,
"COMPort_Enter1");
 BD = new GLabel(this, "Choose BaudRate:",
176, 24, 104, 24);
 optGroup4 = new GOptionGroup();
```

```
  BD38400 = new GOption(this, "38400", 176, 56,
90);
  optGroup4.addOption(BD38400);
  BD38400.addEventHandler(this,
"BD38400_Click1");
  BD57600 = new GOption(this, "57600", 280, 56,
90);
  optGroup4.addOption(BD57600);
  BD57600.setSelected(true);
  BD57600.addEventHandler(this,
"BD57600_Click1");
  BD115200 = new GOption(this, "115200", 384,
56, 90);
  optGroup4.addOption(BD115200);
  BD115200.addEventHandler(this,
"BD115200_Click1");
  SyncQualysis = new GButton(this, "Sync", 336,
520, 72, 24);
  SyncQualysis.setTextAlign(GAlign.CENTER |
GAlign.MIDDLE);
  SyncQualysis.addEventHandler(this,
"SyncQualysis_Click1");
  ResetButton = new GButton(this, "Reset Trial",
688, 608, 56, 23);
  ResetButton.setTextAlign(GAlign.CENTER |
GAlign.MIDDLE);
  ResetButton.addEventHandler(this,
"resettrial_Click1");
  MCUBoard = new GWindow(this, "MCU Gaphs",
0, 0, 430, 270, false, JAVA2D);
  MCUBoard.addDrawHandler(this,
"MCUGraphs");
  AccBoard = new GWindow(this, "Accelerometer
Board Graphs", 0, 0, 430, 270, false, JAVA2D);
  AccBoard.addDrawHandler(this,
"AccBoardGraphs");
  ComboBoard = new GWindow(this, "Combo
Board Graphs", 0, 0, 430, 300, false, JAVA2D);
  ComboBoard.addDrawHandler(this,
"ComboBoardGraphs");
}

// Variable declarations
// autogenerated do not edit
GTextField txtData;
GButton btnStart;
GButton btnStop;
GTextField txtSerialPort;
GTextField txtDataFile;
GImageButton btnImgBiowear;
GButton btnExit;
GButton btnOpenPort;
GOptionGroup optGroup1;
GOption Raw;
GOption Scaled;
GLabel DataFormat;
GLabel filename;
GLabel Name;
GTextField SubjectName;
GLabel Age;
GTextField SubjectAge;
GButton SubmitData;
GLabel Antropometry;
GLabel Leg;
GLabel hip;
GLabel Arm;
GTextField ArmMeasure;
GTextField HipMeasure;
GTextField LegMeasure;
GLabel SubInfoFilename;
GTextField InfoFilename;
GLabel ArmAnalysis;
GOptionGroup optGroup2;
GOption RightArm;
GOption LeftArm;
GLabel CollectionPlane;
GOptionGroup optGroup3;
GOption Shoulder;
GOption Scapula;
GLabel Observations;
GTextField Comments;
GLabel COMPort;
GTextField TextComPort;
GLabel BD;
GOptionGroup optGroup4;
GOption BD38400;
GOption BD57600;
GOption BD115200;
GButton SyncQualysis;
GButton ResetButton;
GWindow MCUBoard;
GWindow AccBoard;
GWindow ComboBoard;
```

Appendix C: Matlab Script

FOS Data Acquisition and Processing

```
------READ POWERMETER---------

clc; clear all; close all;

Path='C:\Users\asilva\Documents\Doutoramen
to\Fiber optic sensor\Data acquisition\';
Desired_Name='FOS_FourLoops';

File=[Path Desired_Name '.csv'];

gpib_h=gpib_usb_prologix_open('COM4');

set_gpib_addr(gpib_h,20); %20
clc
Slot=1;
Channel=1;
n_amostra=1100;
P=zeros(1,n_amostra);
sec=zeros(1,n_amostra);
min=zeros(1,n_amostra);
disp('i=')
for i=1:n_amostra
[power
unit]=power_meter_8163_read(gpib_h,Slot,Chan
nel);
P(i)=power;
fprintf('%d\n',i)
T1=clock;
min(i)=T1(5);

sec(i)=T1(6);

plot(i,P(i),'o');
hold on;
end

fclose(gpib_h);

%csvwrite(File,[P' min' sec']);
dlmwrite(File, [ min' sec' P' ],'delimiter',',');
save([File(1:end-4) '.mat'],'min','sec', 'P');
figure
plot(min+sec/60,P)
%hold on;
-----
function gpib_h=gpib_usb_prologix_open( COM)

gpib_h=serial(COM);
gpib_h.BaudRate=115200;
gpib_h.InputBufferSize=16384*16;
gpib_h.FlowControl='Hardware';
fopen(gpib_h);

-----
function set_gpib_addr(gpib_h, ADDR)

fprintf(gpib_h,['++addr ' num2str(ADDR)]);
fprintf(gpib_h,'++addr');
pause(0.2)
disp(fgetl(gpib_h))

-----
function [power unit]=power_meter_8163_read
(gpib_h,Slot,CH)
if(gpib_h.BytesAvailable)
   fread(gpib_h,gpib_h.BytesAvailable);
end

fprintf(gpib_h,['READ' num2str(Slot) ':CHAN'
num2str(CH) ':POW?']);
pause(0.05); %0.25
str=fgetl(gpib_h);
power=str2num(str);
if(power>1E38)
   power=NaN;
end
fprintf(gpib_h, ['SENS' num2str(Slot) ':CHAN'
num2str(CH) ':POW:UNIT?']);
%pause(0.05); %0.25
if(str2num(fgetl(gpib_h))==1)
   unit='W';
else
   unit='dBm';
end

------
function gpib_close(osa_h)

fclose(osa_h);


------PROCESS DATA---------

clc; clear all;
fileList =
getAllFiles('C:\Users\asilva\Documents\Doutor
amento\Fiber optic sensor\Data
acquisition\sensor characterization\Loop
Configurations\four loops\');
angles = [0 3 6 9 12 15 18 21 24 27 30 33 36 39
42 45 48 51 54 57 60];

for i=1:length(fileList)
   str = fileList{i,1}
   if all(str(end-3:end) == '.mat') %verifica se é
um ficheiro .mat com os dados
```

```
    signal = importdata(str);
    power = signal.P();
    plot(power)

  for j=1:length(angles)

   inicio = input('inicio \n');
   fim = input('fim \n');

   stage(j) = mean(power(:,inicio:fim));

  end

  PowerValues (i,1:j) = stage(:,:);
  end

end
  boxplot(PowerValues)
```

Appendix D: Experimental Protocol Approved by Ethics Committee (in Portuguese)

ESTSP | POLITÉCNICO DO PORTO

FOLHA DE ROSTO DO ESTUDO DE INVESTIGAÇÃO E DESENHO DO PROJECTO

UTILIZAÇÃO OBRIGATÓRIA.

TÍTULO

O BIOFEEDBACK COMO FERRAMENTA DE TREINO/REABILITAÇÃO EM INDIVÍDUOS COM ALTERAÇÃO DA FUNÇÃO DO MEMBRO SUPERIOR

CLASSIFICAÇÃO

Trabalho Académico de Investigação ☒
Não conferidor de grau ☐ Conferidor de grau ☐ (Licenciatura ☐ Mestrado ☐ Doutoramento ☒)
Projecto de Investigação ☐
Ensaio Clínico ☐ (Medicamentos ☐ Dispositivos médicos ☐)
Outro ☐ Qual?

VERSÃO

Novo ☐ Modificação / Adenda ☒ Prolongamento ☐

CALENDARIZAÇÃO

Data início: 01/2012 Data conclusão: 12/2013
PRAZO A CUMPRIR: 2 anos

INVESTIGADORES

É FUNDAMENTAL O E-MAIL, JÁ QUE ESTE CONSTITUIRÁ A FORMA PREFERENCIAL DE CONTACTO COM OS INVESTIGADORES.

Investigador Principal (Nome, Instituição, Serviço, Grupo profissional) Contactos (e-mail, telefone e telemóvel).

CLÁUDIA ISABEL COSTA DA SILVA, ESTSP, ÁREA TÉCNICO-CIENTÍFICA DA FISIOTERAPIA E-MAIL: CCS@ESTSP.IPP.PT, TEL: 938674365

Investigador Responsável na ESTSP (Nome, Serviço, Grupo profissional) (Contactos: e-mail, telefone e telemóvel).

Assinale aqui se for idêntico ao Investigador Principal □

Indique o Investigador Responsável no CHP quando o Investigador Principal não pertencer à Instituição.

MANUEL RUBIM SILVA SANTOS, ESTSP, ÁREA CIENTÍFICA DA FÍSICA, DOUTORAMENTO E-MAIL: RSS@ESTSP.IPP.PT, TEL: 962644773

Outros Investigadores (Nome, Instituição, Serviço, Grupo profissional.)

Indique os restantes elementos da Equipa de Investigação.

ANTÓNIO SALAZAR, FEUP, ENGENHARIA ELECTROTÉC NICA E DE COMPUTADORES, INESCPORTO
E-MAIL: ANTONIO.SALAZAR@GMAIL.COM, TEL: 967401514
ANA SOFIA SILVA, FEUP, ENGENHARIA ELECTROTÉC NICA E DE COMPUTADORES, INESCPORTO
E-MAIL: NITTA.TU@GMAIL.COM, TEL: 938237830
CARLA BORGES, FEUP, ENGENHARIA ELECTROTÉC NICA E DE COMPUTADORES, INESCPORTO
E-MAIL: CARLAMBORGES@GMAIL.COM, TEL: 969494521
MIGUEL VELHOTE CORREIA, FEUP, ENGENHARIA ELECTROTÉC NICA E DE COMPUTADORES, INESCPORTO
E-MAIL: MCORREIA@FE.UP.PT, TEL: 22 508 1888
JOÃO PAULO VILAS-BOAS, FADE-UP, LABORATÓRIO DE BIOMECÂNICA DO PORTO
E-MAIL: JPVB@FADE.UP.PT, TEL: 225074790

ALUNOS E ORIENTADORES

É FUNDAMENTAL O E-MAIL, JÁ QUE ESTE CONSTITUIRÁ A FORMA PREFERENCIAL DE CONTACTO COM OS INVESTIGADORES.

Aluno Nome; Instituição (Universidade / Faculdade ou Escola); Curso e Ano; (Contactos: e-mail, telefone e telemóvel).

NÃO SE APLICA

Orientador / Elo de ligação da Instituição de Ensino

Nome; Instituição (Universidade / Faculdade ou Escola); Grupo e Categoria Profissional; Grau Académico; (Contactos: e-mail, telefone e telemóvel).

MANUEL RUBIM SILVA SANTOS, ESTSP, ÁREA CIENTÍFICA DA FÍSICA, DOUTORAMENTO
E-MAIL: RSS@ESTSP.IPP.PT, TEL: 962644773

Orientador / Elo de ligação na ESTSP (Nome, Serviço, Grupo profissional) (Contactos: e-mail, telefone e telemóvel).

Assinale aqui se for idêntico ao Orientador / Supervisor da Instituição de Ensino □

Indique o Orientador / Supervisor no CHP quando o Orientador / Supervisor da Instituição de Ensino não pertencer à Instituição.

MANUEL RUBIM SILVA SANTOS, ESTSP, ÁREA CIENTÍFICA DA FÍSICA, DOUTORAMENTO
E-MAIL: RSS@ESTSP.IPP.PT, TEL: 962644773

INSTITUIÇÕES E SERVIÇOS

Unidades, Departamentos e Serviço da ESTSP (de entre as indicadas, mencione qual é a proponente)

Área técnico-cientifica de fisioterapia

Outras Instituições intervenientes (Indique outras Instituições, Unidades, Departamentos e Serviços)

Faculdade de Desporto – Universidade do Porto (laboratório de Biomecânica)

CARACTERÍSTICAS DO ESTUDO

1. FUNDAMENTAÇÃO TEÓRICA

Perante situações de alteração da função do membro superior, o objectivo da reabilitação é proporcionar um melhor desempenho nas actividades de vida diária ou no gesto desportivo, de forma a garantir uma melhor performance motora. Tal, tem por base a necessidade de desenvolver oportunidades para que a especificidade de determinada tarefa ou experiência seja repetida, com um significado funcional, através da criação de um contexto motivador e num ambiente que ofereça diferentes modalidades sensoriais (Sveistrup, 2004), e que sobretudo possibilite um adequado feedback da performance. Tal, é de extrema relevância, dado o conhecimento da importância do feedback (quer em tempo real – concomitante à execução da tarefa, ou imediatamente após – "conhecimento de resultados") no processo de aprendizagem motora (Holden, 2005).

Assim, um dos grandes objectivos actualmente consiste no desenvolvimento de sistemas que permitam, com recurso a tecnologia relativamente simples, ao indivíduo em processo de reabilitação, estabelecer uma interacção desafiante, mas segura, num contexto ambiental próprio, com controlo dos vários parâmetros relacionados com as suas necessidades específicas aliado á possibilidade de receber um feedback "aumentativo" e portanto mais eficaz, possibilitando em última instância, um pormenorizado follow-up individual, bem como o desenvolvimento de técnicas de análise standard e protocolos de reabilitação / treino padronizados.

Ainda outra vantagem importante associada ao uso desta tecnologia, é a possibilidade de permitir um aumento na intensidade da prática sem necessitar da presença ou supervisão do terapeuta ou treinador (Dobkin, 2004).

Face ao exposto, o desenvolvimento de sistemas que ofereçam as possibilidades acima referidas, revela-se de total pertinencia. O Wireless Wearable Modular Monitoring (W2M2) constitui um sistema desenvolvido especificamente para dar resposta às necessidades expressas no campo da reabilitação, tendo surgido a partir da criação de uma pareceria entre a ESTSP, faculdade de Desporto e faculdade de Engenharia da Universidade do Porto, no âmbito do doutoramento da investigadora. Trata-se de um equipamento constituído por sistemas modulares contendo acelerómetros e giroscópios que permitem a aquisição de sinais relevantes para a caracterização do movimento. Pretende constituir uma alternativa aos actuais sistemas de aquisição, pela seu baixo custo, aliado à pouca complexidade, eprmitindo assim o seu uso dessiminado, ao invês de confinar a sua aplicabilidade a centros de investigação.

2. OBJECTIVOS

Este estudo tem como objectivo melhorar os conhecimentos sobre o controlo motor associado à função do membro superior, nomadamente na tarefa de alcançar (reach), bem como aprofundar conhecimentos sobre o efeito do biofeedback e a sua relação com as teorias de aprendizagem motora ,a fim de possibilitar uma melhor intervenção na reabilitação de atletas pós lesão desportiva e em indivíduos pós lesão do SNC (AVE), usando tecnologia simple, acessível e de baixo custo.

Pretende-se com este trabalho:

-Caracterizar em termos de acelerometria o gesto humano de alcançar;

- Detectar eventuais erros na performance (de deslocamento, orientação, velocidade angular ou linear, smoothness) e compensações no padrão de moviemento nos casos pós lesão;

-Testar o equipamento desenvolvido (W2M2) no que se refere à sua aplicabilidade como ferramenta de biofeedback, que possibilite ao utilizador, no seu póprio ambiente, a percepção do "erro", aquando da execução do padrão de movimento pretendido.

3. **METODOLOGIA**

3.1. Participantes, tipo de estudo, amostra e procedimentos

TIPO DE ESTUDO:
Prevê-se realizar um estudo observacional.
PARTICIPANTES:
Será constituída uma amostra de individuos voluntários constituída por sujeitos com diagnóstico de Acidente Vascular Encefálico e sujeitos saudáveis (estudantes e funcionários da ESTSP). O investigador contactará individualmente cada individuo convidando-o a participar no estudo
A identificação de cada participante será codificada e será garantido o anonimato.
CRITÉRIOS DE SELECÇÃO
- Critérios de inclusão do grupo de individuos saudáveis: Serão incluídos indivíduos com idade igual ou superior a 18 anos, que não apresentem patologia do foro neuro-músculo-esquelético, nomeadamente ao nível da coluna cervical e ombro, e que concordam em assinar a folha de consentimento informado.
- Critérios de inclusão do grupo de individuos com AVE: confirmação imagiológica de diagnóstico de AVE único e unilateral no território da artéria cerebral média, há pelo menos 3 meses; aus˜encia de neglect; ausência de alterações visuais, perceptivas ou cognitivas e capacidade de realizar movimento activo no membro superior predominantemente afectado de pelo menos 15º no ombro e cotovelo.
- Critérios de exclusão: Serão excluídos os indivíduos que apresentem AVE do tronco encefálico ou cerebelo e presença de dor ao nível dos membros superiores.
As informações serão recolhidas através de um questionário elaborado para esse efeito.
PROCEDIMENTOS:
Cada indivíduo será sentado numa marquesa hidráulica a uma altura equivalente à distância medida da interlinha articular do joelho até ao chão (correspondente ao comprimento da perna), com 75% do comprimento da coxa (medido desde o grande trocânter até à interlinha articular da articulação do joelho) assente e de pés descalços em total contacto com o chão, ou num degrau de madeira. Será colocada uma mesa à frente de cada indivíduo, a uma altura correspondente ao alinhamento das cristas ilíacas, sendo o bordo deste foi alinhado com o limite inferior das coxas do indivíduo, de modo a não interferir com o movimento da mão. A colocação do objecto-alvo na mesa, teve como referência a avaliação no limite anatómico da distância de alcance funcional da mão, usando-se a distância medida desde o acrómio até à interlinha articular da articulação metacarpofalângica do polegar. O indivíduo será instruído, após comando verbal, a executar a tarefa funcional de alcançar o objecto-alvo, e retomar a posição inicial.
O sistema de aquisição dos dados inerciais (acelerometria) - W2M2, constituídos por 3 módulos, será colocado a cada um dos individuos, nos segmentos braço, antebraço e tronco. Este é um sistema não invasivo, que pretende exlusivamente monitorizar parametros relacionados com o movimento funcional, sendo colocado em cada um dos segmentos referidos através do uso de velcros, permitindo a sua correcta fixação. Dado o objectivo deste equipamento, os individuos não necessitam de ser sujeitos a qualquer tipo de preparação prévia, não acarretando por isso quelaquer risco. Os dados obtidos permitirão comparar a performance motora de individuos com AVE vs individuos saudáveis.

3.2. Instrumentos de recolha de dados

Wireless Wearable Modular Monitoring (W2M2)

3.3 Cronograma

	2012-13	2013-14
Revisão bibliográfica e elaboração de protocolos		
Teste piloto dos protocolos de avaliação e ensaios dos protocolos de intervenção		
Selecção da amostra Recolha de dados		
Tratamento estatístico dos dados		
Redacção da tese		